Proposed Nicaragua canal divides scientists *p. 220*

How strain relief pins rings to nitrogen *p. 241*

Early Arctic mammoth hunters *p. 260*

Science

$15
15 JANUARY 2016
sciencemag.org

AAAS

Tuning out

How inhibition protects learned song in zebra finches *p. 267*

CONTENTS

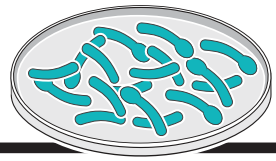

224
Evaluating disease causation

15 JANUARY 2016 • VOLUME 351 • ISSUE 6270

Will an interoceanic canal harm Lake Nicaragua?

220

NEWS

IN BRIEF

208 News at a glance

IN DEPTH

211 ASTRONOMERS SEE ASHES OF THE FIRST STARS
Primordial clouds show how giant stars forged the heavy elements that fill today's universe *By D. Clery*

212 REGULATORS SEEK TO TAME BRAIN TRAINING'S 'WILD WEST'
$2 million fine for Lumosity is latest shot at claims of cognitive benefits from games and apps *By E. Underwood*

213 PUBLISHERS EMBRACE SCHEME TO END NAME CONFUSION
ORCID gives every Smith and Wang a unique number *By J. Bohannon*

214 FEMALE ORGANS REVEALED AS WEAPONS IN SEXUAL ARMS RACE
Researchers broaden their focus beyond male anatomy *By E. Pennisi*

215 INCANDESCENT LIGHTS GO GREEN
Photonic technology boosts efficiency of warm, wasteful bulbs *By R. F. Service*

216 CALTECH SUSPENDS PROFESSOR FOR HARASSMENT
University restricts his access to graduate students after upholding their complaints *By J. Mervis*

FEATURES

217 THE SOCIAL LIFE OF QUARKS
Particles consisting of four and five quarks make a comeback *By A. Cho*

220 A NATION DIVIDED
Some scientists see Nicaragua's plans for a Grand Canal as a boon for an ailing land; others predict ecological catastrophe *By L. Wade*

211

INSIGHTS

PERSPECTIVES

224 ADAPTING KOCH'S POSTULATES
Criteria for disease causation must take microbial interactions into account
By A. L. Byrd and J. A. Segre

226 SMALL PEPTIDES CONTROL HEART ACTIVITY
Peptides from long noncoding RNAs control a muscle calcium pump
By F. Payre and C. Desplan
▸ REPORT P. 272

228 IRES UNPLUGGED
Cap-independent translation by IRESs can occur from various locations in mRNA *By F. Gebauer and M. W. Hentze*
▸ RESEARCH ARTICLE P. 240

PERSPECTIVES

229 TUNING TERAHERTZ LASERS VIA GRAPHENE PLASMONS
The emission of a terahertz laser is controlled by graphene carrier density
By M. Polini
▸ REPORT P. 246

230 SAMPLING THE MOON'S ATMOSPHERE
In situ measurements reveal details of the production and evolution of the lunar exosphere *By C. Dukes and D. Hurley*
▸ REPORT P. 249

BOOKS *ET AL.*

232 WHY WE SNAP
By R. D. Fields, reviewed by P. Wallisch

233 ORPHAN
By P. R. Reilly, reviewed by N. Yang

LETTERS

234 WEATHER STATIONS LACK FOREST DATA
By P. De Frenne and K. Verheyen

234 VISA RULES IMPERIL COLLABORATION
By N. Madani

Science Staff 206
AAAS Meeting Program 290
New Products 303
Science Careers 304

PHOTO: (TOP) REUTERS/OSWALDO RIVAS

Published by AAAS

CONTENTS

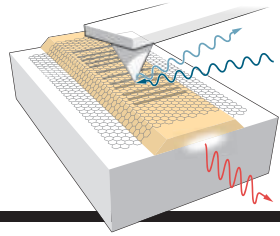

229 & 246
Graphene as a laser tuner

15 JANUARY 2016 • VOLUME 351 • ISSUE 6270

234 MECHANISTIC BIOLOGICAL MODELING THRIVES
By B. O'Shaughnessy and T. D. Pollard

235 TECHNICAL COMMENT ABSTRACTS

RESEARCH

IN BRIEF

236 From *Science* and other journals

REVIEW

239 VIRAL IMMUNITY
Transkingdom control of viral infection and immunity in the mammalian intestine *J. K. Pfeiffer and H. W. Virgin*
REVIEW SUMMARY; FOR FULL TEXT: dx.doi.org/10.1126/science.aad5872

RESEARCH ARTICLES

240 COMPARATIVE GENETICS
Systematic discovery of cap-independent translation sequences in human and viral genomes *S. Weingarten-Gabbay* et al.
RESEARCH ARTICLE SUMMARY; FOR FULL TEXT: dx.doi.org/10.1126/science.aad4939
▸ PERSPECTIVE P. 228

241 ORGANIC CHEMISTRY
Strain-release amination
R. Gianatassio et al.

REPORTS

246 APPLIED OPTICS
Gain modulation by graphene plasmons in aperiodic lattice lasers
S. Chakraborty et al.
▸ PERSPECTIVE P. 229

249 LUNAR ATMOSPHERE
How surface composition and meteoroid impacts mediate sodium and potassium in the lunar exosphere
A. Colaprete et al.
▸ PERSPECTIVE P. 230

252 ORGANIC CHEMISTRY
Functionalization of C(sp^3)–H bonds using a transient directing group
F.-L. Zhang et al.

257 ASTRONOMY
ASASSN-15lh: A highly super-luminous supernova *S. Dong* et al.

260 PALEOANTHROPOLOGY
Early human presence in the Arctic: Evidence from 45,000-year-old mammoth remains *V. V. Pitulko* et al.
▸ PODCAST

264 PHYTOPLANKTON
The fate of photons absorbed by phytoplankton in the global ocean
H. Lin et al.

267 NEURAL CIRCUITS
Inhibition protects acquired song segments during vocal learning in zebra finches *D. Vallentin* et al.

271 MUSCLE PHYSIOLOGY
A peptide encoded by a transcript annotated as long noncoding RNA enhances SERCA activity in muscle
B. R. Nelson et al.
▸ PERSPECTIVE P. 226

275 METABOLISM
AMP-activated protein kinase mediates mitochondrial fission in response to energy stress *E. Q. Toyama* et al.

282 RNA BIOCHEMISTRY
Transcriptome-wide distribution and function of RNA hydroxymethylcytosine
B. Delatte et al.

285 GENE REGULATION
Transcription factors LRF and BCL11A independently repress expression of fetal hemoglobin *T. Masuda* et al.

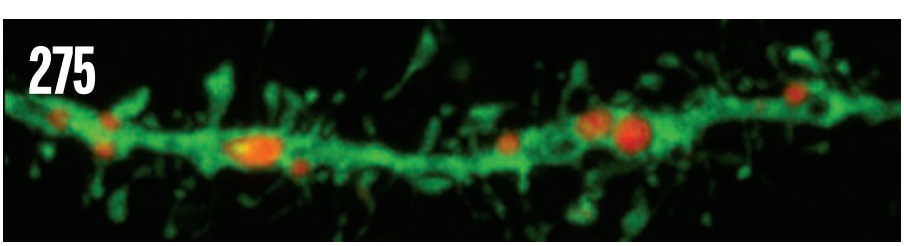

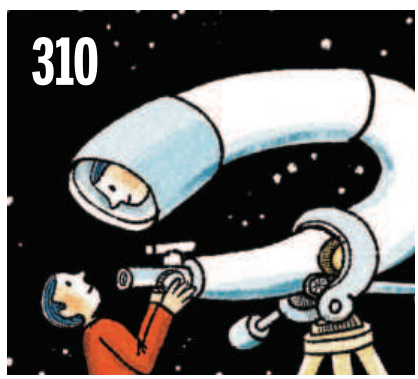

DEPARTMENTS

207 EDITORIAL
Empowering great teachers
By Bruce Alberts

310 WORKING LIFE
My adviser's best advice
By Josh Shiode

ON THE COVER

A young zebra finch (left) attending to his father (right). During development, juvenile birds listen to and imitate their father's courtship song. Through behavioral tracking and synaptic current measurements, Vallentin *et al.* show that neuronal circuit inhibition preferentially targets specific pieces of song that the birds have already mastered, suggesting a new circuit mechanism for observational learning. See page 267.
Photo: Georg Kosche

SCIENCE (ISSN 0036-8075) is published weekly on Friday, except the last week in December, by the American Association for the Advancement of Science, 1200 New York Avenue, NW, Washington, DC 20005. Periodicals mail postage (publication No. 484460) paid at Washington, DC, and additional mailing offices. Copyright © 2016 by the American Association for the Advancement of Science. The title SCIENCE is a registered trademark of the AAAS. Domestic individual membership and subscription (51 issues): $165 ($74 allocated to subscription). Domestic institutional subscription (51 issues): $1522; Foreign postage extra: Mexico, Caribbean (surface mail) $55; other countries (air assist delivery) $89. First class, airmail, student, and emeritus rates on request. Canadian rates with GST available upon request, GST #1254 88122. Publications Mail Agreement Number 1069624. **Printed in the U.S.A.**
Change of address: Allow 4 weeks, giving old and new addresses and 8-digit account number. **Postmaster:** Send change of address to AAAS, P.O. Box 96178, Washington, DC 20090–6178. **Single-copy sales:** $15.00 current issue, $20.00 back issue prepaid includes surface postage; bulk rates on request. **Authorization to photocopy** material for internal or personal use under circumstances not falling within the fair use provisions of the Copyright Act is granted by AAAS to libraries and other users registered with the Copyright Clearance Center (CCC) Transactional Reporting Service, provided that $35.00 per article is paid directly to CCC, 222 Rosewood Drive, Danvers, MA 01923. The identification code for *Science* is 0036-8075. *Science* is indexed in the *Reader's Guide to Periodical Literature* and in several specialized indexes.

Published by AAAS

Science
AAAS
1200 New York Avenue, NW, Washington, DC 20005
Bateman House, 82-88 Hills Road, Cambridge, UK CB2 1LQ

Editor-in-Chief Marcia McNutt
Executive Editor Monica M. Bradford **News Editor** Tim Appenzeller
Managing Editor, Research Journals Katrina L. Kelner
Deputy Editors Barbara R. Jasny, Andrew M. Sugden(UK), Valda J. Vinson, Jake S. Yeston

Research and Insights

SR. EDITORS Caroline Ash(UK), Gilbert J. Chin, Lisa D. Chong, Julia Fahrenkamp-Uppenbrink(UK), Pamela J. Hines, Stella M. Hurtley(UK), Paula A. Kiberstis, Marc S. Lavine(Canada), Kristen L. Mueller, Ian S. Osborne(UK), Beverly A. Purnell, L. Bryan Ray, Guy Riddihough, H. Jesse Smith, Jelena Stajic, Peter Stern(UK), Phillip D. Szuromi, Sacha Vignieri, Brad Wible, Nicholas S. Wigginton, Laura M. Zahn **ASSOCIATE EDITORS** Brent Grocholski, Keith T. Smith **ASSOCIATE BOOK REVIEW EDITOR** Valerie B. Thompson **ASSOCIATE LETTERS EDITOR** Jennifer Sills **CHIEF CONTENT PRODUCTION EDITOR** Cara Tate **SR. CONTENT PRODUCTION EDITORS** Harry Jach, Lauren Kmec **CONTENT PRODUCTION EDITORS** Jeffrey E. Cook, Chris Filiatreau, Cynthia Howe, Barbara P. Ordway, Catherine Wolner **SR. EDITORIAL COORDINATORS** Carolyn Kyle, Beverly Shields **EDITORIAL COORDINATORS** Joi S. Granger, Lisa Johnson, Anita Wynn **PUBLICATIONS ASSISTANTS** Aneera Dobbins, Jeffrey Hearn, Dona Mathieu, Le-Toya Mayne Flood, Shannon McMahon, Scott Miller, Caitlyn Phillips, Jerry Richardson, Rachel Roberts(UK), Alice Whaley(UK), Brian White **EXECUTIVE ASSISTANT** Anna Bashkirova **ADMINISTRATIVE SUPPORT** Janet Clements(UK), Lizanne Newton(UK), Maryrose Madrid, John Wood(UK)

News

NEWS MANAGING EDITOR John Travis **INTERNATIONAL EDITOR** Richard Stone **DEPUTY NEWS EDITORS** Daniel Clery(UK), Robert Coontz, Elizabeth Culotta, David Grimm, David Malakoff, Leslie Roberts **CONTRIBUING EDITOR** Martin Enserink(Europe) **SR. CORRESPONDENTS** Jeffrey Mervis, Elizabeth Pennisi **NEWS WRITERS** Adrian Cho, Jon Cohen, Jennifer Couzin-Frankel, Carolyn Gramling, Eric Hand, Jocelyn Kaiser, Catherine Matacic, Kelly Servick, Robert F. Service, Erik Stokstad(Cambridge, UK), Emily Underwood **INTERNS** Hanae Armitage, Nala Rogers **CONTRIBUTING CORRESPONDENTS** Michael Balter(Paris), John Bohannon, Ann Gibbons, Mara Hvistendahl, Sam Kean, Eli Kintisch, Kai Kupferschmidt(Berlin), Andrew Lawler, Christina Larson(Beijing), Mitch Leslie, Charles C. Mann, Eliot Marshall, Virginia Morell, Dennis Normile(Shanghai), Heather Pringle, Tania Rabesandratana(London), Gretchen Vogel(Berlin), Lizzie Wade(Mexico City) **CAREERS** Donisha Adams, Rachel Bernstein(Editor) **COPY EDITORS** Julia Cole, Dorie Chevlen, Jennifer Levin (Chief) **ADMINISTRATIVE SUPPORT** Jessica Williams

Executive Publisher Rush D. Holt
Acting Publisher Bill Moran **Chief Digital Media Officer** Rob Covey

BUSINESS OPERATIONS AND PORTFOLIO MANAGEMENT DIRECTOR Sarah Whalen **BUSINESS SYSTEMS AND FINANCIAL ANALYSIS DIRECTOR** Randy Yi **MANAGER OF FULFILLMENT SYSTEMS** Neal Hawkins **SYSTEMS ANALYST** Nicole Mehmedovich **ASSISTANT DIRECTOR, BUSINESS OPERATIONS** Eric Knott **MANAGER, BUSINESS OPERATIONS** Jessica Tierney **BUSINESS ANALYSTS** Cory Lipman **FINANCIAL ANALYST** Robert Clark **RIGHTS AND PERMISSIONS ASSISTANT DIRECTOR** Emilie David **PERMISSIONS ASSOCIATE** Elizabeth Sandler **RIGHTS, CONTRACTS, AND LICENSING ASSOCIATE** Lili Kiser

MARKETING DIRECTOR Elise Swinehart **ASSOCIATE DIRECTOR OF ACQUISITION AND RETENTION** Julianne Wielga **MARKETING ASSOCIATE** Elizabeth Sattler **SR. MARKETING EXECUTIVE** Jennifer Reeves **ASSOCIATE DIRECTOR, CREATIVE SERVICES** Tzeitel Sorrosa **ART ASSOCIATE** Seil Lee **JR. ART ASSOCIATE** Kim Huynh **ASSISTANT COMMERCIAL EDITOR** Selby Frame **MARKETING PROJECT MANAGER** Angelissa McArthur **PROGRAM DIRECTOR, AAAS MEMBER CENTRAL** Peggy Mihelich **FULFILLMENT SYSTEMS AND OPERATIONS** membership@aaas.org **MANAGER, MEMBER SERVICES** Pat Butler **SPECIALISTS** Terrance Morrison, Latasha Russell **MANAGER, DATA ENTRY** Mickie Napoleoni **DATA ENTRY SPECIALISTS** Brenden Aquilino, Fiona Giblin

DIRECTOR, SITE LICENSING Tom Ryan **DIRECTOR, CORPORATE RELATIONS** Eileen Bernadette Moran **SR. PUBLISHER RELATIONS SPECIALIST** Kiki Forsythe **PUBLISHER RELATIONS MANAGER** Catherine Holland **PUBLISHER RELATIONS, EASTERN REGION** Keith Layson **PUBLISHER RELATIONS, WESTERN REGION** Ryan Rexroth **SALES RESEARCH COORDINATOR** Aiesha Marshall **MANAGER, SITE LICENSE OPERATIONS** Iquo Edim **SENIOR PRODUCTION SPECIALIST** Robert Koepke **SENIOR OPERATIONS ANALYST** Lana Guz **FULFILLMENT ANALYST** Judy Lillibridge **ASSOCIATE DIRECTOR, MARKETING** Christina Schlecht **MARKETING ASSOCIATES** Thomas Landreth, Isa Sesay-Bah

WEB TECHNOLOGIES SR. DEVELOPER Chris Coleman **DEVELOPERS** Dan Berger, Jimmy Marks, Ryan Jensen **SR. PROJECT MANAGER** Trista Smith **PROJECT MANAGER** Nick Fletcher

MULTIMEDIA DIRECTOR OF ANALYTICS Enrique Gonzales **SR. WEB PRODUCER** Sarah Crespi **WEB PRODUCER** Alison Crawford **VIDEO PRODUCER** Nguyen Nguyen **SOCIAL MEDIA PRODUCER** Brice Russ

DIRECTOR OF OPERATIONS PRINT AND ONLINE Lizabeth Harman **DIGITAL/PRINT STRATEGY MANAGER** Jason Hillman **QUALITY TECHNICAL MANAGER** Marcus Spiegler **PROJECT ACCOUNT MANAGER** Tara Kelly **DIGITAL PRODUCTION MANAGER** Lisa Stanford **ASSISTANT MANAGER DIGITAL/PRINT** Rebecca Doshi **SENIOR CONTENT SPECIALISTS** Steve Forrester, Antoinette Hodal, Lori Murphy, Anthony Rosen **CONTENT SPECIALISTS** Jacob Hedrick, Kimberley Oster

DESIGN DIRECTOR Beth Rakouskas **DESIGN EDITOR** Marcy Atarod **SENIOR DESIGNER** Garvin Grullón **DESIGNER** Chrystal Smith **GRAPHICS MANAGING EDITOR** Alberto Cuadra **SENIOR SCIENTIFIC ILLUSTRATORS** Chris Bickel, Katharine Sutliff **SCIENTIFIC ILLUSTRATOR** Valerie Altounian **SENIOR ART ASSOCIATES** Holly Bishop, Nathalie Cary, Preston Huey **SENIOR PHOTO EDITOR** William Douthitt **PHOTO EDITORS** Leslie Blizard, Christy Steele

DIRECTOR, GLOBAL COLLABORATION, CUSTOM PUBLICATIONS, ADVERTISING Bill Moran **EDITOR, CUSTOM PUBLISHING** Sean Sanders: 202-326-6430 **ASSISTANT EDITOR, CUSTOM PUBLISHING** Tianna Hicklin: 202-326-6463 **ADVERTISING MARKETING MANAGER** Justin Sawyers: 202-326-7061 science_advertising@aaas.org **ADVERTISING MARKETING ASSOCIATE** Javia Flemmings **ADVERTISING SUPPORT MANAGER** Karen Foote: 202-326-6740 **ADVERTISING PRODUCTION OPERATIONS MANAGER** Deborah Tompkins **SR. PRODUCTION SPECIALIST/GRAPHIC DESIGNER** Amy Hardcastle **SR. TRAFFIC ASSOCIATE** Christine Hall **SALES COORDINATOR** Shirley Young **ASSOCIATE DIRECTOR, COLLABORATION, CUSTOM PUBLICATIONS/CHINA/TAIWAN/KOREA/SINGAPORE** Ruolei Wu: +86-186 0082 9345, rwu@aaas.org **COLLABORATION/CUSTOM PUBLICATIONS/JAPAN** Adarsh Sandhu + 81532-81-5142 asandhu@aaas.org **EAST COAST/E. CANADA** Laurie Faraday: 508-747-9395, FAX 617-507-8189 **WEST COAST/W. CANADA** Lynne Stickrod: 415-931-9782, FAX 415-520-6940 **MIDWEST** Jeffrey Dembksi: 847-498-4520 x3005, Steven Loerch: 847-498-4520 x3006 **UK EUROPE/ASIA** Roger Goncalves: TEL/FAX +41 43 243 1358 **JAPAN** Katsuyoshi Fukamizu(Tokyo): +81-3-3219-5777 kfukamizu@aaas.org **CHINA/TAIWAN** Ruolei Wu: +86-186 0082 9345, rwu@aaas.org

WORLDWIDE ASSOCIATE DIRECTOR OF SCIENCE CAREERS Tracy Holmes: +44 (0) 1223 326525, FAX +44 (0) 1223 326532 tholmes@science-int.co.uk **CLASSIFIED** advertise@sciencecareers.org **U.S. SALES** Tina Burks: 202-326-6577, Nancy Toema: 202-326-6578 **EUROPE/ROW SALES** Sarah Lelarge **SALES ASSISTANT** Kelly Grace **JAPAN** Hiroyuki Mashiki(Kyoto): +81-75-823-1109 hmashiki@aaas.org **CHINA/TAIWAN** Ruolei Wu: +86-186 0082 9345 rwu@aaas.org **MARKETING MANAGER** Allison Pritchard **MARKETING ASSOCIATE** Aimee Aponte

AAAS BOARD OF DIRECTORS RETIRING PRESIDENT, CHAIR Gerald R. Fink **PRESIDENT** Geraldine (Geri) Richmond **PRESIDENT-ELECT** Barbara A. Schaal **TREASURER** David Evans Shaw **CHIEF EXECUTIVE OFFICER** Rush D. Holt **BOARD** Bonnie L. Bassler, May R. Berenbaum, Carlos J. Bustamante, Stephen P.A. Fodor, Claire M. Fraser, Michael S. Gazzaniga, Laura H. Greene, Elizabeth Loftus, Mercedes Pascual

SUBSCRIPTION SERVICES For change of address, missing issues, new orders and renewals, and payment questions: 866-434-AAAS (2227) or 202-326-6417, FAX 202-842-1065. Mailing addresses: AAAS, P.O. Box 96178, Washington, DC 20090-6178 or AAAS Member Services, 1200 New York Avenue, NW, Washington, DC 20005

INSTITUTIONAL SITE LICENSES 202-326-6730 **REPRINTS:** Author Inquiries 800-635-7181 **COMMERCIAL INQUIRIES** 803-359-4578 **PERMISSIONS** 202-326-6765, permissions@aaas.org **AAAS Member Services** 202-326-6417 or http://membercentral.aaas.org/discounts

Science serves as a forum for discussion of important issues related to the advancement of science by publishing material on which a consensus has been reached as well as including the presentation of minority of conflicting points of view. Accordingly, all articles published in *Science*—including editorials, news and comment, and books reviews—are signed and reflect the individual views of the authors and not official points of view adopted by AAAS or the institutions with which the authors are affiliated.

INFORMATION FOR AUTHORS See pages 678 and 679 of the 6 February 2015 issue or access www.sciencemag.org/about/authors

SENIOR EDITORIAL BOARD
Robert H. Grubbs, *California Institute of Technology,* **Gary King,** *Harvard University*
Susan M. Rosenberg, *Baylor College of Medicine,* **Ali Shilatifard,** *Northwestern University Feinberg School of Medicine,* **Michael S. Turner,** *U. of Chicago*

BOARD OF REVIEWING EDITORS (Statistics board members indicated with **(S)**)

Adriano Aguzzi, *U. Hospital Zürich*
Takuzo Aida, *U. of Tokyo*
Leslie Aiello, *Wenner-Gren Foundation*
Judith Allen, *U. of Edinburgh*
Sonia Altizer, *U. of Georgia*
Sebastian Amigorena, *Institut Curie*
Kathryn Anderson, *Memorial Sloan-Kettering Cancer Center*
Meinrat O. Andreae, *Max-Planck Inst. Mainz*
Paola Arlotta, *Harvard U.*
Johan Auwerx, *EPFL*
David Awschalom, *U. of Chicago*
Clare Baker, *University of Cambridge*
Jordi Bascompte, *University of Zurich*
Facundo Batista, *London Research Inst.*
Ray H. Baughman, *U. of Texas, Dallas*
David Baum, *U. of Wisconsin*
Carlo Beenakker, *Leiden U.*
Kamran Behnia, *ESPCI-ParisTech*
Yasmine Belkaid, *NIAID, NIH*
Philip Benfey, *Duke U.*
May Berenbaum, *U. of Illinois*
Gabriele Bergers, *U. of California, San Francisco*
Bradley Bernstein, *Massachusettes General Hospital*
Peer Bork, *EMBL*
Bernard Bourdon, *Ecole Normale Supérieure de Lyon*
Chris Bowler, *École Normale Supérieure*
Ian Boyd, *U. of St. Andrews*
Emily Brodsky, *U. of California, Santa Cruz*
Ron Brookmeyer, *U. of California Los Angeles* **(S)**
Christian Büchel, *U. Hamburg-Eppendorf*
Joseph A. Burns, *Cornell U.*
Carter Tribley Butts, *U. of California, Irvine*
Gyorgy Buzsaki, *New York U. School of Medicine*
Blanche Capel, *Duke U.*
Mats Carlsson, *U. of Oslo*
Ib Chorkendorff, *U. of Denmark*
David Clapham, *Children's Hospital Boston*
Joel Cohen, *Rockefeller U., Columbia U.*
James J. Collins, *MIT*
Robert Cook-Deegan, *Duke U.*
Lisa Coussens, *Oregon Health & Science U.*
Alan Cowman, *Walter & Eliza Hall Inst.*
Robert H. Crabtree, *Yale U.*
Roberta Croce, *Vrije Universiteit*
Janet Currie, *Princeton U.*
Jeff L. Dangl, *U. of North Carolina*
Tom Daniel, *U. of Washington*
Frans de Waal, *Emory U.*
Stanislas Dehaene, *Collège de France*
Robert Desimone, *MIT*
Claude Desplan, *New York U.*
Dennis Discher, *U. of Pennsylvania*
Gerald W. Dorn II, *Washington U. School of Medicine*
Jennifer A. Doudna, *U. of California, Berkeley*
Bruce Dunn, *U. of California, Los Angeles*
William Dunphy, *Caltech*
Christopher Dye, *WHO*
Todd Ehlers, *U. of Tuebingen*
David Ehrhardt, *Carnegie Inst. of Washington*
Tim Elston, *U. of North Carolina at Chapel Hill*
Gerhard Ertl, *Fritz-Haber-Institut, Berlin*
Barry Everitt, *U. of Cambridge*
Ernst Fehr, *U. of Zurich*
Anne C. Ferguson-Smith, *U. of Cambridge*
Michael Feuer, *The George Washington U.*
Toren Finkel, *NHLBI, NIH*
Kate Fitzgerald, *U. of Massachusetts*
Peter Fratzl, *Max-Planck Inst.*
Elaine Fuchs, *Rockefeller U.*
Daniel Geschwind, *UCLA*
Karl-Heinz Glassmeier, *TU Braunschweig*
Ramon Gonzalez, *Rice U.*
Julia R. Greer, *Caltech*
Elizabeth Grove, *U. of Chicago*
Nicolas Gruber, *ETH Zurich*
Kip Guy, *St. Jude's Children's Research Hospital*
Taekjip Ha, *U. of Illinois at Urbana-Champaign*
Christian Haass, *Ludwig Maximilians U.*
Michael Hasselmo, *Boston U.*
Martin Heimann, *Max-Planck Inst. Jena*
Yka Helariutta, *U. of Cambridge*
James A. Hendler, *Rensselaer Polytechnic Inst.*
Janet G. Hering, *Swiss Fed. Inst. of Aquatic Science & Technology*
Kai-Uwe Hinrichs, *U. of Bremen*
David Hodell, *U. of Cambridge*
David Holden, *Imperial College*
Lora Hooper, *UT Southwestern Medical Ctr. at Dallas*
Tamas Horvath, *Yale University*
Raymond Huey, *U. of Washington*
Auke Ijspeert, *EPFL Lausanne*
Steven Jacobsen, *U. of California, Los Angeles*
Stephen Jackson, *U. of Arizona*
Kai Johnsson, *EPFL Lausanne*
Peter Jonas, *Inst. of Science & Technology (IST) Austria*
Matt Kaeberlein, *U. of Washington*
William Kaelin Jr., *Dana-Farber Cancer Inst.*
Daniel Kahne, *Harvard U.*
Daniel Kammen, *U. of California, Berkeley*
Masashi Kawasaki, *U. of Tokyo*
V. Narry Kim, *Seoul National U.*
Joel Kingsolver, *U. of North Carolina at Chapel Hill*
Robert Kingston, *Harvard Medical School*
Etienne Koechlin, *Ecole Normale Supérieure*
Alexander Kolodkin, *Johns Hopkins U.*
Thomas Langer, *U. of Cologne*
Mitchell A. Lazar, *U. of Pennsylvania*
David Lazer, *Harvard U.*
Thomas Lecuit, *IBDM*
Virginia Lee, *U. of Pennsylvania*
Stanley Lemon, *U. of North Carolina at Chapel Hill*
Ottoline Leyser, *Cambridge U.*
Wendell Lim, *U.C. San Francisco*
Marcia C. Linn, *U. of California, Berkeley*
Jianguo Liu, *Michigan State U.*
Luis Liz-Marzan, *CIC biomaGUNE*
Jonathan Losos, *Harvard U.*
Ke Lu, *Chinese Acad. of Sciences*
Christian Lüscher, *U. of Geneva*
Laura Machesky, *CRUK Beatson Inst. for Cancer Research*
Anne Magurran, *U. of St. Andrews*
Oscar Marin, *CSIC & U. Miguel Hernández*
Charles Marshall, *U. of California, Berkeley*
C. Robertson McClung, *Dartmouth College*
Graham Medley, *U. of Warwick*
Tom Misteli, *NCI*
Yasushi Miyashita, *U. of Tokyo*
Mary Ann Moran, *U. of Georgia*
Richard Morris, *U. of Edinburgh*
Alison Motsinger-Reif, *NC State U.* **(S)**
Thomas Murray, *The Hastings Center*
Daniel Neumark, *U. of California, Berkeley*
Kitty Nijmeijer, *U. of Twente*
Pär Nordlund, *Karolinska Inst.*
Helga Nowotny, *European Research Advisory Board*
Ben Olken, *MIT*
Joe Orenstein, *U. of California Berkeley & Lawrence Berkeley National Lab*
Harry Orr, *U. of Minnesota*
Andrew Oswald, *U. of Warwick*
Steve Palumbi, *Stanford U.*
Jane Parker, *Max-Planck Inst. of Plant Breeding Research*
Giovanni Parmigiani, *Dana-Farber Cancer Inst.* **(S)**
John H. J. Petrini, *Memorial Sloan-Kettering Cancer Center*
Samuel Pfaff, *Salk Institute for Biological Studies*
Joshua Plotkin, *U. of Pennsylvania*
Albert Polman, *FOM Institute AMOLF*
Philippe Poulin, *CNRS*
Jonathan Pritchard, *Stanford U.*
David Randall, *Colorado State U.*
Felix Rey, *Institut Pasteur*
Trevor Robbins, *U. of Cambridge*
Jim Roberts, *Fred Hutchinson Cancer Research Ctr.*
Barbara A. Romanowicz, *U. of California,Berkeley*
Amy Rosenzweig, *Northwestern University*
Mike Ryan, *U. of Texas, Austin*
Mitinori Saitou, *Kyoto U.*
Shimon Sakaguchi, *Kyoto U.*
Miquel Salmeron, *Lawrence Berkeley National Lab*
Jürgen Sandkühler, *Medical U. of Vienna*
Alexander Schier, *Harvard U.*
Vladimir Shalaev, *Purdue U.*
Robert Siliciano, *Johns Hopkins School of Medicine*
Denis Simon, *Arizona State U.*
Uri Simonsohn, *U. of Pennsylvania*
Alison Smith, *John Innes Centre*
Richard Smith, *U. of North Carolina* **(S)**
John Speakman, *U. of Aberdeen*
Allan C. Spradling, *Carnegie Institution of Washington*
Jonathan Sprent, *Garvan Inst. of Medical Research*
Eric Steig, *U. of Washington*
Paula Stephan, *Georgia State U. and National Bureau of Economic Research*
Molly Stevens, *Imperial College London*
V. S. Subrahmanian, *U. of Maryland*
Ira Tabas, *Columbia U.*
Sarah Teichmann, *Cambridge U.*
John Thomas, *North Carolina State U.*
Shubha Tole, *Tata Institute of Fundamental Research*
Christopher Tyler-Smith, *The Wellcome Trust Sanger Inst.*
Herbert Virgin, *Washington U.*
Bert Vogelstein, *Johns Hopkins U.*
Cynthia Volkert, *U. of Göttingen*
Douglas Wallace, *Dalhousie U.*
David Wallach, *Weizmann Inst. of Science*
Ian Walmsley, *U. of Oxford*
Jane-Ling Wang, *U. of California, Davis* **(S)**
David A. Wardle, *Swedish U. of Agric. Sciences*
David Waxman, *Fudan U.*
Jonathan Weissman, *U. of California, San Francisco*
Chris Wikle, *U. of Missouri* **(S)**
Ian A. Wilson, *The Scripps Res. Inst.* **(S)**
Timothy D. Wilson, *U. of Virginia*
Rosemary Wyse, *Johns Hopkins U.*
Jan Zaanen, *Leiden U.*
Kenneth Zaret, *U. of Pennsylvania School of Medicine*
Jonathan Zehr, *U. of California, Santa Cruz*
Len Zon, *Children's Hospital Boston*
Maria Zuber, *MIT*

BOOK REVIEW BOARD
David Bloom, *Harvard U.,* **Samuel Bowring,** *MIT,* **Angela Creager,** *Princeton U.,* **Richard Shweder,** *U. of Chicago,* **Ed Wasserman,** *DuPont*

EDITORIAL

Empowering great teachers

Long ago, U.S. business learned the benefits of constantly soliciting advice from workers on the shop floor by studying the startling success of the Japanese automobile industry. But the vast majority of U.S. school districts have remained hierarchical operations that ignore the wisdom available from their best classroom teachers. After decades of failed top-down solutions, now is the time to create a massive national movement that empowers and deeply respects our teachers. Scientists and science teachers can lead the way.

Producing an effective system of education is an extremely complex endeavor. Yet despite this complexity, U.S. policy-makers have been employing one simplistic top-down solution after another in attempts to improve schools. The most recent fiasco has been the high-stakes test-based accountability introduced by the federal government's No Child Left Behind Act of 2001. Against the advice of experts, the nation has even been mistreating teachers by grading them according to the annual test gains of their students, ignoring dominant out-of-school influences as well as research showing that teacher differences account for only about 10% of the variance in student test score gains in a single year.* Perhaps not surprisingly, the job satisfaction reported by U.S. teachers has fallen from 62 to 39% in 5 years, and the number of young Americans planning teaching careers has plummeted. How can the United States learn from this failure and make a new start, now that the Every Student Succeeds Act of 2015 has repealed many of the 2001 act's most harmful features? It is way past time to create a major national movement that aims to have outstanding experienced teachers provide effective, regular input that powerfully steers their school district's (and their state's) policies and practices, while remaining in their classrooms with at least a part-time schedule.

Today's students need to learn how to work collaboratively and to communicate effectively using evidence and logic, while sorting, analyzing, and critiquing information. A skilled, experienced teacher creates appropriate challenges for each student, constantly suggesting ideas and connections to follow. A wise friend, with decades of leadership experience in my local public school system, is convinced that "experienced, effective teachers are a vastly underutilized resource in education systems...perhaps the only resource that can truly create the change and improvements that students and teachers deserve." But such teachers are rarely used appropriately, and they can even be resented by school system bureaucracies.

"...now is the time to create a..national movement that empowers...our teachers."

Launching an effective national movement to empower teachers will require casting a wide net to select specific strategies. Such an effort should begin by seeking advice from the best teachers. This can be done immediately for science, where an appropriate set of networks already exists. The organizations that oversee these networks would then form a consortium to select, and strongly advocate for, a small set of specific policies. Collaborations will need to be developed with national institutions that represent other critical aspects of the U.S. education system—in particular, superintendents, principals, teachers' unions, school boards, education schools, parent organizations, and community groups. Such a national movement could, for example, develop a merit-based system for selecting lead teachers, define specific roles for them in schools and school districts, and find ways for them to be paid to stay in the classroom with part-time administrative/professional development roles (rather than being enticed with raises to permanently leave school sites). The situation is urgent: Unless the United States can make dramatic advances in empowering its teachers, the nation will never have public school systems that make the best decisions for their students. Nor will it be able to attract and retain the highly talented teacher corps that every nation needs.†

– Bruce Alberts

Bruce Alberts is the Chancellor's Leadership Chair in Biochemistry and Biophysics for Science and Education at the University of California, San Francisco, CA, and emeritus editor-in-chief of Science. *E-mail: Bruce.Alberts@ucsf.edu*

*E. H. Haertel, 2013; www.ets.org/s/pdf/23497_Angoff%20Report-web.pdf. †This editorial is based on B. Alberts, in *Past as Prologue: The National Academy of Education at 50, Members Reflect*, 2015; www.naeducation.org/cs/groups/naedsite/documents/webpage/naed_169315.pdf.

10.1126/science.aaf2001

PHOTOS: (RIGHT) CHRISTOPHER REIGER; (INSET) FRANCISBLACK/ISTOCKPHOTO.COM

Published by AAAS

NEWS

> "It's frankly so preposterous that I don't believe it."
>
> **U.S. District Court Judge Peter Messite**, sentencing former U.S. National Institute of Standards and Technology (NIST) police officer Christopher Bartley to 42 months in jail. Bartley claimed he cooked methamphetamine in a NIST building as research to train officers about meth.

IN BRIEF

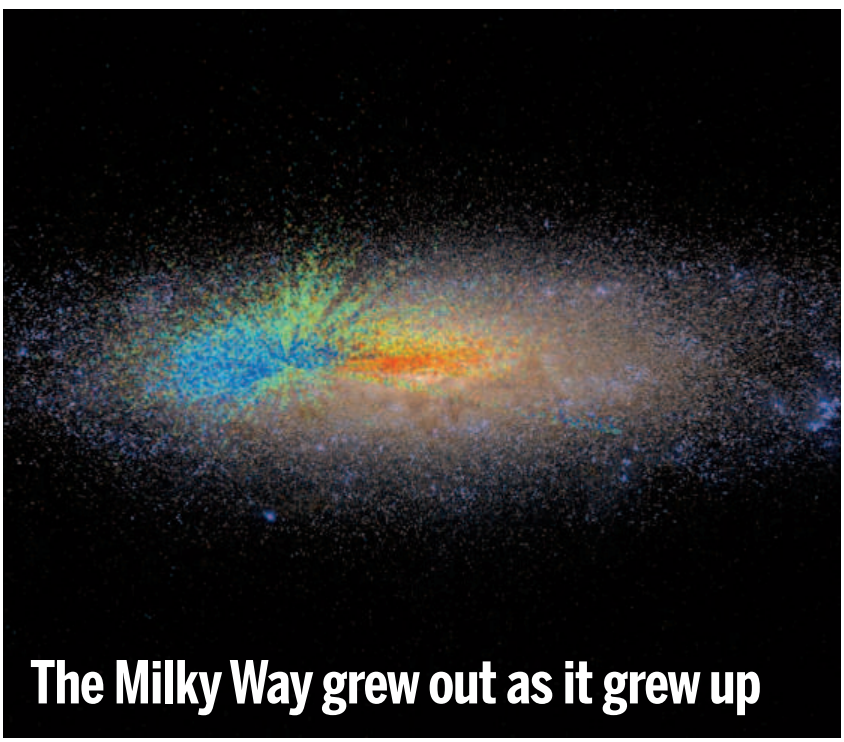

The Milky Way grew out as it grew up

Astronomers have long predicted that the oldest stars in our Milky Way galaxy are in the center, whereas its outer environs are full of younger objects. Now, a team of astronomers has mapped out this prediction in exquisite detail, as they reported last week at the American Astronomical Society meeting in Kissimmee, Florida. The team used the Sloan Digital Sky Survey (SDSS), a 2.5-meter telescope at the Apache Point Observatory in Sunspot, New Mexico, to determine the masses of red giant stars scattered throughout the Milky Way. Red giant stars are bright stars nearing the end of their lives; the older the red giant, generally speaking, the lower its mass. But the SDSS cannot measure mass directly. So the team combined the spectra of light emitted by the red giants with data from NASA's exoplanet-hunting Kepler observatory; from this, they calculated the masses of 70,000 red giants across a large swath of the Milky Way. In the map (above) the focus with lines coming out of it is the location of Earth. To its right are older stars (red) around the galactic center and to its left are younger (blue) stars in the outer parts of the disk.

AROUND THE WORLD

Furor over Indian conference

MYSURU, INDIA | For the second year running, the Indian Science Congress, held last week, has drawn condemnation and scorn from the country's prominent scientists. Amid the legitimate science, a few talks were beyond the pale, some researchers say, including a 5 January lecture on the supposed health benefits of blowing a conch shell, and a scheduled (but not presented) paper on how the Hindu god Shiva was the "greatest environmentalist in the world." Nobel laureate Venkatraman Ramakrishnan, a biologist at the University of Cambridge in the United Kingdom, told *The Times of India* that the congress was a "circus" and said he would never again attend one. Biologist P. M. Bhargava, founder of the Centre for Cellular and Molecular Biology in Hyderabad, told the paper that the event had deteriorated over the years and was now "an absolute waste of money."
http://scim.ag/IndSciCong

Weighing a threat to bees

WASHINGTON, D.C. | The U.S. Environmental Protection Agency (EPA) has for the first time evaluated the risk posed by a pesticide to honey bee colonies. When residues of imidacloprid in plant nectar or pollen exceed 25 parts per billion, they would likely harm the colonies, leading to fewer pollinators or less honey, EPA concluded last week in a draft assessment. Imidacloprid belongs to a controversial group of pesticides called neonicotinoids (*Science*, 10 May 2013, p. 674). Some U.S.

EPA gauged the risk of a pesticide to honey bees.

IMAGES: (LEFT TO RIGHT) G. STINSON/MPIA; © RADIUS IMAGES/ALAMY STOCK PHOTO

Published by AAAS

Haze from peat and forest fires smothered much of western Indonesia last fall, including the city of Palangkaraya on the island of Borneo.

Hazardous haze again threatens Southeast Asia

Forest fires and peat fires in Indonesia blanketed Southeast Asia in a thick, acrid haze from August through October last year. A brief rainy season this winter offered a temporary respite, but the region is beginning to dry out, thanks to this year's strong El Niño—and another bout of haze could form as early as next month. "This is a very big issue," says Mikinori Kuwata, an atmospheric chemist with the Earth Observatory of Singapore at Nanyang Technological University; the haze may not only be a health hazard, he says, but the particulates in the haze may also reduce rainfall, ultimately eroding food security. Kuwata and others are trying to crack the riddle of haze chemistry to better understand its impacts. "The combination of peatland and forest fires leads to a unique composition of the haze," says Rajasekhar Balasubramanian, an environmental engineer at the National University of Singapore who is studying how haze particles behave in the lungs. The chemistry of peat varies at different locations—and at different depths—so that each haze event has a different chemical fingerprint. That, Balasubramanian says, complicates efforts to track smoke constituents and their interactions with the atmosphere and sunlight.

crops, such as citrus trees, may have dangerous residues, EPA noted, but the level of imidacloprid is lower in crops such as corn that do not produce nectar. Environmental groups and some scientists say the proposed threshold is too high, objecting that EPA relied on a single study conducted by a pesticide company. (EPA considered more than 75 studies, but found only the industry study acceptable for reanalysis of raw data.) "It's completely inadequate," says Chris Connolly of the University of Dundee in the United Kingdom. Bayer CropScience welcomed EPA's "science-based apprach." EPA will accept public comments for 60 days, and plans to release preliminary assessments for three other neonicotinoids in December.

Singapore boosts science

SINGAPORE | On 8 January, Singapore's government announced that it will spend 19 billion Singapore dollars ($13.2 billion) on R&D from 2016 to 2020. The Research Innovation Enterprise 2020 Plan, or RIE2020, is an 18% increase over the previous 5-year cycle. "This is an assurance of sustained support for research in Singapore," says Chorh Chuan Tan, president of the National University of Singapore and deputy chairman of the government-backed Agency for Science, Technology and Research (A*STAR). The biggest share—21% of the budget—will go to health and biomedical sciences. That will help address one of Singapore's pressing issues: meeting the needs of a rapidly aging population. The budget also boosts A*STAR's high-profile Biopolis research complex, and places a priority on advanced manufacturing technologies, with emphasis on boosting the aerospace, electronics, chemical, pharmaceutical, and marine sectors.

Outbreak response revamp urged

NEW YORK CITY | A report by a high-profile commission urges the world to revamp how it collectively responds to infectious disease crises, "one of the biggest risks facing humankind." Sponsored by seven leading philanthropies and the U.S. government, *The Neglected Dimension of Global Security* recommends that the world spend about $4.5 billion more each year to bolster the ability of countries to respond to outbreaks, primarily by building their own public health infrastructures. Roughly $1 billion would go toward accelerating R&D for new vaccines and drugs, suggests the report, written by an independent commission organized with help from the U.S. National Academy of Medicine and released 13 January. Similar to other recent reports written in the wake of what the commission called the "sluggish, ill-coordinated, and clumsy" response to Ebola, the report urges the World Health Organization to "make significant changes," including the formation of a new Center for Health Emergency Preparedness and a $100 million contingency fund to help member states mount emergency responses rapidly.

PHOTO: © AP/CORBIS

Published by AAAS

FINDINGS

Soda tax leads to lower sales

In 2012, the first year of Mexico's national tax on soda and other sugar-sweetened beverages, purchases of those goods fell by an average of 6%, according to a study in *The BMJ* last week. Mexico's example shows "a taxation policy can work" to reduce sugary beverage consumption, says Shu Wen Ng, a health economist at the University of North Carolina, Chapel Hill, who co-authored the paper. The drop in soda purchases accelerated over time, reaching 12% by December 2014. Low-income households altered their behavior the most. Still, "it's too early to tell" whether Mexico's tax will help reduce the country's high rates of obesity and diabetes, Ng says. Tom Sanders, a nutritional scientist at King's College London, says the drop averages to about one sugar cube per day, "which is a drop in the caloric ocean. Long-term reductions in total energy in the range of 300–500 [calories per day] are probably needed to prevent obesity."

NEWSMAKERS

Three Q's

Qais Rasheed is the chairman of Iraq's State Board of Antiquities and Heritage. *Science* spoke with him recently in his office at The Iraq Museum in Baghdad about the Islamic State (IS) group, the museum, and more.

Q: Much of northern Iraq is under the control of the IS group. What is your biggest worry?
A: Our biggest concern is that ISIS [the group] will set booby traps at ancient sites in Mosul. After its liberation, we will send in teams to assess the damage. It will not be easy or even possible to rebuild, and we will need an international campaign to assist in conservation.

Q: You recently reopened the Iraq Museum, which was closed for 12 years following its 2003 looting. How many visitors do you have, and how many objects are on display?
A: On average we have about 400 people a day. For Iraqis, the entrance fee is 2000 Iraqi dinar [$1.80] and 250 Iraqi dinar [$0.23] for school children. We have some 10,000 objects on display, and about 500,000 in storage, but we don't yet have a full inventory.

Q: How strongly does the government support antiquities and heritage?
A: Antiquities rank at the bottom of the list of government priorities. There is a very limited budget. For 2015, we had 67 billion Iraqi dinar [$61 million] and 63 billion Iraqi dinar [$57 million] of that goes to salaries. There's not much left for conservation and excavation. We do have some financial support from Japan, Italy, and the United States.

Levels of nitrogen and other nutrients in leaves offer clues to the health of seagrass meadows, such as this one on the coast of Wales.

PHOTO: BEN JONES

U.K. seagrass meadows suffering

Eelgrass (*Zostera marina*) provides important habitat for young fish, shrimp, mussels, and other organisms living along the North Atlantic and North Pacific coastlines. But excess nutrients pouring into the sea are degrading this habitat, especially near cities, crops, or livestock: The nutrients spur the growth of algae and phytoplankton, which can smother the grass and dim the sunlight it needs to grow. Seagrass around the United Kingdom is in a particularly bad state, researchers report this week in *Royal Society Open Science*. They measured nutrient levels in leaf tissue at 11 locations around the U.K. coast, and discovered that, on average, nitrogen was 75% higher than reported in *Z. marina* elsewhere in the world. Phosphorus, meanwhile, was lower—both indications of poor water quality. In addition, boat moorings and anchors and bait-digging during low tides have damaged many seagrass meadows. "There's a lack of recognition of how degraded the marine habitats are in the U.K.," says co-author and marine ecologist Richard Unsworth of Swansea University in the United Kingdom, who has set up a conservation group called Project Seagrass to study techniques to restore seagrass meadows.

BY THE NUMBERS

23%

Decline in U.S. cancer death rates between 1991 and 2012, according to a new report by the American Cancer Society. The reduction is due to a combination of less smoking, better care, and better screening.

4 million

Record-setting number of hectares of U.S. land burned by wildfires (about half of them in Alaska) in 2015, according to the National Interagency Fire Center in Boise.

800

Force, in multiples of a cockroach's body weight, needed to smash the insects, as reported last week at the Society for Integrative and Comparative Biology meeting in Portland, Oregon.

Published by AAAS

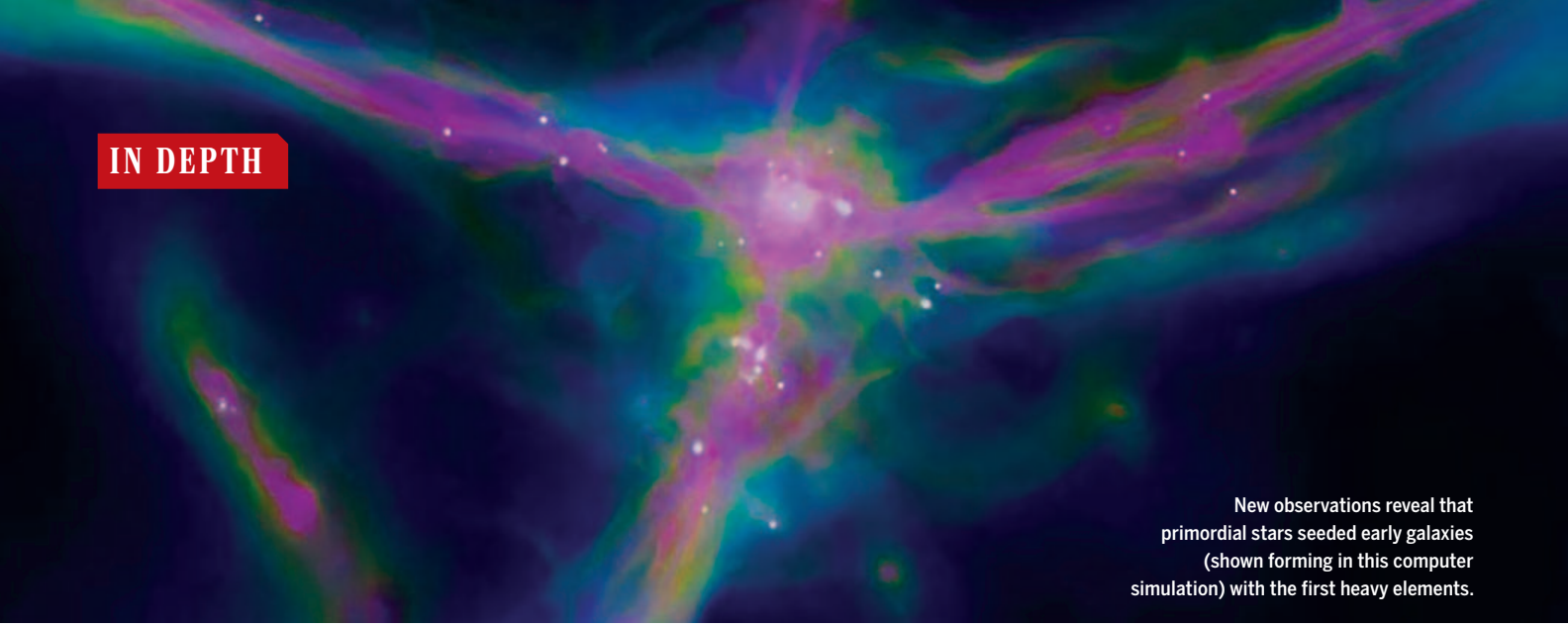

New observations reveal that primordial stars seeded early galaxies (shown forming in this computer simulation) with the first heavy elements.

SPACE

Astronomers see ashes of the first stars

Primordial clouds show how giant stars forged the heavy elements that fill today's universe

By **Daniel Clery**, *in Kissimmee, Florida*

The universe of today is a rich banquet of elements, from the silicon and oxygen in rocky planets to the carbon and nitrogen in our bodies. But in its early days, the cosmic offerings were monotonous: mostly hydrogen, some helium, and a pinch of lithium, all made in the big bang. At a meeting of the American Astronomical Society (AAS) here last week, researchers announced that they have seen signs of how, starting in those early days, truly monstrous stars 100 times as massive as our sun began transforming those simple ingredients into today's feast of elements.

Until recently, says astronomer John O'Meara of Saint Michael's College in Colchester, Vermont, this ancient—hence distant—epoch remained in "the realm of computer simulations." But now, teams using some of the world's biggest telescopes are beginning to probe it by studying light from ancient quasars, superbright galaxy cores that shone in the early universe. As the light passes through clouds of gas en route to Earth, the gas absorbs specific wavelengths, creating an absorption spectrum that reveals what the cloud was made of and how new ingredients were added to the early universe.

These elements were forged in the earliest stars, which formed about 150 million years after the big bang and were unlike any today. They were giant puffballs, made from gas so hot that it was slow to compress to the density needed to ignite fusion in their cores. These unlit protostars kept piling on mass until, finally, their cores became hot and dense enough to ignite. Because they had become so huge, these giants—known as population III stars—burned hot and fast; after only a few million years their cores ran out of fuel, collapsed, and exploded. But in the meantime, their fusion furnaces had forged hydrogen into numerous heavier elements, and their end-of-life explosions—while making still more elements—helped to spread them across the cosmos.

That was the beginning of the process by which the pristine gas clouds from the big bang have become "enriched" with heavier elements (which astronomers call "metals")—a process that continues in stars today and provided the ingredients for planets and life.

In 2011, O'Meara and colleagues used quasar spectra to discover two gas clouds at the very beginning of this process: They appeared completely devoid of elements heavier than hydrogen (*Science*, 2 December 2011, p. 1245). These clouds existed about 2 billion years after the big bang—long after the first population III stars ignited—showing that some pristine clouds survived to that later time. Then last year, a team led by David Sobral of the University of Lisbon detected a bright galaxy just a billion years after the big bang that seemed to have some stars made from hydrogen, helium, and nothing else.

Now, O'Meara and his colleagues at Swinburne University of Technology, Hawthorn, in Australia have found a gas cloud that existed when the universe was 1.8 billion years old and has just a wisp of heavier elements: 1/3000 of the level in our solar system. This suggests that it contains only the remains of population III stars dispersed by their violent deaths.

The team identified the cloud in quasar spectra collected using high-resolution spectrographs on the Keck telescopes in Hawaii and the Very Large Telescope in Chile. They focused on a portion of the spectrum that is so crammed with absorption lines from hydrogen gas clouds that it is known as the Lyman-α forest. "We dared to go down into the weeds and study a few hundred quasars," O'Meara says. It took considerable modeling to derive element abundances from the spectral lines. "This is a prototype of a new avenue of study," he says.

"It's quite exciting," says Sobral, now at the United Kingdom's Lancaster University. "It shows that extremely metal-poor clouds exist even out at [1.8 billion years]." Avi Loeb, chair of Harvard University's astronomy department, says such studies help answer the question of when life could have arisen in the universe. There has to be carbon and oxygen, but at what stage are they abundant enough? "We're getting close to the sensitivity to probe the transition between the formation of massive [population III] stars and those similar to what we have around today."

Teasing the faint fingerprints of the first heavy elements from light that has crossed the universe taxes today's most powerful instruments. Researchers hope to probe deeper into the workings of early stars with the James Webb Space Telescope, due for launch in 2018, and the next generation of giant ground-based telescopes in the 2020s. "This is a really exciting game to play with 30-meter telescopes. There will be no problem doing thousands of spectra," O'Meara says. ■

IMAGE: CEVERINO, DEKEL & PRIMACK

Published by AAAS

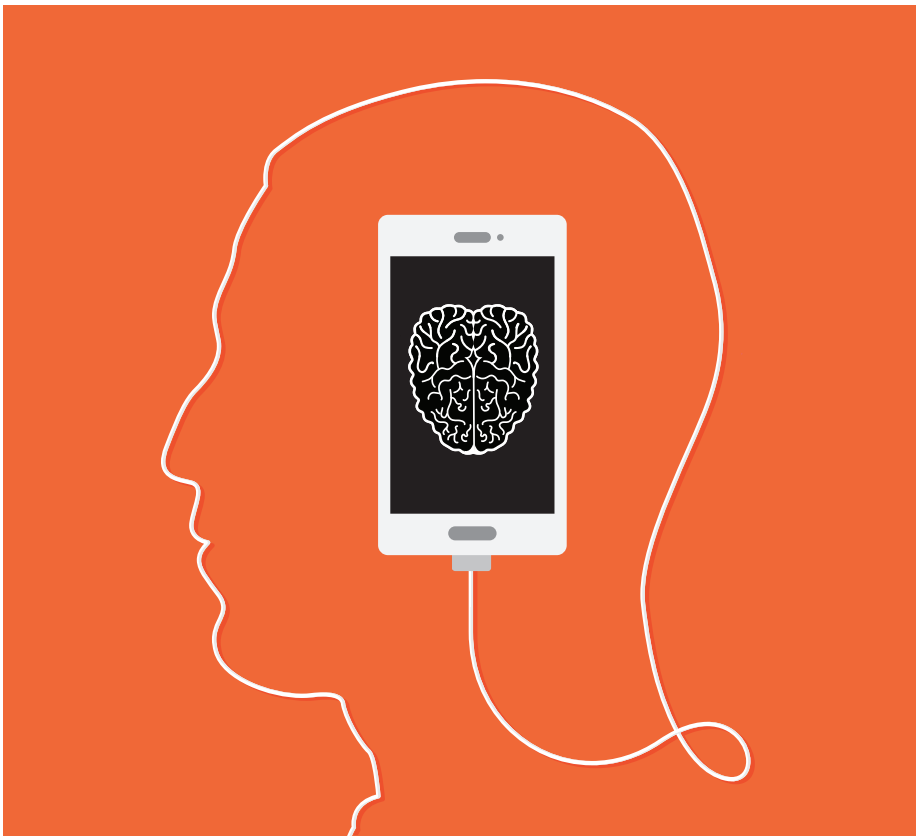

NEUROSCIENCE

Regulators seek to tame brain training's 'Wild West'

$2 million fine for Lumosity is latest shot at claims of cognitive benefits from games and apps

By **Emily Underwood**

If you watch cable TV news or listen to NPR, you've likely been barraged with ads for Lumosity, a set of digital "brain-training" games that, for $14.95 a month, purportedly sharpens the mind based on the "science of neuroplasticity." By playing the games for just 10 to 15 minutes per day several days a week, the ads claim, consumers can improve their performance in work and school, and perhaps even stave off Alzheimer's and other serious medical conditions.

Last week Lumosity hit the news for a different reason, as the Federal Trade Commission (FTC) made it the latest target in a crackdown on companies selling products that purportedly enhance memory, provide some other cognitive benefit, or reduce the serious side effects of dementia. It fined the games' maker, Lumos Labs, Inc., $2 million for false advertising and required it to create a pop-up screen that alerts players to FTC's order and allows them to avoid future billing.

It's the third FTC complaint against the industry in 4 months, and many neuroscientists and psychologists say action is long overdue. Still, some worry that games based on solid science may be unfairly tarnished, and that the agency may be imposing a standard of evidence that game developers can't meet.

Both FTC and the Food and Drug Administration (FDA) have authority to regulate brain-training games and apps, but FTC is particularly interested in deceptive advertising practices, says Michelle Rusk, a spokesperson with FTC in Washington, D.C. For some time now, FTC has been "concerned about some of the claims we're seeing out there," she says. After evaluating the few available studies on Lumos Labs's products as well as the broader literature on brain-training games, "our assessment was they didn't have adequate science for the claims that they're making," she says. "The most that they have shown is that with enough practice you get better on these games, or on similar cognitive tasks … there's no evidence that training transfers to any real-world setting."

Susanne Jaeggi, a psychologist at the University of California (UC), Irvine, agrees, saying, "there's little to no evidence" Lumosity works the way the company says it does. Lumos Labs's claims of benefitting seriously ill people, and its use of testimonials solicited from customers via prize contests, are "egregious" examples of irresponsible advertising, adds Michael Merzenich, a neuroscientist at UC San Francisco and co-founder of Posit Science, which develops a different type of brain-training software.

Although Lumos Labs is not granting interviews, a company statement says its games are based on rigorous science. (One of its owners, Michael Scanlon, left a Stanford University Ph.D. program in neuroscience in 2005 to start the company.) The statement cites the company's recent study in the journal *PLOS ONE*, showing that 4700 participants who trained with Lumosity for 10 weeks showed small improvements on an aggregate assessment of cognition.

Although Jaeggi is skeptical of Lumos Labs's claims, she says "we have to be careful not to overgeneralize." There is "growing evidence" that brain-training games related to skills such as working memory—the short-term ability to learn and use new information—"can be beneficial for a variety of tasks," she says. Some 70 prominent researchers came to the defense of Carrot Neurotechnology in 2015 after FTC fined Aaron Seitz, a psychologist at UC Riverside, and his partner $75,000 each for ads promoting the company. Now called Ultimeyes, the company sells a training program aimed at improving visual acuity by increasing the efficiency with which the brain processes information from the eyes. The agency took aim at assertions that the app improved acuity by an average of 31%—a figure plucked from Seitz's small, peer-reviewed study in *Current Biology* in February 2014, which tracked a baseball team's performance after training on the app. Such claims must be supported with statistically significant results from randomized, blinded, placebo-controlled human clinical trials, the agency said.

Although some of Ultimeyes's claims were too strong, its defenders concede, they say the app's basic scientific premise is based on decades of research in vision science and has been vetted by top experts in the field.

ILLUSTRATION: ADAPTED FROM MUSTAFAHACALAKI/ISTOCKPHOTO.COM BY G. GRULLÓN/*SCIENCE*

Published by AAAS

"Carrot Neurotechnology has been a model for presenting well researched methods," wrote Michael Posner, an emeritus professor at the University of Oregon, Eugene, in public comments on the FTC website. Daphne Bavelier, a cognitive neuroscientist at the University of Rochester in New York, wrote to FTC that the double-blind standard "is untenable in the case of behavioral interventions—patients cannot be blind to the game they are asked to play or the exercises they are asked to do."

Rusk notes FTC does not expect trials for such apps to be of the size, scale, and duration that are typically needed for FDA drug approval. But "they do have to have a valid design and be reliably conducted," she says.

The debate about FTC's actions mirrors a larger scientific dispute: whether any brain-training game, or even such venerated activities as playing the violin, can provide general cognitive benefits. Several meta-analyses have found little to no evidence that brain-training provides any real-world benefits, says Randall Engle, a psychologist at the Georgia Institute of Technology in Atlanta. In a 2014 consensus statement, researchers at Stanford University in Palo Alto, California, and the Max Planck Institute in Berlin, said there is "little evidence that playing brain games improves underlying broad cognitive abilities, or that it enables one to better navigate a complex realm of everyday life." The Lumosity settlement—and FTC's skepticism—is "fully consistent" with that conclusion, says Ulman Lindenberger, a psychologist at Max Planck.

> ***"The most that they have shown is that with enough practice you get better on these games, or on similar cognitive tasks ... there's no evidence that training transfers to any real-world setting."***
>
> **Michelle Rusk**, Federal Trade Commission

Merzenich remains confident that a few brain-training programs—including his own, called BrainHQ—are effective. Still, he and others are calling for an independent scientific entity to evaluate companies' claims, to sort the wheat from the chaff. Such a body of experts will likely form this year, he says. Until then, he says, it's up to FTC to tame the brain-training industry's "Wild West." ■

DATA: ORCID

SCIENTIFIC PUBLISHING

Publishers embrace scheme to end name confusion

ORCID gives every Smith and Wang a unique number

By **John Bohannon**

Name ambiguity can be a nuisance. If you are a Williams or a Johnson—among the most common surnames in the United States—it can be tricky to find you on the Internet, especially if you also have a common first name such as Mary or James. But for academic researchers, whose careers are measured largely by authorship on papers, name ambiguity can be a killer. For example, search for papers by Weizhe Hong, a neuroscience postdoc at the California Institute of Technology in Pasadena, using his last name and initial, and you "get more than 10,000 hits," Hong says. "It's a disaster."

Now, the scientific community is coalescing around what could be a solution: a standard system for giving every researcher a unique identifying number that would map to all of their papers, projects, and grants. In a letter released online 7 January, some of the world's largest academic publishers and scientific societies announced that they will not just encourage, but ultimately require, researchers to sign up with ORCID (Open Researcher and Contributor ID), a nonprofit organization that assigns members a 16-digit identifier.

The move gives ORCID a big boost in a long competition to set an ID standard. In 2009, when ORCID was launched, several competing systems already existed. Publishing giant Thomson Reuters offered one called ResearcherID, while Elsevier offered Scopus. But those tagging systems were proprietary, so a group of scientific organizations—including the Wellcome Trust research charity and CrossRef, which provides the digital object identifier system for papers—decided to create a nonprofit alternative.

ORCID now has about 2 million users. U.S.-based scientists make up the largest group, says Laurel Haak, ORCID's executive director, who is located in Bethesda, Maryland. But "China is our No. 2 country," he says.

Researchers with Asian names often face several ambiguity problems. Not only are certain surnames very common (see box, below), but transliteration to the Roman alphabet often results in multiple spellings. "And if you get married and change your name," Hong says, "then you've got another problem."

ORCID will relieve these "pain points," Haak says. Searching for papers with Hong's ORCID number, for instance, yields only his papers. But scientists will have to do some of the work. Although ORCID will tag new papers, researchers will have to use the group's website to curate work.

ORCID is so far dodging another problem: what to do about assigning numbers to dead scientists. That job may be left to private companies such as Elsevier, which has been steadily assigning Scopus IDs to the authors—many of them deceased—of millions of papers in their database that were published before 1996. That could keep the Scopus ID system relevant well into an ORCID-dominated future.

The signers of the new pledge—the American Geophysical Union, eLife, the European Molecular Biology Organization, Hindawi, the Institute of Electrical & Electronics Engineers, the Public Library of Science, and the Royal Society—will mostly require the use of ORCID IDs by year's end, although the Royal Society began the practice on 1 January. AAAS (the publisher of *Science* and other journals), will also start requiring the use of ORCID IDs later this year, says *Science* Editor-in-Chief Marcia McNutt. The Springer Nature publishing company says it will continue to encourage, but not require, the use of ORCID IDs in its 3000 journals. ■

Who's who?

Asian names dominate a top 10 list of ORCID users with identical monikers.

GIVEN NAMES	FAMILY NAMES	COUNT
Wei	Wang	185
Yang	Liu	161
Wei	Li	156
Wei	Zhang	149
Jing	Wang	131
Lei	Zhang	124
Lei	Wang	119
Yang	Li	115
Li	Li	113
Jun	Li	111

Published by AAAS

Even though she's surrounded by male suitors, a female garter snake may still have some control over mating.

COMPARATIVE BIOLOGY

Female organs revealed as weapons in sexual arms race

Researchers broaden their focus beyond male anatomy

By **Elizabeth Pennisi**, *in Portland, Oregon*

For decades, biologists have marveled at the diversity of penises across the animal kingdom—straight, forked, spiraled, spiny. But in anatomy, as in other fields, females are getting more credit. A symposium during the annual meeting of the Society for Integrative and Comparative Biology held here last week was ostensibly about the male organ. But the complexity of some female genitalia and their role in shaping phallic diversity stole the show. "Everyone feels females are the understudied sex," says Teri Orr, a reproductive evolutionary ecologist at the University of Utah in Salt Lake City.

Researchers studying whales, snakes, and other animals are finding that female sex organs have some of the same baroque complexity seen in males. They now see females as active participants in an arms race, likely evolving more complex genitalia to help control mating and create barriers to forced matings, which in turn leads to male countermeasures. "It's likely that female form and function drive male form and function," says Patricia Brennan, an evolutionary biologist at Mount Holyoke College in South Hadley, Massachusetts.

Thirty years ago, the comparative evolutionary biology of intromittent organs—penises and their equivalents—was born when evolutionary biologist William Eberhard at the Smithsonian Tropical Research Institute in Panama drew attention to the wild variations among male genitalia. These come in all shapes and sizes, from modified anal fins to spiraling penises covered with hooks and spines. Eberhard wondered why and how this astonishing diversity had evolved. But he described the female equivalents as "relatively uniform," a characterization that led other researchers to ignore them.

As Eberhard continued his studies of flies, wasps, and spiders, however, he began to suspect that females might be more interesting than he first thought, in part because males in so many species rub, bite, eat, or otherwise interact with females during copulation, apparently to prevent them from sabotaging the act. He also wondered whether forced copulation might prompt females to evolve defensive strategies.

During copulation, the male garter snake uses one of his spiny penises to insert a plug into his partner.

That's just what Brennan discovered in ducks in 2007. She showed that duck penises are elaborately spiraled to get into the similarly twisted vaginas of potential mates, and suggested these elaborations arose through an anatomical arms race. To combat the forced matings common in ducks and so thwart insemination by a male not of her own choosing, females evolved ever more convoluted reproductive tracts; males evolved longer penises in response. At the time, researchers considered these complicated shapes a novelty among vertebrates.

But it's not just ducks, Sarah Mesnick reported at the meeting. Mesnick, a marine biologist at the National Oceanic and Atmospheric Administration's Southwest Fisheries Science Center in San Diego, California, started looking at cetacean genitalia as a way of gleaning clues about the mating systems of whale populations in decline. Over the past 10 years, she, graduate student Dara Orbach at Texas A&M University, Galveston, and their colleagues have examined the vaginas of 24 whale and dolphin species by studying stranded specimens and reviewing the literature. They found internal folds that range from thin, leaflike structures to convoluted labyrinths.

The finding supports 19th century anatomists who had noted the folds, which some researchers explained as a mechanism for preventing seawater from seeping in and diluting or damaging sperm. But Mesnick and Orbach's work, though still preliminary, argues against that hypothesis: Some dolphins have very reduced folds despite mating in saltwater, the pair reported.

Highly convoluted folds are found in species including the harbor porpoise and bowhead whale, which have relatively large testes—often a sign that each female mates with multiple males. The researchers suggest that the folds may give females some influence over which sperm fertilize their eggs: Like the duck's corkscrew vagina, the folds create an additional "gauntlet" that the male must navigate to mate successfully, Mesnick says.

Because researchers are unable to get a close-up view of copulations, they can only guess at the detailed mechanics of the event. In whales and even in most terrestrial vertebrates, "we have no idea how

PHOTOS: PATRICIA BRENNAN

Published by AAAS

male and female genitalia interact and how those interactions affect reproductive success," cautions Matthew Dean, an evolutionary biologist at the University of Southern California in Los Angeles. "But it's superimportant."

At the meeting, some researchers reported initial steps in figuring out those details. Brennan is now studying the copulatory tug-of-war in red-sided garter snakes, working with Christopher Friesen from the University of Sydney in Australia and others. In this species, males have spines at the tips of their penises, which may help them counteract a female tactic: contracting the opening of their reproductive tracts to push the penis out. As they finish copulating, male snakes deposit a plug of sperm and other material that may keep sperm from leaking out as well as prevent other males from transferring their own sperm.

The researchers removed the penile spines from some males and anesthetized the openings of some females, then allowed the snakes to mate. The plugs—a mark of male success—were much bigger in males with spines and in anesthetized females that couldn't expel the penis, Brennan, Friesen, and colleagues reported at the meeting. Thus, the male's spines give him an edge, one that the female counters through her contractions. "It's absolutely critical to look at these systems as pairs," Kelly says.

Orr is trying to determine whether her organisms, bats, are in an arms race as well. She had been characterizing penile spines in the males, but she is now looking at females to see whether they have thicker vaginal linings in species with bigger-spined males.

As researchers delve into coevolved genital traits, they are realizing they need better ways to describe the details of the organs and the act of copulation. Dean and his colleagues have developed a grid system for pelvic bones that should provide a set of landmarks. So far they have measured the baculum, a bone in the penis of many mammals, and are beginning to describe diversity in the baubellum, a small bone in the clitoris of some mammals. The more precise measurements are helping Dean and others to better tease out the genetic underpinnings of male and female anatomy, he says.

Compared with penises, female organs are harder to map, and dissecting the intricate combination of behavior and anatomy in copulation is harder still. But Brian Langerhans, an evolutionary biologist at North Carolina State University in Raleigh, says both participants in nature's crucial act are coming into focus. Five years from now, he predicts, "I don't think we'll be talking about a lack of attention on females anymore." ■

PHOTO: O. ILIC *ET AL.*/MIT

TECHNOLOGY

Incandescent lights go green

Photonic technology boosts efficiency of warm, wasteful bulbs

By **Robert F. Service**

Thomas Edison would be pleased. Researchers have come up with a way to dramatically improve the efficiency of his signature invention, the incandescent light bulb. The approach uses nanoengineered mirrors to recycle much of the heat from the filament. The new-age incandescents are still far from a commercial product, but already they are nearly as efficient as commercial LED bulbs while retaining a warm, old-fashioned glow.

"This is beautiful work," says Shawn-Yu Lin, an electrical engineer and optics expert at the Rensselaer Polytechnic Institute in Troy, New York. He and others note that there is plenty of room for further improving the mirrors, which could ultimately push the efficiency of the bulbs well beyond that of today's lighting technologies. And because lighting consumes 11% of all electricity in the United States, any such improvement could help reduce carbon dioxide emissions.

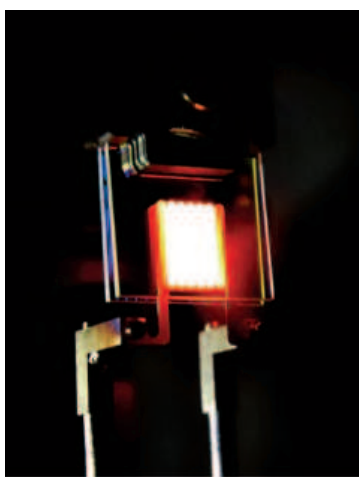

In the reinvented bulb, photonic crystals flank a sheetlike tungsten filament.

Incandescent lights have changed little since Edison first perfected them. The bulbs send electricity through a curly tungsten filament; electrical resistance boosted by the long, twisting path heats the filament to some 3000 K, causing it to glow with warm, yellowish white light. Only about 2% of the energy fed into an incandescent is emitted as visible light; most emerges at longer infrared (IR) wavelengths and is wasted as heat. Other technologies do somewhat better. Compact fluorescent bulbs typically reach an efficiency between 7% and 13%; LEDs manage between 5% and 15%. But the most efficient ones don't quite match the familiar glow of an incandescent.

Researchers at the Massachusetts Institute of Technology in Cambridge led by physicists Ognjen Ilic, Marin Soljačić, and John Joannopoulos set out to boost incandescent efficiencies with the help of an intricately structured material called a photonic crystal. Photonic crystals can act as both filters and mirrors, depending on the wavelength. So the team set out to create one that would allow visible light to pass through while reflecting IR photons. The hope was that the filament would reabsorb the IR photons and re-emit some of that energy as visible light.

The researchers started with millimeter-thick sheets of glass and deposited 90 alternating layers of tantalum oxide and silicon dioxide, in thicknesses determined through extensive computer modeling. They also redesigned the bulb's filament. In place of the curly wire, they folded a tungsten ribbon back and forth, creating a thin tungsten sheet. Electrons still follow a long, circuitous path that generates heat and light, but the larger surface area of the tungsten sheet makes it easier for the metal to absorb the IR photons reflected by the photonic crystals.

The team flanked the sheetlike tungsten emitter with two sheets of the glass-coated photonic crystals and turned on the power. As they report this week in *Nature Nanotechnology*, the crystals allowed virtually all the visible light to pass through but reflected the majority of IR photons back to the emitter, where they were reabsorbed. The energy recycling ultimately improved the efficiency of the bulb to 6.6%, triple that of conventional light bulbs. "I think they can do even better than this," says Alejandro Rodriguez, an electrical engineer and photonic crystal expert at Princeton University, perhaps by adding other materials and more complex structures to the crystals.

Ilic and Soljačić say with further engineering it may even be possible to reach efficiencies of 40%, far beyond what commercially available LEDs can muster. Then they will have to show that they can make their photon recyclers cheaply enough for a mass market. If the approach lives up to its promise, cutting-edge photonics could give Edison's glowing filaments a new lease on life. ■

Published by AAAS

SCIENTIFIC COMMUNITY

Caltech suspends professor for harassment

University restricts his access to graduate students after upholding their complaints

By **Jeffrey Mervis**

For what is believed to be the first time in its history, the California Institute of Technology (Caltech) in Pasadena has suspended a faculty member for gender-based harassment. The researcher has been stripped of his university salary and barred from campus for 1 year, is undergoing personalized coaching to become a better mentor, and will need to prove that he has been rehabilitated before he can resume advising students without supervision. Caltech has not curtailed his research activities.

The university has not disclosed the name of the faculty member, but *Science* has learned that it is Christian Ott, a professor of theoretical astrophysics who studies gravitational waves and other signals from some of the most violent events in the cosmos. Born and educated in Germany, Ott joined the Caltech faculty in 2009 and was awarded tenure in early 2014.

According to Ott's website, as of last week he was advising five graduate students. He is the principal investigator on two active grants from the National Science Foundation, including a prestigious, 5-year CAREER award for promising young investigators. Part of that award helps support a summer workshop for dozens of graduate students in astrophysics from around the world.

The case comes to light as harassment has become a major flashpoint within the astronomy community in the wake of an investigation by the University of California, Berkeley, that found astronomer Geoffrey Marcy had committed serial harassment over a decade (*Science*, 23 October 2015, p. 364). The university faced a storm of criticism after giving Marcy little more than a warning; he ultimately resigned. Caltech took a different approach, says Fiona Harrison, head of Caltech's physics, mathematics, and astronomy division. "I think that Caltech was extremely responsive and proactive and did the right thing," she asserts.

The Caltech investigation began in June 2015, after two graduate students filed complaints under Title IX of a 1972 federal law aimed at preventing gender discrimination in higher education. The university has released neither the names of the complainants nor the details of the complaints. Two faculty members led a committee that found the complaints to be valid and recommended action. This past September the provost meted out the penalty, Harrison says, and an appeal was denied later that month.

Christian Ott and other Caltech astronomers are housed in the Cahill Center on campus.

In an email to *Science*, Ott wrote that "I cannot comment on, confirm, or deny anything at this time."

The university issued a brief statement in late September saying only that there had been a "violation" of university harassment policies and that it had taken "disciplinary action." More details became known last week, after a website posted a two-page letter from Caltech's president, Thomas Rosenbaum, to faculty and students.

> ***"[Caltech] has absolutely no tolerance for harassment and discrimination."***
>
> **Fiona Harrison**, Caltech division head

The 4 January missive, which includes the actions taken against Ott, described "[t]his painful incident," as well as the university's plans for improving support for all graduate students. Those steps include forming a council that will conduct a campus-wide review of "student experiences with their advisors," adding staff to assist graduate students, and initiating activities, such as discussion groups, aimed specifically at supporting female graduate students.

The 3-month gap between the two statements, Harrison says, was the result of university efforts to balance privacy and transparency. The goal of last week's letter, she says, "was to make clear that the university has absolutely no tolerance for harassment and discrimination."

Meg Urry of Yale University, president of the American Astronomical Society, says that she's heartened by Caltech's response. "The letter says the institution is committed to doing better and that it plans to do a variety of things to make women feel welcome and supported on campus. So good on them."

Those who have studied gender disparities in science say that the broader challenge for Caltech and other elite research institutions is creating a more welcoming environment for women. That may require increasing the number of women in certain scientific fields. (There are roughly six men for every woman among faculty in Caltech's physics, mathematics, and astronomy division, and in engineering and applied science the ratio is nine to one.)

Large egos may also contribute to the problem, Urry believes. "The more practitioners in a field talk about themselves as the second coming, the fewer women there are in that field," she says.

This week a member of Congress said she would propose legislation requiring universities to share the results of a Title IX investigation of a faculty member with a new employer if that person changes jobs. Representative Jackie Speier (D–CA) says that the current rules allow universities to "protect sexual predators."

Ott, whom Harrison refers to only as "the faculty member," has begun the coaching program, which "is specific to his particular situation," she says. It is not part of the regular orientation on harassment given to faculty members and students, she notes.

Harrison says "a third party" is mediating the faculty member's interactions with his graduate students. The university decided that such an arrangement was the best way to intervene while allowing the students to remain on course for their degree. Rosenbaum's letter explains that the faculty member must exhibit "a demonstrable change in behavior and mentoring" before he is allowed normal interactions. Harrison says she is responsible for determining "when and if" those changes have taken place.

The faculty member was banned from campus for a year "for the protection of students," Harrison says. His courses have been reassigned, she adds. At the same time, Harrison says, "there are no restrictions on continuing with his research." ■

PHOTO: LANCE HAYASHIDA/CALTECH STRATEGIC COMMUNICATIONS

Published by AAAS

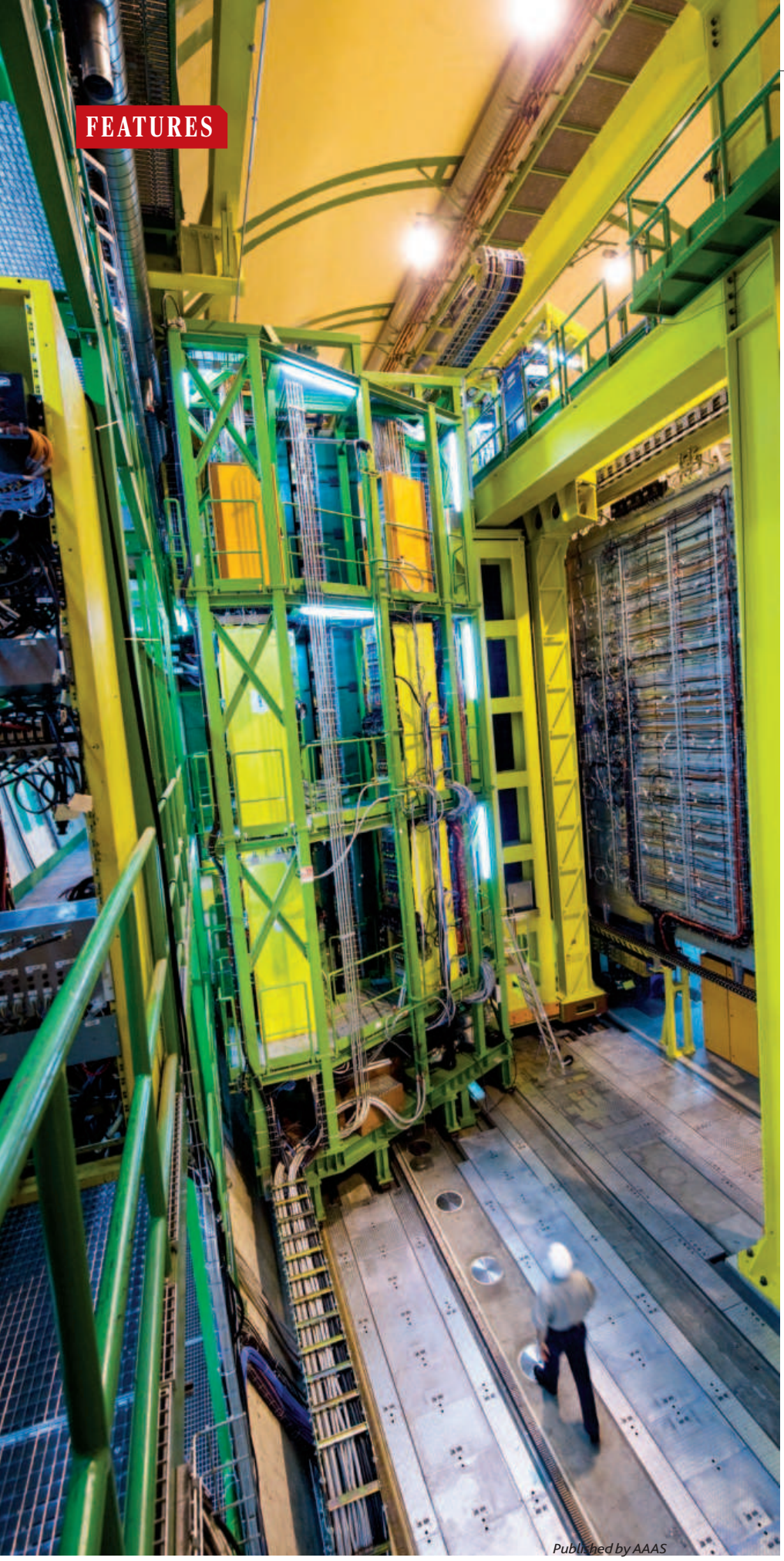

PHOTO: CERN

Inside the LHCb detector at CERN, colliding protons blast exotic particles into fleeting existence.

THE SOCIAL LIFE OF QUARKS

Particles consisting of four and five quarks make a comeback

By **Adrian Cho**

Among particle physicists, Sheldon Stone has a reputation for high standards and brutal honesty. He's been known to challenge a tenuous claim by shouting in the middle of a colleague's talk. So when Stone discusses recent observations that he and his colleagues have made, his words carry weight. "I really do think there is a chance this will become a big breakthrough," he says.

Stone works with a huge particle detector called LHCb, one of four fed by the world's biggest atom smasher—the Large Hadron Collider (LHC) at the European particle physics laboratory, CERN, in Switzerland. He and colleagues say they have observed bizarre new cousins of the protons and neutrons that make up the atomic nucleus. Protons and neutrons consist of other particles called quarks, bound together inextricably by the strong nuclear force. By smashing particles at high energies, physicists have blasted into fleeting existence hundreds of other hadrons—particles made of quarks. They fall into just two classes: baryons, including the proton and neutron, which contain three quarks; and mesons, which contain two. But last year, LHCb researchers spotted particles made of five quarks. The year before, they confirmed the existence of one with four.

Known as pentaquarks and tetraquarks and lasting only a quadrillionth of a nanosecond, those oddball particles defy the existing picture of the strong force, captured in a vexingly complex theory called quantum chromodynamics (QCD). "They have the potential for revolutionizing the way we understand QCD," says Eric Swanson, a

Published by AAAS

theorist at the University of Pittsburgh in Pennsylvania. Marek Karliner, a theorist at Tel Aviv University in Israel, says, "You don't really understand your theory unless you know what combinations [of quarks] are stable and what ones aren't."

LHCb's observations also mark a rare event in science, the comeback of a discredited idea. Twelve years ago, multiple groups spied a different pentaquark, only to see those results crumble. However, LHCb's observations appear to have resurrected the pentaquark. "This stuff I believe is real," Swanson says.

QUARKS, the fundamental constituents of most matter, have a complex social life. Like the electromagnetic force that binds negatively charged electrons to the atom's positively charged nucleus, the strong force acts on "charges." But whereas there is only one type of electric charge, which can be positive or negative, there are three types of strong charge, denoted arbitrarily by the colors red, blue, and green, each with its negation antired, antiblue, or antigreen. In allowed combinations of quarks, the color charges add up to colorless or white. So, a baryon contains a red quark, a blue quark, and a green quark, as red, blue, and green add to make white. A two-quark meson contains a quark and an anticolored antiquark, for example, red and antired, which combine to make it colorless.

Adding variety to the mix, quarks come in six types or "flavors": the up and down quarks found in ordinary matter, and the heavier charm, strange, top, and bottom quarks that can be made in particle collisions. Combining flavors produces a panoply of particles, most of them highly unstable and transient. A proton consists of two ups and a down; the fleeting baryon called a Λ_b (pronounced "lambda B") contains an up, a down, and a bottom quark. A meson called the K^- (pronounced "K minus") contains a strange quark and an anti–up quark.

The evidence for all of this is indirect, because physicists can never observe an isolated quark. The strong force is so strong that if you blast a quark out of a proton, it will yank quarks and antiquarks out of the vacuum to create more baryons and mesons. Moreover, within hadrons, countless "virtual" quark-antiquark pairs flit in and out of existence. The quarks cling to one another by exchanging particles called gluons, which themselves exchange gluons. That "brown muck" of virtual quarks and gluons typically makes up most of a particle's mass and renders theoretical predictions very difficult.

As soon as physicists worked out QCD in the 1970s, they realized that quarks might clump in groups of more than three. The color charges of two quarks and two antiquarks (a tetraquark) or four quarks and an antiquark (a pentaquark) can add up to white (see diagram, below). "There's no reason why they don't exist," says Valentina Santoro, an experimenter at the European Spallation Source (ESS) in Lund, Sweden. "If you really don't find them, you should justify why."

In 2003, physicists thought they had spotted one: a pentaquark called the θ^+ (pronounced "theta plus"). Supposedly containing two up quarks, two down quarks, and one anti–strange quark, that particle was glimpsed by experimenters with the Laser Electron-Photon (LEPS) facility at the SPring-8 accelerator laboratory in Hyōgo Prefecture, Japan, which fired high-energy photons into a carbon target. Nine other experiments also reported the particle, which was thought to have a mass about 1.5 times that of a proton.

Then the θ^+ vanished. Other experiments found no sign of it, and some of the experiments that had seen it could not reproduce it. Physicists still aren't sure how so many groups could be so badly mistaken, says Kenneth Hicks of Ohio University in Athens, who worked on one of the teams that originally saw the particle. "It was the strangest situation I've ever been involved in," Hicks says, "and I was right in the middle of it."

Others say the results were never as convincing as claimed. Physicists looked for the θ^+ by assuming it decayed into a particular combination of particles—in the LEPS experiment, a neutron and a K^+ meson (an up quark and an anti–strange quark). For each neutron-K^+ pair they observed, they used the particles' momenta to calculate the mass of their presumed θ^+ parent. If some pairs were coming from real θ^+ decays, then a plot of the calculated masses should show a peak, corresponding to the parent particle. But researchers can fool themselves in such simple analyses, Stone says. "These guys never did anything but look at bumps in mass plots," he says, "and that makes you vulnerable to fluctuations that you can tune up to make a peak."

The θ^+ misadventure cast a shadow over the search for tetraquarks and pentaquarks, says Robert Jaffe, a theorist at the Massachusetts Institute of Technology (MIT) in Cambridge. "People got the impression that the field was somehow flaky and that the experiments weren't trustworthy," he says.

Even so, tantalizing hints of such particles kept turning up. In 2003, physicists in Japan spotted a particle that looked like a tetraquark containing a beefy charm quark, an anti–charm quark, and a light quark–antiquark pair. They called it the X(3872). In 2008, the same experiment—the Belle particle detector, fed by the KEKB electron-positron collider at the Japanese particle physics lab KEK in Tsukuba—spotted a heavier apparent tetraquark, Z(4430). In the past few years, physicists at several labs have found a handful of other possible tetraquarks.

NOW, LHCb researchers have confirmed the Belle tetraquark and reported strong evidence for two pentaquarks, consisting of two

What's in the bag?

Quarks come in three colors, three anticolors, and six flavors. Pentaquarks might be bags of five quarks and force-carrying gluons, or they might be "molecules" made of known particles—physicists aren't sure.

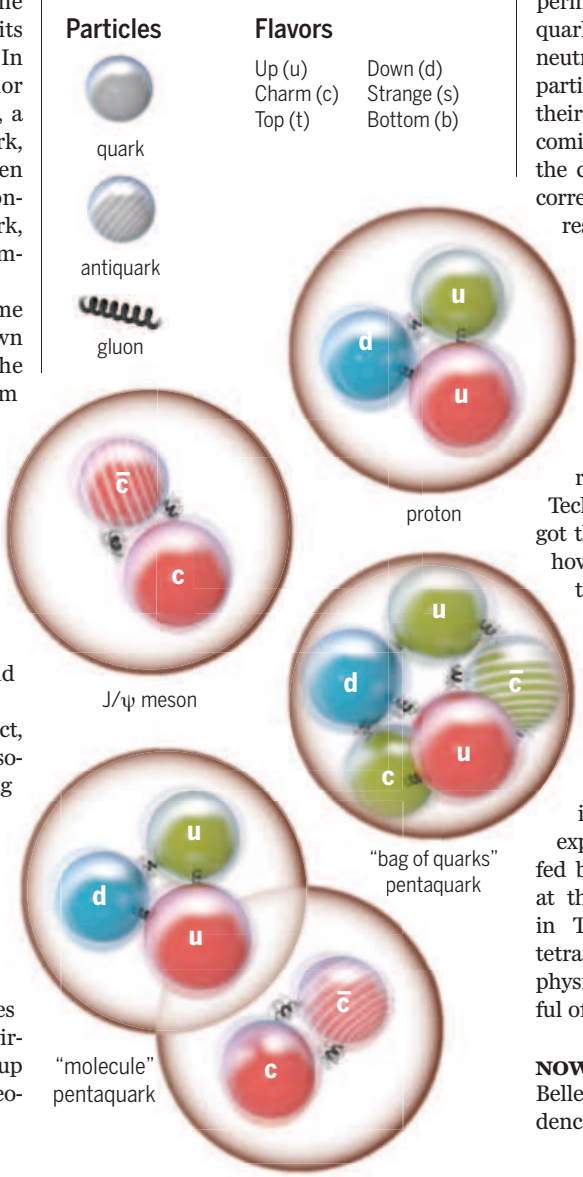

DIAGRAM: V. ALTOUNIAN/SCIENCE

Published by AAAS

up quarks, a down quark, a massive charm quark, and an anti–charm quark.

The main goal of LHCb, a 4500-ton assemblage of iron, high-tech electronics, and light-emitting crystals, is to study the decays of particles containing a massive bottom quark, whose behavior could provide clues to physics beyond physicists' standard model. To understand the "background" of another particle decay, Stone and colleagues asked a student to analyze debris from the decays of a Λ_b (the up, down, and bottom quark combination). "The student complained," Stone says. "He didn't want to do it—there wasn't going to be a signal. And he came back, and there was a huge signal"—one that suggested entirely new particles were taking shape during the decay.

In fact, the results point to two pentaquarks with slightly different masses, a heavier one weighing 4.74 times as much as a proton and a lighter one weighing 4.67 times as much as a proton, as the team reported in August in *Physical Review Letters*.

The analysis is tricky. Stone and colleagues had expected that the Λ_b would first decay to a J/ψ (quark content: charm and anticharm) and a Λ (up, down, strange) and that the Λ would then decay into a proton and the K^-. However, they found that sometimes the Λ_b appeared to take an alternate route to the same final destination, decaying instead into a K^- and a pentaquark. The pentaquark then decayed into the proton and the J/ψ. The two pentaquarks show up as peaks in the mass plot for proton-J/ψ pairs.

However, the LHCb researchers did far more than spot a couple of mass peaks. Squeezing information out of their data, they also worked out the complete wavelike quantum amplitude that describes the decay from a Λ_b to a pentaquark and a K^- and on to the J/ψ and the proton and encodes the probabilities for the particles to emerge at different angles, momenta, and spins. That monumental task requires teasing out how those amplitudes mix with others for the parallel decay the researchers had expected to see. The analysis clearly reveals amplitudes for two pentaquarks—signatures far more specific than bumps on mass plots, Stone says.

At first, LHCb researchers themselves doubted the result, Stone says. "We said, 'Oh, pentaquarks! It's got to be crap!'"he says. "We spent more time doing checks on this than on anything else ever." Using similar methods in 2014, the LHCb team also confirmed the sighting of the Z(4430) tetraquark, which consists of a down quark, an anti–up quark, and a charm-anticharm pair.

BUT IF SUCH PARTICLES ARE REAL, how are they put together? Tetra- and pentaquarks could be bona fide bags of four and five quarks, respectively. Or both could be more like molecules made of two-quark mesons and three-quark baryons. Such binding would resemble that between the protons and neutrons in a nucleus, which is best described by the exchange not of gluons, but of quark-containing particles called π mesons, or pions. In fact, Karliner and Jonathan Rosner, a theorist at the University of Chicago in Illinois, have developed a model that they argue already explains most of the candidate tetraquarks and one of LHCb's pentaquarks as molecules.

PHOTO: STEVE SARTORI/SYRACUSE UNIVERSITY

"I really do think there is a chance this will become a big breakthrough."

Sheldon Stone, Syracuse University

The molecule picture would also help explain why pentaquarks and tetraquarks, though fleeting, last a surprisingly long time. Physicists can't measure that lifetime directly, but they can infer it from the uncertainty in a particle's mass or its "width": The narrower the width, the longer the lifetime. The tetraquarks and pentaquarks are narrower than physicists would expect for particles that can decay through strong interactions. A moleculelike structure could favor longevity, as it would sequester the quarks from one another and keep them from instantly forming new particles and falling apart. "There has to be some sort of barrier to the recombining," Hicks says. "If they're all in a bag, I don't see what that barrier is."

But molecular models can't account for the two different pentaquarks LHCb sees, Stone says. And they can't explain other details of the pentaquarks: their spin and a property called parity.

The debate could have much deeper implications for the theory of QCD, says the University of Pittsburgh's Swanson. If the molecule picture is correct, then a relatively minor tweak to QCD will enable physicists to apply the pion-exchange picture developed in the 1940s for the atomic nucleus to more fleeting particles. If, however, the bag-of-quarks picture applies, then it may be wrong to think of the innards of the exotic particles in terms of discrete quarks and gluons. Instead, Swanson says, each particle may be more like a continuous "quark field" in which knots in the field form the constituent particles.

For example, in the 1970s, MIT's Jaffe suggested that the quarks within hadrons may dance around one another to form fleeting correlated pairs called diquarks. If so, a baryon might best be described as an ever-evolving state of a quark and a diquark. However, Jaffe cautions that theoretically there may be no real distinction between a molecule and bag of quarks.

It's still possible that the penta- and tetraquarks aren't real after all. For example, LHCb researchers see their pentaquarks emerging in the decays of another particle, the Λ_b. However, it could be that the production of a different combination of mesons and baryons exerts a shadow effect that generates a false signal for the supposed pentaquark decay. Such "threshold" effects are hard to rule out, ESS's Santoro says, because it's easy to find another combination of particles that would add up to give the observed mass. "There are very few [tetraquarks and pentaquarks] that are far from a threshold," she says.

TO TELL WHICH DESCRIPTION of pentaquarks and tetraquarks is right, physicists say they'll have to find more of the things. The bag-of-quarks and molecule models should predict different rosters of tetraquarks and pentaquarks with different masses, spins, and parities. For example, Karliner says, because of the parity of the pion, his molecular model allows some meson combinations to bind but forbids others. Those restrictions would limit the spectra of tetraquarks and pentaquarks that experimenters will see.

But even if a plethora of new particles are found, the experimental data may prove less telling than hoped. The models are flexible, Jaffe says. "When experimenters find a state that a model can't explain there will always be some lever [theorists] can pull to incorporate it."

Ultimately, enormously demanding computer simulations may yield insights, physicists say. But even if the simulations can handle the exotic particles, they might not provide a clear answer to their nature. "It's more likely to be, 'Well, [a pentaquark] spends 40% of its time in a baryon-meson molecule, and 40% of its time in a five-quark bag,'" Hicks says.

At least, physicists now seem to think that pentaquarks and tetraquarks are real. Whether they'll ever figure out how they're put together remains to be seen. ■

Published by AAAS

A NATION DIVIDED

Some scientists see Nicaragua's plans for a Grand Canal as a boon for an ailing land; others predict ecological catastrophe

By **Lizzie Wade**, *in Managua*

When the Nicaraguan government vowed in 2012 to revive a long-dormant idea to carve a canal through the heart of the country, Jorge Huete-Pérez expected a national debate on the project's merits. More than three times as long and twice as deep as the recently enlarged Panama Canal, the $40 billion Grand Canal linking the Atlantic and Pacific oceans would be the largest civil earthmoving project in history, with a social and environmental footprint to match. But in June 2013, when Nicaragua's government asked its National Assembly to grant a 50-year concession for the canal to the Chinese firm Hong Kong Nicaragua Canal Development (HKND) Group, approval took just 2 days.

Now, after the release of a massive impact assessment of the project commissioned by HKND, and just months before the company says it will break ground, the debate has begun in earnest. Huete-Pérez, a molecular biologist at Central American University (UCA) here, is firmly on one side. The canal, he

PHOTO: FRANCK GUIZIOU/CORBIS

Published by AAAS

Lake Nicaragua, Central America's largest source of freshwater, is a flashpoint in plans for an interoceanic canal.

says, "is going to be an environmental disaster of enormous dimensions."

Huete-Pérez had already published editorials in *Nature* and *Science* (23 January 2015, p. 355) decrying the project's downsides, including the possible salinization of Lake Nicaragua—Central America's largest source of freshwater—and the forced relocation of indigenous communities in the eastern part of the country. He views the 11,000-page impact assessment, conducted by Environmental Resources Management (ERM), a consulting firm headquartered in London, as inadequate. Many others expressed similar qualms at a meeting of Nicaraguan and international scientists that Huete-Pérez organized in November 2015 to review the assessment. "It's irresponsible" to commit to building the canal with so little data, says Katherine Vammen, a water expert at UCA. "There are just too many left-open doubts."

But among Nicaragua's small community of biologists, some take a sunnier view. Deforestation and pollution are already ravaging Nicaragua's environment, they note, and they applaud HKND's plans to replant forests near the canal to halt erosion and control runoff. They also view the project as a possible boon to science: a chance to collect a windfall of environmental data through HKND-funded studies in a country too impoverished to support much fieldwork. "We should provide help and support, so that the [impact] study is as complete as possible and the canal's impact on the environment is as minor as possible," says Ricardo Rueda, a botanist at the National Autonomous University of Nicaragua (UNAN), León.

The scientific debate is unlikely to dissuade President Daniel Ortega's Sandinista government from pursuing a megaproject that it claims is vital to the nation's future. Nicaragua is the second poorest country in the Americas, after Haiti, and "we don't have many development opportunities," says Manuel Coronel Kautz, president of the Nicaraguan canal authority. Nicaragua stands to gain a 1% stake in the canal each year, which means that after a half-century of operation it will have accumulated a controlling stake. In the meantime, the canal law states that HKND will pay the Nicaraguan government up to $10 million a year for 10 years. "We want to transform the economic lives of Nicaraguans—that's what makes us revolutionaries," says Coronel, a long-time Sandinista. "And there is no other option that makes as big of an impact."

> ***"The canal is going to be an environmental disaster of enormous dimensions."***
>
> **Jorge Huete-Pérez**, Central American University

Far from posing a further threat to Nicaragua's dwindling forests and wetlands, asserts engineer Bill Wild, HKND's chief project adviser, the canal will benefit conservation by bringing economic development. "I personally believe that the only thing that will save Nicaragua's environment is the canal," Wild says. "There is nothing else."

FOUR CENTURIES AGO, Spain dreamt of what Nicaragua is bent on doing today. Tired of schlepping gold and silver across Panama on foot and by mule from mines in western South America to ships in the Atlantic, the empire began eyeing Nicaragua as an alternative route. Although wider than both Costa Rica and Panama, Nicaragua offered a hydrological advantage. The navigable San Juan River allowed large ships to sail from the Atlantic 200 kilometers inland to Lake Nicaragua. Crossing the lake's roughly 100-kilometer span left a mere 20 kilometers to the Pacific coast. But when an engineer surveyed the potential canal route, he found that ships would need to be raised and lowered more than 30 meters as they traversed the Nicaraguan terrain: too great an elevation to overcome with 17th century technology. Other countries thought to pick up where Spain left off, but time and again their plans fell through.

Hoping to succeed where empires stumbled is HKND's founder, a Chinese magnate named Wang Jing. His plans, too, face skepticism because of the project's costs and scale. "Practically every week there's a reason to believe the canal is going to happen and another reason to believe it won't," says Edmundo Jarquín, an opposition politician here. HKND says it plans to finance the project by attracting investors on the open market. But he says that "if the canal is built, it won't be for financial reasons." Instead, Jarquín says, it would be part of a larger "geopolitical vision" backed by the Chinese government. If Beijing doesn't step up to fund the canal's construction, the project could collapse, says R. Evan Ellis, an expert on Chinese–Latin American relations at the U.S. Army War College Strategic Studies Institute in Carlisle, Pennsylvania. An economic feasibility study HKND commissioned has not been made public.

Since securing the preliminary concession, HKND has been investigating possible canal routes, including the one Spain considered. After determining that commandeering the San Juan River would be too destructive—and would surely anger Costa Rica, which shares the river as a border—HKND settled on a route running from Brito through Lake Nicaragua to the mouth of the Punta Gorda River (see map, p. 222).

Although Lake Nicaragua was once considered a boon to a canal, it now presents a daunting engineering challenge. The lake's average depth—13 meters—is far too shallow for supertankers and cargo ships. To create the necessary 30-meter-deep channel, HKND must carve 17 meters into the lakebed. ERM estimates that would require removing 715 million cubic meters of sediment: "the largest wet excavation ever," Vammen says.

She worries about what it might stir up. In the single sediment core from Lake Nicaragua analyzed for the impact study,

Published by AAAS

ERM found relatively high concentrations of heavy metals and other pollutants, including mercury, arsenic, and pesticides, possibly from rice paddies along the lake's eastern shore. Dredging could release the contaminants into the water, making it unsafe to drink or use for irrigation. Lake sediments also likely contain nutrients such as phosphorus and nitrogen; stirring those up could fuel algae blooms, poison fish, and destabilize the ecosystem.

The channel itself could transform the lake, if saltwater were to leak through the locks that will raise and lower ships. Not only would such an intrusion make the water undrinkable, it could bring invasive marine species and harm the plankton and invertebrates that form the base of the lake's food web. "The lake is a place where so much could be lost," says panelist Gerald Urquhart, a tropical ecologist at Michigan State University in East Lansing.

Others raise a direr scenario. "There is a serious risk of [volcanic] eruptions" near Lake Nicaragua, says Sergio Espinosa, a Nicaraguan geoscientist based in Vancouver, Canada, who consults on seismic risks and participated in the academy panel. "Eruptions cause landslides, and landslides cause lake tsunamis." If a catastrophe destroyed the locks, Lake Nicaragua might drain down the channel to the Pacific. How HKND and the government plan for such low-probability but high-risk events could "make or break the canal," says panelist Julio Miranda, a Nicaraguan structural engineer with CH2M HILL in San Jose, California.

Over the long term, the canal's ecological toll would run coast to coast. The canal could dump sediment into both oceans, harming coral reefs, says Jorge Cortés Núñez, a marine biologist at the University of Costa Rica, San José. And the planned route would sever the Mesoamerican Biological Corridor, a string of protected areas and buffer zones from southern Mexico to Panama intended to safeguard habitat for jaguars and other large mammals.

Although HKND has not started digging, the mere prospect of the Grand Canal has ignited social unrest in Nicaragua. The canal will run through indigenous lands, and the last village where the Rama language is spoken will have to be relocated to make room for it, according to ERM's report. And the concession law gives HKND the right to expropriate land anywhere in Nicaragua, not just along the canal route. "We're on a state of alert," says Manuel Abines Jiménez, a community leader from the town of Jícaro who attended the academy panel and has protested against the canal. "We won't go easily."

According to Urquhart, who does fieldwork in Nicaragua's rural east, other farmers are already fleeing to avoid the prospect of being violently relocated to less desirable land. He says some have moved into the Indio Maíz Biological Reserve, the largest continuous area of rainforest north of the Amazon. The government has claimed that the canal would keep people out of Indio Maíz by serving as a barrier on its northern border.

In its impact study, ERM "rightly described the social and environmental issues as serious," Urquhart says. However, he says, the report's "great optimism that these impacts can be mitigated" is not matched by a mitigation strategy. Other scientists say the assessment is based on too little data. For example, Vammen says, little is known about Lake Nicaragua's bathymetry and the composition of its sediments, leaving a major question mark about the safety and feasibility of dredging. "Those are really essential things you need to know if you're going to build a canal," she says.

Nor did the report fully weigh the risks of a catastrophic failure, Miranda says. The study used Chinese building codes to evaluate the canal's safety, he says, rather than develop new standards that would ensure the "one-of-a-kind project" remains "operational before, during, and after a quake."

Huete-Pérez argues that ERM's impact study, paid for by HKND, is tainted and has called on the government to fund a new study—ideally one that would evaluate the canal against other possible development projects. But Wild defends the report, noting that ERM was paid in advance: "They wrote whatever report they wanted with us not owing them a cent," he says. In the meantime, the academy panel has recommended that construction be put on hold while independent scientists fill gaps in ERM's report. Nicaragua, the panel contends, needs more data and analyses to accurately weigh the canal's risks and benefits.

"We do share the scientists' frustration with the lack of data in some critical areas,"

The biggest dig

World powers have long dreamed of carving a shipping canal through Nicaragua. Critics assail HKND's preferred route, which would bisect Central America's largest lake.

Profile of the canal

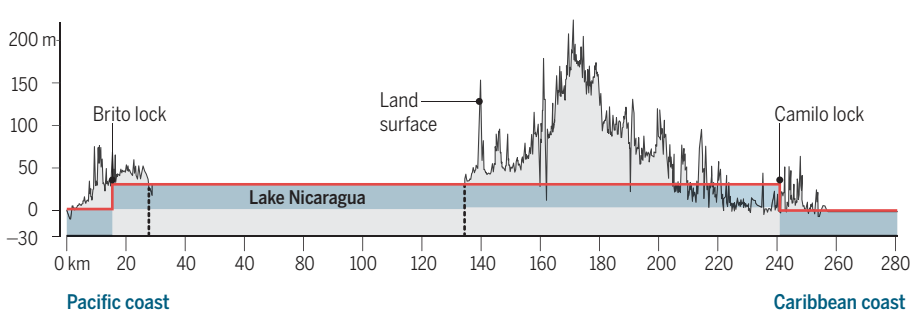

ILLUSTRATION: A. CUADRA/*SCIENCE*

Published by AAAS

Canal opponents fear the project will wreak havoc on Nicaragua's environment and lead to forced relocations of farmers and indigenous communities.

PHOTO: OSWALDO RIVAS/REUTERS

says ERM partner David Blaha, who led the impact study. ERM's report lists nine studies, including a complete bathymetric survey of Lake Nicaragua and a study of seismic risks, that should be carried out before construction begins. Such studies should be done after HKND completes its final design, says the canal authority's Coronel. For example, he says, "it's not until the lock designs are finished that we can analyze the specific geology of the exact place where [they are] going to be." Wild anticipates the canal's final design will be completed around the end of this year. Well before then, he says, the company plans to break ground on the Pacific port.

JEFFREY MCCRARY used to share Huete-Pérez's feelings about the canal. When ERM asked McCrary to survey freshwater fish species along the canal route as part of the impact study, the biologist, who has lived in Nicaragua for 3 decades and now works for the Nicaraguan Foundation for Integral Community Development here, remembers thinking, "I'm going to give you the best reasons not to do the canal." But as he traveled around the eastern portion of the country, he was struck by the lawlessness and environmental destruction he saw. Slash-and-burn agriculture and cattle ranching had devastated the Punta Gorda watershed and was threatening the Indio Maíz reserve, he says. "This is a really doomed place," he recalls thinking. Now, he wonders, "what in the world are we going to do if we don't get a canal?"

For McCrary and other converts, the Grand Canal's main selling point is reforestation. "Between 2002 and 2012, half of [Nicaragua's] forest cover was lost," heightening erosion and runoff, says Norving Torres, director of the Friends of the Upper San Juan River Foundation here. "The amount of clearing is a disaster for water management," Wild adds. If HKND doesn't put a stop to the erosion, he says, "we're going to be dredging all that stuff [out of the canal] forever." As a result, the company plans to reforest the Punta Gorda River catchment, an area covering roughly 20,000 hectares.

> ***"The only thing that will save Nicaragua's environment is the canal."***
> **Bill Wild**, HKND

Wild says HKND has tweaked the canal's route in response to ERM's concerns. The original location for the Pacific port, he says, would have "completely wiped out" a mangrove lagoon and destroyed the mouth of the Brito River. "So we moved it," Wild says. The firm also moved the Atlantic port to skirt Indio Maíz. And it shifted where the canal would connect to the eastern shore of Lake Nicaragua to avoid El Tule, a town that has been roiled by protests against relocation. "We've made a lot of changes," Wild says. "We will react positively wherever we can to honest and objective criticism."

McCrary, for one, is ready to work on HKND's terms. "I guess my strategic tack is, if there's going to be a canal in Nicaragua, I want to be sure it gets done right," he says. He's "disappointed" that Huete-Pérez and other canal opponents have shut themselves out of that conversation by adopting a confrontational stance, he says. Rueda, the UNAN botanist, agrees. Nicaraguan scientists, he says, should be "looking for ways to help so that more and more is known" about the country's natural resources and the best ways to protect them during canal construction.

Driving along the shore of Lake Nicaragua, Vammen points out drainage ditches that funnel raw sewage from the city of Granada into the lake. "No one ever said the whole area was pristine," she says. But Vammen and like-minded scientists reject the idea of anointing the canal as Nicaragua's savior. And Huete-Pérez bristles at the suggestion that cooperation is the only path forward. "It's always easier to take the side of the powerful," he says. "It requires more courage to align yourself with the powerless." ■

Published by AAAS

Functional small peptides p. 226 ▸

Graphene tuners for terahertz lasers p. 229

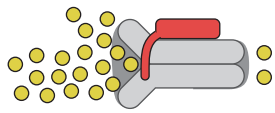

PERSPECTIVES

INFECTIOUS DISEASE

Adapting Koch's postulates

Criteria for disease causation must take microbial interactions into account

By **Allyson L. Byrd**[1,2] *and* **Julia A. Segre**[1]

In the late 19th century, Robert Koch established his famous postulates as stringent guidelines to evaluate causation in infectious disease (*1*). These original postulates require isolation of the putative pathogen and reinfection of a healthy host to prove causation. Over the years, Koch's postulates have been continually restated to incorporate the latest scientific findings and technologies (*2*–*5*). Modern molecular techniques have demonstrated that current or previous members of a microbial community can affect disease outcome, providing a nuanced view of strict causation as originally proposed by Koch. There is thus a need to incorporate microbial communities into rigorous modern guidelines for evaluating disease causation.

1 PATHOGEN = 1 DISEASE. Koch's original postulates can be summarized as follows: First, the microorganism occurs in every case of the disease; second, it is not found in healthy organisms; and third, after the microorganism has been isolated from a diseased organism and propagated in pure culture, the proposed pathogen can induce disease anew. Koch did not include the often

[1]*Microbial Genomics Section, Translational and Functional Genomics Branch, National Human Genome Research Institute, Bethesda, MD 20892, USA.* [2]*Department of Bioinformatics, Boston University, Boston, MA 02215, USA. E-mail: jsegre@nhgri.nih.gov*

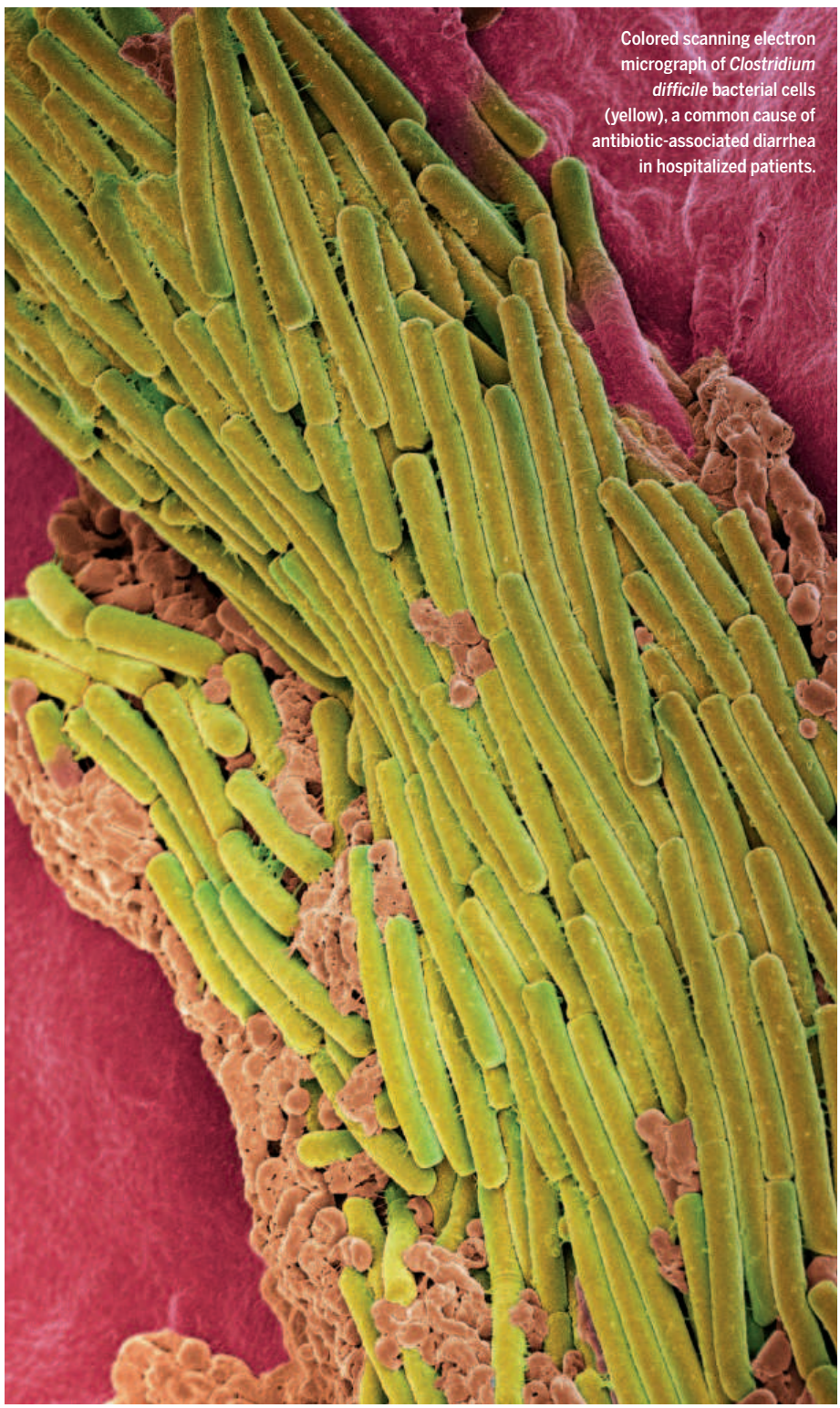

Colored scanning electron micrograph of *Clostridium difficile* bacterial cells (yellow), a common cause of antibiotic-associated diarrhea in hospitalized patients.

PHOTO: PAUL GUNNING/SCIENCE SOURCE

Published by AAAS

cited fourth postulate that the microorganism must then be reisolated from the experimentally infected host, but it has come to be viewed as necessary to complete the loop asserting causation. Although revolutionary for the time, the postulates have since been a double-edged sword. For example, the third postulate was implemented to guard against misassignment of causality due to mixed cultures. However, blind adherence to this postulate would mean excluding obligate parasites and viruses as infectious agents.

Over the past decade, sequencing technologies and advanced analytic tools have enabled whole-genome sequencing of both microbial isolates and communities. These advances raise new questions of how Koch's postulates can be updated to incorporate these molecular techniques. For example, when assigning causality to an organism, can a fully sequenced genome act as a surrogate for pure culture, even when the suspected organism requires additional microbes for successful propagation? Also, how do you address the role of microbial communities in disease pathogenesis? Here we address these questions and introduce new variables into Koch's one organism = one disease equation.

1 PATHOGEN + 1 COLONIZATION RESISTOR = 0 DISEASE . A modern test of Koch's postulates is the risk to patients of becoming colonized with a pathogen while hospitalized. In this setting, it has become clear that some commensal organisms can protect the host against pathogenic enemies, a process termed "colonization resistance." These commensal protectors defend the host either by directly inhibiting the pathogen or by enhancing host immunity (*6*). Recent evidence for both varieties of colonization resistance highlights how the presence of specific commensal bacteria can alter the pathology induced by Koch-verified infectious bacteria (*7, 8*). These studies demonstrate how microbial community sequencing can be used to differentiate when an infectious agent induces disease in some but not all hosts.

In one study, Buffie *et al.* (*7*) showed that mice treated with antibiotics exhibited varied susceptibility to infection by *Clostridium difficile*, a major cause of antibiotic-induced diarrhea. The authors also performed a similar analysis with a cohort of patients undergoing stem-cell transplant. Because of antibiotic treatment and compromised immune function, these patients are particularly susceptible to *C. difficile* infection. With microbial community sequencing and subsequent modeling of microbial interactions, the authors identified *Clostridium scindens* as a commensal associated with colonization resistance. This was validated when mice precolonized with a commercially available strain of *C. scindens* exhibited amelioration of symptoms associated with *C. difficile* infection. Mechanistically, it was demonstrated that *C. scindens* modifies endogenous bile acids to inhibit *C. difficile* growth (*7, 9*). Buffie *et al.* provide a well-validated example of how one organism can protect against a common pathogen (see the figure).

In addition to direct inhibition, a commensal organism can mediate colonization resistance through activation of the immune system. Recently, Schieber *et al.* demonstrated how a commensal *Escherichia coli* strain protects against muscle wasting associated with gut trauma and/or infection (*8*). By sequencing the microbial communities of mice with differential colitis severity, the authors identified an outgrowth of *Escherichia* species in the more resistant mice. *E. coli* isolate O21:H$^+$ was subsequently isolated and administered to the susceptible mice, which were then protected from colitis-induced wasting. Notably, an unrelated commensal *E. coli* strain did not provide a protective effect. This strain specificity highlights the importance of using linked primary, rather than banked isolates, since strains of the same species can display extensive functional variation. Similarly, when mice were infected with *Salmonella* Typhimurium or *Burkholderia thailandensis*, precolonization with *E. coli* O21:H$^+$ reduced the degree of wasting (*8*). With additional experiments, the authors showed that this protective effect was not due to inhibition of pathogen colonization, but rather that commensal *E. coli* O21:H$^+$, acting through the innate immune system, down-regulates muscle atrophy and promotes muscle regeneration. In this example, the pathogenesis of an infectious disease is altered because of a single commensal activating the immune system rather than a commensal directly inhibiting the growth of a pathogen.

The idea of distinct *E. coli* strains conferring colonization resistance is not new. In 1917, the *E. coli* strain Nissle was isolated from a soldier who did not develop diarrhea during an outbreak of shigellosis (*10*). Since then, research on this probiotic strain has identified several mechanisms by which it outcompetes pathogens, including an efficient iron acquisition system (*11*). Despite this early example of colonization resistance, previous updates to Koch's postulates have not considered the overall community context in which a pathogen does or does not induce a disease. As described

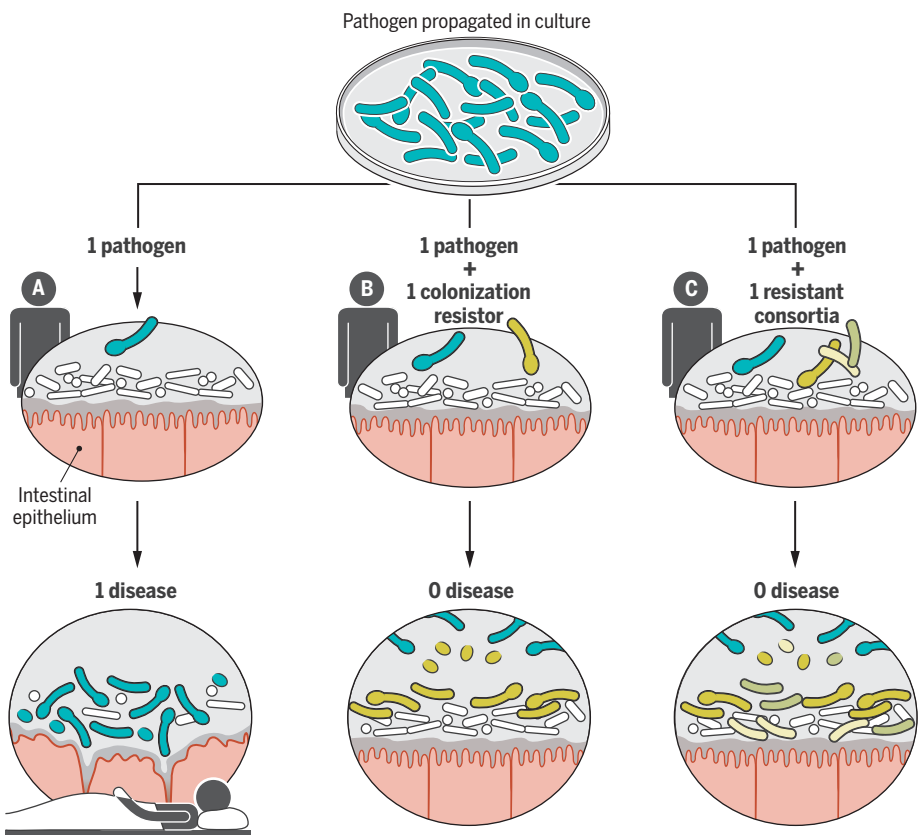

Microbial protectors. (**A**) According to Koch's original postulates, a pathogenic organism in a host will induce disease. (**B**) This assumption is challenged when an organism is present that can protect against the pathogen. (**C**) In some cases, consortia of microbes can have an ever greater protective effect.

ILLUSTRATION: K. SUTLIFF/*SCIENCE*

Published by AAAS

in (*7*, *8*), the role of specific members of the microbial community in disease pathogenesis could only be identified with antibiotic treatment and subsequent microbial community sequencing, technical advances that Koch could not have imagined as nucleic acids and antibiotics were not discovered until years after his death.

1 PATHOGEN + 1 COMMUNITY = 0 DISEASE. The previous examples highlighted comparatively simple cases of disease causation in which single colonization resistors were important. However, multiple microbes can also have an enhanced protective effect.

As described above, Buffie *et al*. find that *C. scindens* provides colonization resistance to *C. difficile* (*7*). However, the authors present evidence that even better outcomes are achieved when *C. scindens* cocolonizes with three other microbes. Similarly, Lawley *et al*. have reported that *C. difficile*–infected mice become less sick and clear the pathogen more efficiently after the administration of healthy donor feces (*12*). To define a more tractable resistant community, Lawley *et al*. cultured individual isolates from the feces and combined them into phylo-

"...do all members of the community have to be grown in pure culture and tested individually, or is it sufficient to grow and test a group culture?"

genetically distinct mixtures until they had found a six-member community that reproducibly reduced *C. difficile* infection and bacterial load.

These findings force us to consider under what circumstances a consortium of microbes can fulfill Koch's postulates. For example, do all members of the community have to be grown in pure culture and tested individually, or is it sufficient to grow and test a group culture? This is important in both scientific and translational arenas as researchers strive to create artificial communities capable of recapitulating the positive effects of fecal transplant in patients with recurrent *C. difficile* infections (*13*).

In the future, artificial communities could also be created to treat other infections associated with antibiotic-induced alterations of the microbial community. For example, women taking antibiotics are prone to develop mucosal candidiasis due to a depletion of beneficial microbes (*14*). Instead of traditional probiotic treatments, could a vaginal artificial community be designed to restore normal microbial community dynamics?

TOWARD DYNAMIC ADAPTATION. Combining sequencing and culturing represents a powerful way to explore and define the microorganisms affecting disease outcome. With sequencing, all organisms present in a sample can be observed without the constraints imposed by pure culture requirements. Based on conclusions drawn and hypotheses generated from sequencing results, researchers can then proceed with a more targeted culturing approach to identify organisms of interest.

In summary, updated Koch's postulates incorporating sequencing and culturing would involve the following steps: first, sequencing to classify all members of the microbial community; second, using computational models to assess microbes both necessary and sufficient for disease induction; third, targeted culturing to isolate microbes of interest from the diseased host; and fourth, testing primary isolates and consortia in relevant disease models.

In regards to steps 3 and 4, it should be emphasized that working with primary isolates cultured directly from a diseased host, rather than commercially available strains, lends scientific accuracy given the extensive genetic variability within a species. As an additional step, testing nonprimary isolates can be done to evaluate how widespread the capability is across strains of a species.

In light of recent appreciation of microbial consortia, the scientific community should consider infectious disease causation in a broader systems biology context in which host genetic variability, health status, past exposure history, and microbial strains and communities are all important. As technology advances and new scientific discoveries are made, we must dynamically adapt Koch's postulates so today's science maintains the integrity that Koch originally fostered. ■

REFERENCES

1. R. Koch, in *Xth International Congress of Medicine, Berlin* (1890).
2. A. S. Evans, *Yale J. Biol. Med.* **49**, 175 (1976).
3. T. M. Rivers, *J. Bacteriol.* **33**, 1 (1937).
4. S. Falkow, *Rev. Infect. Dis.* **10** (suppl. 2), S274 (1988).
5. D. N. Fredricks, D. A. Relman, *Clin. Microbiol. Rev.* **9**, 18 (1996).
6. C. G. Buffie, E. G. Pamer, *Nat. Rev. Immunol.* **13**, 790 (2013).
7. C. G. Buffie *et al.*, *Nature* **517**, 205 (2015).
8. A. M. Schieber *et al.*, *Science* **350**, 558 (2015).
9. J. A. Sorg, A. L. Sonenshein, *J. Bacteriol.* **192**, 4983 (2010).
10. A. Nissle, *Med. Welt* **29-30**, 1519 (1961).
11. M. Sassone-Corsi, M. Raffatellu, *J. Immunol.* **194**, 4081 (2015).
12. T. D. Lawley *et al.*, *PLOS Pathogens* **8**, e1002995 (2012).
13. E. van Nood *et al.*, *N. Engl. J. Med.* **368**, 407 (2013).
14. T. J. Break *et al.*, *Infect. Immun.* **83**, 958 (2015).

10.1126/science.aad6753

RNA

Small peptides control heart activity

Peptides from long noncoding RNAs control a muscle calcium pump

By **François Payre**[1] *and* **Claude Desplan**[2]

A growing body of evidence shows that so-called long noncoding RNAs (lncRNAs) often produce short peptides from small open reading frames (smORFs) (*1*). Whether and how smORF-encoded peptides fulfill specific functions remain poorly understood. Recent studies in flies (*2*) and mammals (*3*) have revealed that transcripts annotated as lncRNAs encode smORF peptides that bind to, and inhibit, the sarco/endoplasmic reticulum calcium adenosine triphosphatase (SERCA), an ion pump that is a key player in handling calcium in striated muscles. On page 271 of this issue, Nelson *et al*. (*4*) report that a lncRNA-encoded small peptide competes with SERCA-inhibitory peptides, thereby favoring heart contractility in mammals. These findings open new ways to understand cardiac function and pathologies, and show that smORF peptides act as versatile regulators of protein activity.

Muscle contraction relies on bursts of calcium released from the sarcoplasmic reticulum into the cytosol. The released calcium activates movement of the molecular motor myosin along actin filaments, enabling a "power stroke" mechanism. The SERCA pump moves calcium from the cytosol back into the sarcoplasmic reticulum, allowing actomyosin relaxation. Cycles of contraction and relaxation thus underlie muscular function. In the early 1970s, biochemical approaches in mammalian muscle cells revealed the inhibitory activity of a 52–amino acid peptide called phospholamban (PLN; also called PLB) (*5*). PLN is a transmembrane α-helix that fits a groove in the SERCA structure, favoring a conformational state that

[1]*Centre de Biologie du Développement, CNRS UMR5547, Université Paul Sabatier, Toulouse, France.* [2]*Department of Biology, New York University, New York, NY, USA. E-mail: claude.desplan@nyu.edu*

Published by AAAS

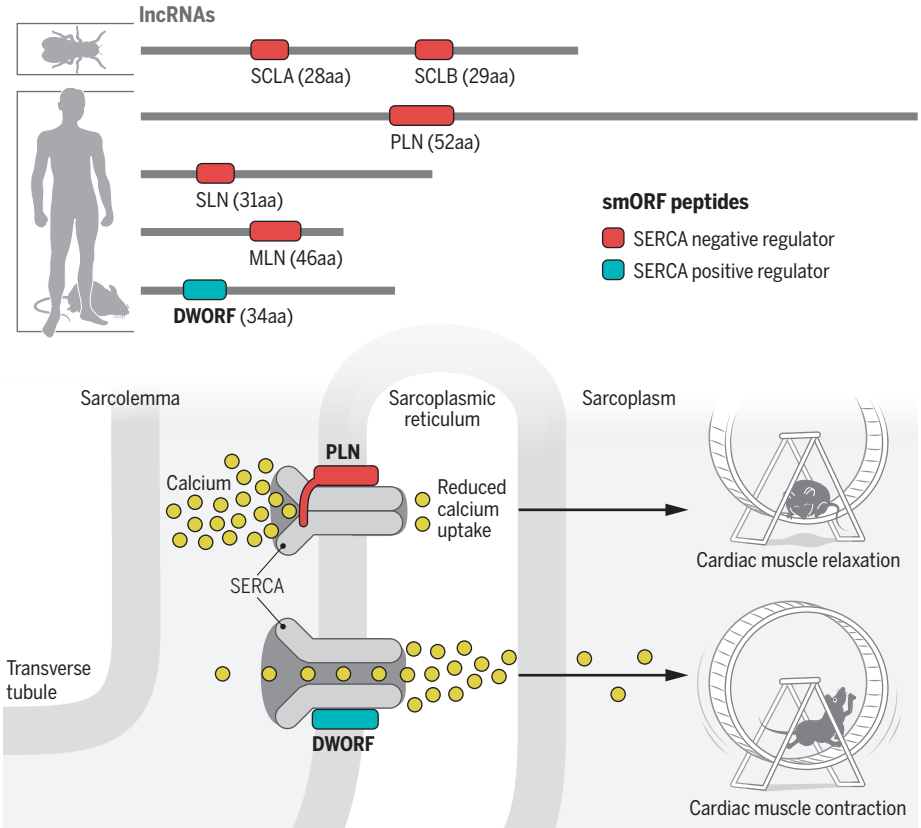

Competing peptides. Large RNAs annotated as noncoding produce a family of smORF peptides that regulate activity of the SERCA calcium pump, from flies to mice and humans. The DWORF peptide prevents the binding of SLN, PLN, and MLN inhibitory peptides, resulting in increased calcium uptake into the sarcoplasmic reticulum, which improves muscle contractility.

reduces calcium uptake (*6, 7*). A second, unrelated peptide of 31 amino acids, sarcolipin (SLN), was later identified in mammals (*8*) and shown to similarly bind to and inhibit the SERCA (*6, 9*). Both PLN and SLN are translated from distinct smORFs in transcripts that would be predicted as lncRNAs by current genomic annotation methods.

Whereas the SERCA protein from the fruit fly *Drosophila melanogaster* bears >70% sequence identity with the human protein, no annotated genes in *Drosophila* encode SLN- or PLN-like peptides. However, profiling lncRNAs allowed the identification of a muscle-specific transcript (*pncr003:2L*) in *Drosophila* that produces two related smORF peptides (*2*). Computer simulations suggest that these peptides, called sarcolamban A and B (SCLA and SCLB), fit the groove of the SERCA and, consistently, they bind to *Drosophila* and human SERCA. Furthermore, mutant fruit flies lacking SCL peptides display severe defects in muscle function, including cardiac arrhythmias (*2*). These results suggested that additional SERCA regulatory peptides could be hidden in the large number of apparently noncoding RNAs in mammals. Indeed, recent work has identified a 46–amino acid smORF peptide, myoregulin (MLN), produced from a transcript specifically expressed in skeletal muscles in mice and humans (*3*). Again, a similar conformation allows MLN to bind the SERCA and to decrease calcium uptake. Genetic experiments demonstrated the importance of MLN in vivo: Reducing the expression of MLN leads to improved performance in treadmill tests when compared to control mice (*3*). Therefore, lncRNAs produce a variety of smORF peptides that inhibit SERCA activity, providing tissue-specific control of striated muscle physiology.

Nelson *et al.* now provide evidence that a smORF peptide positively regulates SERCA activity in mammals. The authors identified an alleged lncRNA, predominantly expressed in the heart muscle of mice and humans, and demonstrated that it produces a 34–amino acid smORF peptide, called DWORF. Genome editing [with clustered regularly interspaced short palindromic repeats (CRISPR)–Cas9] leading to frameshifts in the DWORF peptide sequence resulted in reduced SERCA activity, delayed calcium clearance from the cytoplasm, and slowed relaxation of muscle fibers. Conversely, overexpression of DWORF in the heart increased calcium load in the sarcoplasmic reticulum and accelerated cytoplasmic calcium decay, thereby enhancing contractility. Although DWORF peptides bind to the SERCA protein, they do not intrinsically activate the SERCA. Instead, DWORF displaces the binding of MLN, PLN, or SLN peptides, relieving their inhibitory activity. The DWORF peptide thus appears as an antagonist of negative regulators, competing for binding to the SERCA.

Both the rationale of the antagonistic activities of these peptides and their intimate mechanisms of action remain to be elucidated. Whereas releasing inhibition may favor fast control and fine-tuning of protein activity, the dynamics of exchanges between regulatory peptides and the SERCA—which are both embedded in the sarcoplasmic reticulum membrane—are not known. In addition, PLN phosphorylation is sufficient to prevent its inhibitory activity, providing fast and signal-dependent control (*10*). Moreover, how DWORF prevents the binding of inhibitory peptides needs to be clarified. Although the DWORF peptide lacks sequence similarity with SLN, PLN, or MLN, it may—like SCL—dock into the same groove in the SERCA. In that case, how could a similar binding event inhibit (SLN, PLN, and MLN) SERCA activity, or not (DWORF)? Perhaps DWORF binds to a different domain of the SERCA, thus masking the regulatory groove. Structural studies, ideally including time-resolved methods, should further our understanding of muscle contraction and might help in the development of smORF-peptide–inspired therapeutics to prevent heart failure.

From a broader perspective, the findings of Nelson *et al.* highlight the importance of smORF peptides in the control of animal development and physiology, expanding the functional repertoire of protein-coding regions of our genome. Although still in its infancy, the emerging field of smORF peptides suggests that they represent an overlooked reservoir of versatile protein-binding interfaces, well suited to regulate the activity of various protein complexes (*1–4, 11*). Future work should explore the full range of smORF peptide activities and their role in the function and evolution of living organisms. ■

REFERENCES

1. A. Saghatelian, J. P. Couso, *Nat. Chem. Biol.* **11**, 909 (2015).
2. E. G. Magny *et al.*, *Science* **341**, 1116 (2013).
3. D. M. Anderson *et al.*, *Cell* **160**, 595 (2015).
4. B. R. Nelson *et al.*, *Science* **251**, 271 (2016).
5. M. Tada, M. A. Kirchberger, A. M. Katz, *J. Biol. Chem.* **250**, 2640 (1975).
6. A. M. Winther *et al.*, *Nature* **495**, 265 (2013).
7. B. L. Akin, T. D. Hurley, Z. Chen, L. R. Jones, *J. Biol. Chem.* **288**, 30181 (2013).
8. A. Odermatt *et al.*, *Genomics* **45**, 541 (1997).
9. C. Toyoshima *et al.*, *Nature* **495**, 260 (2013).
10. D. H. MacLennan, E. G. Kranias, *Nat. Rev. Mol. Cell Biol.* **4**, 566 (2003).
11. J. Zanet *et al.*, *Science* **349**, 1356 (2015).

10.1126/science.aad9873

ILLUSTRATION: K. SUTLIFF/*SCIENCE*

Published by AAAS

GENETICS

IRES unplugged

Cap-independent translation by IRESs can occur from various locations in mRNA

By **Fátima Gebauer**[1,2] *and* **Matthias W. Hentze**[3]

All cellular messenger RNAs (mRNAs) have a 7-methylguanosine (m7GpppN) cap structure at their 5′ ends, which promotes efficient translation and mRNA stability. The cap is recognized by the translation initiation factor eIF4F. eIF4F recruits the 40*S* small ribosomal subunit near the mRNA cap, which then scans the 5′ untranslated region (UTR) toward the initiation codon for subsequent protein synthesis. In conditions of stress or during viral infections, cap-dependent translation is compromised. Internal ribosome entry sites (IRESs) can bypass the cap to recruit ribosomes internally to the transcript, helping to secure appropriate protein synthesis under such conditions. On page 240 of this issue, Weingarten-Gabbay *et al.* (*1*) report the systematic discovery of cellular and viral IRESs, identifying a substantial fraction of mRNAs (~10%) and viruses (~20%) with the potential to be translated by this cap-independent mechanism.

IRESs were first discovered as complex structures in the 5′UTRs of picornavirus transcripts and were later found to occur in other viral and cellular mRNAs (*2*). IRESs interact with translation initiation factors, with bridging RNA-binding proteins, or with the small ribosomal subunit itself, leading to ribosomal positioning at or near the initiation codon and typically promoting translation initiation with little or no ribosomal scanning. IRESs have also been found as short sequence elements that can form base pairs with ribosomal RNA (rRNA), similar to Shine-Dalgarno sequences in bacterial translation initiation (*3*). IRESs lack common features that allow bioinformatic prediction, calling for experimental approaches to identify them.

The standard test to detect IRES activity within a given sequence is the bicistronic reporter assay, where the candidate sequence is placed between two open reading frames (ORFs) or "cistrons" and is tested for its ability to direct translation of the downstream cistron (*4*). The typically modest activities of cellular IRESs in the bicistronic assay, together with some poorly controlled published experiments, have fueled skepticism regarding the prevalence of IRESs in cellular mRNAs. However, the existence of ribosomal proteins seemingly dedicated to IRES-dependent translation supports IRESs as potentially important effectors of cellular mRNA translation (*5*, *6*). Segal and colleagues (*1*) established a high-throughput bicistronic reporter assay to quantify IRES-dependent translation driven by thousands of fragments, 174 nucleotides in length, derived from cellular and viral mRNAs. A set of 583 cellular and 471 viral novel 5′UTR IRESs emerged, with suitably rigorous controls showing they are neither cryptic promoter artifacts nor splice site artifacts.

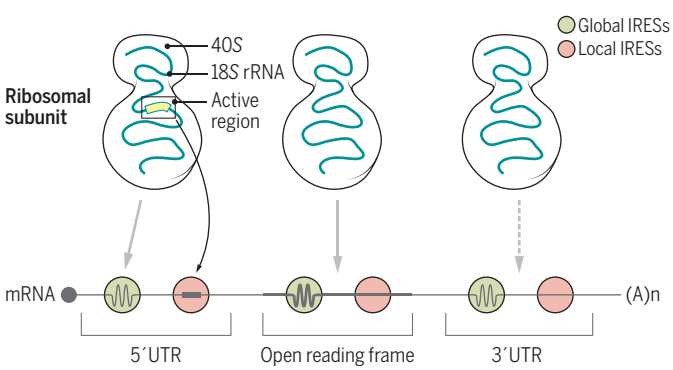

Cap-independent translation. Two types of IRESs are depicted in an mRNA, "global" (green) and U-rich "local" IRESs (pink), frequently with complementarity to the "active region" (yellow) of 18*S* rRNA, shown as part of the 40*S* ribosomal small subunit.

IRESs revealed by mutagenesis experiments can be classified into two types: "global" IRESs where complex, extended RNA structures are required to drive cap-independent translation, and "local" IRESs defined by short sequence motifs typically located within 60 nucleotides upstream of the initiation codon. Interestingly, some of these "local" IRES sequences display complementarity to a region of 18*S* rRNA, helices h23 and h26, that was previously shown to contact mRNA (see the figure). Using scanning oligonucleotides with complementarity to the entire 18*S* rRNA sequence in the bicistronic assay, a distinct region of 18*S* rRNA (nucleotides 812 to 1233) including h23 and h26 was systematically defined as "active" for mediating IRES function by mRNA complementarity. Whereas "global" IRESs could aid in ribosome recruitment by the interaction with translation initiation or other bridging RNA-binding factors, the "local" IRESs could in large part be based on Shine-Dalgarno–like mRNA-rRNA complementarity.

IRESs populate not only the 5′UTR but also the ORF itself and, surprisingly, the 3′UTR. Although the latter is intriguing and may suggest "shunting" of ribosomes from the 3′UTR to the initiation codon, possibly mediated by mRNA circularization (*7*), their unnatural placement upstream of an ORF in the bicistronic reporter assay calls for evaluation of these sequences within their natural contexts. Furthermore, the 3′UTR may contain cap-independent translation enhancers (CITEs), which can also function when placed at the 5′UTR (*8*). CITEs, found in plant viruses, recruit translation initiation factors and deliver them to the 5′ end of the mRNA via long-distance base pairing with the 5′UTR. Translation from CITEs requires scanning and therefore differs from IRES-mediated translation.

The article by Weingarten-Gabbay *et al.* suggests that IRES-mediated translation is also widespread among viral RNAs. Fragments with IRES activity have been found along the polyprotein region of several viruses, implying that IRESs might drive the independent expression of viral proteins from within the major polyprotein ORF. This in turn might stimulate research into new antiviral strategies.

Recent findings indicate that adenosine methylation (m^6A) in the 5′UTR can also stimulate cap-independent translation through interactions with eIF3 (*9*). This type of translation differs from IRES-driven translation because it requires scanning and a free 5′ end. Together with the work of Weingarten-Gabbay *et al.*, these results illustrate the diversity of cap-independent translation initiation mechanisms in mammalian cells. ■

[1]*Gene Regulation, Stem Cells and Cancer Programme, Centre for Genomic Regulation, Barcelona Institute of Science and Technology, 08003 Barcelona, Spain.* [2]*Universitat Pompeu Fabra, 08003 Barcelona, Spain.* [3]*European Molecular Biology Laboratory, 69117 Heidelberg, Germany. E-mail: hentze@embl.de*

REFERENCES

1. S. Weingarten-Gabbay *et al.*, *Science* **351**, aad4939 (2016).
2. R. J. Jackson, *Biochem. Soc. Trans.* **33**, 1231 (2005).
3. J. Dresios, S. A. Chappell, W. Zhou, V. P. Mauro, *Nat. Struct. Mol. Biol.* **13**, 30 (2006).
4. S. R. Thompson, *Wiley Interdiscip. Rev. RNA* **3**, 697 (2012).
5. D. M. Landry, M. I. Hertz, S. R. Thompson, *Genes Dev.* **23**, 2753 (2009).
6. S. Xue *et al.*, *Nature* **517**, 33 (2015).
7. S. E. Wells, P. E. Hillner, R. D. Valle, A. B. Sachs, *Mol. Cell* **2**, 135 (1998).
8. I. N. Shatsky, S. E. Dmitriev, D. E. Andreev, I. M. Terenin, *Crit. Rev. Biochem. Mol. Biol.* **49**, 164 (2014).
9. K. D. Meyer *et al.*, *Cell* **163**, 999 (2015).

10.1126/science.aad8540

ILLUSTRATION: P. HUEY/*SCIENCE*

Published by AAAS

APPLIED OPTICS

Tuning terahertz lasers via graphene plasmons

The emission of a terahertz laser is controlled by graphene carrier density

By **Marco Polini**

Plasmons (*1*) are collective density oscillations that pertain to charged particles, such as electrons and holes in solids. Although plasmons are often associated with metals, they are being actively explored for graphene and related two-dimensional materials (2DMs). Graphene plasmons (GPs) (*2*) can achieve active functionalities in diverse device types. For example, mid-infrared (mid-IR) GPs have been used to enhance mid-IR photodetectors (*3*), vibrational sensing of surface-adsorbed polymers (*4*), and label-free detection of protein monolayers (*5*). On page 246 of this issue, Chakraborty *et al.* (*6*) show that tunable graphene optical properties and GPs can be used to modulate the emission of a terahertz (THz) quantum cascade laser (*7*). Electromagnetic waves in the THz range (frequencies ν between 0.3 and 10 THz, or wavelengths λ between 50 μm and 1 mm) can penetrate many materials and have many applications in imaging and spectroscopy.

In bulk metals, plasmons occur at high frequencies, typically from the visible to the ultraviolet. In low-dimensional semiconductors, they typically fall in the band extending from the THz to the IR. If the right tricks are played to compensate the mistmatch between the momentum of photons and plasmons, plasmons can couple to light, yielding composite propagating quasiparticles called surface plasmon polaritons (SPPs). The hybrid light-matter nature of these quasiparticles yields SPPs with a wavelength λ_p shorter than the free-space wavelength λ_0. Plasmonics takes advantage of this ability to confine light to very small volumes to create nanoscale optoelectronic devices.

The recent marriage between graphene and plasmonics stems from two simple considerations. First, graphene and related 2DMs have carrier densities that can be tuned by electrical field-effect gating or chemical gating. For a fixed photon frequency, SPPs in 2DMs have a tunable wavelength, unlike ordinary metal-based plasmonics, where such field effects are blocked by strong screening. Second, high-quality 2DMs tend to host electron systems with large room-temperature mobility, which should lead to long SPP lifetimes and weak losses. In ordinary metal-based plasmonics, losses hamper many applications (*8*).

Graphene Labs, Istituto Italiano di Tecnologia, Via Morego 30, I-16163 Genova, Italy. E-mail: marco.polini@iit.it

ILLUSTRATION: P. HUEY/*SCIENCE*

Scattering-type scanning near-field optical microscopy (SNOM) (*9*–*13*) provides an unprecedented ability to visualize GPs in real space. Illuminating the tip of an atomic force microscope launches propagating plasmons that are reflected by edges or defects (see the figure). The plasmons that reach the tip again are converted to light. Recording this light with a photodetector while moving the tip enables spatial mapping of propagating GPs. Such measurements of mid-IR plasmons in high-quality graphene sheets encapsulated between hexagonal boron nitride crystals demonstrated ultralarge field confinement ($\lambda_p/\lambda_0 \approx 1/150$), an ultralow group velocity ($v_g \approx v_F$, where $v_F \approx 10^6$ m/s is the graphene Fermi velocity), and a lifetime exceeding 500 fs (*13*).

Chakraborty *et al.* consider a metal-based SPP waveguide inside a THz quantum cascade laser. Such plasmonic structures are used to control the properties of THz lasers. When their regularity is broken—for example, by introducing an aperiodic series of subwavelength slits into the metal part of the waveguide—control of the spectral properties of the THz laser is achieved at multiple frequencies. Large-area graphene flakes produced by chemical vapor deposition are then transferred over the waveguide, and the entire device is covered by a polymer electrolyte, which is used to tune the carrier density in graphene.

Two regimes were identified, depending on the value of the carrier density n_s in graphene. When n_s is low [corresponding to a Fermi energy $E = \hbar v_F(\pi n_s)^{1/2} \approx 50$ meV], the

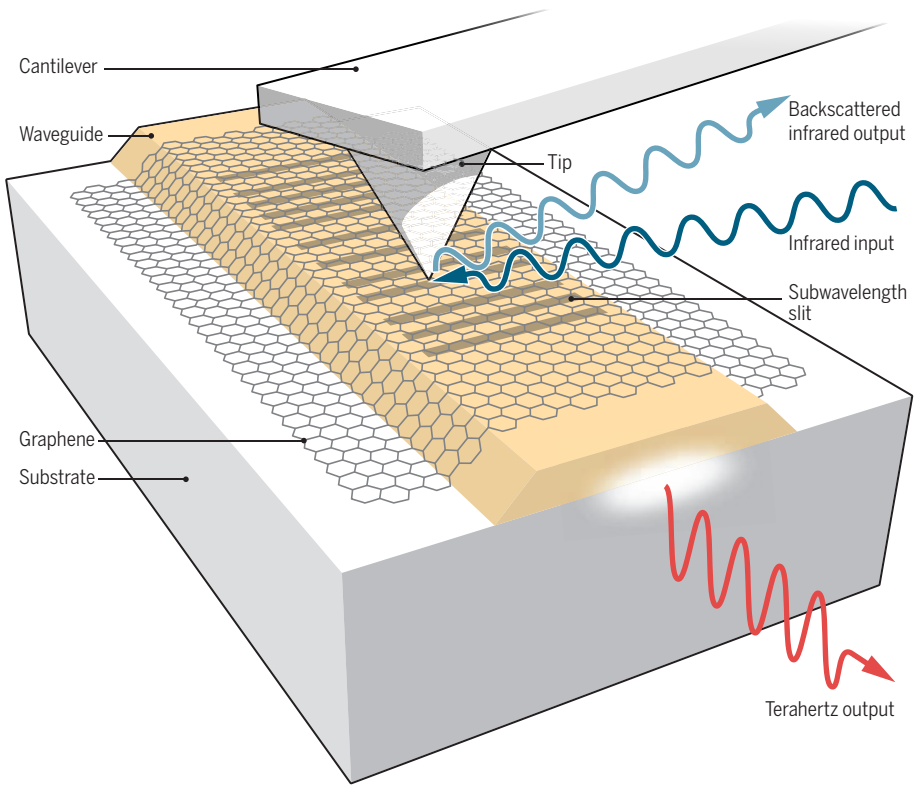

Probing plasmons in aperiodic lattice lasers. A component of the laser of Chakraborty *et al.* is a metallic waveguide covered by large-area graphene. Scanning near-field optical microscopy can probe the plasmons in graphene that control the laser; infrared light launches graphene plasmons from the metallized tip of an metallized atomic force microscope that are then imaged as backscattered light. Imaging plasmons in the laser device itself will require imaging through the polymer electrolyte that covers the graphene and imaging at ambient temperatures.

Published by AAAS

GP wavelength is on the order of the slit width. In this case, it is as if the GPs repair the patterned waveguide, yielding a laser emission spectrum that is similar to that of an unpatterned waveguide (i.e., of a waveguide without subwavelength slits). By contrast, when n_s is large (corresponding to $E_F \approx 300$ meV), the GP plasmon wavelength is much larger than the slit width. In this case, propagating THz SPP modes are efficiently scattered by the subwavelength slits, and the laser emission spectrum is forced to be controlled by the collection of slits.

Unfortunately, it is not yet possible to carry out THz SNOM spectroscopy on the existing devices for two reasons. The thick polymer electrolyte prevents the SNOM tip from getting close enough to the graphene sheet. This obstacle could be bypassed with a more complex architecture in which the patterned metal ridge is covered by a thin, optically transparent, electrically gated heterostructure, such as graphene–hexagonal boron nitride–graphene. Also, SNOM measurements (*9*–*13*) are typically performed at room temperature, whereas THz quantum cascade lasers operate at cryogenic temperatures. Several labs are now working on low-temperature SNOM setups.

The experimental results of Chakraborty *et al*. pave the way for the creation of a new generation of THz semiconductor lasers where gate-tunable spectral control is enabled by graphene. One can imagine device architectures in which the properties of a single subwavelength slit are programmable by local gating. More generally, this work is further proof of the great potential of graphene in THz technologies (*14*), including modulators, detectors, generators, and reflectarray antennas. ■

REFERENCES AND NOTES

1. G. F. Giuliani, G. Vignale, *Quantum Theory of the Electron Liquid* (Cambridge Univ. Press, 2005).
2. A. N. Grigorenko, M. Polini, K. S. Novoselov, *Nat. Photonics.* **6**, 749 (2012).
3. M. Freitag *et al*., *Nat. Commun.* **4**, 1951 (2013).
4. Y. Li *et al*., *Nano Lett.* **14**, 1573 (2014).
5. D. Rodrigo *et al*., *Science* **349**, 165 (2015).
6. S. Chakraborty *et al*., *Science* **351**, 246 (2016).
7. J. Faist, *Quantum Cascade Lasers* (Oxford Univ. Press, 2013).
8. Focus Issue on Plasmonics Applications, *Nat. Nanotechnol.* **10** (January 2015).
9. Z. Fei *et al*., *Nature* **487**, 82 (2012).
10. J. Chen *et al*., *Nature* **487**, 77 (2012).
11. P. Alonso-González *et al*., *Science* **344**, 1369 (2014).
12. S. Dai *et al*., *Nat. Nanotechnol.* **10**, 682 (2015).
13. A. Woessner *et al*., *Nat. Mater.* **14**, 421 (2015).
14. A. Tredicucci, M. S. Vitiello, *IEEE J. Sel. Top. Quantum Electron.* **20**, 8500109 (2014).

ACKNOWLEDGMENTS

Supported by the Graphene Flagship program (contract no. CNECT-ICT-604391) and Fondazione Istituto Italiano di Tecnologia.

10.1126/science.aad7995

PLANETARY SCIENCE

Sampling the Moon's atmosphere

In situ measurements reveal details of the production and evolution of the lunar exosphere

By **Catherine Dukes**[1] *and* **Dana Hurley**[2]

In H. G. Wells' 1901 science fiction classic *The First Men in the Moon*, two protagonists, English businessman Mr. Bedford and the eccentric physicist Dr. Cavor, knock back a special enervating concoction designed to expand their lungs, followed by the requisite fortifying brandy, before venturing onto the Moon's surface to breathe the rarefied lunar atmosphere. Even more tenuous than Wells' imagined environment, the lunar exosphere is an atmosphere so thin that atoms never collide, bounded on one side by the lunar surface and extending thousands of kilometers out into space. This low-density envelope results from a balance among the influx of material from the Sun, outgassing from the Moon's interior, delivery from meteoritic bombardment, and the loss of material to space as well as recycling in the lunar surface (see the figure). The precise formula for the formation of the lunar exosphere is unknown, but recent data from orbital spacecraft are being used to delineate the relative contributions from different processes. On page 249 of this issue, Colaprete *et al*. (*1*) report measurements of sodium and potassium (Na and K) in the lunar exosphere based on observations from the Ultraviolet and Visible Spectrometer (UVS) aboard NASA's Lunar Atmosphere and Dust Environment Explorer (LADEE), which acquired continuous dayside and nightside measurements of exospheric Na and K over multiple lunar orbits.

The UVS measurements provide a step toward determining the composition of the lunar atmosphere and the processes that control the distribution and variability of its components. Although Na and K are only minor constituents of the Moon's mostly inert (argon, helium, and neon) atmosphere, they have strong resonant scattering signals and can be readily observed with ground-based telescopes to monitor the health of the lunar environment (*2*, *3*).

Variation of the Na and K density appears diurnal—tied to the day-night periodicity that occurs with the Moon's rotation—in a more dramatic manner than previously measured (*1*, *4*). This temporal pattern suggests that volatile Na and K from the lunar regolith (a planetesimal's outer layer of loose rock and dust) are liberated from the surface by radiation from the Sun, either by solar photons that desorb Na and K from the lunar surface (*5*) or by solar wind ions, which can sputter atoms from alkali-containing minerals such as the plagioclase feldspars that make up a large fraction of the lunar highland and mare crust. Solar wind ions may play an additional role, as the keV protons and helium atoms impact the lunar surface, breaking bonds within the irradiated material and facilitating the diffusion of volatile atoms to the mineral surface to be subsequently removed by photodesorption or sputtering (*6*).

One way to better differentiate between the photon-generated exosphere and one populated by sputtered atoms is to moni-

PHOTO: NASA

[1]*Laboratory for Astrophysics and Surface Physics, University of Virginia, Charlottesville, VA 22904, USA.* [2]*Applied Physics Laboratory, Johns Hopkins University, Laurel, MD 20723, USA. E-mail: cdukes@virginia.edu*

Published by AAAS

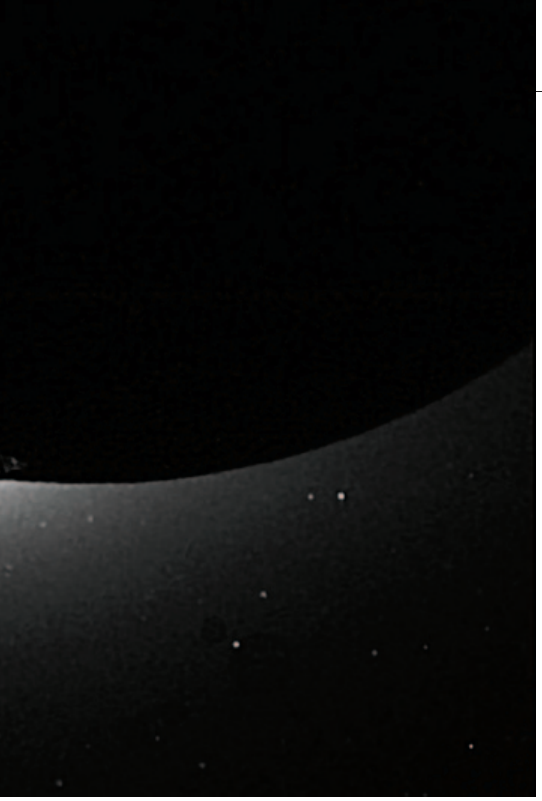

tor Na and K densities during the time the Moon moves through Earth's magnetotail. The magnetotail is a portion of Earth's magnetic field that extends away from the Sun, pushed outward by the force of the solar wind. Here, ions and electrons from the Sun are deflected, creating a region that is generally free of solar wind charged-particle irradiation. When the Moon passes through this region, approximately 3 days preceding and then following the full Moon, it can be assumed that photons dominate any surface interaction.

The first studies of lunar exospheric sodium measured a decrease in Na density during the Moon's transit through Earth's magnetotail (*2*), suggesting that solar wind sputtering is the primary initiator of the lunar Na exosphere. However, subsequent measurements contradicted this result (*7*–*9*). LADEE UVS data reveal a much more complicated dependence for Na: decreasing as the Moon moves into the magnetosphere, then increasing to a local maximum before declining again. Simultaneous observation of the K density, about an order of magnitude lower than that of Na, does not clarify the picture, as no change to the diurnal variation appears to occur during the Moon's transit through the magnetotail. This may be merely a function of the decreased intensity, or may be an additional indication that the evolution of the exosphere is a highly complex process.

One conclusion from the new LADEE data is the intimate association between the lunar surface and exosphere, which implies a strong correlation between the K abundance in the lunar exosphere and KREEP (potassium, rare earth elements, and phosphorus) regions on the Moon's surface. Potassium incorporated in lunar minerals is relatively rare and found in a few well-defined regions on the Moon's surface (*10*), allowing a straightforward comparison. The exosphere-surface relationship is less pronounced for Na, which is more uniformly distributed across the lunar map.

The role of meteoritic bombardment has also been investigated by monitoring the lunar environment as the Earth-Moon system passed through known meteor streams. As meteorites impact the lunar surface, thermal heating occurs and material from the regolith is ejected with a composition similar to the surface mineralogy. Colaprete *et al.* report short-term increases in Na and K during the Moon's transit through meteor streams, but more tellingly, they find strong evidence for a Na annual cycle that strongly influences the exospheric budget. Colaprete *et al.* suggest that this is caused by the impact exposure of fresh Na-containing surfaces and redeposition of Na released into the exosphere (*11*). This is consistent with a trend hinted at by the Japanese Kaguya mission, which observed a local maximum for exospheric Na during its 7-month scrutiny of the lunar nightside (*2*). Interestingly, the variations induced by meteor streams are comparable to the magnitude of the diurnal variations.

For now, the production and evolution of the lunar atmosphere remains an open question, one that is particularly relevant to understanding exospheres across the solar system, from Mercury to the asteroid belt to Saturn's moons and beyond. With such an amalgam of competing processes and variability on multiple time scales, Mr. Bedford and Dr. Cavor would need multiple forecasts to determine the required lung expansion for venturing onto the lunar surface. ■

REFERENCES

1. A. Colaprete *et al.*, *Science* **351**, 249 (2016).
2. A. L. Sprague, R. W. H. Kozlowski, D. M. Hunten, W. K. Wells, F. A. Grosse, *Icarus* **96**, 27 (1992).
3. A. E. Potter, T. H. Morgan, *Geophys. Res. Lett.* **21**, 2263 (1994).
4. M. Kagitani *et al.*, *Planet. Space Sci.* **58**, 1660 (2010).
5. T. E. Madey, B. V. Yakshinskiy, V. N. Ageev, R. E. Johnson, *J. Geophys. Res.* **103**, 5873 (1998).
6. C. A. Dukes, W. Y. Chang, M. Famá, R. A. Baragiola, *Icarus* **212**, 463 (2011).
7. A. E. Potter, R. M. Killen, T. H. Morgan, *J. Geophys. Res.* **105**, 15073 (2000).
8. M. Mendillo, J. Baumgardner, J. Wilson, *Icarus* **137**, 13 (1999).
9. M. Sarantos, R. M. Killen, A. S. Sharma, J. A. Slavin, *Geophys. Res. Lett.* **35**, L04105 (2008).
10. T. H. Prettyman *et al.*, *J. Geophys. Res.* **111**, E12007 (2006).
11. S. Yokota *et al.*, *J. Geophys. Res.* **119**, 798 (2014).

10.1126/science.aad8245

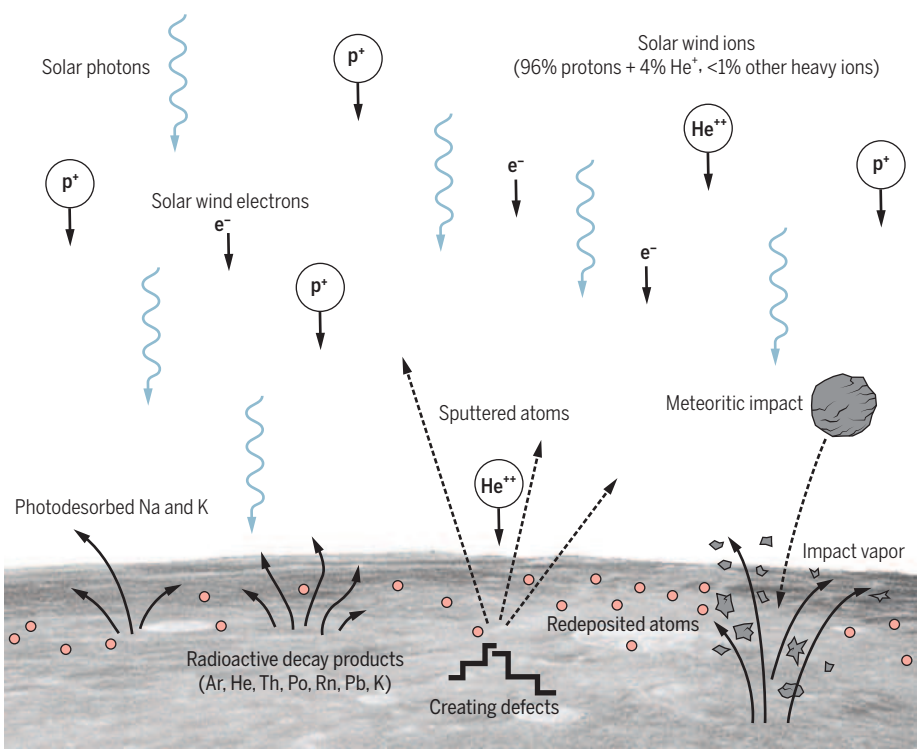

Creating an atmosphere. The lunar exospheric composition and density result from a time-varying balance between production and loss. Primary mechanisms generating exospheric atoms include photostimulated desorption, solar wind ion sputtering, meteoritic bombardment, radioactive decay, and thermal desorption. Exospheric atoms may be lost to space, photoionized, and swept away by the solar wind or Earth's magnetosphere, trapped in cold, permanently shadowed regions, or bonded to chemically active surface atoms.

ILLUSTRATION: P. HUEY/*SCIENCE*; (MOON) NASA

Published by AAAS

BOOKS *et al.*

NEUROSCIENCE

Unleashing the beast within

Adaptations that gave our ancestors an evolutionary edge can cause major problems for modern humans

By **Pascal Wallisch**

Why We Snap
Understanding the Rage Circuit in Your Brain
R. Douglas Fields
Dutton, 2015. 416 pp.

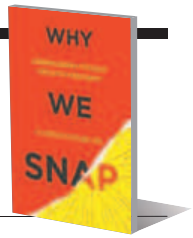

Economists like to assert that humans are cool calculators of maximal utility, considering all options, then deciding on a course of action that leads to the best outcome possible, given the situation. In this light, it seems puzzling that the news is chock full of reports of people who seem to violate this presumption, sometimes violently.

Why We Snap by R. Douglas Fields attempts to explain this seeming paradox from the perspective of neuroscience. The book nicely illustrates an irony of evolution: Much of what evolved to keep us safe can get us into serious trouble in the modern world.

Bouts of rage that lead to violence are akin to black swan events—unpredictable often even to the perpetrator but extremely memorable and momentous in hindsight. Fields outlines nine specific triggers that are likely to unleash rage: threats to life and limb; threats to mates, family members, and the tribe; insults to oneself or the social order; encroachment on territory or resources; and being prevented from freely pursuing one's actions.

Throughout evolutionary history, each of these triggers represented an existential threat to our continued survival. For instance, nonphysical insults, although not inherently life threatening, potentially endanger one's social standing, which for our ancestors meant that one's access to resources and/or mates was directly at risk.

The circuitry that kicks in when engaged by these triggers involves areas deep within the brain, particularly the amygdala (to perceive the threat) and the hypothamalus (to initiate the violent response). The circuitry involved is extremely trigger-specific, at least in rodents: Threats to life and limb, triggered by the presence of a cat, activate regions of the hypothamalus different from those activated by territory encroachment, triggered by introducing another rat, for example. Although the details of this subcortical circuitry are still an area of active research, it seems apparent that we are subject to the outputs of a system that continuously performs an analysis of ancient threats.

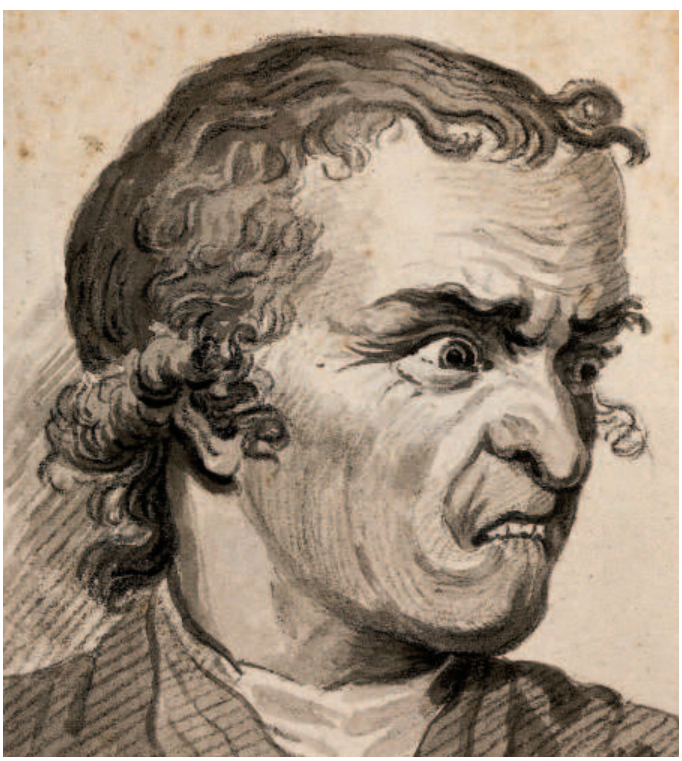

Everyone knows what rage looks like, but to understand what triggers it and why, it helps to take a closer look at the underlying brain circuitry.

Today, if someone commits a violent act, it often seems out of proportion to the events that triggered it. Most barroom brawls, for example, are started by trivial insults or minor disagreements. Modern environments constantly trigger false alarms of this ancient circuitry—false alarms that can lead to violence.

Fortunately, we are not entirely at the mercy of our subcortical brain. The prefrontal cortex can quench violent urges before we take action. The trigger threshold is not constant; it varies between and within individuals. Alcohol and stress can lower the threshold, whereas behaviors that reinforce one's commitment to nonviolence, such as those practiced by Jains and Quakers, can raise it. Unfortunately, the book's discussion of individual differences is surprisingly light.

A book of such an ambitious scope cannot be expected to be without flaws. In an attempt to ground the rage circuitry in a broader framework of unconscious information processing, the book goes on various tangents that are ultimately a distraction, including discussions of the nature of intuition and how the visual cortex of blind individuals can sometimes extract information from other senses, allowing the blind to "see" with their fingers. In contrast, a discussion of psychoactive drugs and their relation to violent behavior is entirely missing. The book would also have benefited from clearer distinctions between the science (performed mostly in rodents) and Fields's personal opinions about the implications of this research.

Much of western philosophy and our current societal structure, including the legal system, presumes that humans are rational actors who know right from wrong, making us culpable in the case of wrongdoing. However, this model was conceived thousands of years before modern neuroscience. If we are to have any hope of stemming violent behavior, it may be time to start incorporating our understanding of this ancient circuitry into public policy. *Why We Snap* is an important and timely book that uses neuroscience to illustrate why society must come to terms with our evolutionary heritage.

The reviewer is in the Department of Psychology at New York University, New York, NY 10012, USA. E-mail: pascal.wallisch@nyu.edu

10.1126/science.aad7138

CREDIT: WELLCOME LIBRARY, LONDON

Published by AAAS

MEDICINE

Evening the odds

Researchers tweak the genetic lottery for children with rare diseases

By **Nora Yang**

Nearly 40,000 individuals with phenylketonuria live normal lives today, thanks to the development of a highly accurate newborn screening test in the 1960s.

PHOTO: © ROMMEL/MASTERFILE/CORBIS

"Few quests are as seductive or as demanding as the search to cure a disease," affirms Philip R. Reilly in his new book, *Orphan: The Quest to Save Children with Rare Genetic Disorders*. The courage to mend nature's mistakes, the desire to provide a child with a healthy life, and the aspiration to understand the inner workings of life itself drive those who set out to find cures for diseases. The journey, however, is an arduous one, often lasting for decades and laden with setbacks and defeat.

In his book, Reilly chronicles the quest to end a particular subset of human diseases: rare genetic disorders that arise when our DNA goes awry. Like any lottery, these genetic mishaps are merely a matter of probability. Many genetic errors are innocuous to their DNA bearers. Some genetic errors are lethal to the embryo and will never get passed on to offspring. For the rest, the genetic errors manifest themselves through various forms of disease. In the United States, 1 out of 33 babies are born every year with genetic defects that cause disorders characterized by a wide range of debilitating symptoms, including misshapen and dysfunctional organs, mental disability, severe immune deficiency, and metabolic disorders (*1*). A rare disease, sometimes called an "orphan disease" since the passing of the Orphan Drug Act of 1983, is defined by the U.S. Food and Drug Administration (FDA) as any disease that affects fewer than 200,000 patients in the United States.

Orphan begins with the rare genetic disorders' "dark age," recounting the pain and suffering of sick children, the desperation and financial ruin to their families, and the relentless pursuit by parents, physicians, and scientists of ways to improve their lives. Owing to their heroic efforts, we now have treatments or even cures for numerous genetic diseases. The book is a magnificent gift for those on the quest to conquer genetic disorders, retracing roads to successful treatments and providing suggestions for the next trails to be blazed.

If no one in your extended family has one of the more than 4000 rare genetic disorders that have been identified, you belong to the lucky few winners of the genetic coin toss. Collectively, an estimated 30 million (1 in 10) Americans suffer from rare diseases. The occurrence of "rare" diseases in societies can be as frequent as the occurrence of cancer or diabetes.

A close examination of rare diseases reveals that scores of seemingly unrelated rare disorders with completely different symptoms share common genetic causes. The story of enzyme replacement therapy (ERT), as told by Reilly, is a case in point. After decades of searching, Cerezyme, the first ERT, was approved by the FDA to treat Gaucher's disease. A protein product made in a factory, Cerezyme carries out the job that the inherited, defective enzyme fails to do, allowing patients to live unobstructed by the genetic defect they carry. This approach has been applied to many other disorders whose origins are rooted in the existence of a missing or defective enzyme.

Now, more progressive approaches such as gene therapy, gene editing, cell therapy, microbiome therapy, and system biology are all poised to deliver new curative therapies for genetic diseases. New technologies are being developed that may someday give us the tools to beat the odds of the genetic lottery and provide every fetus with a fully functional genome when it enters our world.

Orphan
The Quest to Save Children with Rare Genetic Disorders
Philip R. Reilly
CSH Press, 2015. 420 pp.

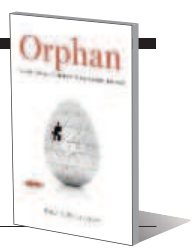

As we acquire technologies to more precisely shape the human genome, fierce ethical debate ensues. Where do we draw the line between treating a genetic disorder and eugenics? When we change DNA composition in a fetus to cure an immune deficiency disorder, can we not also change the genes that enhance its immune system, so that it can better fight diseases in life? While correcting a fetus's gene to avoid stunted mental development, could we also change its genetic makeup to enhance its intelligence? Who should decide and regulate how to use the knowledge and technologies that can change a person's life?

Societies will grapple with these and many other related questions for years to come. For now, we focus on continuing the quest to save as many children as possible from the devastating effects of rare genetic disorders.

The reviewer is at the National Center for Advancing Translational Sciences, National Institutes of Health, Bethesda, MD 20892, USA. E-mail: nora.yang@nih.gov

REFERENCES AND NOTES

1. www.cdc.gov/ncbddd/birthdefects/data.html.

10.1126/science.aad7104

Published by AAAS

LETTERS

Edited by **Jennifer Sills**

Weather stations lack forest data

ACROSS THE GLOBE, weather stations record temperatures for numerous purposes, including real-time weather analyses, climatological and biological studies, and agriculture. Yet, virtually all weather stations on land follow the World Meteorological Organization's guidelines that sensors should be installed well away from trees (*1*–*3*). Thus, although warming of the terrestrial macroclimate is clearly evident from weather station data, we actually do not know how temperatures are changing beneath trees.

This is a major concern because forests cover 27% of the land surface on Earth and harbor two-thirds of all terrestrial biodiversity (*4*, *5*). Much of this diversity lives below the upper foliage of trees. The scarce microclimatic data that are available from forest understories record non-uniform and nonlinear responses of subcanopy temperatures to above-canopy warming (and even buffering against temperature changes), due to factors such as canopy structure, season, tree species, and management (*3*). This makes subcanopy temperatures hard to predict from open-field measurements.

Weather radar station in Germany.

The fact that standard terrestrial weather stations are not installed in forests is of paramount importance for climate effects on processes that take place in the shade, such as tree regeneration, biodiversity dynamics, and nutrient, water, and carbon cycling, and thus also for macroclimate modeling (*6*, *7*). To further our understanding of climate change, we urgently need to better quantify how temperatures are changing inside the world's forests.

***Pieter De Frenne*[1,2]** and Kris Verheyen*[2]**

[1]Department of Plant Production, Ghent University, 9090, Melle, Belgium. [2]Department of Forest and Water Management, Ghent University, 9090, Gontrode, Belgium.

*Corresponding author: E-mail: Pieter.DeFrenne@UGent.be

REFERENCES

1. World Meteorological Organization, *Guide to Meteorological Instruments and Methods of Observation* (WMO-No. 8, Geneva, 2008).
2. M. B. Ashcroft, *J. Biogeogr.* **37**, 1407 (2010).
3. B. R. Scheffers *et al.*, *Global Change Biol.* **20**, 495 (2014).
4. Food and Agriculture Organization of the United Nations, *Global Forest Resources Assessment* (FAO, Rome, 2015).
5. Millennium Ecosystem Assessment, *Ecosystems and Human Well-Being: Biodiversity Synthesis* (World Resources Institute, Washington, DC, 2005).
6. P. De Frenne *et al.*, *Proc. Natl. Acad. Sci. U.S.A.* **110**, 18561 (2013).
7. S. P. Good , D. Noone, G. Bowen, *Science* **349**, 175 (2015).

Visa rules imperil collaboration

THE TRAGIC EVENTS in Paris, France, and San Bernardino, California, have led to an unfortunate response by U.S. lawmakers. In an amendment to the recently signed omnibus bill, changes to the Visa Waiver Program (VWP) were enacted that will substantially affect global scientific collaborations and exchanges. The program previously allowed citizens of 38 nations to travel to the United States without a visa for up to 90 days—a great boon to scientists and academics who wished to participate in conferences or take part in research projects. Indeed, the goal of the program was to encourage such interactions by reducing barriers to travel.

The changes to this program focus on four countries in the Middle East and North Africa (MENA) region (*1*). Dual nationals of Iran, Iraq, Syria, and Sudan, as well as others who have traveled to those countries since 2011, are prohibited from traveling to United States without a visa by the VWP (*2*). Given the potential for reciprocal restrictions upon American travelers by other countries (*3*), this change will impede global scientific exchanges and dialogue and will obstruct the work of scientists and health professionals who travel to the MENA region, including members of charitable organizations such as Doctors Without Borders, UNICEF, and Save the Children. As scientists, we need to work diligently to create communities that model successful and peaceful collaborations [e.g., (*4*, *5*)], and the changes to the VWP stand in the way of that mission.

During the Cold War, American and Russian scientists collaborated to develop groundbreaking prototypes to the oral polio vaccine (*6*). The danger posed by the Cold War was at least as great and arguably greater than the current danger from terrorism; yet, despite open enmity between nations, scientific collaborations produced a breakthrough that prevented millions of people from dying or becoming disabled due to polio. Are we willing to sacrifice that kind of progress out of fear of terrorism?

Navid Madani

Department of Global Health and Social Medicine, Harvard Medical School, and Department of Cancer Immunology and Virology, Dana-Farber Cancer Institute, Boston, MA 02215, USA.
E-mail: Navid_Madani@dfci.harvard.edu

REFERENCES

1. T. C. Brown, "Proposed changes to the Visa Waiver Program," Bipartisan Policy Center (2015); http://bipartisanpolicy.org/blog/proposed-changes-to-the-visa-waiver-program/.
2. BBC News, "Five things you need to know about US visa changes" (2015); www.bbc.com/news/world-us-canada-35162916.
3. The Hill, "What the Visa Waiver Program means to Europe" (2015); http://thehill.com/blogs/congress-blog/foreign-policy/262999-what-the-visa-waiver-program-means-to-europe.
4. NIH Record, "U.S.-Iran Scientific Partnerships Hold Promise" (2013); https://nihrecord.nih.gov/newsletters/2013/01_18_2013/story6.htm.
5. "Iran winning praise for effective—and increasingly open—response to HIV/AIDS, experts say" (2012); www.aaas.org/news/iran-winning-praise-effective%E2%80%94and-increasingly-open%E2%80%94response-hivaids-experts-say.
6. W. Swanson, "Revealed: How Cold War scientists joined forces to conquer polio," *Scientific American* (2012); www.scientificamerican.com/article/birth-of-a-cold-war-vaccine/.

Mechanistic biological modeling thrives

IN THEIR PERSPECTIVE "Systems biology (un)certainties" (23 October 2015, p. 386), P. D. W. Kirk *et al.* may give readers the impression that mathematical modeling and computer simulations of biological systems have fallen on hard times, owing to difficulties in measuring parameter values. The authors write that quantitative modeling in biology is under attack for applying data-driven models whose structure and parameters lack physical meaning. They suggest that such abstract models are necessary because biological parameters are hard to measure. In spite of their intrinsic limitations (*1*), we agree that abstract models can be powerful tools to address systems such as gene networks. We also agree that uncertainties should be reported.

However, we wish to stress that physically motivated, mechanistic modeling of complex biological systems is thriving,

PHOTO: © FRIDMAR DAMM/CORBIS

Published by AAAS

driven in large part by increasingly accurate measurements of molecular numbers, activities, and organization in live cells (*2*) and even in whole organisms (*3*). Whenever available, such information should be incorporated to constrain the structure and parameters, as it improves the model's ability to identify the mechanism. Thus, it is misleading to write that "fundamental physical laws…often do not provide a good starting point for understanding how biological organisms and systems work" or that "the abundances of all the key players (molecules, cells, or individuals) cannot be measured simultaneously and continuously."

Microscopically realistic modeling, constrained by independent parameter measurement, has driven the physical sciences for centuries. As in these fields, model predictions in modern quantitative biology often motivate new experiments that yield parameter values and structural revisions, and successful models converge on the actual molecular mechanism over time. Only mechanistic models allow physical principles and intuition gleaned from countless previous studies to be called upon to guide model development.

Ben O'Shaughnessy[1] and Thomas D. Pollard[2]

[1]Department of Chemical Engineering, Columbia University, New York, NY 10027, USA. [2]Department of Molecular, Cellular, and Developmental Biology, Yale University, New Haven, CT 06520, USA.

*Corresponding author. E-mail: bo8@columbia.edu

REFERENCES

1. S. Brenner, *Philos. Trans. R. Soc. London Ser. B Biol. Sci.* **365**, 207 (2010).
2. D. Vavylonis, J.-Q. Wu, S. Hao, B. O'Shaughnessy, T. D. Pollard, *Science* **319**, 97 (2008).
3. F. B. Shipley, C. M. Clark, M. J. Alkema, A. M. Leifer, *Front. Neural Circuits* **8**, 28 (2014).

TECHNICAL COMMENT ABSTRACTS

Comment on "Broken translational and rotational symmetry via charge stripe order in underdoped $YBa_2Cu_3O_{6+y}$"

B. V. Fine

Comin *et al.* (Reports, 20 March 2015, p. 1335) have interpreted their resonant x-ray scattering experiment as indicating that charge inhomogeneities in the family of high-temperature superconductors $YBa_2Cu_3O_{6+y}$ (YBCO) have the character of one-dimensional stripes rather than two-dimensional checkerboards. The present Comment shows that one cannot distinguish between stripes and checkerboards on the basis of the above experiment.

Full text at http://dx.doi.org/10.1126/science.aac4454

Response to Comment on "Broken translational and rotational symmetry via charge stripe order in underdoped $YBa_2Cu_3O_{6+y}$"

R. Comin, R. Sutarto, E. H. da Silva Neto, L. Chauviere, R. Liang, W. N. Hardy, D. A. Bonn, F. He, G. A. Sawatzky, A. Damascelli

Fine questions our interpretation of unidirectional stripes over a bidirectional checkerboard and illustrates his criticism by simulating a momentum space structure consistent with our data and corresponding to a checkerboard-looking real space density. Here, we use a local rotational-symmetry analysis to demonstrate that the simulated image is actually composed of locally unidirectional modulations of the charge density, consistent with our original conclusions.

Full text at http://dx.doi.org/10.1126/science.aac4778

TECHNICAL COMMENT

SUPERCONDUCTIVITY

Comment on "Broken translational and rotational symmetry via charge stripe order in underdoped $YBa_2Cu_3O_{6+y}$"

B. V. Fine[1,2]*

Comin *et al.* (Reports, 20 March 2015, p. 1335) have interpreted their resonant x-ray scattering experiment as indicating that charge inhomogeneities in the family of high-temperature superconductors $YBa_2Cu_3O_{6+y}$ (YBCO) have the character of one-dimensional stripes rather than two-dimensional checkerboards. The present Comment shows that one cannot distinguish between stripes and checkerboards on the basis of the above experiment.

Comin *et al.* (*1*) conducted a resonant x-ray scattering (RXS) experiment for three different compounds belonging to the family of high-temperature superconductors $YBa_2Cu_3O_{6+y}$ (YBCO). The experiment focused on the accurate measurements of the shapes of four charge-ordering peaks appearing in the RXS structure factor $S(q_x, q_y)$ at positions $\{\pm Q_0, 0\}$ and $\{0, \pm Q_0\}$, where $Q_0 \approx \pi/2$ in the units of inverse lattice period. These peaks can originate from either two-dimensional (2D) checkerboard-like modulations of charge density or 1D stripe-like modulations. The stripe interpretation implies that the sample can be fully partitioned into regions of mutually orthogonal 1D modulations. Each such region would generate only two dominant peaks at either $\{\pm Q_0, 0\}$ or $\{0, \pm Q_0\}$. The checkerboard interpretation implies that, under any partition, there will be regions generating all four peaks with comparable intensity. Distinguishing between stripes and checkerboards was the goal of Comin *et al.* In other families of high-temperature superconductors, this goal proved to be notoriously difficult to achieve [see, for example, (*2*–*5*)]. In particular, the experimental effort of (*3*) and the discussion given in (*4*) are very reminiscent of the present case.

Comin *et al.* have found that the shapes of measured charge peaks are elongated in the direction perpendicular to the wave vectors defining the centers of the peaks. In their analysis, the above authors associated the finite width of the peaks with the finite size of either stripe or checkerboard domains and then, in the main text of the Report, they pointed out that, in the case of checkerboards, the shapes of individual peaks should either have the fourfold symmetry—i.e., not be elongated—or the orientation of the elongation should be different. At the same time, stripe domains could reproduce the observed elongated peak shapes. The supplementary materials, however, indicated that the difference was not so clear-cut, because "canted" checkerboard domains would reproduce the observed elongation of the charge peaks as well. Comin *et al.* then introduced a quantitative constraint on the canted checkerboard scenario (equation S16 of their supplementary materials) and, in supplementary table S3, showed that their experimental results violate this constraint. Finally, Comin *et al.* concluded that their experimental observations are incompatible with checkerboard modulations and hence indicate stripe-like modulations.

The goal of this Comment is to raise the objection to the above conclusion. The problem with the reasoning of Comin *et al.* is that, instead of doing the Fourier analysis directly, they adopted various oversimplifying assumptions involving rigid domains of perfectly periodic structures for both stripes and checkerboards. Adopting a domain picture amounts to an implicit assumption of a certain kind of phase coherence between different Fourier components of the charge modulation, for which, to the best of this author's knowledge, there is no experimental evidence. At the same time, in the opposite limit of no coherence between different modulation harmonics, sufficiently narrow charge peaks, such as those observed by Comin *et al.*, are consistent with a rather routine-looking checkerboard modulation irrespective of the shape of the peaks.

To demonstrate the above statement, let us assume Gaussian peak shapes (which will not be essential for the conclusions) and represent the four peaks in the structure factor as

$$S(q_x, q_y) = \sum_{i=1}^{4} A_i \exp\left\{-\frac{(q_x - Q_{x,i})^2}{2\sigma_{x,i}^2} - \frac{(q_y - Q_{y,i})^2}{2\sigma_{y,i}^2}\right\} \quad (1)$$

where i is the index of the peaks; $\{Q_{x,i}, Q_{y,i}\}$ are the positions of the centers of the peaks admitting values $\{Q_0, 0\}$, $\{-Q_0, 0\}$, $\{0, Q_0\}$, and $\{0, -Q_0\}$; $\sigma_{x,i}$, $\sigma_{y,i}$ are the peak widths in the directions indicated by the subscripts; and $A_i = \frac{1}{8\pi\sigma_{x,i}\sigma_{y,i}}$ are the normalization constants.

Let us choose $Q_0 = \pi/2$ and then $\sigma_{x,i} = 0.085\ Q_0$, $\sigma_{y,i} = 0.2\ Q_0$ for peaks centered at $\{Q_0, 0\}$ and $\{-Q_0, 0\}$, and $\sigma_{x,i} = 0.15\ Q_0$, $\sigma_{y,i} = 0.1\ Q_0$ for peaks centered at $\{0, Q_0\}$ and $\{0, -Q_0\}$. The resulting structure factor $S(q_x, q_y)$ is plotted in Fig. 1A. Such a choice of parameters violates the constraint [equation S16 of (*1*)] on the canted checkerboards by a factor of about 2. In the framework of the assumptions adopted in (*1*), these four peaks cannot correspond to a checkerboard.

Figure 1B demonstrates the 2D Fourier transforms of the above structure factor, which gives the correlation function $C(x, y) \cong \langle \delta\rho(x + x_0, y + y_0)\delta\rho(x_0, y_0)\rangle_{x_0,y_0}$, where $\delta\rho(x, y)$ describes the fluctuation of the charge density with respect to the average value, and $\langle \ldots \rangle_{(x_0, y_0)}$ denotes averaging over x_0 and y_0. Independently of the shape of the four narrow peaks, $C(x, y)$ is bound to show strong checkerboard correlations of the kind appearing in Fig. 1B.

Now, to generate a possible pattern of 2D density fluctuations $\delta\rho(x, y)$ underlying the peaks in $S(q_x, q_y)$, let us recall that the $S(q_x, q_y)$ also represents the square of the amplitude of a harmonic with wave numbers $\{q_x, q_y\}$. Therefore, for the sake of producing an example, let us resolve the spectral peaks around $\{Q_0, 0\}$ and $\{0, Q_0\}$ into two 41 x 41 grids of discrete Fourier components uniformly spanning the ranges $[-4\sigma_{x,i}, 4\sigma_{x,i}]$ and $[-4\sigma_{y,i}, 4\sigma_{y,i}]$ around the peak centers

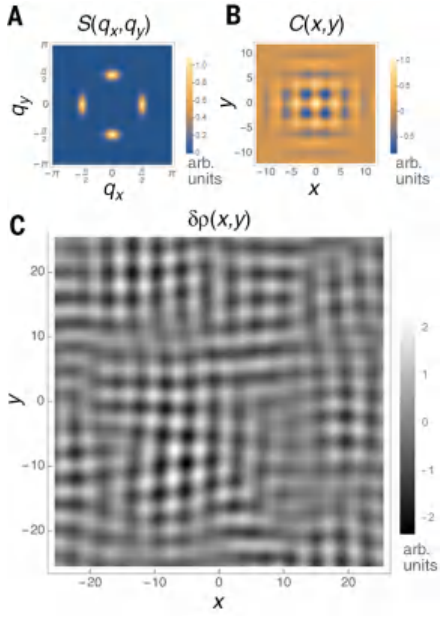

Fig. 1. Fluctuating checkerboard modulation of charge density. (**A**) Four charge modulation peaks in the structure factor $S(q_x, q_y)$ with parameters given in the text. (**B**) Density-density correlation function $C(x, y)$ obtained as the 2D Fourier transform of $S(q_x, q_y)$ given in (A). (**C**) Example of density modulation $\delta\rho(x, y)$ corresponding to $S(q_x, q_y)$ given in (A).

[1]Skolkovo Institute of Science and Technology, 100 Novaya Street, Skolkovo, Moscow Region 143025, Russia.
[2]Institute for Theoretical Physics, University of Heidelberg, Philosophenweg 12, 69120 Heidelberg, Germany.
*E-mail: b.fine@skoltech.ru

in the x and y directions, respectively. [The apparent character of the resulting function $\delta\rho(x, y)$ does not change, if a denser $\{q_x, q_y\}$ grid is used.] The density modulations in the real space are then obtained as

$$\delta\rho(x, y) = \sum_m a_m \cos(q_{x,m}x + q_{y,m}y + \varphi_m) \quad (2)$$

where index m labels all $2 \times 41 \times 41$ discrete Fourier components participating in the expansion, $a_m = \sqrt{S(q_{x,m}, q_{y,m})}$ the corresponding amplitude (up to a normalization constant), and φ_m is the random phase of each component.

The numerically generated function $\delta\rho(x, y)$ for one possible set of random phases φ_m is shown in Fig. 1C. It conveys a clear impression of a fluctuating checkerboard, in fact not much different from the results of the scanning tunneling microscopy experiments (*6*, *7*) for other cuprate compounds. As seen in Fig. 1C, the randomness of the phases φ_m implies that the correlation length controlling the width of the charge modulation peaks originates from the distortions of mostly continuous superstructures rather than from the domains of perfectly periodic modulations.

To conclude, the experimental results reported in (*1*) represent new valuable microscopic information that has implications for both the stripe and the checkerboard scenarios of charge modulations in cuprates. As such, however, the above results do not rule out the checkerboard modulations.

REFERENCES AND NOTES

1. R. Comin *et al*., *Science* **347**, 1335–1339 (2015).
2. B. V. Fine, *Phys. Rev. B* **70**, 224508 (2004).
3. N. B. Christensen *et al*., *Phys. Rev. Lett.* **98**, 197003 (2007).
4. B. V. Fine, *Phys. Rev. B* **75**, 060504 (2007).
5. B. V. Fine, *J. Supercond. Nov. Magn.* **24**, 1207–1211 (2011).
6. T. Hanaguri *et al*., *Nature* **430**, 1001–1005 (2004).
7. W. D. Wise *et al*., *Nat. Phys.* **4**, 696–699 (2008).

ACKNOWLEDGMENTS

I am grateful to V. K. Bhartiya for drawing my attention to the subject of this Comment.

28 April 2015; accepted 10 December 2015
10.1126/science.aac4454

TECHNICAL RESPONSE

SUPERCONDUCTIVITY

Response to Comment on "Broken translational and rotational symmetry via charge stripe order in underdoped $YBa_2Cu_3O_{6+y}$"

R. Comin,[1,2]* R. Sutarto,[3] E. H. da Silva Neto,[1,2,4,5] L. Chauviere,[1,2,5] R. Liang,[1,2] W. N. Hardy,[1,2] D. A. Bonn,[1,2] F. He,[3] G. A. Sawatzky,[1,2] A. Damascelli[1,2]*

Fine questions our interpretation of unidirectional stripes over a bidirectional checkerboard and illustrates his criticism by simulating a momentum space structure consistent with our data and corresponding to a checkerboard-looking real space density. Here, we use a local rotational-symmetry analysis to demonstrate that the simulated image is actually composed of locally unidirectional modulations of the charge density, consistent with our original conclusions.

We recently found that the symmetry of the underlying instability responsible for the charge order observed in the cuprate superconductor $YBa_2Cu_3O_{6+y}$ (YBCO) is of a unidirectional (1D) stripe rather than bidirectional (2D) checkerboard type (*1*). Fine (*2*) questions this conclusion by providing an example of charge modulation seemingly consistent with a bidirectional checkerboard modulation, but having the necessary characteristics of 1D order as per the definitions in (*1*). In the following, we will show that this is not the case.

The charge modulation patterns presented in figure 1, B and C, of Fine's Comment give the overall impression of a globally 2D order. However, establishing whether this corresponds to a true checkerboard or stems from the coexistence of two independent 1D modulations is a much subtler issue, even in the simple case of Fine's figure 1C. A unidirectional charge order instability is accompanied by the breaking of fourfold symmetry, but its detection can be obscured by the presence of 90° rotated domains, giving rise to what might appear as a globally 2D modulation. We have analyzed the density wave pattern in Fine's figure 1C and determined that it locally breaks D_{4h} symmetry and is thus best described as the superposition of two independent, locally 1D modulations.

[1]Department of Physics and Astronomy, University of British Columbia, Vancouver, British Columbia V6T 1Z1, Canada. [2]Quantum Matter Institute, University of British Columbia, Vancouver, British Columbia V6T 1Z4, Canada. [3]Canadian Light Source, Saskatoon, Saskatchewan S7N 2V3, Canada. [4]Quantum Materials Program, Canadian Institute for Advanced Research, Toronto, Ontario M5G 1Z8, Canada. [5]Max Planck Institute for Solid State Research, D-70569 Stuttgart, Germany.
*Corresponding author. E-mail: r.comin@utoronto.ca (R.C.); damascelli@physics.ubc.ca (A.D.)

In (*1*) we implemented an analysis based on these symmetry considerations, which allows discriminating the two scenarios discussed above. We note that our conclusion in favor of charge stripe order is supported by two completely independent pieces of evidence: (i) the symmetry analysis of the RXS structure factor performed for a variety of configurations, including domains as well as canted domains (this is what Fine questions in his Comment); and (ii) the intrinsic unidirectionality observed for the competition between charge order and superconductivity [see figure 3 in (*1*) and the discussion of the strong anisotropy in the temperature evolution of the charge-order correlation length].

Hereafter, we will present quantitative counterarguments to the thesis outlined in Fine's Comment. Stripe order is a smectic charge-ordered state (*3*)—i.e., one breaking both translational and fourfold rotational (D_{4h}) symmetry. To reveal and characterize the local breaking of these symmetries, we have analyzed the real-space density map proposed by Fine in his figure 1C in terms of its local D_{4h}-symmetry breaking. We seek to isolate the two real-space density components that are modulated along x and y [$\delta\rho_x(\mathbf{r})$ and $\delta\rho_y(\mathbf{r})$]. We do this by taking a local Fourier transform that is often used to analyze scanning tunneling microscopy (STM) data [see e.g., the supplementary materials of (*4*)]

$$\delta\rho_x(\mathbf{r}) = \frac{1}{2\pi\Gamma^2}\sum_{\mathbf{r}'}\delta\rho(\mathbf{r}')\cdot e^{i\mathbf{Q}_x\cdot\mathbf{r}'}\cdot e^{-\frac{|\mathbf{r}'-\mathbf{r}|^2}{2\Gamma^2}} \quad (1)$$

and similarly for $\delta\rho_y(\mathbf{r})$. Here, $\delta\rho(\mathbf{r})$ is the original real-space density pattern, and Γ is chosen to be appropriate to the domain sizes observable in $\delta\rho(\mathbf{r})$ ($\Gamma \sim 0.22Q^{-1}$). As a formally defined metric for the checkerboard state, we use two similar definitions of a local-order parameter, following a previous theoretical study (*5*) and more recent experimental STM work (*6*). These two quantities, respectively denominated $\Sigma_1(\mathbf{r})$ and $\Sigma_2(\mathbf{r})$, are defined as follows

$$\Sigma_1(\mathbf{r}) = (|\delta\rho_y(\mathbf{r})|^2 - |\delta\rho_x(\mathbf{r})|^2)/(|\delta\rho_y(\mathbf{r})|^2 + |\delta\rho_x(\mathbf{r})|^2) \quad (2)$$

$$\Sigma_2(\mathbf{r}) = (|\delta\rho_y(\mathbf{r})| - |\delta\rho_x(\mathbf{r})|)/(|\delta\rho_y(\mathbf{r})| + |\delta\rho_x(\mathbf{r})|) \quad (3)$$

These local order parameters are bound between –1 and 1; whereas +1 (–1) corresponds to stripes propagating along y (x), 0 is a pure checkerboard state (i.e., fourfold symmetric), where the two density modulations need to have locally the same amplitude, a necessary condition for D_{4h} point group symmetry to be preserved.

The plot of $\Sigma_1(\mathbf{r})$ is superimposed on the real-space density map (Fig. 1, A and B). The presence of multiple colorful patches implies the existence of extended regions with local stripe modulations predominantly along y [i.e., $\Sigma_1(\mathbf{r}) = 1$, red] or predominantly along x [i.e., $\Sigma_1(\mathbf{r}) = -1$, blue]. The choice of a threshold value for $\Sigma_1(\mathbf{r})$ separating bidirectional from unidirectional nanoregions would be arbitrary, and ultimately, only the extremal values correspond to well-defined order parameters. However, the existence of extended stripy regions reveals a clear tendency of the charge density to locally break D_{4h} point group symmetry. Similar observations can be made for the corresponding plots of $\Sigma_2(\mathbf{r})$(Fig. 1, C and D), where blue and red ellipses in Fig. 1C illustrate the location of x and y stripy domains, respectively, confirming the existence of extended regions with local stripe modulations.

We note that, even in the original density pattern, it can be observed that most regions approach a unidirectional character, even though the general appearance of the image gives an overall impression of a checkerboard motif. This is visualized in the x- and y-projected density maps of Fig. 1E [$\delta\rho_x(\mathbf{r})$] and 1F [$\delta\rho_y(\mathbf{r})$].

The overall picture is essentially what one would obtain by taking the real-space schematics in figure 2A of (*1*) and partially overlapping the stripy domains on top of each other. An equivalent configuration (from the perspective of the reciprocal space representation) would be obtained with a criss-cross pattern of stripes in adjacent CuO_2 planes within a bilayer because of our inability to resolve the c-axis–projected structure of the charge-ordered state. In (*1*), we showed only disjointed stripy domains for illustrative purposes; we did not assume that the individual stripy domains have to be segregated.

Finally, we can also calculate the cross-correlation coefficient

$$r_{\rho_x,\rho_y} = \frac{1}{n}\sum_{\mathbf{r}}\frac{(\rho_x(\mathbf{r}) - \overline{\rho_x})\cdot(\rho_y(\mathbf{r}) - \overline{\rho_y})}{\sigma_{\rho_x}\cdot\sigma_{\rho_y}} \quad (4)$$

where ρ_x (ρ_y) are the density amplitudes along x (y), σ_{ρ_x} (σ_{ρ_y}), the corresponding standard deviation, and n is the number of discretized

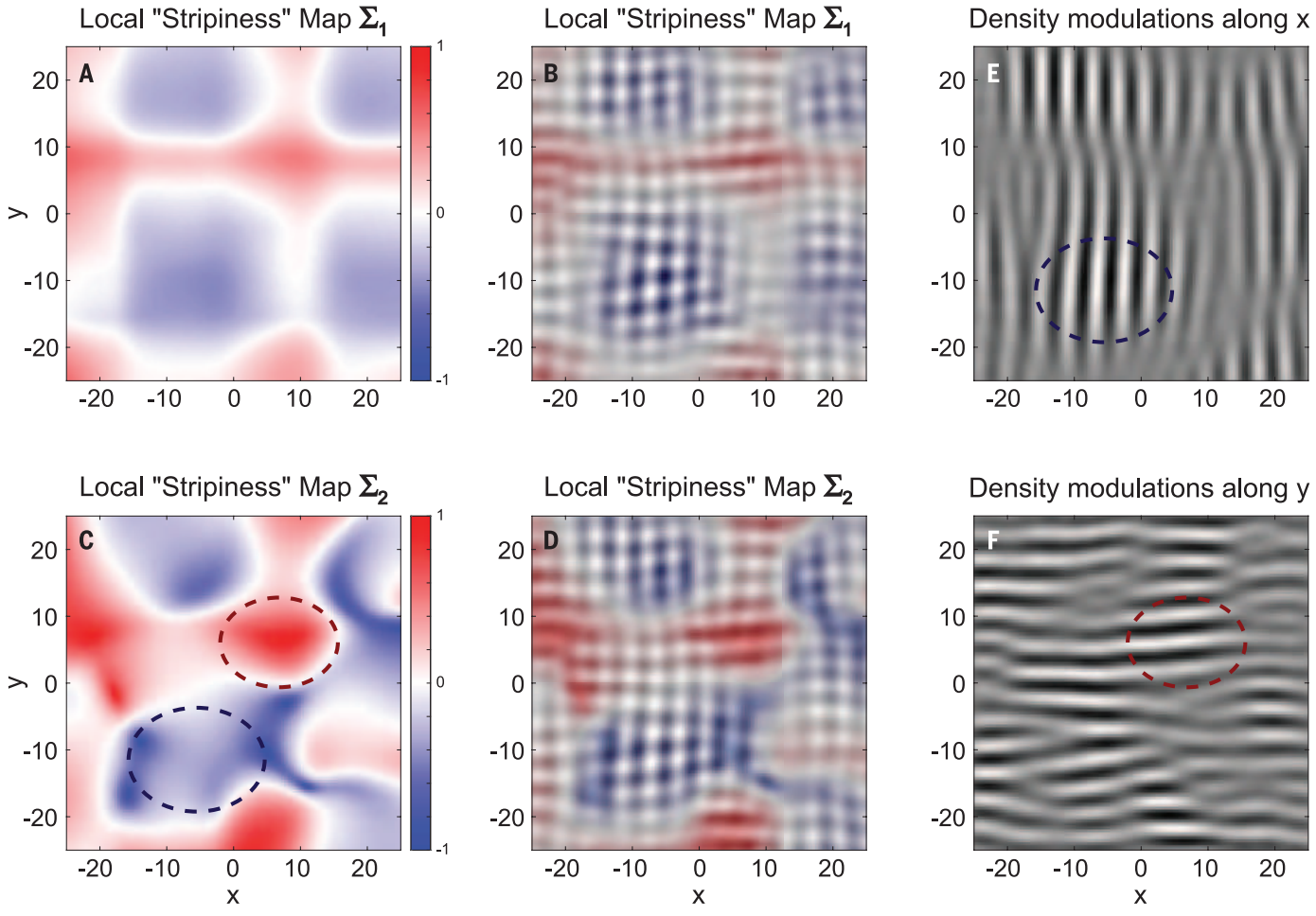

Fig. 1. Symmetry analysis in real and reciprocal space. (**A**) Map of the order parameter (local "stripiness") $\Sigma_1(\mathbf{r})$, calculated as outlined in the text, overlaid on top of the original map in (**B**). (**C** and **D**) Same as (A) and (B), but for the $\Sigma_2(\mathbf{r})$ order parameter. Density modulations along *x* (**E**) and *y* (**F**), extracted from the data set used in figure 1C of Fine's Comment [blue and red ellipses are the same as in (C)].

spatial points. This leads to $r_{\rho_x,\rho_y} \sim 0.25$, once again closer to the limit of pure stripe ($r_{\rho_x,\rho_y} = 0$) than checkerboard ($r_{\rho_x,\rho_y} = 1$) order.

In conclusion, the specific counterexample provided by Fine also belongs to the general case of a locally unidirectional charge modulation, albeit with partially overlapping 90°-rotated domains, as opposed to an actual checkerboard. Such a topology is more straightforward to distinguish from a native checkerboard in reciprocal space than it is in real space. Our analysis here highlights the compatibility of an overlapping stripe-domains' configuration with the momentum-space structure determined experimentally in our study. Finally, this also reaffirms our conclusion in favor of a microscopic symmetry breaking via charge stripe order, consistent with the strong anisotropy observed for the temperature evolution of the correlation length.

REFERENCES

1. R. Comin *et al.*, *Science* **347**, 1335–1339 (2015).
2. B. V. Fine, *Science* **351**, 235 (2016).
3. S. Kivelson *et al.*, *Rev. Mod. Phys.* **75**, 1201–1241 (2003).
4. K. Fujita *et al.*, *Science* **344**, 612–616 (2014).
5. A. Del Maestro, B. Rosenow, S. Sachdev, *Phys. Rev. B* **74**, 024520 (2006).
6. M. H. Hamidian *et al.*, arXiv:1507.07865 (2015).

28 June 2015; accepted 10 December 2015
10.1126/science.aac4778

REVIEW SUMMARY

VIRAL IMMUNITY

Transkingdom control of viral infection and immunity in the mammalian intestine

Julie K. Pfeiffer* and Herbert W. Virgin*

BACKGROUND: Viruses that infect the mammalian gastrointestinal tract have intimate relationships with the host, as well as members of the complex community of microbes that inhabit the intestine. The mammalian intestine contains the highest density of microbes in the body. These microbes, collectively referred to as the intestinal microbiota, include bacteria, archaea, fungi, viruses, and eukaryotes. Emerging data indicate that enteric viruses regulate, and are regulated by, these other microbes through a series of processes termed "transkingdom interactions." Recent advances have shed light on the nature and importance of these transkingdom interactions for enteric virus replication, transmission, and disease.

ADVANCES: The study of enteric virus pathogenesis has traditionally focused on viral virulence genes of classical pathogens and host immunity to these agents. Recent analysis of the viruses present in the intestine has revealed a dynamic and diverse taxonomic intestinal viral world (the enteric virome) featuring, in addition to recognized enteric viral pathogens, many new viruses and new relationships between known viral types and disease. We now know that enteric viral infection must be considered in light of the fact that viruses are part of a complex milieu of microbes and microbial products that directly and indirectly regulate viral pathogenesis. Thus, interactions of enteric viruses with other microbes are increasingly recognized as critical to viral infectivity, disease, and control. Studies leveraging the simple paradigm of examining enteric viruses in the intestine after natural oral infection have driven the field forward. It is now clear that members of the intestinal microbiome promote replication and transmission of enteric viruses from four different families: noroviruses, picornaviruses, retroviruses, and reoviruses. Therefore, the standard reductionist approach of understanding the pathogenesis of, and immunity to, viral infection in the context of a single virus interacting with a single host is too limited to capture the full range of relevant pathogenic mechanisms. This simple concept has broad implications for prevention and therapy of viral infections of great medical importance.

ON OUR WEB SITE

Read the full article at http://dx.doi.org/10.1126/science.aad5872

OUTLOOK: Despite recent rapid advances, there are still major gaps in our understanding of transkingdom control of enteric virus replication, pathogenesis, and transmission. Recognition of the important impact of the bacterial microbiota has advanced more rapidly than for any other component of the intestinal microbiota. A particular challenge for studies to comprehensively identify viruses within the enteric virome is their diversity and extreme sequence variability. A key direction for the field is to identify functional relationships governing transkingdom interactions in the intestine, including the dynamic coevolved relationship between the intestinal microbiota and innate and adaptive immunity. The field is now poised to define, in structural and biochemical terms, specific molecular mechanisms responsible for such transkingdom interactions. Future studies on the mammalian virome and transkingdom factors that influence viral infection may inspire new therapeutic approaches. In this Review, we explore the interplay between viruses, the microbiota, and host immune responses. We highlight how transkingdom interactions influence infection with mammalian enteric viruses, including pathogens. ■

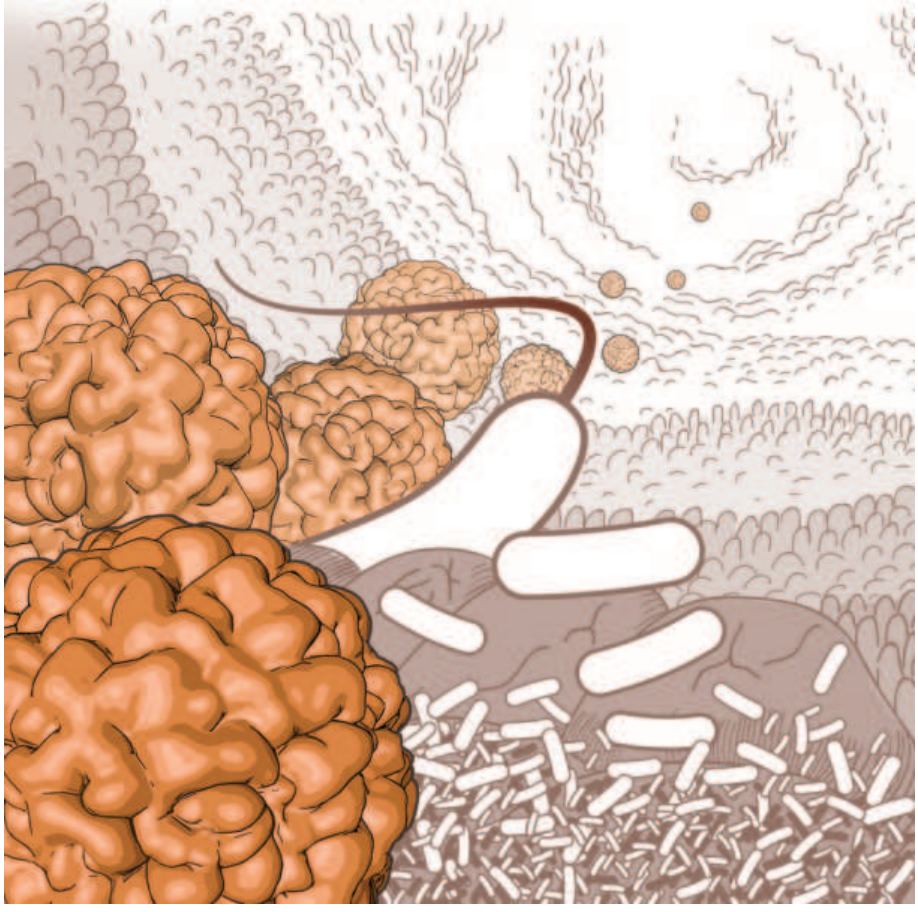

Intestinal microbiota promote enteric virus replication. Enteric viruses can interact with bacteria before initiating replication in the mammalian intestine. This illustration shows norovirus interacting with bacteria. Through these interactions, and/or through microbiota-mediated alteration of host immune responses, intestinal microbiota facilitate enteric virus replication in the gut. [Credit: K. Sutliff/*Science*]

The list of author affiliations is available in the full article online.
*Corresponding author. E-mail: julie.pfeiffer@utsouthwestern.edu (J.K.P.); virgin@wustl.edu (H.W.V.)
Cite this article as J. K. Pfeiffer and H. W. Virgin, *Science* 351, aad5872 (2016). DOI: 10.1126/science.aad5872

REVIEW

VIRAL IMMUNITY

Transkingdom control of viral infection and immunity in the mammalian intestine

Julie K. Pfeiffer[1]* and Herbert W. Virgin[2]*

Viruses that infect the intestine include major human pathogens (retroviruses, noroviruses, rotaviruses, astroviruses, picornaviruses, adenoviruses, herpesviruses) that constitute a serious public health problem worldwide. These viral pathogens are members of a large, complex viral community inhabiting the intestine termed "the enteric virome." Enteric viruses have intimate functional and genetic relationships with both the host and other microbial constituents that inhabit the intestine, such as the bacterial microbiota, their associated phages, helminthes, and fungi, which together constitute the microbiome. Emerging data indicate that enteric viruses regulate, and are in turn regulated by, these other microbes through a series of processes termed "transkingdom interactions." This represents a changing paradigm in intestinal immunity to viral infection. Here we review recent advances in the field and propose new ways in which to conceptualize this important area.

Enteric viruses include important human pathogens that spread in food, water, and through contact. These viruses encounter an incredible environment on entry into the gastrointestinal tract and have evolved their outer layers, either proteinaceous capsids or lipid envelopes, to manage and leverage this complex milieu. Peristalsis moves enteric viruses through an assortment of pH gradients, digestive enzymes, and microbes before they penetrate the mucus layer or cross intestinal M cells to infect the host. Both direct and indirect interactions of enteric viruses with other microbes and the host immune system are increasingly recognized as a critical aspect of their infectivity, disease induction, and control (Fig. 1). Perhaps this is not surprising, since these viruses must complete their life cycle in the intestine, which is one of the most complex microbial environments on Earth (*1*–*4*).

Over the past decade, many studies have examined the composition and, to a lesser extent, the function of microbes that inhabit the intestine and other body sites (*5*–*7*). In addition to bacteria, the intestine contains multiple other types of organisms that can have profound effects on mucosal and systemic immune responses, including viruses (*8*–*14*), fungi (*15*, *16*), and eukaryotes such as the protozoa *Blastocystis* (*17*) or helminths (*18*, *19*). Together, these organisms have been referred to as the microbiome or the microbiota. Given the emerging understanding of transkingdom interactions as determinants of host immunity and virus infection, it is possible that a large proportion of the unexplained variation in mammalian responses to infection may be due to interhost variation in the microbiota (*1*, *3*, *4*, *9*, *10*, *20*–*27*).

[1]Department of Microbiology, University of Texas Southwestern Medical Center, Dallas, TX 75390, USA. [2]Department of Pathology and Immunology, Washington University School of Medicine, St. Louis, MO 63110, USA. *Corresponding author. E-mail: julie.pfeiffer@utsouthwestern.edu (J.K.P.); virgin@wustl.edu (H.W.V.)

The enteric virome

Analysis of the intestinal virome has revealed a dynamic environment featuring both bacteriophages and multiple eukaryotic viruses. Viruses that infect systemic tissues or other mucosal surfaces such as the lung also influence the intestine in important ways, including via control of tissue homeostasis, healing, and the outcome of infection with bacterial pathogens (*23*, *28*). Viruses can even benefit the host by promoting immune development and influencing tissue architecture (*10*, *20*, *22*, *23*). It is now possible to understand, albeit incompletely, the taxonomic structure of the viruses present in the intestine. The task of identifying the individual viruses present is in its infancy because many sequences obtained in random or "shotgun" libraries of DNA and RNA from intestinal contents or mucosae cannot be effectively annotated, owing to weaknesses in databases and the lack of easy-to-use software. A particular problem has been a focus on sequencing only entities with DNA genomes when so many enteric viruses have RNA genomes.

It is nevertheless clear that the viral contents of the intestine are remarkably complex (*2*, *4*, *13*, *29*–*31*). It has been estimated that the intestine contains about 100 trillion prokaryotic cells (*32*), many of which carry temperate bacteriophages in their genomes. Bacteriophages that infect these prokaryotic organisms may be ~10-fold more abundant than their host cells (*1*, *4*, *33*). In addition, there is a eukaryotic virome in the asymptomatic host, with humans averaging at least 10 permanent systemic eukaryotic viral infections (*3*, *4*, *20*). A variety of enteric viruses infect humans, including members of the *Retroviridae*, *Adenoviridae*, *Astroviridae*, *Caliciviridae*, *Reoviridae*, and *Picornaviridae*, *Picobirnaviridae*, *Annelloviridae*, *and Circoviridae* families. Some of these infections are very common (e.g., norovirus and reovirus), whereas others are rare (e.g., poliovirus, a picornavirus). Infections range from asymptomatic to severe acute disease to severe chronic disease. Asymptomatic people can shed noroviruses for prolonged periods (*34*), and some strains of murine norovirus (MNoV) establish lifelong intestinal infection of mice (*34*–*36*). Several studies have identified enteric viruses in feces from asymptomatic people or other mammals (*3*, *37*–*42*); the intestine of healthy children can contain various eukaryotic viruses, including picobirnaviruses, adenoviruses, anelloviruses, astroviruses, caliciviruses, bocaviruses, enteroviruses, circoviruses, rotaviruses, and sapoviruses (*13*, *43*–*47*). Together, these data indicate that the enteric virome has been vastly underestimated. Thus, the number of prokaryotic and eukaryotic viruses that might contribute to, or be regulated by, transkingdom interactions relevant to the intestine is daunting.

Replication and transmission of mammalian enteric viruses

For successful propagation and transmission, enteric viruses must navigate several unique niches within the gastrointestinal tract. Fewer than 100 viral particles are frequently sufficient for infection with human enteric viruses such as norovirus, rotavirus, and poliovirus (*48*–*50*). Enteric viruses encounter low pH, proteolytic enzymes, microbiota, and intestinal mucus before replication in the intestine. Therefore, initiation of viral replication from the intestinal lumen is likely to be far more difficult than subsequent cycles of viral replication initiated by spread from previously infected intestinal cells or between cells in tissue culture. Different enteric viruses replicate in different cell types, ranging from enterocytes to lymphocytes to myeloid cells. After viral replication, progeny viruses are shed into the lumen, leading to transmission to new hosts.

Promotion of enteric viral infection by bacteria

To examine how intestinal microbes influence viral infection and transmission, many investigators use mouse models of infection, including antibiotic-treated animals or germ-free mice; each approach has pros and cons (*51*, *52*). Antibiotic treatment is relatively simple and inexpensive, but depletion of bacteria is incomplete and selective, depending on the antibiotic(s) used. Germ-free mice, while providing a "clean slate" devoid of all microbes, require specialized facilities and have immature intestinal architecture and immune responses compared with conventional mice; the organ targeted by enteric viruses is therefore abnormal. Mice are relatively resistant to a variety of human enteric pathogens, including many viruses and bacteria (*53*), rarely develop diarrhea, and cannot vomit. As a result, the general

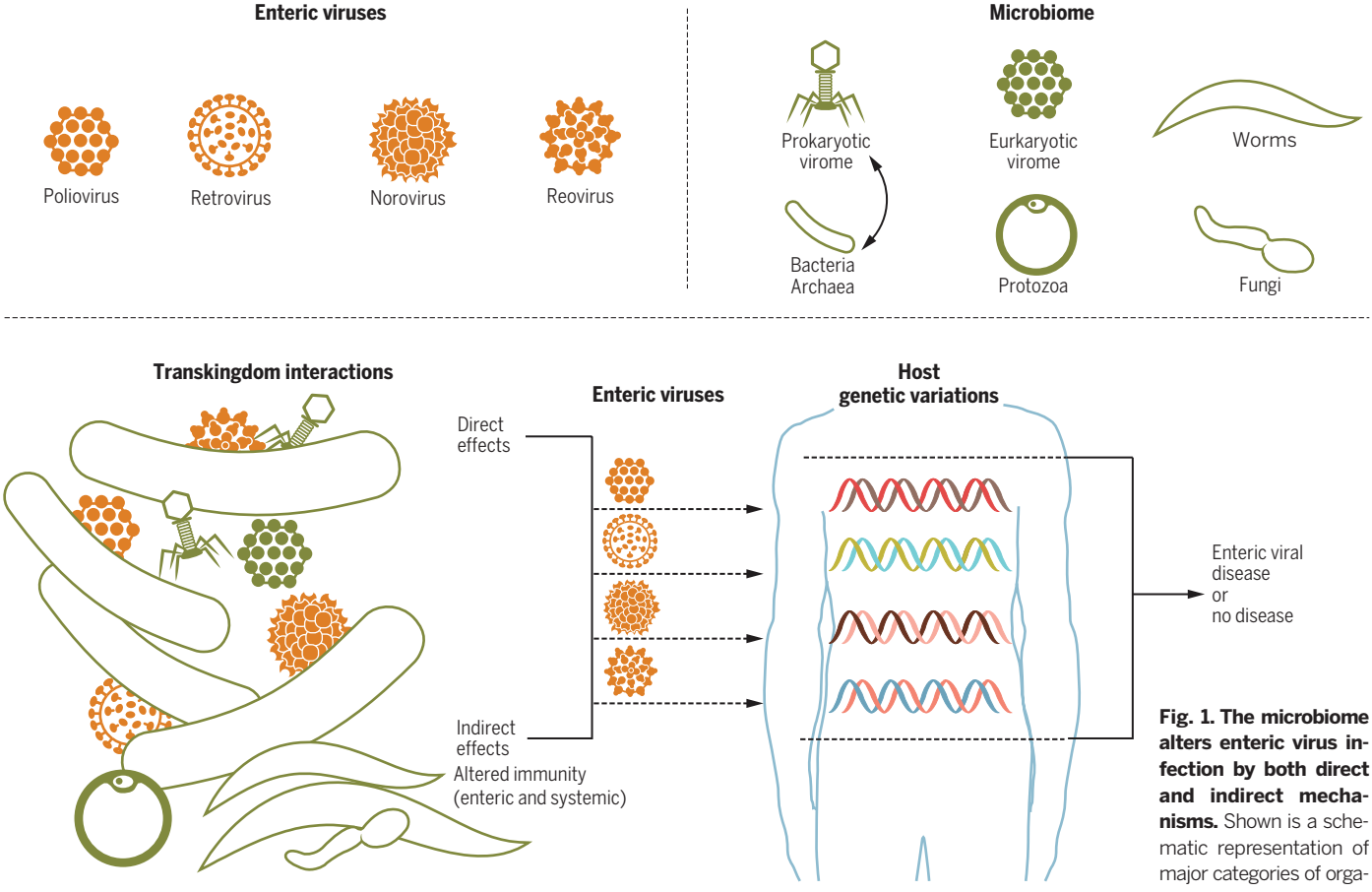

Fig. 1. The microbiome alters enteric virus infection by both direct and indirect mechanisms. Shown is a schematic representation of major categories of organisms in the intestinal microbiome that, in aggregate, affect enteric infection with the four viral taxa shown. In some cases, transkingdom interactions affect enteric viruses directly through physical interactions between viruses and organisms or components of organisms within the intestinal microbiome. In other cases, the microbiome regulated viral infection indirectly by altering immunity. Systemic viral infection can also alter intestinal virus infection. Host genes also affect these transkingdom interactions, and the ultimate outcome of virus-triggered disease, as shown on the right.

approach has been to examine human pathogens in immune-deficient and/or young mice and to examine mouse pathogens that are closely related to human pathogens in their natural host.

A combination of experiments using germ-free and antibiotic-treated mice infected with human and murine viruses has provided compelling evidence that the bacterial microbiota, through transkingdom interactions, influences viral infection (Fig. 2). Intestinal bacteria promote replication and transmission of enteric viruses from four different families in orally infected mice. Mouse mammary tumor virus (MMTV), a member of the *Retroviridae*, is spread from mother to offspring through milk. Experiments in germ-free mice demonstrate that intestinal bacteria are required for efficient MMTV transmission (*54*). Poliovirus, a member of the *Picornaviridae*, is spread by the fecal-oral route and can disseminate to the central nervous system. Intestinal bacteria enhance poliovirus replication, systemic pathogenesis, and fecal-oral transmission in mice (*55*, *56*). Intestinal microbes enhance replication and pathogenesis of reovirus and rotavirus, both members of the *Reoviridae*, in mice (*55*, *57*). MNoV, a member of the norovirus genus within the *Caliciviridae*, is commonly present in mouse facilities and is spread by the fecal-oral route. Several groups have shown that intestinal bacteria promote MNoV replication and persistence (*10*, *58*, *59*). Notably, the beneficial effects of the bacterial microbiota on enteric viruses are not observed when viruses are delivered by intraperitoneal injection that bypasses the natural oral infection route (*55*, *59*, *60*). This may explain why effects of the microbiota on enteric viruses were unrecognized until recently; many previous studies delivered virus by injection rather than the natural oral route.

Several enteric viruses that benefit from the bacterial microbiota bind bacterial surface polysaccharides, resulting in enhanced viral infectivity and pathogenesis. MMTV, a virus with a lipid bilayer envelope, binds lipopolysaccharide (LPS), a glycan on the surface of Gram-negative bacteria (*54*, *61*). As a consequence, viral infection initiates innate immune responses that culminate in host tolerance, viral replication, and transmission (Fig. 2). Poliovirus, a nonenveloped virus, binds LPS as well as peptidoglycan, a major component of the bacterial cell wall, enhancing viral attachment to host cells and promoting transmission by stabilizing viral particles and limiting thermal inactivation (*55*, *56*) (Fig. 2). Human norovirus, a nonenveloped virus, binds carbohydrate histo–blood group antigens (HBGAs) present on host cells and certain bacterial cells (*58*, *62*), facilitating human norovirus infection of B cells, likely through enhanced viral attachment to host cells (*58*) (Fig. 2). Collectively, these studies indicate that diverse viruses have evolved to bind to and benefit from bacterial surface glycans.

Regulation of intestinal immunity to viruses by the microbiota

The intestinal immune system has been extensively reviewed (*63*, *64*). Here we focus on recent data relevant to the role of immunity in transkingdom interactions that regulate virus infection.

The bacterial microbiota influences immunity to a variety of viruses. Recently, it has been shown that preexisting antibodies to enteric bacteria can skew vaccine responses to cross-reacting HIV-1 antigens, arguably rendering a vaccine less protective (*65*). Enteric bacterial components regulate vaccine responses to influenza in mice through activation of the innate immune receptor, Toll-like receptor 5 (TLR5) (*66*). Antibiotic treatment of mice has profound effects on antiviral immunity at another mucosal surface, the lung, since antibiotic treatment prevents normal innate and

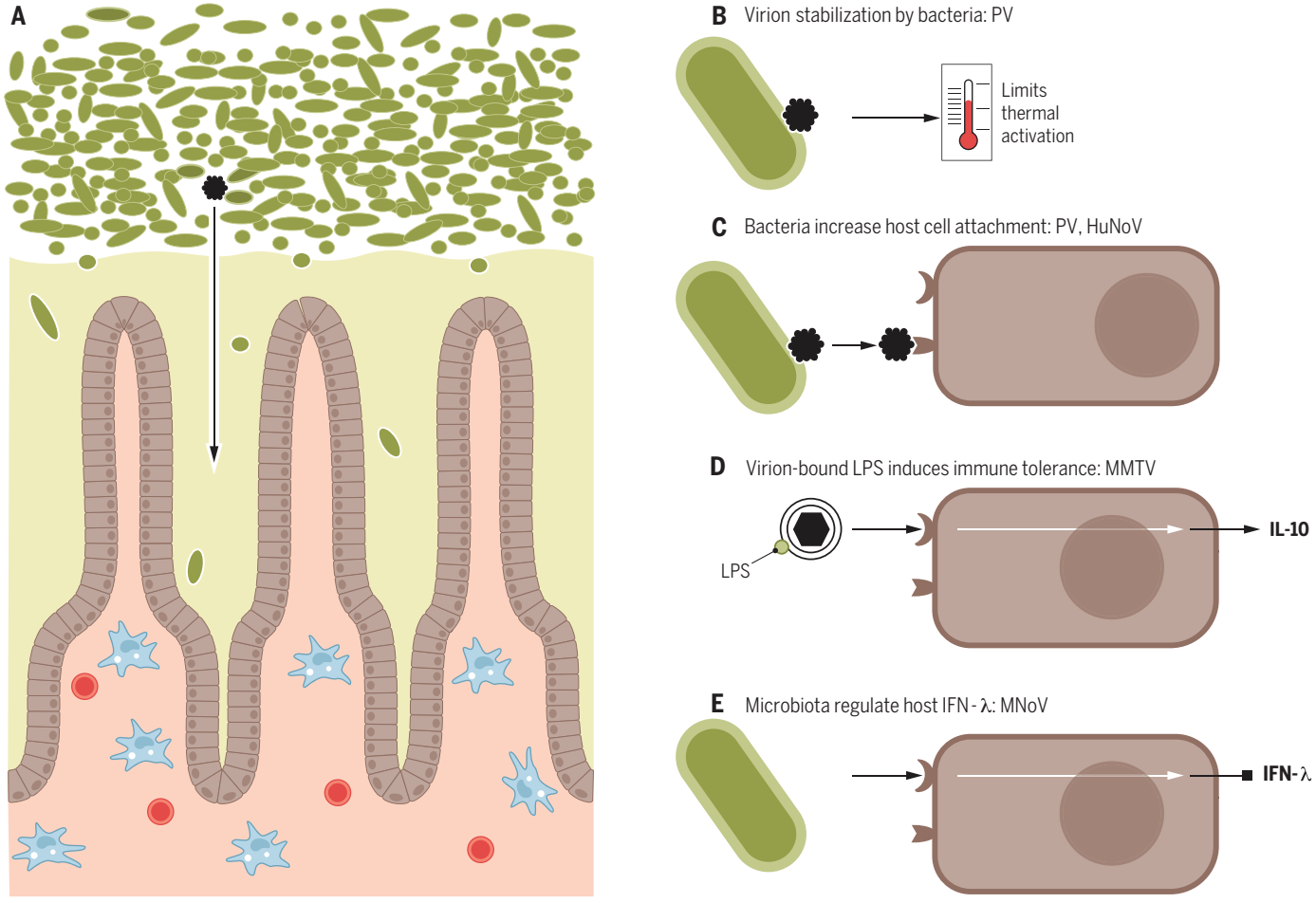

Fig. 2. Transkingdom interactions and mechanisms by which bacteria enhance enteric virus replication and transmission. (**A**) The intestinal environment includes bacteria (green) and other components of the microbiome, the mucus layer (yellow), host enterocytes (brown), and underlying immune cells (blue and red). Enteric viruses (black) are exposed to bacteria before initiating replication in host cells (enterocytes or immune cells, depending on the virus type). Bacteria promote enteric virus replication and transmission by several mechanisms. (**B**) Poliovirus (PV) binds bacteria, which stabilizes virions and limits premature RNA release to promote transmission. (**C**) PV and human norovirus (HuNoV) bind bacteria, which increases viral attachment to host cells. (**D**) Mouse mammary tumor virus (MMTV) binds LPS, which induces host TLR signaling and IL-10–mediated immune tolerance. (**E**) Murine norovirus (MNoV) replication is enhanced by bacteria, likely through regulation of IFN-λ responses.

adaptive immune responses to influenza, resulting in death of the host (*67*–*69*). These results underscore the importance of the bacterial microbiota for antiviral immune responses.

Members of the enteric microbiota in addition to bacteria, such as helminthic worms, also have profound effects on intestinal antiviral immunity. Helminth infection of mice inhibits intestinal antiviral immune CD8 T cell responses to MNoV (*70*), an effect that is independent of other members of the microbiota as it is observed in germ-free mice. Intestinal helminth infection also affects the control of systemic herpesvirus infection in mice (*71*). Here, helminths induce secretion of cytokines such as interleukin-4 (IL-4) or IL-13, which triggers transcription from specific viral promoters and subsequent reactivation from latency. This effect is evolutionarily conserved between murine and human γ-herpesviruses. Interestingly, in both of these studies, the effect of helminth infection was associated with worm-induced changes in macrophage differentiation. The role of macrophages in the control of intestinal biology is also suggested by the fact that systemic virus infection results in the production of type 1 interferons (IFNs), which through their effects on macrophages, substantially increase proliferation of intestinal epithelial cells, resulting in improved wound healing (*28*).

Bacterial molecules also have striking effects on immune signaling pathways relevant to enteric virus infection. Virus-associated LPS induces TLR4 signaling, culminating in IL-10–mediated immune tolerance and increased transmission of MMTV (*54*). Antibiotic treatment of mice prevents persistent enteric MNoV infection, an effect that is reversed by fecal transplantation (*59*). This action of antibiotics required the presence of the IFN-λ receptor, indicating that this signaling pathway is involved in transkingdom regulation of persistent enteric virus infection (Fig. 2). Together, these data indicate that, in addition to direct binding of bacterial components to viruses, the indirect effects of the enteric microbiota on immunity can have profound effects on viral infection.

One of the most interesting findings to come from studies of transkingdom interactions and viral infection is the discovery of sterilizing innate immunity in the intestine (*72*, *73*). Treatment of mice with IFN-λ effectively cured persistent MNoV infection in mice lacking T cells and B cells and therefore unable to mount an antigen-specific adaptive immune response. It is intriguing that enteric bacteria also control persistent enteric norovirus infection in a manner requiring the IFN-λ receptor, although the mechanisms connecting these two observations remain to be elucidated (*59*). In the case of rotavirus infection, treatment of mice with bacterial flagellin cured virus infection via a mechanism involving TLR signaling and induction of the cytokines IL-22 and IL-18. Again, viral clearance did not require adaptive immunity. It has recently been reported that IL-22 and IFN-λ can synergize to clear enteric rotavirus infection, suggesting a common

pathway for sterilizing innate immunity in the intestine (*74*). Strategies to enhance these innate immune mechanisms, perhaps by manipulating the enteric bacterial microbiota, may be useful for treating enteric virus infection independent of vaccine responses. These studies indicate the importance of analyzing transkingdom interactions that control enteric viral infection as a window into fundamental mechanisms of immunity.

Complex genetic interactions dictate outcomes

Given that transkingdom interactions govern enteric virus infection, it is not surprising that viral disease is dependent on interaction of microbes and viruses with host genes (Fig. 1). In one example, the combination of MNoV and a murine mutation in a human Crohn's disease susceptibility gene, *ATG16L1*, results in pathological abnormalities in intestinal Paneth cells when neither the host gene mutation nor the virus infection alone can induce these abnormalities (*9*, *75*). A similar process has been shown in studies of MNoV in combination with mutation of the immunoregulatory cytokine IL-10 (*24*). Notably, virus-triggered colonic pathology in each of these studies is dependent on intestinal bacteria. In the case of MNoV-*ATG16L1* interactions, treatment of mice with antibiotics ameliorated pathology, whereas in studies of MNoV–IL-10 interactions, pathology was ameliorated in germ-free mice. Thus, virus-induced pathology in the intestine can be driven by a transkingdom interaction with bacteria.

Viruses may also control intestinal bacteria by transferring genes between bacteria and through predator-prey relationships in which bacteriophages alter the taxonomic structure of the bacterial microbiota (*1*, *8*, *14*, *47*). These types of transkingdom interactions may have disease relevance. For example, in human Crohn's disease and ulcerative colitis, enteric bacteriophages become more taxonomically complex even as the bacterial microbiota becomes less diverse and taxonomically rich (*8*). This is consistent with disease-associated changes in predatory-prey relationships between viruses and bacteria. Taken together, these studies underscore the importance of transkingdom interactions, and the association of these events with host genetic variation, in dictating responses to infectious agents and inflammatory disease.

Future challenges

Although we have expanded our understanding of the virome and transkingdom control of enteric virus infection, several key challenges remain. First, a more thorough examination of the enteric virome, including both DNA and RNA viruses, and how it changes over time is essential. We do not fully understand all of the players in the complex dance of transkingdom interactions. Further, comparatively few studies have evaluated the intestinal mycobiome, the archaea, or the meiofauna. Characterizing the virome and other members of the enteric microbiota will allow investigators to more thoroughly explore the phenomenology of transkingdom control of viral infection, setting the stage for more mechanistic studies and therapeutic translation of novel concepts that arise.

Another challenge is making sense of multifactorial interactions that frequently have so many components related in nonlinear ways that they seem to defy analysis. It is likely that there will be more examples of mechanisms revealed only upon combined analysis of host genetics, components of the microbiota, and viral infection (*9*, *24*, *54*–*56*). Furthermore, environmental factors such as diet and circadian rhythms are likely to influence enteric viral infections (*76*–*78*). We are only taking the first steps on a long road into a new area of research in virology, but it is clear that we need to embrace this complexity if we are to fully understand viral pathogenesis and immunity.

Finally, we need to address whether new knowledge about enteric viruses gained by studies of transkingdom interactions can be used therapeutically. Although recent work implies that antibiotic treatment can have antiviral effects, this is clearly not a viable treatment option for enteric virus infections because of logistical issues and side effects, including disruption of the many positive effects that the bacterial microbiota has for the host. However, targeted therapies based on mechanistic insights into transkingdom interactions are more realistic. For example, treatment with IFN-λ or bacterial flagellin could have substantial effects on enteric virus infection (*72*, *73*). Furthermore, it is possible that some enteric viruses may benefit the host by providing immunoregulatory cues (*4*, *10*, *20*). Alterations of the infectivity of viruses by binding of bacterial or other microbiota components might alter virulence and immunogenicity. Identification of beneficial human enteric or systemic viruses may inform fecal transplant therapies.

Conclusion

The proviral effect of other microbes for enteric virus infection was revealed only recently, which is surprising considering that the technology required for most of the experiments has existed for many years. A simple conceptual advance, examining enteric viruses in the intestine after natural oral infection, was key for driving the field forward. Therefore, although reductionist experiments are important and aid our understanding of viral replication and pathogenesis, removing the complexity of the intestinal environment has apparently masked important biology.

Enteric viruses do not exist in a vacuum. They have evolved in the unique environment of the intestine for optimal replication and transmission. A complex interplay between viruses, bacteria, the host, and the environment determines the efficiency of viral replication, disease, and transmission. Recent work has shed light on factors that influence enteric virus infection. However, there are still major gaps in our understanding of enteric virus infection. Future studies on the mammalian virome and transkingdom factors that influence enteric viral infection may inspire new therapeutic approaches.

REFERENCES AND NOTES

1. B. A. Duerkop, L. V. Hooper, Resident viruses and their interactions with the immune system. *Nat. Immunol.* **14**, 654–659 (2013). doi: 10.1038/ni.2614; pmid: 23778792
2. J. M. Norman, S. A. Handley, H. W. Virgin, Kingdom-agnostic metagenomics and the importance of complete characterization of enteric microbial communities. *Gastroenterology* **146**, 1459–1469 (2014). doi: 10.1053/j.gastro.2014.02.001; pmid: 24508599
3. E. F. Foxman, A. Iwasaki, Genome-virome interactions: Examining the role of common viral infections in complex disease. *Nat. Rev. Microbiol.* **9**, 254–264 (2011). doi: 10.1038/nrmicro2541; pmid: 21407242
4. H. W. Virgin, The virome in mammalian physiology and disease. *Cell* **157**, 142–150 (2014). doi: 10.1016/j.cell.2014.02.032; pmid: 24679532
5. S. Naik *et al*., Commensal-dendritic-cell interaction specifies a unique protective skin immune signature. *Nature* **520**, 104–108 (2015). doi: 10.1038/nature14052; pmid: 25539086
6. D. T. Pride *et al*., Evidence of a robust resident bacteriophage population revealed through analysis of the human salivary virome. *ISME J.* **6**, 915–926 (2012). doi: 10.1038/ismej.2011.169; pmid: 22158393
7. J. Oh *et al*., NISC Comparative Sequencing Program, Biogeography and individuality shape function in the human skin metagenome. *Nature* **514**, 59–64 (2014). doi: 10.1038/nature13786; pmid: 25279917
8. J. M. Norman *et al*., Disease-specific alterations in the enteric virome in inflammatory bowel disease. *Cell* **160**, 447–460 (2015). doi: 10.1016/j.cell.2015.01.002; pmid: 25619688
9. K. Cadwell *et al*., Virus-plus-susceptibility gene interaction determines Crohn's disease gene Atg16L1 phenotypes in intestine. *Cell* **141**, 1135–1145 (2010). doi: 10.1016/j.cell.2010.05.009; pmid: 20602997
10. E. Kernbauer, Y. Ding, K. Cadwell, An enteric virus can functionally replace the beneficial cues provided by commensal bacteria. *Nature* **516**, 94 (2014).pmid: 25409145
11. S. Minot, S. Grunberg, G. D. Wu, J. D. Lewis, F. D. Bushman, Hypervariable loci in the human gut virome. *Proc. Natl. Acad. Sci. U.S.A.* **109**, 3962–3966 (2012). doi: 10.1073/pnas.1119061109; pmid: 22355105
12. A. Reyes *et al*., Viruses in the faecal microbiota of monozygotic twins and their mothers. *Nature* **466**, 334–338 (2010). doi: 10.1038/nature09199; pmid: 20631792
13. A. Reyes *et al*., Gut DNA viromes of Malawian twins discordant for severe acute malnutrition. *Proc. Natl. Acad. Sci. U.S.A.* **112**, 11941–11946 (2015). doi: doi:10.1073/pnas.1514285112; pmid: 26351661
14. A. Reyes, M. Wu, N. P. McNulty, F. L. Rohwer, J. I. Gordon, Gnotobiotic mouse model of phage-bacterial host dynamics in the human gut. *Proc. Natl. Acad. Sci. U.S.A.* **110**, 20236–20241 (2013). doi: 10.1073/pnas.1319470110; pmid: 24259713
15. I. D. Iliev *et al*., Interactions between commensal fungi and the C-type lectin receptor Dectin-1 influence colitis. *Science* **336**, 1314–1317 (2012). pmid: 22674328
16. D. M. Underhill, I. D. Iliev, The mycobiota: Interactions between commensal fungi and the host immune system. *Nat. Rev. Immunol.* **14**, 405–416 (2014). doi: 10.1038/nri3684; pmid: 24854590
17. S. M. Fletcher, D. Stark, J. Harkness, J. Ellis, Enteric protozoa in the developed world: A public health perspective. *Clin. Microbiol. Rev.* **25**, 420–449 (2012). doi: 10.1128/CMR.05038-11; pmid: 22763633
18. H. J. McSorley, J. P. Hewitson, R. M. Maizels, Immunomodulation by helminth parasites: Defining mechanisms and mediators. *Int. J. Parasitol.* **43**, 301–310 (2013). doi: 10.1016/j.ijpara.2012.11.011; pmid: 23291463
19. E. Stelekati, E. J. Wherry, Chronic bystander infections and immunity to unrelated antigens. *Cell Host Microbe* **12**, 458 (2012).
20. H. W. Virgin, E. J. Wherry, R. Ahmed, Redefining chronic viral infection. *Cell* **138**, 30–50 (2009). doi: 10.1016/j.cell.2009.06.036; pmid: 19596234
21. C. Moon *et al*., Vertically transmitted faecal IgA levels determine extra-chromosomal phenotypic variation. *Nature* **521**, 90–93 (2015). doi: 10.1038/nature14139; pmid: 25686606
22. E. S. Barton *et al*., Herpesvirus latency confers symbiotic protection from bacterial infection. *Nature* **447**, 326–329 (2007). doi: 10.1038/nature05762; pmid: 17507983

23. D. A. MacDuff *et al*., Phenotypic complementation of genetic immunodeficiency by chronic herpesvirus infection. *eLife* **4**, e04494 (2015). doi: 10.7554/eLife.04494; pmid: 25599590
24. M. Basic *et al*., Norovirus triggered microbiota-driven mucosal inflammation in interleukin 10-deficient mice. *Inflamm. Bowel Dis.* **20**, 431–443 (2014). doi: 10.1097/01.MIB.0000441346.86827.ed; pmid: 24487272
25. S. G. Hansen *et al*., Profound early control of highly pathogenic SIV by an effector memory T-cell vaccine. *Nature* **473**, 523–527 (2011). doi: 10.1038/nature10003; pmid: 21562493
26. S. G. Hansen *et al*., Effector memory T cell responses are associated with protection of rhesus monkeys from mucosal simian immunodeficiency virus challenge. *Nat. Med.* **15**, 293–299 (2009). pmid: 19219024
27. D. Furman *et al*., Cytomegalovirus infection enhances the immune response to influenza. *Sci. Transl. Med.* **7**, 281ra43 (2015). doi: 10.1126/scitranslmed.aaa2293; pmid: 25834109
28. L. Sun *et al*., Type I interferons link viral infection to enhanced epithelial turnover and repair. *Cell Host Microbe* **17**, 85–97 (2015). doi: 10.1016/j.chom.2014.11.004; pmid: 25482432
29. C. Moon, T. S. Stappenbeck, Viral interactions with the host and microbiota in the intestine. *Curr. Opin. Immunol.* **24**, 405–410 (2012). doi: 10.1016/j.coi.2012.05.002; pmid: 22626624
30. P. J. Turnbaugh *et al*., The human microbiome project. *Nature* **449**, 804–810 (2007). doi: 10.1038/nature06244; pmid: 17943116
31. R. E. Ley *et al*., Evolution of mammals and their gut microbes. *Science* **320**, 1647–1651 (2008). doi: 10.1126/science.1155725; pmid: 18497261
32. W. B. Whitman, D. C. Coleman, W. J. Wiebe, Prokaryotes: The unseen majority. *Proc. Natl. Acad. Sci. U.S.A.* **95**, 6578–6583 (1998). doi: 10.1073/pnas.95.12.6578; pmid: 9618454
33. S. Minot *et al*., Rapid evolution of the human gut virome. *Proc. Natl. Acad. Sci. U.S.A.* **110**, 12450–12455 (2013). doi: 10.1073/pnas.1300833110; pmid: 23836644
34. S. M. Karst, C. E. Wobus, I. G. Goodfellow, K. Y. Green, H. W. Virgin, Advances in norovirus biology. *Cell Host Microbe* **15**, 668–680 (2014). doi: 10.1016/j.chom.2014.05.015; pmid: 24922570
35. L. B. Thackray *et al*., Murine noroviruses comprising a single genogroup exhibit biological diversity despite limited sequence divergence. *J. Virol.* **81**, 10460–10473 (2007). doi: 10.1128/JVI.00783-07; pmid: 17652401
36. T. J. Nice, D. W. Strong, B. T. McCune, C. S. Pohl, H. W. Virgin, A single-amino-acid change in murine norovirus NS1/2 is sufficient for colonic tropism and persistence. *J. Virol.* **87**, 327–334 (2013). doi: 10.1128/JVI.01864-12; pmid: 23077309
37. L. Li *et al*., The fecal viral flora of California sea lions. *J. Virol.* **85**, 9909–9917 (2011). doi: 10.1128/JVI.05026-11; pmid: 21795334
38. S. R. Finkbeiner *et al*., Metagenomic analysis of human diarrhea: Viral detection and discovery. *PLOS Pathog.* **4**, e1000011 (2008). doi: 10.1371/journal.ppat.1000011; pmid: 18398449
39. S. A. Handley *et al*., Pathogenic simian immunodeficiency virus infection is associated with expansion of the enteric virome. *Cell* **151**, 253–266 (2012). doi: 10.1016/j.cell.2012.09.024; pmid: 23063120
40. T. Shan *et al*., The fecal virome of pigs on a high-density farm. *J. Virol.* **85**, 11697–11708 (2011). doi: 10.1128/JVI.05217-11; pmid: 21900163
41. T. G. Phan *et al*., The fecal viral flora of wild rodents. *PLOS Pathog.* **7**, e1002218 (2011). doi: 10.1371/journal.ppat.1002218; pmid: 21909269
42. I. Smith, L. F. Wang, Bats and their virome: An important source of emerging viruses capable of infecting humans. *Curr. Opin. Virol.* **3**, 84–91 (2013). doi: 10.1016/j.coviro.2012.11.006; pmid: 23265969
43. B. Kapusinszky, P. Minor, E. Delwart, Nearly constant shedding of diverse enteric viruses by two healthy infants. *J. Clin. Microbiol.* **50**, 3427–3434 (2012). doi: 10.1128/JCM.01589-12; pmid: 22875894
44. T. G. Phan *et al*., A third gyrovirus species in human faeces. *J. Gen. Virol.* **93**, 1356–1361 (2012). doi: 10.1099/vir.0.041731-0; pmid: 22422066
45. J. G. Victoria *et al*., Metagenomic analyses of viruses in stool samples from children with acute flaccid paralysis. *J. Virol.* **83**, 4642–4651 (2009). doi: 10.1128/JVI.02301-08; pmid: 19211756
46. S. Roux, S. J. Hallam, T. Woyke, M. B. Sullivan, Viral dark matter and virus-host interactions resolved from publicly available microbial genomes. *eLife* **4**, e08490 (2015). doi: 10.7554/eLife.08490; pmid: 26200428
47. E. S. Lim *et al*., Early life dynamics of the human gut virome and bacterial microbiome in infants. *Nat. Med.* **21**, 1228–1234 (2015). doi: 10.1038/nm.3950; pmid: 26366711
48. R. L. Ward *et al*., Human rotavirus studies in volunteers: Determination of infectious dose and serological response to infection. *J. Infect. Dis.* **154**, 871–880 (1986). doi: 10.1093/infdis/154.5.871; pmid: 3021869
49. M. Katz, S. A. Plotkin, Minimal infective dose of attenuated poliovirus for man. *Am. J. Public Health Nations Health* **57**, 1837–1840 (1967). doi: 10.2105/AJPH.57.10.1837; pmid: 4293371
50. P. F. Teunis *et al*., Norwalk virus: How infectious is it? *J. Med. Virol.* **80**, 1468–1476 (2008). doi: 10.1002/jmv.21237; pmid: 18551613
51. C. M. Robinson, J. K. Pfeiffer, Viruses and the microbiota. *Annu. Rev. Virol.* **1**, 55–69 (2014). doi: 10.1146/annurev-virology-031413-085550; pmid: 25821837
52. L. V. Hooper, D. R. Littman, A. J. Macpherson, Interactions between the microbiota and the immune system. *Science* **336**, 1268–1273 (2012). doi: 10.1126/science.1223490; pmid: 22674334
53. A. B. Sabin, Pathogenesis of poliomyelitis; reappraisal in the light of new data. *Science* **123**, 1151–1157 (1956). doi: 10.1126/science.123.3209.1151; pmid: 13337331
54. M. Kane *et al*., Successful transmission of a retrovirus depends on the commensal microbiota. *Science* **334**, 245–249 (2011). doi: 10.1126/science.1210718; pmid: 21998394
55. S. K. Kuss *et al*., Intestinal microbiota promote enteric virus replication and systemic pathogenesis. *Science* **334**, 249–252 (2011). pmid: 21998395
56. C. M. Robinson, P. R. Jesudhasan, J. K. Pfeiffer, Bacterial lipopolysaccharide binding enhances virion stability and promotes environmental fitness of an enteric virus. *Cell Host Microbe* **15**, 36–46 (2014). pmid: 24439896
57. R. Uchiyama, B. Chassaing, B. Zhang, A. T. Gewirtz, Antibiotic treatment suppresses rotavirus infection and enhances specific humoral immunity. *J. Infect. Dis.* **210**, 171–182 (2014). doi: 10.1093/infdis/jiu037; pmid: 24436449
58. M. K. Jones *et al*., Enteric bacteria promote human and mouse norovirus infection of B cells. *Science* **346**, 755–759 (2014). pmid: 25378626
59. M. T. Baldridge *et al*., Commensal microbes and interferon-λ determine persistence of enteric murine norovirus infection. *Science* **347**, 266–269 (2015). doi: 10.1126/science.1258025; pmid: 25431490
60. J. Schaffer, P. R. Beamer, P. C. Trexler, G. Breidenbach, D. N. Walcher, Response of germ-free animals to experimental virus monocontamination. I. Observation on Coxsackie B virus. *Proc. Soc. Exp. Biol. Med.* **112**, 561–564 (1963). doi: 10.3181/00379727-112-28105; pmid: 13976644
61. J. Wilks *et al*., Mammalian lipopolysaccharide receptors incorporated into the retroviral envelope augment virus transmission. *Cell Host Microbe* **18**, 456–462 (2015). doi: 10.1016/j.chom.2015.09.005; pmid: 26468748
62. T. Miura *et al*., Histo-blood group antigen-like substances of human enteric bacteria as specific adsorbents for human noroviruses. *J. Virol.* **87**, 9441–9451 (2013). doi: 10.1128/JVI.01060-13; pmid: 23804639
63. K. Honda, D. R. Littman, The microbiome in infectious disease and inflammation. *Annu. Rev. Immunol.* **30**, 759–795 (2012). doi: 10.1146/annurev-immunol-020711-074937; pmid: 22224764
64. I. I. Ivanov II, K. Honda, Intestinal commensal microbes as immune modulators. *Cell Host Microbe* **12**, 496–508 (2012). doi: 10.1016/j.chom.2012.09.009; pmid: 23084918
65. W. B. Williams *et al*., Diversion of HIV-1 vaccine-induced immunity by gp41-microbiota cross-reactive antibodies. *Science* **349**, aab1253 (2015). doi: 10.1126/science.aab1253; pmid: 26229114
66. J. Z. Oh *et al*., TLR5-mediated sensing of gut microbiota is necessary for antibody responses to seasonal influenza vaccination. *Immunity* **41**, 478–492 (2014). doi: 10.1016/j.immuni.2014.08.009; pmid: 25220212
67. W. C. Dolowy, R. L. Muldoon, Studies of germfree animals. I. Response of mice to infection with influenza A virus. *Proc. Soc. Exp. Biol. Med.* **116**, 365–371 (1964). doi: 10.3181/00379727-116-29249; pmid: 14189140
68. T. Ichinohe *et al*., Microbiota regulates immune defense against respiratory tract influenza A virus infection. *Proc. Natl. Acad. Sci. U.S.A.* **108**, 5354–5359 (2011). doi: 10.1073/pnas.1019378108; pmid: 21402903
69. M. C. Abt *et al*., Commensal bacteria calibrate the activation threshold of innate antiviral immunity. *Immunity* **37**, 158–170 (2012). doi: 10.1016/j.immuni.2012.04.011; pmid: 22705104
70. L. C. Osborne *et al*., Coinfection. Virus-helminth coinfection reveals a microbiota-independent mechanism of immunomodulation. *Science* **345**, 578–582 (2014). pmid: 25082704
71. T. A. Reese *et al*., Helminth infection reactivates latent γ-herpesvirus via cytokine competition at a viral promoter. *Science* **345**, 573–577 (2014). pmid: 24968940
72. B. Zhang *et al*., Viral infection. Prevention and cure of rotavirus infection via TLR5/NLRC4-mediated production of IL-22 and IL-18. *Science* **346**, 861–865 (2014). pmid: 25395539
73. T. J. Nice *et al*., Interferon-λ cures persistent murine norovirus infection in the absence of adaptive immunity. *Science* **347**, 269–273 (2015). doi: 10.1126/science.1258100; pmid: 25431489
74. P. P. Hernández *et al*., Interferon-λ and interleukin 22 act synergistically for the induction of interferon-stimulated genes and control of rotavirus infection. *Nat. Immunol.* **16**, 698–707 (2015). pmid: 26006013
75. K. Cadwell *et al*., A key role for autophagy and the autophagy gene Atg16l1 in mouse and human intestinal Paneth cells. *Nature* **456**, 259–263 (2008). doi: 10.1038/nature07416; pmid: 18849966
76. D. Hickman *et al*., The effect of malnutrition on norovirus infection. *MBio* **5**, e01032-e13 (2014). doi: 10.1128/mBio.01032-13; pmid: 24595373
77. X. Yu *et al*., T_H17 cell differentiation is regulated by the circadian clock. *Science* **342**, 727–730 (2013). pmid: 24202171
78. C. A. Thaiss *et al*., Transkingdom control of microbiota diurnal oscillations promotes metabolic homeostasis. *Cell* **159**, 514–529 (2014). pmid: 25417104

ACKNOWLEDGMENTS

We thank members of our laboratories for useful discussions and comments on the manuscript. J.K.P. is supported by NIH grants R01 AI074668 and R21 AI114927 and a Burroughs Wellcome Fund Investigators in the Pathogenesis of Infectious Diseases Award. H.W.V. is supported by U19 AI109725, R24 OD019793, R01 AI111918, R01 DK 101354, Kenneth Rainin Foundation grant no. 14H16, and Juvenile Diabetes Research Foundation grant 2-SRA-2015-305-Q-R.

10.1126/science.aad5872

RESEARCH ARTICLE

ORGANIC CHEMISTRY

Strain-release amination

Ryan Gianatassio,[1*] Justin M. Lopchuk,[1*] Jie Wang,[1] Chung-Mao Pan,[1] Lara R. Malins,[1] Liher Prieto,[1] Thomas A. Brandt,[2] Michael R. Collins,[3] Gary M. Gallego,[3] Neal W. Sach,[3] Jillian E. Spangler,[3] Huichin Zhu,[3] Jinjiang Zhu,[3] Phil S. Baran[1]†

To optimize drug candidates, modern medicinal chemists are increasingly turning to an unconventional structural motif: small, strained ring systems. However, the difficulty of introducing substituents such as bicyclo[1.1.1]pentanes, azetidines, or cyclobutanes often outweighs the challenge of synthesizing the parent scaffold itself. Thus, there is an urgent need for general methods to rapidly and directly append such groups onto core scaffolds. Here we report a general strategy to harness the embedded potential energy of effectively spring-loaded C–C and C–N bonds with the most oft-encountered nucleophiles in pharmaceutical chemistry, amines. Strain-release amination can diversify a range of substrates with a multitude of desirable bioisosteres at both the early and late stages of a synthesis. The technique has also been applied to peptide labeling and bioconjugation.

Systematic structural tuning of drug candidates, or leads, is an essential feature of medicinal chemistry research. Exchanging substituents that exhibit similar yet distinct properties in biological environments, termed "bioisosteres," can address a myriad of structural liabilities, circumventing issues such as unwanted metabolic clearance. Such structures also serve to combat the continued challenge of narrowing intellectual property space (*1*). These motifs can be rather unusual in that they are often not found in natural products: Fluoroalkyl groups (*2*, *3*) and strained ring systems that include small spirocycles and bicycles are examples (*4*). Interest in the latter area was fueled by an ongoing program at Pfizer (*5*), where difficulties in the synthesis of bicyclo[1.1.1]pentan-1-amine (**2**, Fig. 1A) led to the abandonment of a lead oncology clinical candidate (*6*). Developments in the synthesis of this strained motif date back to 1970 with Wiberg's classic synthesis of **2** from bicyclo[1.1.1]pentane in four steps via the intermediacy of bicyclo[1.1.1]pentan-1-carboxylic acid (see fig. S1) (*7*). Although this pioneering work allowed synthetic access to **2** and subsequent studies pointed to the counterintuitive stability of **A**, many improvements were carried out over the ensuing 46 years (*8*–*10*). All of these reports required ≥3 steps to form amine **2** because of the need for multiple functional group interconversions, rendering Pfizer's current in-house approach unsustainable (*10*). More globally, conventional preparations of substituted bicyclo[1.1.1]pentan-1-amine **1** have required the synthesis of the parent amine **2**, followed by amide formation (*11*) or substitution chemistry (*12*), limiting the retrosynthetic analysis of lead compounds such as **3** (*13*). The goal of this work was to solve both of these issues by (i) the invention of a process-friendly synthesis of amine **2**; and (ii) development of a route to **1** that does not even require the intermediacy of **2**, bypassing conventional retrosynthetic logic. Our strategy to address these challenges was to embrace the innate reactivity of the most strained C–C bond present in propellane **A** (~60 kcal/mol are stored in this bond) (*14*) by engaging it directly with an amine. This concept was then extended to other systems containing "spring-loaded" bonds (*15*, *16*) as a general tool to append small, cyclic bioisoteric motifs (**4** → **5**–**7**, Fig. 1B). We describe the preparation and use of convenient "strain-release reagents" (such as **A** to **C**) to expand chemical space for drug discovery: Specifically, the introduction of motifs such as bicyclo[1.1.1.]pentanes, azetidines, and cyclobutanes is delineated. The exquisite chemoselectivity of this approach has also been established, and initial applications to the areas of peptide labeling and bioconjugation are reported (see below). This work lays a foundation for the synthesis of new chemical entities, probe molecules, and clicklike

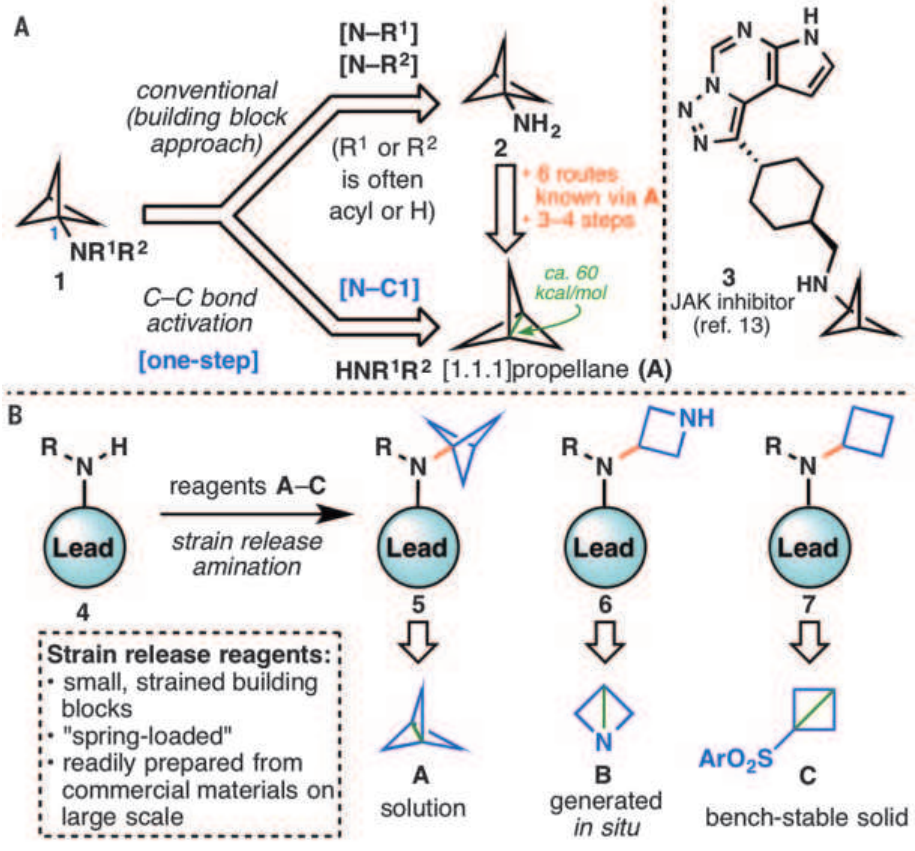

Fig. 1. Synthetic methods for incorporating small, strained ring systems. (**A**) Revisiting the retrosynthetic disconnection of an important scaffold in medicinal chemistry, bicyclo[1.1.1]pentan-1-amine. (**B**) Strain-release amination: "any-stage" functionalization of lead compounds in drug discovery.

[1]Department of Chemistry, The Scripps Research Institute, 10550 North Torrey Pines Road, La Jolla, CA 92037, USA. [2]Chemical Research and Development, Pfizer Worldwide Research and Development, Eastern Point Road, Groton, CT 06340, USA. [3]Department of Chemistry, La Jolla Laboratories, Pfizer Inc., 10770 Science Center Drive, San Diego, CA 92121, USA.
*These authors contributed equally to this work.
†Corresponding author. E-mail: pbaran@scripps.edu

connections that rely on the native activation of strained C–C bonds.

Application of propellane strain-release amination

As mentioned above, efforts in this area were initiated on account of the practical difficulties encountered at Pfizer in procuring large quantities of bicyclo[1.1.1]pentan-1-amine **2** (Fig. 2A). The tendency of propellane **A** to react with strong nucleophiles such as *t*-BuLi and aryl Grignard reagents inspired our approach (*17*, *18*). Extensive exploration (see table S1) identified Davies-type amine nucleophiles (Bn_2N-Li) (*19*) as a good starting point, furnishing **9** in ~20% yield. The key breakthrough was the finding that the corresponding turbo-amide (*20*) ($Bn_2NMgCl{\bullet}LiCl$) led to clean formation of **9** even on a >100 g scale. The use of PhLi leads to reproducible, scalable, and clean formation of propellane **A**. The dibenzyl group was then easily removed, and the HCl salt of **2** was precipitated (30 g scale). This protocol was successfully scaled up at an outsourcing vendor and can now be used in a process setting to deliver bicyclo[1.1.1]pentan-1-amine–containing clinical candidates economically on scale.

With a reliable route to stock solutions of propellane **A** (after codistillation with Et_2O, solution is stable for weeks to months at –20°C or –78°C, respectively), the scope of this direct "propellerization" was explored (Fig. 2B). Strain-release amination of **A** using a variety of in situ–derived turbo amides delivered a wide range of tertiary amines containing the valuable bicyclo[1.1.1]pentane bioisosteric motif. Figure 2 illustrates 29 different amines varying in complexity that can be easily accessed. In cases when the reaction did not go to completion, the starting amine could be recovered (e.g., **16**, **24**, **38**). The method tolerates a variety of functional groups, including acetals (**16**), benzyl ethers (**17**), ketals (**23**), and Lewis-basic groups (**21, 22, 27, 28, 30–32, 37, 38**).

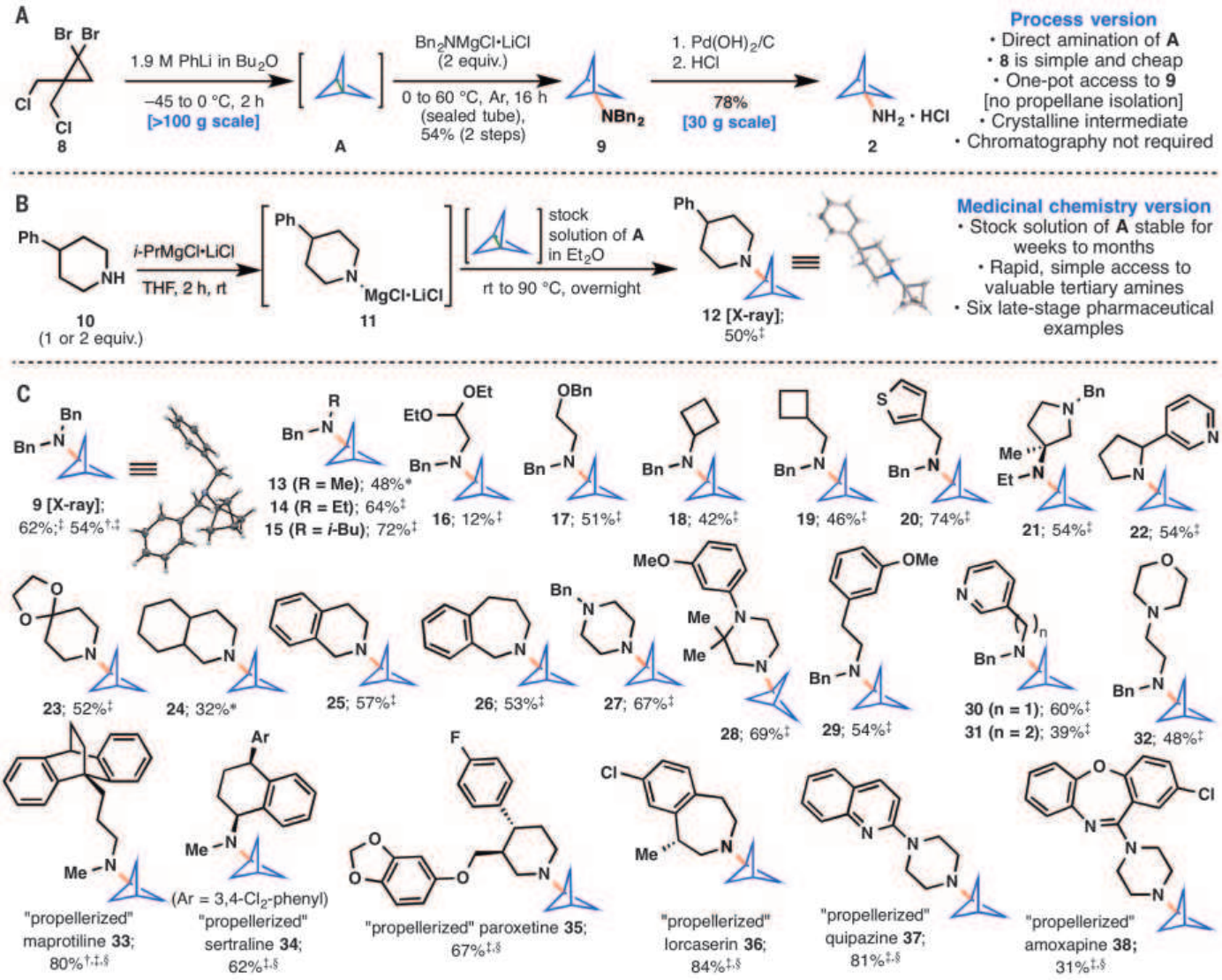

Conditions: *Amine substrate (1 equiv.); †The HCl salt of the amine starting material was used; ‡Conditions: Amine substrate (2 equiv.); §The extra equivalent of the amine starting material was recovered in *ca.* 90% yield (See SM for details); ‖rt = room temperature

Fig. 2. "Propellerization" of amine-containing substrates. Isolated yields are reported. (**A**) An improved synthesis of the known bicyclo[1.1.1]pentan-1-amine. (**B**) A general "propellerization" of amines enabled by strain-release reagents. (**C**) Substrate scope of amine-containing substrates.

Late-stage incorporation of this challenging bioisostere onto six different commercial drugs (Fig. 2C, **33**-**38**) obviated otherwise laborious multistep sequences to access these analogs. The use of turbo-amides is key to enabling the "any-stage" functionalization of both simple and complex amines with **A**. We anticipate that the path to these bioisosteres will find immediate and widespread use in medicinal chemistry. Indeed, this chemistry has already been field-tested at Pfizer (for example, compounds **14, 15, 17, 19, 21,** and **30** were prepared at Pfizer for use in ongoing programs).

Introduction of azetidine via strain release

The documented use of azetidines as a tactic to both rigidify amine backbones and serve as phenyl bioisosteres inspired the evaluation of a similar approach (*1*, *20*). Like the propellane systems, access to amino-azetidines is largely limited to a building-block approach that relies on the multistep synthesis of protected azetidinones (*21*). Strain-release amination of **B** was therefore evaluated as a means to simplify the preparation of such compounds. Isolated examples of the addition of nucleophiles to **B** are known but require superstoichiometric amounts of Lewis acids and only work with dibenzyl amine, anilines, and thiols (*22*). As depicted in Fig. 3, the addition of in situ–generated turbo-amides to a solution of in situ–generated **B** leads cleanly to azetidinylated products (**42**–**59**) that are subsequently trapped with a variety of acylating agents to simplify isolation and handling (free azetidines can be generated if desired). Using this protocol, azetidines were directly appended to 18 different amines varying in complexity, including three pharmaceutical agents.

Introduction of cyclobutane via strain release

Given the variety of medicinal contexts in which cyclobutane derivatives have been enlisted (*23*), we next explored a strain-release approach for this motif. The goal was to generate a stable reagent that would enable both rapid and mild "cyclobutylation" of amines but also permit further functionalization of intermediate adducts. Bicyclobutane and its substituted derivatives, since their first preparation in 1959 (*24*), have been the subject of many synthetic studies, most of which either engaged the strained system as a nucleophile or cleaved the center bond via a transition metal–mediated process (*25*, *26*). Rather than pursuing the parent bicyclobutane (a gas at room temperature) (*27*), we appended an arylsulfonyl group as a means to both activate the strained C–C bond and render the reagent bench stable. Encouragingly, a few examples have been reported wherein benzylamine, when employed as a solvent, could be added to phenylsulfonyl-substituted bicyclobutanes at 140°C (*28*, *29*). In seeking a reagent that would allow for more mild reaction conditions and the use of the amine as a limiting reagent, we synthesized a variety of substituted phenylsulfonylated bicyclobutanes (**C2** to **C7**, Fig. 4) and evaluated them in a strain-release amination with amine **39**. Not surprisingly, aryl sulfones containing electron-withdrawing substituents were the most reactive, and the addition of LiCl further accelerated the amination. Removal of the arylsulfonyl group could be easily achieved in the same pot under mild reductive conditions (Mg, MeOH). This protocol was applied to 16 diverse amines with the use of reagent **C7**, including four commercial drugs, to append the cyclobutyl group (Fig. 4B). The reaction of **C7** is chemoselective for amines in the presence of free hydroxyl groups; **71** could be prepared from 4-hydroxypiperidine in 43% yield over three steps (see supplementary materials for details). The arylsulfonyl group could also be used as a handle to generate other useful cyclobutane building blocks containing deuterium (**77**), alkyl (**78**), fluorine (**79**), and olefin (**80**) substituents. Strain-release amination is not limited to the three ring systems described here, as illustrated in Fig. 4D, wherein cyclopentane (*30*) could be easily appended to 1,2,3,4-tetrahydroisoquinoline (**81** → **83**) and *N*-benzylpiperazine (**84** → **85**). Given these collective findings, we anticipate that a wide range of strained C–C bonds

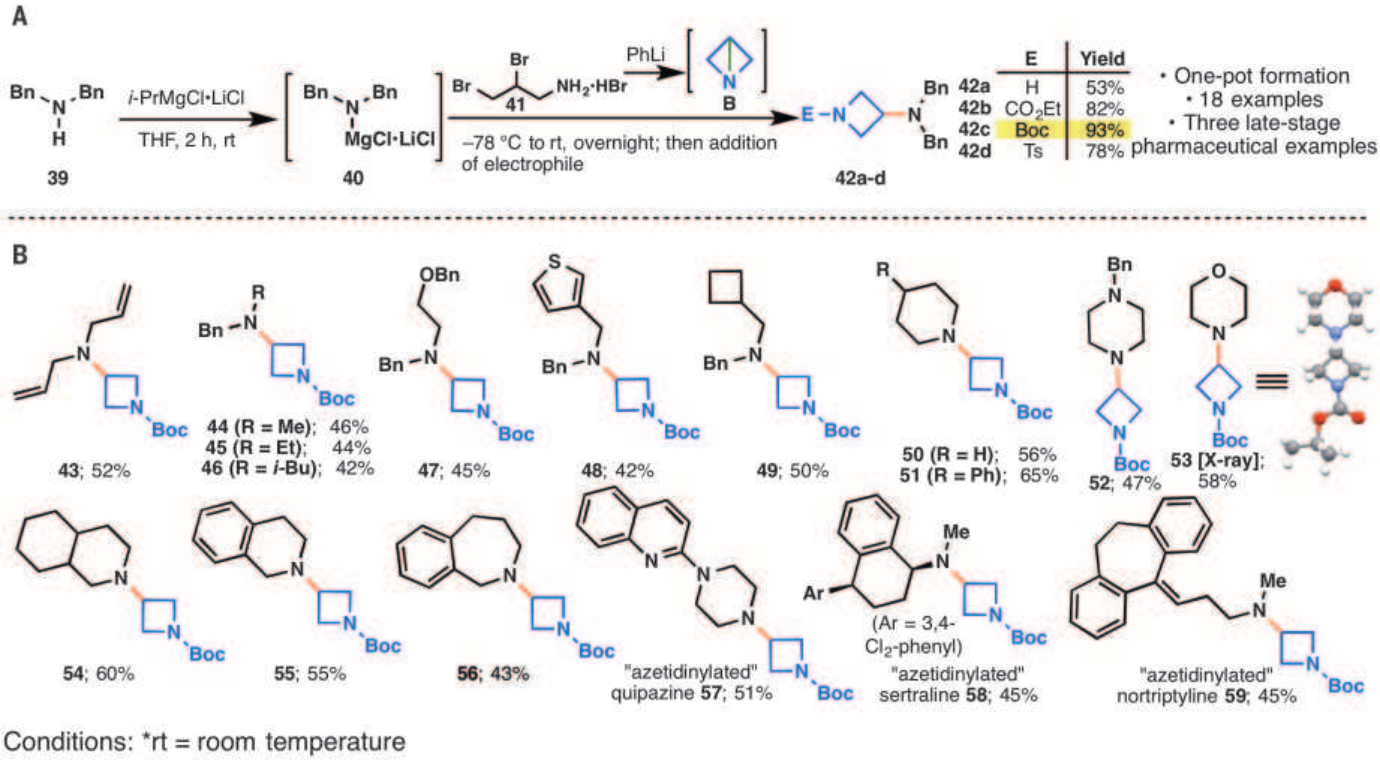

Fig. 3. "Azetidinylation" of amine-containing substrates. (**A**) A general "azetidinylation" of amines enabled by strain-release reagents. (**B**) Scope of amine-containing substrates.

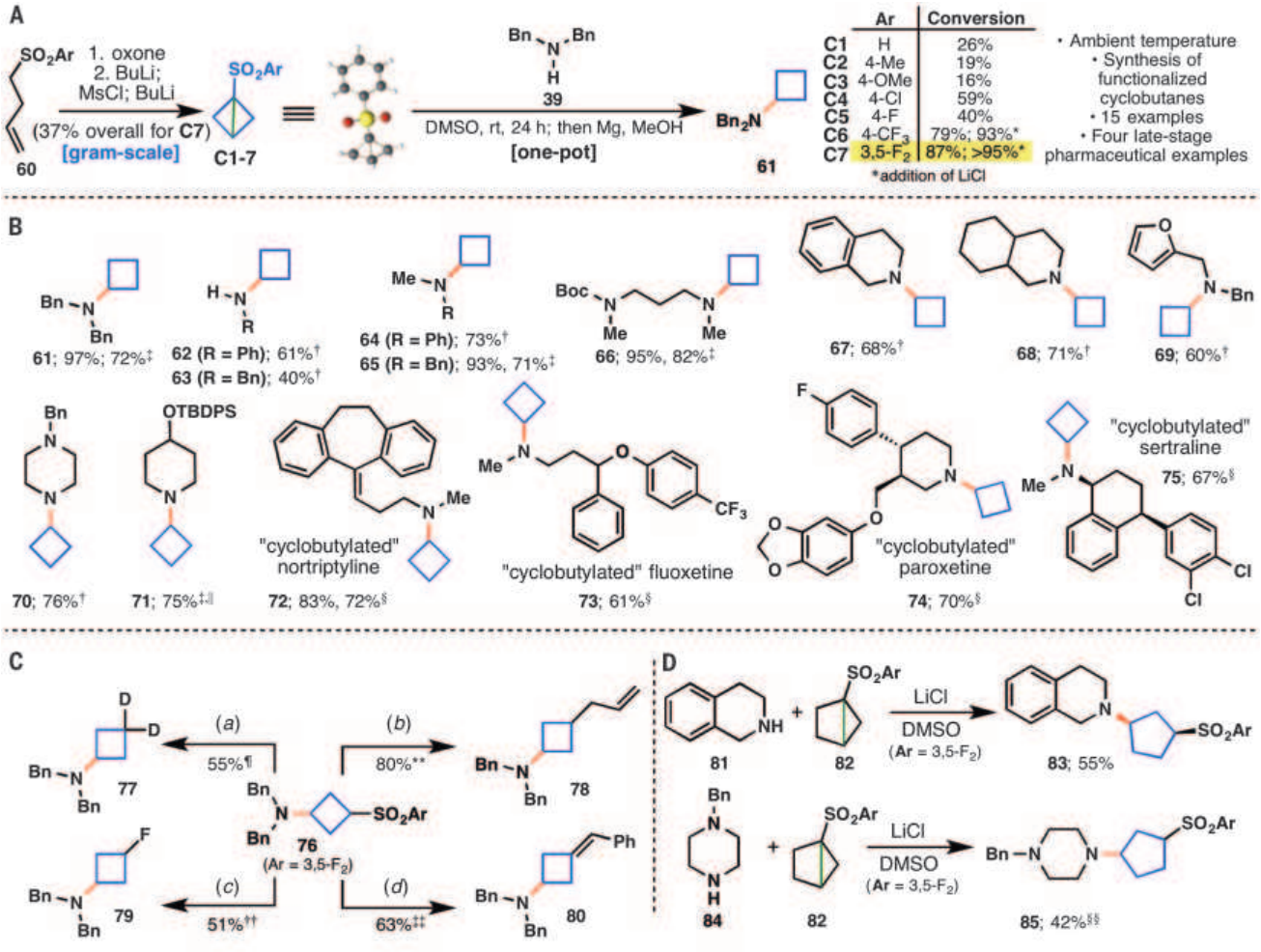

*LiCl, DMSO, room temperature; †General procedure A with **C7**: one-pot, no purification of intermediates; ‡General procedure B with **C7**: intermediates isolated by column chromatography; §General procedure C with **C7**: one-pot, no purification of intermediates, reduction initiated by sonication; ‖This compound was also prepared from 4-hydroxypiperidine (43% over three steps, see SM for details); ¶(a) i) CD_3OD/CD_3ONa, ii) Na/Hg; **(b) i) LHMDS, allyl bromide, ii) Mg/MeOH; ††(c) i) LHMDS, NFSI, ii) Na/Hg; ‡‡(d) i) PhCHO, *t*-BuOK, ii) DMAP, Et_3N, Ac_2O, iii) Na/Hg; §§ Mixture of isomers (see SM for details); ‖‖rt = room temperature

Fig. 4. "Cyclobutylation" of amine-containing substrates. (**A**) A general "cyclobutylation" of amines with **C7** enabled by strain-release reagents. (**B**) Substrate scope of amine-containing substrates. (**C**) Diversification of intermediate cyclobutylsulfone **76**. (**D**) Installation of cyclopentane onto primary and secondary amines by strain-release amination.

will be amenable to amination and further functionalization.

Applications to peptide labeling

The "spring-loaded" electrophiles described herein exhibit a broad substrate scope for amination and inspired exploration of this platform in a more biologically relevant context. A model peptide (**86**, Fig. 5) was therefore prepared containing an assortment of proteinogenic nucleophilic functional groups and exposed to strain-release reagent **C7** in a mixed organic/aqueous solvent system. Remarkably, complete selectivity was observed for labeling of the cysteine thiol [91% isolated yield of **88** after 5 hours; see HPLC (high-performance liquid chromatography) trace in Fig. 5B]. In the presence of cysteine-free peptide **87**, no background reaction was observed (Fig. 5C) after 24 hours. In marked contrast, the commonly employed maleimide electrophile led to multiple adducts with **87** after only 1 hour of exposure. The complete chemoselectivity observed for cysteine shows promise for the use of strain-release functionalization in a variety of contexts, such as site-selective bioconjugation (*31*–*34*) and peptide stapling (*35*–*38*). The efficient tagging of other thiols, including glutathione and cysteine methyl ester, attests to the generality of the approach (see supplementary materials for details). Further, by modifying the electronic character of the aryl sulfone group, we could adjust the temporal parameters of the functionalization (Fig. 5D). This tunable click reaction may facilitate the strategic design of electrophilic covalent warheads for enzyme inhibition and activity-based protein profiling.

Outlook

The operational simplicity, mild reaction conditions, inexpensive preparation, and chemoselectivity exhibited by strain-release reagents **A** to **C** will facilitate their rapid adoption. More globally, an enormous variety of reagents based on this concept can be envisaged. For the task of procuring a specific target, this approach to bond formation will enable practitioners to refocus on the challenge of synthesizing a molecular scaffold rather than on the difficulty posed by small ring systems. We anticipate that this approach will also enable formation of distinct connections in the materials, polymer, and bioconjugation arenas.

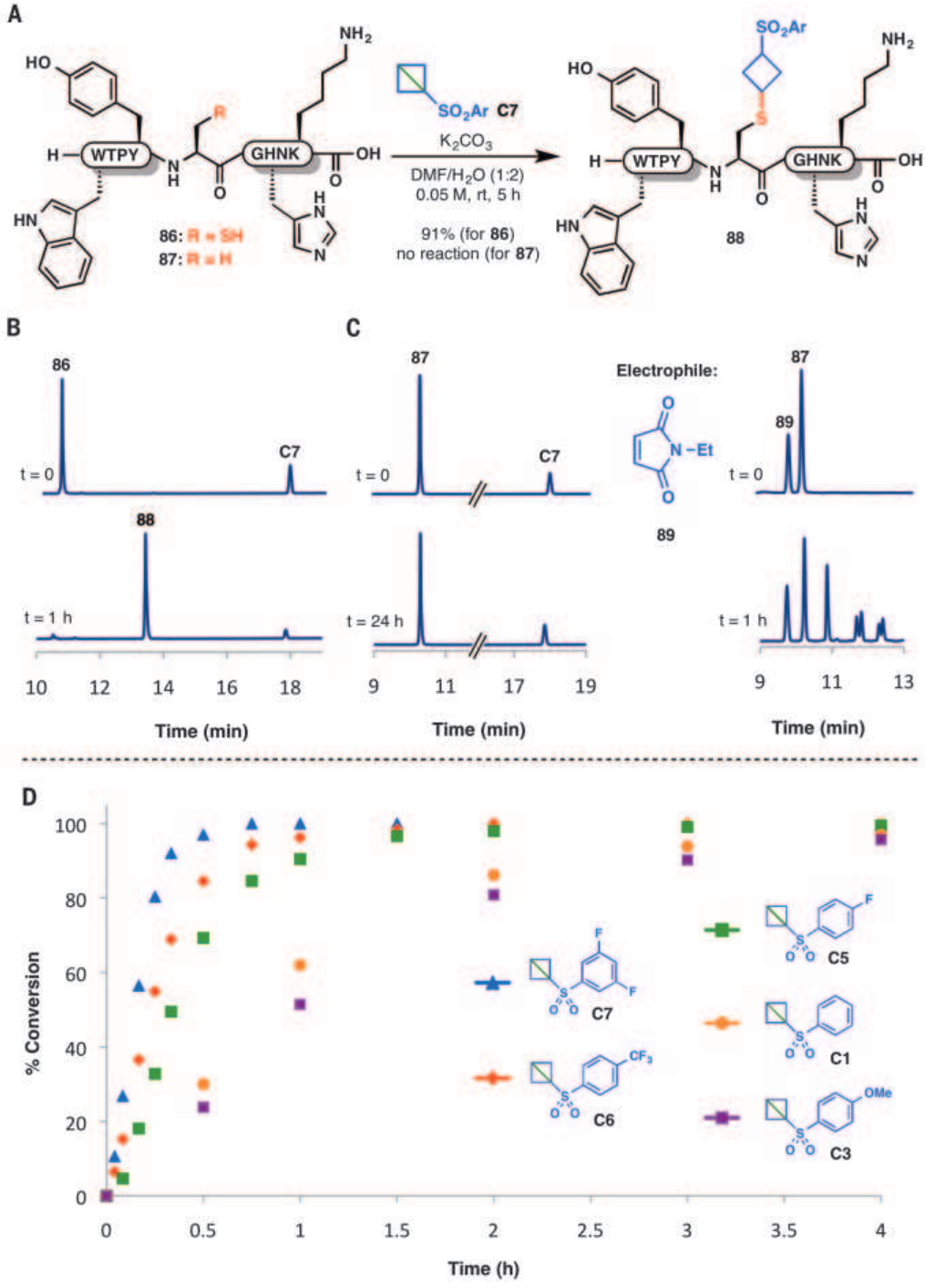

Fig. 5. Use of reagent C as a chemoselective cysteine tag for peptide and protein labeling. (**A**) Reaction of **C7** with functionalized peptides **86** and **87**. (**B**) HPLC chromatogram depicting rapid and clean conversion of **86** to cysteine-labeled product **88** after 1 hour. (**C**) Superior chemoselectivity of reagent **C7** relative to maleimide **89** in the presence of cysteine-free peptide **87**. (**D**) Reaction kinetics demonstrating the tunable functionalization of **86** with substituted arylsulfonyl bicyclobutane reagents.

REFERENCES AND NOTES

1. N. A. Meanwell, *J. Med. Chem.* **54**, 2529–2591 (2011).
2. C. Ni, M. Hu, J. Hu, *Chem. Rev.* **115**, 765–825 (2015).
3. Y. Fujiwara *et al.*, *Nature* **492**, 95–99 (2012).
4. M. V. Westphal, B. T. Wolfstädter, J. M. Plancher, J. Gatfield, E. M. Carreira, *ChemMedChem* **10**, 461–469 (2015).
5. Q. Michaudel, Y. Ishihara, P. S. Baran, *Acc. Chem. Res.* **48**, 712–721 (2015).
6. A. F. Stepan *et al.*, *J. Med. Chem.* **55**, 3414–3424 (2012).
7. K. B. Wiberg, V. Z. Williams, *J. Org. Chem.* **35**, 369–373 (1970).
8. M. D. Levin, P. Kaszynski, J. Michl, *Chem. Rev.* **100**, 169–234 (2000).
9. K. B. Wiberg, *Chem. Rev.* **89**, 975–983 (1989).
10. K. D. Bunker, N. W. Sach, Q. Huang, P. F. Richardson, *Org. Lett.* **13**, 4746–4748 (2011).
11. L. Zehnder *et al.*, *J. Med. Chem.* **54**, 3368–3385 (2011).
12. B. L. Bennett *et. al.*, PCT Int. Appl. WO 2012145569 (2012).
13. K. Hayashi *et. al.*, PCT Int. Appl. WO 2013024895 (2013).
14. K. B. Wiberg, F. H. Walker, *J. Am. Chem. Soc.* **104**, 5239–5240 (1982).
15. K. B. Wiberg, *Angew. Chem. Int. Ed. Engl.* **25**, 312–322 (1986).
16. H. C. Kolb, M. G. Finn, K. B. Sharpless, *Angew. Chem. Int. Ed.* **40**, 2004–2021 (2001).
17. E. W. Della, D. K. Taylor, J. Tsanaktsidis, *Tetrahedron Lett.* **31**, 5219–5220 (1990).
18. M. Messner, S. I. Kozhushkov, A. de Meijere, *Eur. J. Org. Chem.* **2000**, 1137–1155 (2000).
19. S. G. Davies, A. M. Fletcher, P. M. Roberts, J. E. Thomson, *Tetrahedron Asymmetry* **23**, 1111–1153 (2012).
20. C. J. Rohbogner, G. C. Clososki, P. Knochel, *Angew. Chem. Int. Ed. Engl.* **47**, 1503–1507 (2008).
21. A. Brandi, S. Cicchi, F. M. Cordero, *Chem. Rev.* **108**, 3988–4035 (2008).
22. Y. Ikee *et al.*, *Chem. Pharm. Bull. (Tokyo)* **56**, 346–356 (2008).
23. M. L. Wrobleski *et al.*, *Bioorg. Med. Chem. Lett.* **16**, 3859–3863 (2006).
24. K. B. Wiberg, R. P. Ciula, *J. Am. Chem. Soc.* **81**, 5261–5262 (1959).
25. K. B. Wiberg, in *Advances in Alicyclic Chemistry* (Academic Press, New York, 1968), vol. 2, pp. 185–254.
26. M. A. A. Walczak, T. Krainz, P. Wipf, *Acc. Chem. Res.* **48**, 1149–1158 (2015).

27. G. M. Lampman, J. C. Aumiller, *Org. Synth.* **51**, 55–59 (1971).
28. Y. Gaoni, *Tetrahedron Lett.* **29**, 1591–1594 (1988).
29. Y. Gaoni, *Org. Prep. Proced. Int.* **27**, 185–212 (1995).
30. S. M. Jeffery, C. J. M. Stirling, *J. Chem. Soc., Perkin Trans.* **2**, 1617–1624 (1993).
31. O. Boutureira, G. J. L. Bernardes, *Chem. Rev.* **115**, 2174–2195 (2015).
32. C. S. McKay, M. G. Finn, *Chem. Biol.* **21**, 1075–1101 (2014).
33. N. Stephanopoulos, M. B. Francis, *Nat. Chem. Biol.* **7**, 876–884 (2011).
34. J. Kalia, R. T. Raines, *Curr. Org. Chem.* **14**, 138–147 (2010).
35. Y. H. Lau, P. de Andrade, Y. Wu, D. R. Spring, *Chem. Soc. Rev.* **44**, 91–102 (2015).
36. A. M. Spokoyny *et al.*, *J. Am. Chem. Soc.* **135**, 5946–5949 (2013).
37. Y. Wang, D. H.-C. Chou, *Angew. Chem. Int. Ed.* **54**, 10931–10934 (2015).
38. S. P. Brown, A. B. Smith 3rd, *J. Am. Chem. Soc.* **137**, 4034–4037 (2015).

ACKNOWLEDGMENTS

Financial support for this work was provided by Pfizer, Inc., and the National Institutes of Health (GM106210). The National Institutes of Health provided a postdoctoral fellowship to J.M.L.; the Shanghai Institute of Organic Chemistry, Zhejiang Medicine Co., and Pharmaron provided a postdoctoral fellowship to J.W.; and the University of the Basque Country provided a predoctoral fellowship to L.P. We thank Y. Ishihara for assistance with the initial preparation of the manuscript. We are grateful to D.-H. Huang and L. Pasternack (The Scripps Research Institute) for assistance with nuclear magnetic resonance (NMR) spectroscopy and A. L. Rheingold and C. E. Moore (University of California, San Diego) for x-ray crystallographic analysis. Crystallographic data for compounds **9**, **12, 53**, **C1**, and **S23** are available free of charge from the Cambridge Crystallographic Data Centre under accession numbers CCDC 1431179, 1438966, 1431180, 1431182, and 1431183, respectively.

SUPPLEMENTARY MATERIALS

www.sciencemag.org/content/351/6270/241/suppl/DC1
Materials and Methods
Figs. S1 to S68
Tables S1 to S6
References (*39*–*68*)
NMR Spectra

21 October 2015; accepted 2 December 2015
10.1126/science.aad6252

REPORTS

APPLIED OPTICS

Gain modulation by graphene plasmons in aperiodic lattice lasers

S. Chakraborty,[1]* O. P. Marshall,[1,2] T. G. Folland,[1] Y.-J. Kim,[2] A. N. Grigorenko,[2] K. S. Novoselov[2]*

Two-dimensional graphene plasmon-based technologies will enable the development of fast, compact, and inexpensive active photonic elements because, unlike plasmons in other materials, graphene plasmons can be tuned via the doping level. Such tuning is harnessed within terahertz quantum cascade lasers to reversibly alter their emission. This is achieved in two key steps: first, by exciting graphene plasmons within an aperiodic lattice laser and, second, by engineering photon lifetimes, linking graphene's Fermi energy with the round-trip gain. Modal gain and hence laser spectra are highly sensitive to the doping of an integrated, electrically controllable, graphene layer. Demonstration of the integrated graphene plasmon laser principle lays the foundation for a new generation of active, programmable plasmonic metamaterials with major implications across photonics, material sciences, and nanotechnology.

Among the many intriguing properties of graphene, its plasmonic characteristics are some of the most fascinating and potentially useful (*1*, *2*). Long-lived, tunable intrinsic graphene surface plasmons (SPs) have already been demonstrated in a number of experiments (*3*–*9*), including optical modulators (*10*, *11*), providing the potential for applications (*12*, *13*). In contrast to the noble metals that are usually used in SP devices (*13*, *14*), graphene's Fermi energy, E_F, and carrier concentration, n_s (and therefore its conductivity and SP mode properties), can be altered, for example, by electrical gating and surface doping (*3*, *15*, *16*). Consequently, the behavior of graphene SP-based structures can be modified in situ, without the need for structural device changes. In particular, graphene's optical and plasmonic properties are tunable in the terahertz (THz) spectral region (*3*, *17*), giving rise to the possibility of compact electrically controllable THz optical components (*18*). We incorporated graphene into a plasmonic THz laser microcavity to dynamically modulate round-trip modal gain values and therefore laser emission via E_F. In this way, gated graphene becomes a powerful tool with which to control the fundamental properties of a laser—a tool that is potentially extremely fast and all electrical in nature, with negligible electrical power requirements.

The interaction between light and matter can be altered by manipulating the electromagnetic density of states (DOS) using a microresonator (*19*, *20*). By incorporating a photonic lattice or plasmonic structure into a laser, one can control the frequency and amplification of resonant modes and hence manipulate the properties of lasing emission (*21*–*23*). Furthermore, by breaking the regularity of these structures it is possible to modulate the photon DOS and hence light-matter interaction at several frequencies simultaneously. This technique was used recently to develop an aperiodic distributed feedback (ADFB) cavity laser with a lattice that is in essence a computer-generated hologram (*24*, *25*). The hologram digitally encodes the Fourier transform of a desired optical filter function (multiple reflection resonances within the gain bandwidth of the laser), enabling photonic DOS manipulation at precise filter frequencies. In real space, a typical hologram lattice contains a multitude of phase shifts; the locations and sizes of scattering sites and defects are set such that via coherent backscattering the device enters a slow light regime. Transfer matrix method (TMM) calculations of the group delay transfer function (which is intrinsically linked to the photonic DOS) of an ADFB microcavity under the influence of gain reveal infinite-gain singularities [fig. S4; see (*26*) for further details]. These singularities represent the frequency and gain values at which self-oscillation occurs. The ADFB microcavity can produce coherent amplification of the cavity photons via stimulated emission processes because of the build-up of phase coherence at the singularities (*20*).

ADFB structures were realized in THz quantum cascade lasers (QCLs)—extremely long wavelength semiconductor lasers with active regions based on precisely engineered inter-subband transitions (*27*). Such ADFB THz QCLs provide an ideal proving ground for graphene-controlled gain modulation because they use SP-based waveguides (at a metal-semiconductor interface, Fig. 1A) (*28*). The first crucial step is to excite two-dimensional (2D) plasmons in an integrated, atomically thin graphene sheet to take full leverage of the computer-generated hologram principle. Hologram pixels are introduced to the QCL waveguide as plasmonic scattering sites along the longitudinal axis of the laser ridge (Fig. 1B). By depositing an electrically gateable graphene film onto these devices, our goal is to switch the THz SP at each pixel "on" or "off" by tuning n_s, thereby altering the photonic DOS and the degree to which the THz intersubband gain spectra follows the hologram response. For example, by modulating the hologram pixel scattering strength we approach the DOS singularities, resulting in a dramatic increase of light-matter interaction within the QCL gain media (*20*). Photon lifetimes (and hence modal gain values) are thereby enhanced, leading to selective enhancement of competing laser modes and a concomitant suppression of others.

A hologram with relatively weak feedback was chosen so that any subtle influence of graphene plasmons on laser emission was not hidden by

[1]School of Electrical and Electronic Engineering, University of Manchester, Manchester M13 9PL, UK. [2]School of Physics and Astronomy, University of Manchester, Manchester M13 9PL, UK.
*Corresponding author. E-mail: s.chakraborty@manchester.ac.uk (S.C.); kostya@manchester.ac.uk (K.S.N.)

strongly amplified photonic filtering. The hologram was designed to define multi-color THz QCL emission (*25*, *29*) and was introduced to the metalized laser ridge surface as a series of subwavelength slits (Fig. 1E) (*27*). At each slit, the localized removal of metal strongly influences the fundamental transverse magnetic THz eigenmode of the waveguide (*25*). Finite element modeling (FEM) of the electric field across a single slit reveals strong radiative scattering of the propagating THz mode (Fig. 1B). The single-pass reflection gain (G) (essentially the modal gain), calculated in the frequency (f) and material gain (gL, where L is the hologram length) plane by using the TMM, reveals the possibility of selective mode enhancement from the microcavity resonances at reasonably achievable values of the normalized coupling factor κL (Fig. 1, C and D). This coupling is in turn dictated by the scattering strength of the hologram pixels. For further details of the FEM and TMM, see (*26*). Last, the key element of our design—switchable graphene plasmons—are excited in a graphene layer placed on the top of the hologram.

Four devices were fabricated and characterized, each demonstrating similar behavior, with minor differences attributable to their individual active region and hologram properties. Here we concentrate on a single representative device. Details of fabrication and testing, along with experimental results for a second device (fig. S1), are presented in (*26*). The unpatterned Fabry-Perot (FP) cavity lased on numerous longitudinal cavity modes (Fig. 1A), many of which were suppressed by implementation of the ADFB microstructure (Fig. 1E). Introduction of graphene partially "repaired" the waveguide, reducing individual pixel scattering strengths and leading to the return of many FP modes (Fig. 1F). Laser spectra were evaluated in terms of N, the observed number of lasing modes (Fig. 2A), revealing the FP-like behavior of the graphene-ADFB QCL over a wide range of laser operating currents (I). For reference, the electrical and output power characteristics of the QCL at each stage of waveguide modification are also presented (Fig. 2B). At each stage the device displays typical THz QCL band structure alignment and misalignment features, with no appreciable changes in the absolute lasing threshold (I_{th}) because g is clamped by laser facet feedback.

In order to demonstrate electrical modification of fundamental laser gain dynamics by varying E_F in the graphene, a polymer electrolyte was deposited over the device (Fig. 3A). FEM simulations of THz scattering at a single slit provide a basic understanding of the mechanisms involved (Fig. 3B). The presence of low-n_s (low-E_F) graphene leads to strongly suppressed intraslit fields. Experimentally, application of gate voltage (V_{gate}) leads to high n_s (*16*). In this case, the simulated intraslit field intensities are larger. Our understanding of these results is helped by an analytical estimate of the plasmon wavelength $\lambda_{pl} = \frac{2\alpha E_F}{\varepsilon \hbar \omega_0}\lambda_0$, where α is the fine structure constant, ω_0 and λ_0 are the lasing mode frequency and wavelength, respectively, and ε the average permittivity surrounding the graphene (we use $\varepsilon = 7$, the average of vacuum and GaAs) (*6*, *8*). For E_F = 50 meV (typical for intrinsically doped graphene), we estimate $\lambda_{pl} \sim 1$ μm, comparable with the slit width. Consequently the electron plasma in graphene introduces a second dipole field (localized SP) within the slit, oriented opposite to the existing field, greatly reducing THz scattering (fig. S2) (*26*). On the other hand, for E_F = 300 meV (a reasonably achievable level by electrochemical doping) the plasmon wavelength is six times longer (large relative to the slit width), and the electron plasma moves coherently inside the slit, leading to efficient THz scattering. TMM calculations of reflection gain in the f-κL plane enable us to calculate the changes in modal amplification induced by raising n_s. Graphene-induced changes in individual pixel scattering strength (κ) can alter modal G values by almost two orders of magnitude (Fig. 3, C and D) and the group index (n_g) by almost one order of magnitude (fig. S4) (*26*). Owing to the reduced group velocity (slow light regime), the photon DOS is strongly enhanced around the infinite-gain singularities (*20*).

This effect has important experimental consequences (Fig. 3, E and F). At low E_F, the DOS does not offer a dominant channel for inter-subband emission, and a large fraction of the emission is channeled into the FP-like lasing modes. Laser emission just above I_{th} is modified when we apply V_{gate}. By increasing E_F by almost an order of magnitude, many of the FP-like lasing modes (seen at V_{gate} = 0 V) are inhibited, and inter-subband emission is predominantly channeled into singularities. Therefore, the high-E_F graphene plasmons force laser emission to be governed by the hologram response, with pure single-mode emission within each resonance band. Such a redistribution of spectral power is further observed experimentally in the light-current behavior of the four dominant modes near I_{th} (Fig. 4, A and B); with V_{gate} = 1 V applied, we observed a strongly favored (highest n_g) mode. The most dramatic

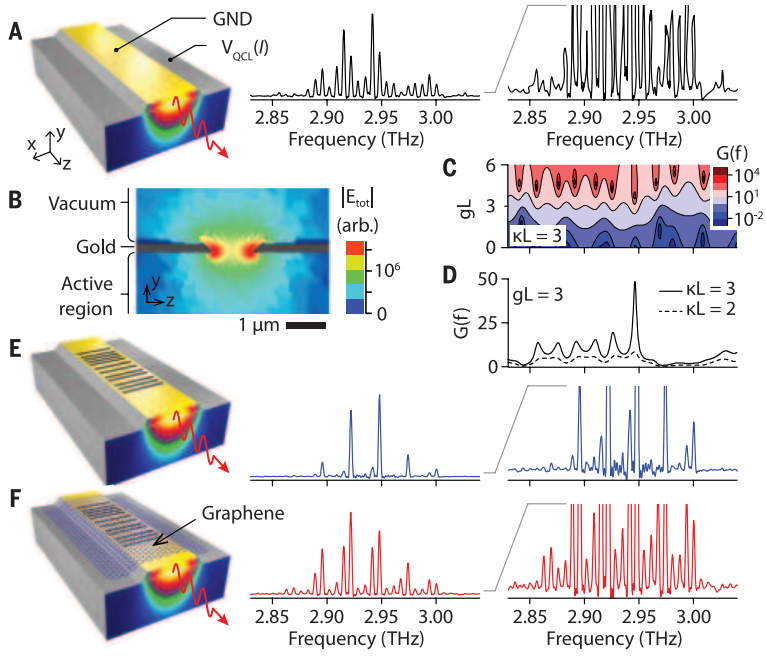

Fig. 1. Hologram-defined laser emission. (**A**) Schematic and typical measured emission spectra of the unperturbed Fabry-Perot QCL. (**B**) Simulated electric field intensity profile within a single hologram pixel (slit), f = 2.8 THz. (**C**) Calculated reflection gain, $G(f)$, for a range of dimensionless material gain (gL, where L is the hologram length) values. The hologram coupling $\kappa = \Delta n / n_{eff}\Lambda$, where n_{eff} is the effective refractive index, Δn the refractive index contrast, and Λ the minimum pixel spacing. (**D**) $G(f)$ for low and high E_F (and κL). Schematics and emission spectra are also shown for (**E**) the hologram-patterned and (**F**) the graphene-covered QCL.

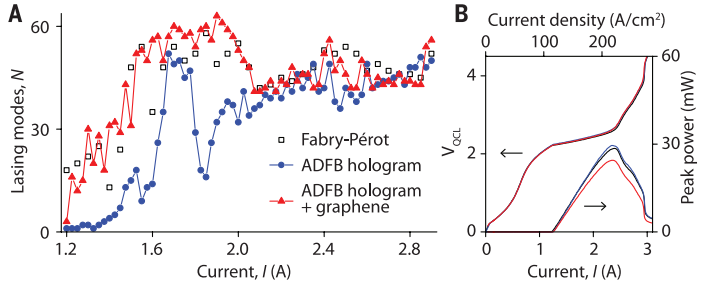

Fig. 2. Influence of graphene deposition. (**A**) Number of measured lasing modes N as a function of laser driving current (I). (**B**) Laser output power and electrical characteristics.

reversible changes in N also occurred close to I_{th} (Fig. 4C) but remained appreciable over a wide current range. In contrast, when electrolyte was applied without graphene, N was insensitive to V_{gate} (Fig. 4D). In this specific case, the resulting macroscale optoelectronic functionality (close to I_{th}) is graphene-controlled switching between dual- and single-mode operation. The switching behavior is reversible up to a small finite hysteresis, as is typically observed when graphene devices are gated by solid electrolyte (*16*). Demonstration of reversible graphene control is the key result of this work (not single-mode lasing, which is achievable by a number of techniques). This use of graphene to define and control the fundamental gain dynamics of a laser is what sets this work apart from previously reported optical filtering in passive graphene waveguides (*10*, *11*). Time domain modeling (TDM) provides further insight into the spatial-temporal interplay between light-field and population inversion in ADFB lasers, revealing the localization caused by the underlying aperiodicity within the hologram. Furthermore, it reveals substantial changes in the inhomogeneity of the population inversion profile within the microcavity as κ is varied (fig. S6) (*26*). Any change in this profile has implications for the gain dynamics of the laser, altering the competition between lasing modes.

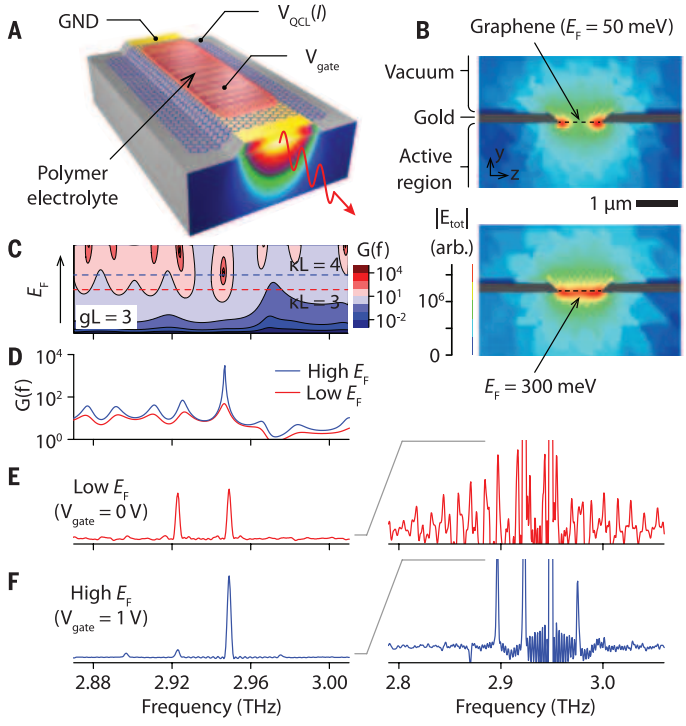

Fig. 3. Sensitivity of laser emission to graphene doping. (**A**) Schematic of the polymer electrolyte-covered device. (**B**) Simulated electric field intensity profiles within a single hologram pixel containing low doped (top) and highly doped (bottom) graphene, f = 2.8 THz. (**C** and **D**) Calculated $G(f)$ as E_F (and κL) is varied. Laser emission spectra measured after electrolyte deposition for (**E**) ungated (low n_s, low E_F) and (**F**) gated (high n_s, high E_F) graphene, collected just above laser threshold.

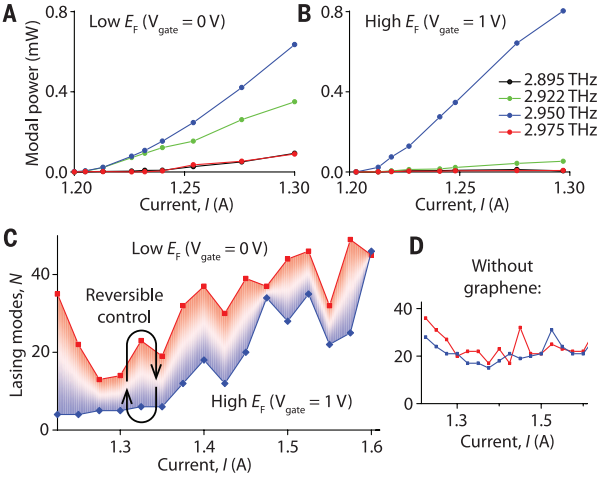

Fig. 4. Graphene-controlled modal gain modulation. Light-current behavior of four dominant emission frequencies for (**A**) ungated and (**B**) gated graphene. (**C**) Reversible spectral filtering (variation in N) is achieved via V_{gate}. (**D**) Results for electrolyte-covered QCL without graphene.

Last, a correlation between N and pixel scattering is also seen in the TDM, indicating a direct link between the graphene-controlled electromagnetic DOS and the modal gain of the laser (fig. S5) (*26*). We stress that the possibility to effectively control the operation of a semiconductor microcavity laser by graphene ultimately stems from unique properties of 2D graphene plasmons that allow unprecedented wavelength compression (by a factor of ~30) at small gating voltage and hence excitation of localized SP modes within the hologram pixels.

The use of electrically controllable graphene plasmons to modify active photonic systems offers a number of interesting device possibilities. In principle, each pixel (or small group of pixels) in an ADFB hologram could be independently gated, allowing individual tailoring of scattering strengths. Combined with the highly flexible multiband digital hologram approach, this would allow an operator to electronically rewrite the spectral response of a laser on demand. Furthermore, whereas programmable graphene plasmonic structures are particularly appealing for incorporation into THz lasers where spectral control is traditionally difficult, they can also be scaled to shorter-wavelength optoelectronic systems, greatly expanding their potential technological impact.

REFERENCES AND NOTES

1. K. S. Novoselov *et al.*, *Science* **306**, 666–669 (2004).
2. A. K. Geim, K. S. Novoselov, *Nat. Mater.* **6**, 183–191 (2007).
3. L. Ju *et al.*, *Nat. Nanotechnol.* **6**, 630–634 (2011).
4. T. Eberlein *et al.*, *Phys. Rev. B* **77**, 233406 (2008).
5. J. T. Kim, S.-Y. Choi, *Opt. Express* **19**, 24557–24562 (2011).
6. J. Chen *et al.*, *Nature* **487**, 77–81 (2012).
7. Z. Fei *et al.*, *Nature* **487**, 82–85 (2012).
8. A. N. Grigorenko, M. Polini, K. S. Novoselov, *Nat. Photonics* **6**, 749–758 (2012).
9. H. Yan *et al.*, *Nat. Photonics* **7**, 394–399 (2013).
10. X. Wang, Z. Cheng, K. Xu, H. K. Tsang, J.-B. Xu, *Nat. Photonics* **7**, 888–891 (2013).
11. E. O. Polat, C. Kocabas, *Nano Lett.* **13**, 5851–5857 (2013).
12. K. S. Novoselov *et al.*, *Nature* **490**, 192–200 (2012).
13. W. L. Barnes, A. Dereux, T. W. Ebbesen, *Nature* **424**, 824–830 (2003).
14. E. Ozbay, *Science* **311**, 189–193 (2006).
15. C. J. Docherty *et al.*, *Nat. Commun.* **3**, 1228 (2012).
16. A. Das *et al.*, *Nat. Nanotechnol.* **3**, 210–215 (2008).
17. F. Bonaccorso, Z. Sun, T. Hasan, A. C. Ferrari, *Nat. Photonics* **4**, 611–622 (2010).
18. A. Tredicucci, M. S. Vitiello, *IEEE J. Sel. Top. Quantum Electron.* **20**, 130–138 (2014).
19. E. Yablonovitch, *Phys. Rev. Lett.* **58**, 2059–2062 (1987).
20. T. Pickering, J. M. Hamm, A. F. Page, S. Wuestner, O. Hess, *Nat. Commun.* **5**, 4972 (2014).
21. J. P. Dowling, M. Scalora, M. J. Bloemer, C. M. Bowden, *J. Appl. Phys.* **75**, 1896 (1994).
22. M. Engel *et al.*, *Nat. Commun.* **3**, 906 (2012).
23. J. Li *et al.*, *Sci. Rep.* **5**, 9263 (2015).
24. S. Chakraborty, M. C. Parker, R. J. Mears, *Photonics Nanostruct. Fundam. Appl.* **3**, 139–147 (2005).
25. S. Chakraborty *et al.*, *Appl. Phys. Lett.* **101**, 121103 (2012).
26. See supplementary materials available on *Science* Online.
27. O. P. Marshall *et al.*, *J. Appl. Phys.* **113**, 203103 (2013).
28. L. Mahler *et al.*, *Appl. Phys. Lett.* **84**, 5446–5448 (2004).
29. S. Chakraborty *et al.*, *Opt. Express* **20**, B306–B314 (2012).

SUPPLEMENTARY MATERIALS

www.sciencemag.org/content/351/6270/246/suppl/DC1
Materials and Methods
Figs. S1 to S6
References (*30*, *31*)

7 September 2015; accepted 6 November 2015
10.1126/science.aad2930

LUNAR ATMOSPHERE

How surface composition and meteoroid impacts mediate sodium and potassium in the lunar exosphere

A. Colaprete,[1]* M. Sarantos,[2,3] D. H. Wooden,[1] T. J. Stubbs,[4] A. M. Cook,[1,5] M. Shirley[1]

Despite being trace constituents of the lunar exosphere, sodium and potassium are the most readily observed species due to their bright line emission. Measurements of these species by the Ultraviolet and Visible Spectrometer (UVS) on the Lunar Atmosphere and Dust Environment Explorer (LADEE) have revealed unambiguous temporal and spatial variations indicative of a strong role for meteoroid bombardment and surface composition in determining the composition and local time dependence of the Moon's exosphere. Observations show distinct lunar day (monthly) cycles for both species as well as an annual cycle for sodium. The first continuous measurements for potassium show a more repeatable variation across lunations and an enhancement over KREEP (Potassium Rare Earth Elements and Phosphorus) surface regions, revealing a strong dependence on surface composition.

The Lunar Atmosphere and Dust Environment Explorer (LADEE) mission, which operated in lunar orbit between 6 October 2013 and 18 April 2014, had the goal to determine the composition of the lunar atmosphere and investigate the processes that control its distribution and variability, including sources, sinks, and surface interactions (*1*). The Ultraviolet and Visible Spectrometer (UVS) (*2*) was designed to make observations of the lunar exosphere and search for dust. The LADEE orbit was retrograde and equatorial; thus, observations were restricted to between about ±20° latitude. However, this orbit did provide synoptic observations of lunar exospheric species with temporal cadence of typically less than 12 hours. These observations provide new constraints on the processes, sources, and sinks that govern concentrations of species in the lunar exosphere. UVS observed resonant scattering from sodium (Na) and potassium (K). Although Na and K are minor constituents in the lunar exosphere, the brightness of their emission lines makes them readily observable, and thus they serve as excellent proxies to understanding the processes that govern the composition of the lunar exosphere (*3*–*6*).

Potential sources of Na and K in the exosphere include photon-stimulated desorption (PSD), sputtering, and impact vaporization (Fig. 1). The role of PSD and sputtering have been estimated by evaluating the change in Na abundances as the surface is shielded from solar wind sputtering as the Moon passed through Earth's magnetotail (*7*). From these previous Earth-based observations and modeling, PSD was generally considered to be the dominant source, by a factor of ~10 to 100, over sputtering or impact vaporization (*6*, *7*). However, the question of whether photons simply re-excite material that has been previously vaporized by other processes or whether they act as a primary source process of atoms from glasses and minerals has not been previously answered. The only other space-based observations of Na were made by the Telescope for Visible Light (TVIS) instrument on board the Kaguya spacecraft (*8*). Kaguya TVIS observations were limited to the lunar nightside, looking in the antisolar direction toward the extended Na tail; thus, they preferentially observed the "hottest" portion of the Na population and were not continuous across the entire lunation (*9*). These observations showed a continuous decrease of the inferred Na surface density from first to third quarter, including phases when the Moon passes through Earth's magnetosphere, with a variation of about 50% across a lunation.

Observations of K from Earth are more difficult than for Na because a strong telluric O_2 band overwhelms the stronger of the two K lines, whereas the smaller scale height for K results in relatively small concentrations at altitudes where Earth-based observations can be made. Besides its initial discovery (*3*), only two other K observations have been published (*10*, *11*), and these were limited to observations on single days. There are therefore no observations of K over the course of a lunation.

Earth-based observations have detected increases in the overall concentration of Na in the lunar exosphere associated with some meteoroid streams (*12*–*16*). However, these observations were intermittent and limited in time, often focusing on only a few measurements about an individual stream; thus, Na variability associated with meteoroid streams has been inconclusive (*17*). Annual variability of lunar-sodium tail brightness has been found, with a peak in the Na tail brightness in

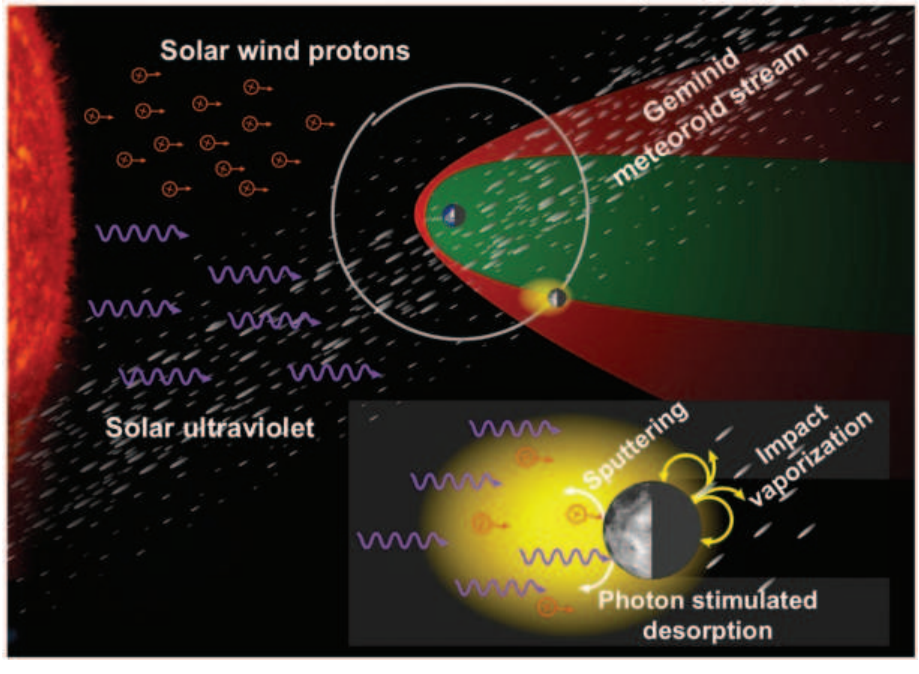

Fig. 1. The primary sources and sinks of the lunar Na and K exosphere. The yellow region represents the sodium exosphere having a greater extent on the dayside due to higher sodium temperatures. The sources and sinks include photon-stimulated desorption (from solar ultraviolet), sputtering (from solar wind protons) and meteoroid impact vaporization (e.g., the Geminid meteoroid stream). These processes are affected as the Moon passes through Earth's magnetosphere (green region) and sheath (red region).

[1]Space Science Division, NASA Ames Research Center, Moffett Field, Mountain View, CA, USA. [2]Heliophysics Science Division, NASA Goddard Space Flight Center, Greenbelt, MD, USA. [3]University of Maryland, Baltimore County, Baltimore, MD, USA. [4]Solar System Exploration Division, NASA Goddard Space Flight Center, Greenbelt, MD, USA. [5]Millennium Engineering and Integration Services, Moffett Field, CA 94035, USA.
*Corresponding author. E-mail: anthony.colaprete-1@nasa.gov

February, but no explanation for the annual variations has been provided (*9*, *17*). The UVS observations allow for continuous monitoring of the exosphere, both during and outside intervals of increased stream activity, through the course of more than five lunations, which allows for a much less ambiguous measure of immediate Na activity associated with meteoroid streams. In addition to these Na observations, these observations are the first to assess the response of K to meteoroid stream activity.

The emission line strengths for both Na and K were derived from UVS limb observations at around local noon. These noon limb-viewing activities typically covered spacecraft solar longitudes between –25° and +55° with a telescope viewing altitude of around 40 km (*2*, *18*).

The derived tangent column densities of Na and K show variations by a factor of 2 to 3 over the course of a lunation (Fig. 2). The minimum-to-maximum ratio of Na column density changes continuously during the five lunations measured by LADEE, but the factor of 2 for Na seen on the last month is significantly different from the ~50% seen in Kaguya observations (*9*). A factor of two change in the lunar Na content was inferred from modeling ground-based observations taken before UVS observations (*7*) and attributed to the solar wind increasing the PSD rate via ion-enhanced diffusion inside grains (*18*). However, the model in (*18*) predicted that the exosphere rose continuously between exit and subsequent reentry to the magnetosphere. The Kaguya TVIS data showed a continuous decline in Na through the magnetotail, whereas LADEE UVS data show Na peaks near full Moon. These differences are perhaps a difference in vantage points as suggested to reconcile the Kaguya results with the analysis of ground-based observations (*9*).

As the Moon passes into Earth's magnetotail, the total Na is seen by UVS first to decrease and then increase through full Moon to a maximum about 30° of lunar phase, after which it begins to decrease again. Although detailed modeling is required to understand the cause of these trends, some of this variation could be the result of adsorbed species being released by solar wind sputtering as particles spend more time on the surface than on ballistic trajectories. The absence of sputtering in the magnetotail should allow for the Na surface reservoir to increase, perhaps explaining the increase in exospheric concentration several days after the full Moon; then, as the Moon comes out of the magnetotail, sputtering begins to release adsorbed particles again and exospheric Na decreases as it is lost to space. This paradigm suggests then that most of the Na particles do not get lost to the surface on their first bounce, unlike hypothesized in recent models based on ground-based observations (*7*, *15*). It was suggested that some of the daily variation observed by Kaguya could be explained if there were surficial enhancements of Na in selenographic longitudes around 90°± 90°, resulting in differences in PSD rates between near-side and far-side regolith (*9*). Consistent with this idea of a surface dependency, the new LADEE UVS data are suggestive of a different dependence in PSD between mare versus highlands soils (Fig. 3).

Potassium shows a much more regular trend over time, with intensity variations over a lunation of approximately a factor of 2 (Fig. 2). This more systematic monthly trend for K (compared to Na) is reminiscent of the extreme variation of K surface abundance due to the enrichment found in KREEP (Potassium Rare Earth Elements and Phosphorus) soils (*19*), which can be as much as a factor of 10. Any variation introduced by the solar wind appears to be masked by the strong variation of surface K. In addition to the much larger variation in K over the course of a lunation, the K dependence on surface composition is more clearly shown by the location of the peak tangent column densities (Fig. 3). Given the anticipated influence of the magnetotail on sputtering (*7*, *18*), a minimum in column density for both Na and K could be expected to be centered at around a longitude of 0°, with maxima to either side. However, the K peak occurs to the west, centered on the Oceanus Procellarum and the Mare Imbrium regions, areas of maximum surface K as measured by the Lunar Prospector mission (*20*). Sodium is more symmetric about 0° longitude, with a local

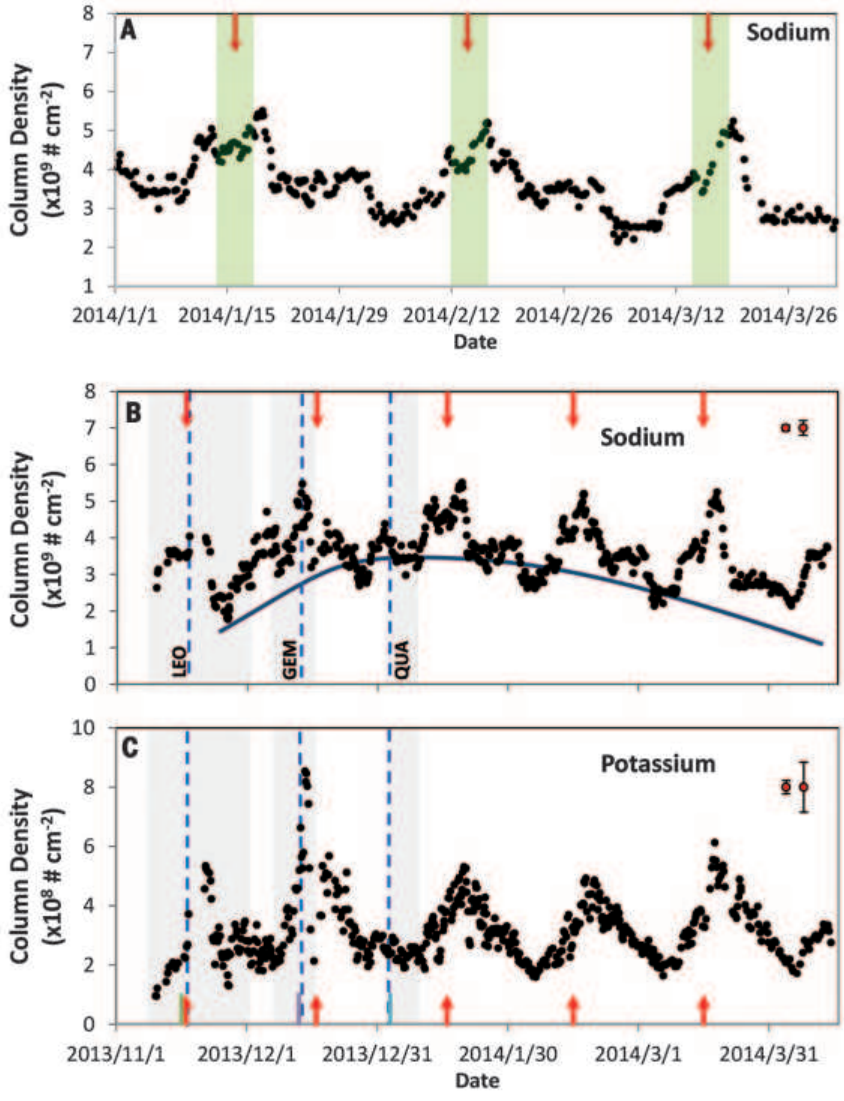

Fig. 2. The total line-of-site column densities for sodium and potassium. (**A** and **B**) Sodium. (**C**) Potassium. The column densities were derived from data taken while the telescope grazing point was between a spacecraft solar longitude of 165° to 180° (near local noon). In (A), the last three observed lunations are shown with green-shaded regions indicating when the Moon was in Earth's magnetotail. (B) and (C) show the Na and K column densities, respectively, for the entire mission period. In (B), a fit to the minima in column concentration (solid blue curve) is shown to highlight the long-term Na trend. Also shown in (B) and (C) are the approximate beginning and end dates (gray-shaded regions) for three meteoroid streams (Leo, Gem, and Qua) and the observed peak (blue dashed lines) and the approximate dates of the full Moon (red arrows). Average absolute and relative (point-to-point) uncertainties are shown by the red points toward the upper right corner of (B) and (C).

minimum at 0°. There is some correlation of Na with surface albedo (Fig. 3), which suggests a possible dependence on composition (e.g., Mare or Highlands composition); however, albedo is also a function of surface maturity and roughness, and these factors are expected to influence how adsorbates bind on grains. Additionally, the structure around 0° longitude could also be a reaction to being inside the magnetotail.

Some individual meteoroid streams led to a significant increase in these exospheric species. Three major streams that occurred during the LADEE mission are indicated in Fig. 2. In the Na data set, although there are peaks in the Na column abundance, it is not obvious that these are the result of the streams (as opposed to whatever is causing the monthly variation). Indeed the noon-time immediate response to streams of an exosphere populated by previously adsorbed atoms is expected to be rather small, because most streams have radiants on the lunar nightside (*21*, *22*), with larger variations in response to the streams expected at around dawn. However, in the K noon-time data there is a clear increase at around the time of the Geminid (Gem) meteoroid stream (approximately between 4 and 16 December) and also smaller signatures at around the time of the Leonid (Leo) (6 to 30 November) and Quadrantid (Qua) (1 to 10 January) streams. In addition to these enhancements at or around individual streams, the overall rise in Na from October 2013 to a peak in December 2013, and then a gradual decline until the end of the mission, can be attributed to a cumulative response to meteoroid streams. A similar trend was apparent in Kaguya data (*9*), but, as with earlier studies (*17*), it could not be correlated to any particular process. The UVS data suggest a strong link between these streams and the exosphere, lasting far beyond the initial encounter. The meteoroid impacts expose fresh Na and K, but also supply these species directly to the exosphere at increased rates.

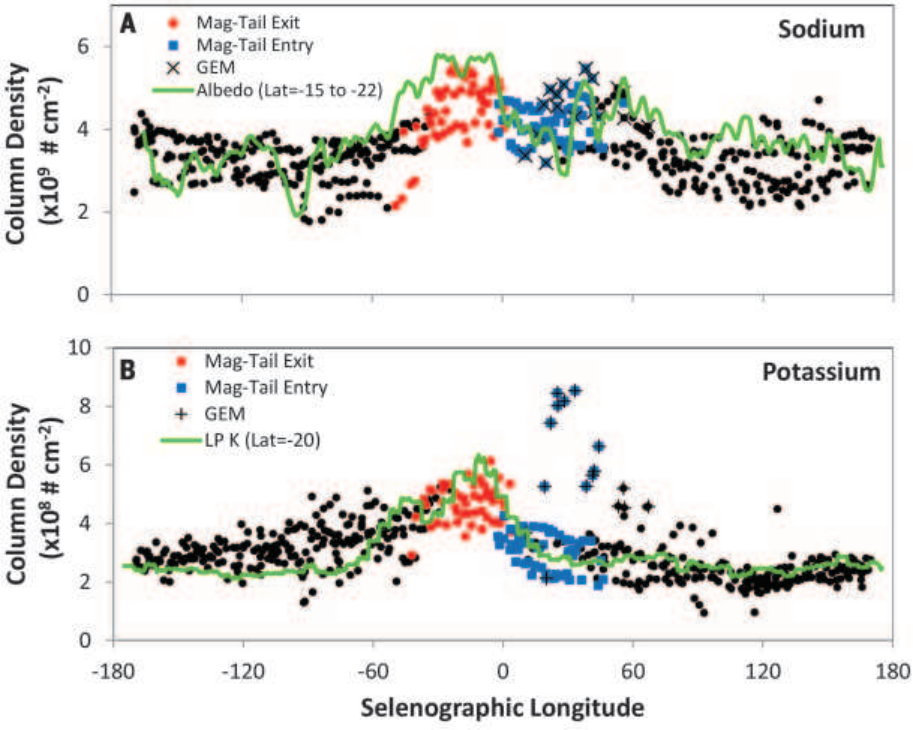

Fig. 3. Column densities for sodium and potassium as a function of selenographic longitude. (**A**) Sodium. (**B**) Potassium. The approximate entry into (blue squares) and exit out of (red points) Earth's magnetotail are shown. Data was acquired at about solar noon. Data acquired during the Geminids stream are indicated with an X or a +. Also shown is the scaled surface albedo averaged between –15° and –22° latitude [green line in (A)] and in the relative concentration of K at the latitude of –20° in the lunar soil as a function of selenographic longitude as derived from Lunar Prospector observations [green line in (B)].

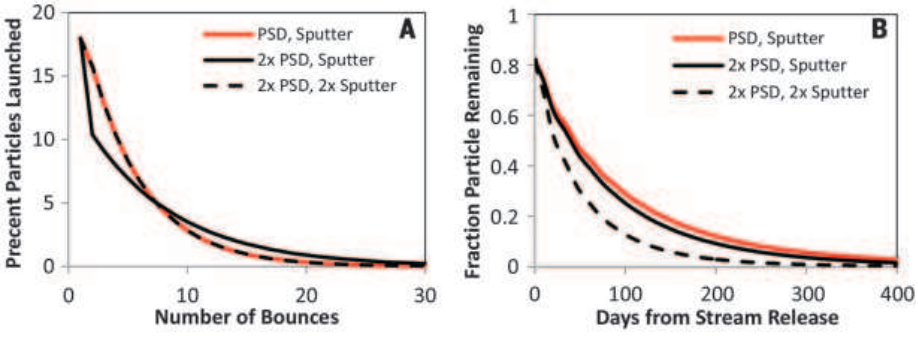

Fig. 4. The lifetimes of sodium released by meteoroid impacts, as estimated with a Monte Carlo method. In these simulations, the effect of a meteoroid stream is modeled by a sudden release of Na test particles, which are tracked until loss by photoionization, sputtering, or deposition into permanently shadowed regions (*18*). The fraction of atoms lost on the first bounce much exceeds gravitational escape, reflecting losses to sputtering after particles recycle for the first time (**A**). Prolonged residence of released Na on surficial grains between bounces would continue to affect the exosphere well after the meteoroid stream encounter, with an exponential time decay as long as 90 days (**B**).

The large instantaneous responses of the dayside to meteor showers are indirect evidence of the role of adsorbed particles. If all particles were lost to the surface in one bounce, it would take more than an order of magnitude enhancement of impact vaporization during showers over sporadic impacts for this source to reach the rate of 2×10^6 Na atoms cm^{-2} s^{-1} required to explain the Na atmosphere (*7*). Hence, vapor introduced by meteoroid impacts can reside for considerable periods on the surface, adding to the overall adsorbed Na and K surface reservoir. We performed Monte Carlo simulations to estimate the total residence time for Na and K in the exosphere and soil. In the simulations, a one-second injection of Na or K was assumed to occur from the nightside hemisphere, with the duration between hops and loss rates for sputtering and photoionization taken from published values (see the supplementary materials). The simulations show that a release of ejecta from a single injection will persist in the exosphere-surface system for much longer than the ionization lifetime would suggest (Fig. 4). This is the result of each particle residing in the soil for approximately an ionization lifetime (i.e., several days) between bounces, combined with the many bounces that it has to take before being lost from the exosphere. Residence times in the lunar environment of 45 to 90 days (mainly on the lunar surface) can be expected before escape to the solar wind, which would explain the long-term smooth increase and decrease in the Na column density observed as the result of meteoroid streams (Fig. 2). Shorter times are predicted if some fraction (but smaller than 50%) of recycled particles are trapped permanently between bounces.

These observations provide constraints on the sources and sinks of Na and K in the lunar exosphere. The nearly continuous, synoptic nature of the observations illustrates the contribution of impacts and surface composition. The independent

confirmation by Kaguya and LADEE of the lunar Na trend between November and April provides the strongest evidence yet for an annual variation of the Na exosphere. This trend is likely the cumulative response of Na to meteoroid streams, whose annual activity peaks from November through January and then subsides until the summer. The substantial residence time for Na at the surface suggested by this interpretation inevitably leads to the conclusion that Na migrates toward the poles like other volatiles (e.g., water) in these cycles of adsorption and redesorption. The K measurements show a strong but, contrary to Na, short-lived response to the Geminids meteoroid shower. Outside of the meteoroid streams, K shows a regular variation across a lunation that correlates strongly with the abundance of potassium in the lunar bulk soil. Combined, these results and recent studies of the Mercurian exosphere (*23*, *24*) indicate a pronounced role for meteoroid impact vaporization and surface exchange in determining the composition of surface-bounded exospheres. However, the details of how the exosphere depends on surface composition and responds to meteoroid streams are not yet understood.

REFERENCES AND NOTES

1. R. C. Elphic *et al*., *Space Sci. Rev.* **185**, 3–25 (2014).
2. A. Colaprete *et al*., *Space Sci. Rev.* **185**, 63–91 (2014).
3. A. E. Potter, T. H. Morgan, *Science* **241**, 675–680 (1988).
4. A. S. Stern, *Rev. Geophys.* **37**, 453–491 (1999).
5. A. L. Sprague, M. Sarantos, D. M. Hunten, R. E. Hill, R. W. H. Kozlowski, *Can. J. Phys.* **90**, 725–732 (2012).
6. D. Hunten, A. L. Sprague, *Adv. Space Res.* **19**, 1551–1560 (1997).
7. M. Sarantos, R. M. Killen, A. S. Sharma, J. A. Slavin, *Icarus* **205**, 364–374 (2010).
8. M. Kagitani *et al*., *Earth Planets Space* **61**, 1025–1029 (2009).
9. M. Kagitani *et al*., *Planet. Space Sci.* **58**, 1660–1664 (2010).
10. R. W. H. Kozlowski, A. L. Sprague, D. M. Hunten, *Geophys. Res. Lett.* **17**, 2253–2256 (1990).
11. A. L. Sprague, R. W. Kozlowski, D. M. Hunten, W. K. Wells, F. A. Grosse, *Icarus* **96**, 27–42 (1992).
12. D. M. Hunten *et al*., *Icarus* **136**, 298–303 (1998).
13. S. M. Smith, J. K. Wilson, J. Baumgardner, M. Mendillo, *Geophys. Res. Lett.* **26**, 1649–1652 (1999).
14. S. Verani, C. Barbieri, C. Benn, G. Cremonese, *Planet. Space Sci.* **46**, 1003–1006 (1998).
15. V. Tenishev, M. Rubin, O. J. Tucker, M. R. Combi, M. Sarantos, *Icarus* **226**, 1538–1549 (2013).
16. A. A. Berezhnoy *et al*., *Planet. Space Sci.* **96**, 90–98 (2014).
17. M. Matta *et al*., *Icarus* **204**, 409–417 (2009).
18. Materials and methods are available as supplementary materials on *Science* Online
19. A. E. Potter, R. M. Killen, T. H. Morgan, *J. Geophys. Res.* **105** (E6), 15073–15084 (2000).
20. B. L. Jolliff, J. J. Gillis, L. A. Haskin, R. L. Korotev, M. A. Wieczorek, *J. Geophys. Res.* **105** (E2), 4197–4216 (2000).
21. D. J. Lawrence *et al*., *Science* **281**, 1484–1489 (1998).
22. T. J. Stubbs *et al*., Influence of Meteoroid Streams on the Lunar Environment: Results from LADEE, 46th Lunar and Planetary Science Conference, held March 16–20, 2015, in The Woodlands, Texas. LPI Contribution No. 1832, p. 2984 (2015).
23. M. Horányi *et al*., *Nature* **522**, 324–326 (2015).
24. R. M. Killen, J. Hahn, *Icarus* **250**, 230 (2015).

ACKNOWLEDGMENTS

We thank R. Killen for constructive discussions and the three reviewers who helped to greatly improve this paper. LADEE UVS was supported through the NASA Lunar Quest Program. Additional funding for M.S. was through NASA grants NNX14AG14A, NNX13AP94G, and NNX13AO74G. All LADEE UVS data are available online at the NASA Planetary Data System (PDS), including all raw and calibrated spectra and derived sodium and potassium line strengths.

SUPPLEMENTARY MATERIALS

www.sciencemag.org/content/351/6270/249/suppl/DC1
Materials and Methods
Supplementary Text
Figs. S1 to S5
References (*25*–*34*)

13 August 2015; accepted 30 November 2015
Published online 17 December 2015
10.1126/science.aad2380

ORGANIC CHEMISTRY

Functionalization of C(sp^3)–H bonds using a transient directing group

Fang-Lin Zhang,* Kai Hong,* Tuan-Jie Li,* Hojoon Park, Jin-Quan Yu†

Proximity-driven metalation has been extensively exploited to achieve reactivity and selectivity in carbon–hydrogen (C–H) bond activation. Despite the substantial improvement in developing more efficient and practical directing groups, their stoichiometric installation and removal limit efficiency and, often, applicability as well. Here we report the development of an amino acid reagent that reversibly reacts with aldehydes and ketones in situ via imine formation to serve as a transient directing group for activation of inert C–H bonds. Arylation of a wide range of aldehydes and ketones at the β or γ positions proceeds in the presence of a palladium catalyst and a catalytic amount of amino acid. The feasibility of achieving enantioselective C–H activation reactions using a chiral amino acid as the transient directing group is also demonstrated.

Precoordination of a metal with functional groups in substrates has been extensively exploited to control selectivity and promote reactivity in metal-catalyzed or -mediated reactions (*1*–*5*). The same approach has been successfully implemented in directed C–H activation reactions (*6*–*11*). However, the covalent installation and removal of directing groups is a major drawback for synthetic applications. First, an additional two steps must be added to the synthetic sequence. Second, the conditions for installation or removal of the directing groups are sometimes incompatible with other functional groups present in advanced synthetic intermediates. It is therefore highly desirable to devise a functionally tolerant reagent that can be reversibly linked to the substrate and can serve as a directing group. Upon C–H activation and subsequent functionalization, this reagent would dissociate from the product and transiently link to another substrate molecule so that only a catalytic quantity of the directing group would be needed (Fig. 1A). This approach has been successfully implemented in Rh(I)-catalyzed C(sp^2)–H activation reactions in a number of pioneering examples. Jun *et al*. reported the use of 2-amino pyridine as a transient directing group for Rh-catalyzed activation of aldehydic C–H bonds (*12*) (Fig. 1B). Recently, using a related strategy, Mo and Dong reported a Rh-catalyzed α-alkylation of ketones via a vinyl C–H activation step, featuring an enamine intermediate with a pyridine moiety as the transient directing group (*13*). Bedford *et al*. developed a Rh-catalyzed ortho-arylation through reversible in situ transesterification of catalytic amounts of phosphinite ligands with the phenol substrate (*14*). The strategy of using catalytic directing groups has also been employed by Lightburn *et al*. (*15*) and Grünanger and Breit (*16*) to achieve selectivity in Rh-catalyzed hydroformylation reactions.

In conjunction with our efforts to develop Pd-catalyzed C(sp^3)–H functionalizations (*17*, *18*), we have extensively investigated the feasibility of Pd(II)-catalyzed C(sp^3)–H activation of aldehydes and ketones using a wide range of potential transient directing groups, including those previously developed for Rh(I) catalysts. Unfortunately, the resultant Pd(II) complexes bound to the bidentate iminopyridine or iminooxazoline are unreactive toward cleavage of sp^3 C–H bonds under various conditions. The development of monoprotected amino acid ligands (*19*, *20*) and the recent use of amino acids as bidentate directing groups in C–H functionalizations of peptides (*21*) led us to speculate that an amino acid could serve as a suitable transient directing group. We reasoned that the amino acid could be reversibly tethered to an aldehyde or ketone substrate via an imine linkage under appropriate conditions. In a similar manner to that operative in our dipeptide chemistry, the imine moiety and the carboxylate could form a bidentate directing group to enable subsequent C–H functionalization (Fig. 1C).

The Scripps Research Institute, 10550 North Torrey Pines Road, La Jolla, CA 92037, USA.
*These authors contributed equally to this work.
†Corresponding author. E-mail: yu200@scripps.edu

We chose arylation of 2-methylbenzaldehyde **1a** with 4-iodoanisole as the model reaction for optimization. Benzaldehyde derivatives are known to readily form imine linkages with amino acids (*22*). After extensive experimentation, we found that the desired C(sp^3)–H selective mono-arylation product **2a** could be observed in 18% nuclear magnetic resonance (NMR) yield when the reaction was conducted in hexafluoroisopropyl alcohol (HFIP) with 10 mol % $Pd(OAc)_2$ (OAc, acetate), 40 mol % glycine, and 1.5 equivalents of silver trifluoroacetate (see table S1, entry 5). The use of acetic acid (AcOH) as the solvent improved the yield to 52%, albeit with considerable decomposition of the starting material (table S1, entry 6). We speculated that the low mass balance stemmed from a rate mismatch between the imine formation step and the following C–H cleavage step, leading to decomposition of the accumulated imine species. Therefore, we reasoned that the addition of water would reduce the concentration of the imine intermediate and prevent decomposition during the reaction. Indeed, when a 9:1 mixture of AcOH and H_2O was used as the solvent, we were able to achieve 93% conversion and 71% NMR yield, along with formation of the diarylated product in 11% yield (table S1, entry 8). By switching the limiting reagent to the aryl iodide, we obtained the desired mono-arylated product exclusively in 81% NMR yield (table S1, entry 10). We also evaluated a variety of amino acids and found that the side chain of the amino acid does not have a marked effect on the efficiency of this transformation (table S1, entries 10 to 13). As expected, N-protected glycine led to a complete loss of reactivity, consistent with the hypothesis that imine formation is crucial for enabling C–H activation (table S1, entry 14).

Under optimal conditions, we next examined the scope of C–H arylation (Fig. 2). The arylation of 2-methylbenzaldehyde **1a** proceeded with a wide range of aryl iodides in good yields. Both electron-donating (**2a** to **2c**) and electron-withdrawing (**2f** to **2n**) substituents are well tolerated at either the para or meta position of the aryl iodide (72 to 83% yield). The use of a sterically hindered ortho-substituted aryl iodide led to a reduced yield (**2d**, 43%). The reaction can accommodate a range of functional groups, including halides (F and Br), nitro groups, aldehydes, ketones, esters, and even free carboxylic acid groups. More importantly, this reaction is compatible with heteroaryl iodides as coupling partners (**2o** to **2v**), overriding the strong coordination of heteroatoms to the metal catalyst. This feature renders the reaction particularly useful for the synthesis of biologically active compounds bearing heterocycles. Finally, benzaldehydes with various ortho, meta, and para substituents were effectively arylated with 1-iodo-3-nitrobenzene, providing the corresponding products in good yields under the standard conditions (**2w** to **2ad**). The use of the analogous ketone substrate 2′-methylacetophenone produced the arylated product in low yield, presumably because that ketimine is more difficult to form.

We next investigated whether the same strategy could be applied to aliphatic ketone substrates, which are versatile and widely used synthetic intermediates (*23*). Although β-arylation of ketones via reaction pathways other than β-metal insertion has been limited to the substrates without α-substitution (*24*, *25*), directed C(sp^3)–H activation of ketones has only been studied through the intermediacy of preformed oximes (*9*, *26*, *27*). We were aware that direct arylation of ketones using a transient directing

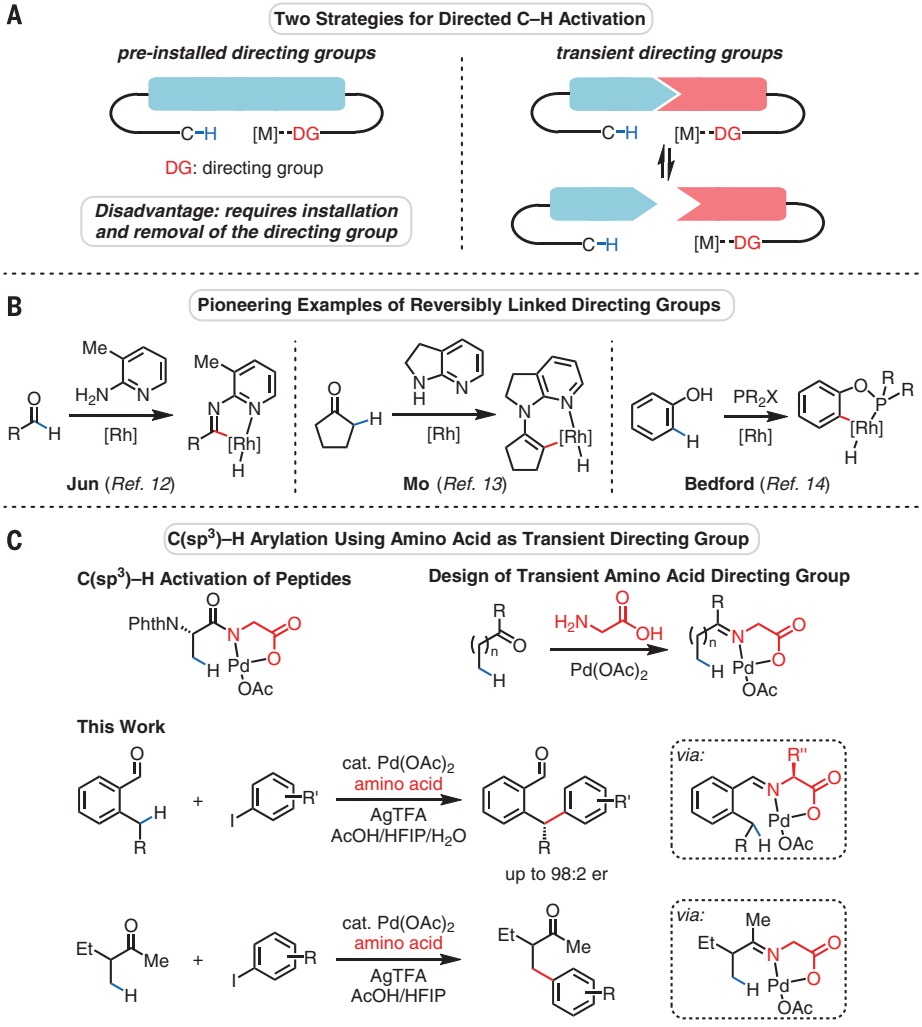

Fig. 1. C–H activation using transient directing groups. (**A**) Two strategies for directed C–H activation. M, metal. (**B**) Pioneering examples of reversibly linked directing groups. Me, methyl; X, leaving group. (**C**) C(sp^3)–H arylation using an amino acid as a transient directing group. Phth, phthalimido; Et, ethyl; TFA, trifluoroacetic acid.

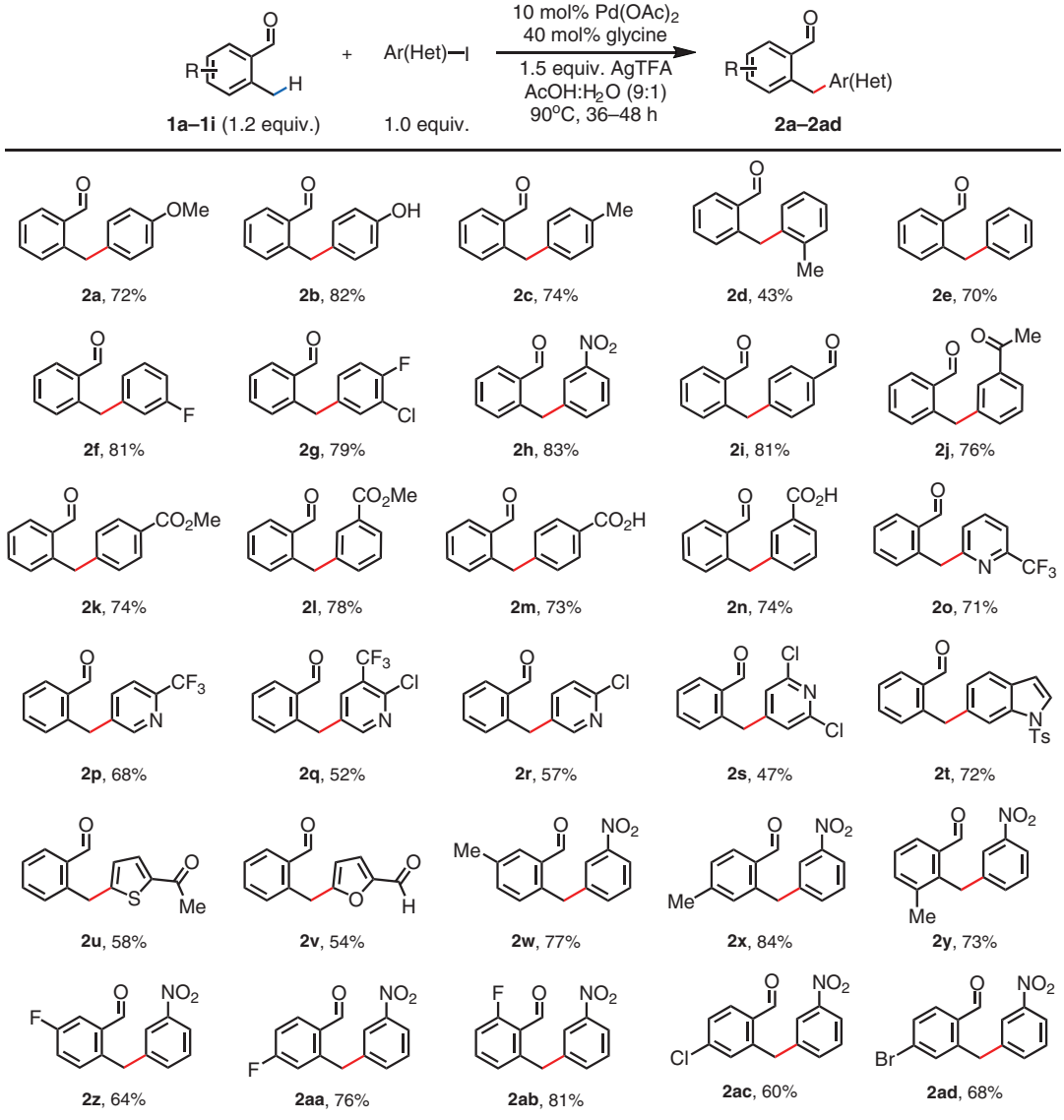

Fig. 2. Palladium-catalyzed benzylic C(sp^3)–H arylation of aldehydes. Ar(Het), (hetero)aryl.

For each entry number (in boldface), data are reported as isolated yield. See supplementary materials for experimental details.

group would pose several challenges: First, in situ formation of ketimines is generally less favored than that of aldimines. Second, one of the ketimine *E*/*Z* isomers may not be reactive if the orientation of the imino acid directing group is not suitable for directing palladium in proximity to the target C–H bond. Third, tautomerization of imines to enamines may occur as a competing pathway, which would generate an ineffective directing group. With these considerations in mind, we further optimized the reaction conditions for ketone arylation. Although the initial investigation with 3-methyl-2-pentanone (**3a**) provided <2% yield of the desired product under the optimal conditions for aldehydes (table S2, entry 1), we found that by using 50 mol % glycine and a 3:1 mixture of HFIP:AcOH as the solvent, the yield of β-arylation product **4a** could be substantially improved to 71% (table S2, entry 7). However, a variety of amino acids with side chains proved inferior and led to diminished yields (table S2, entries 9 to 11).

We then explored the scope of ketones and aryl iodides under the new conditions. As illustrated in Fig. 3, a wide range of aryl iodides with electron-donating or -withdrawing substituents were well tolerated (**4a** to **4f**). Moderate to good yields were achieved after conducting the reaction with a variety of linear, α-branched, and cyclic ketones (**4g** to **4r**). We found that this method can activate methylene C(sp^3)–H bonds in cyclic substrates, producing the corresponding syn products with excellent diastereoselectivity (**4o** to **4q**). Furthermore, one example of γ-arylation was observed when β-C(sp^3)–H bonds were absent in the substrate (**4s**). However, aliphatic aldehydes are not suitable substrates because competing reaction pathways lead to the decomposition of the starting material under the current conditions.

Because carrying out Pd-catalyzed enantioselective C–H insertion reactions remains a substantial challenge (*19*, *28*–*30*), we wondered whether the enantioselective C–H arylation could be achieved by using a chiral reversible directing agent. Thus, benzaldehydes bearing methylene C(sp^3)–H bonds were investigated in the presence of a chiral amino acid. This transformation is difficult due to the more sluggish C–H activation, as well as the requirement of discrimination between the two enantiotopic C–H bonds. On the basis of our proposed intermediate in Fig. 1C, we envisioned that the enantioselection could be realized through the steric interaction between the R group (R ≠ H) and the bulky side chain R″ of the amino acid. Indeed, when 40 mol % L-valine (R″ = isopropyl)

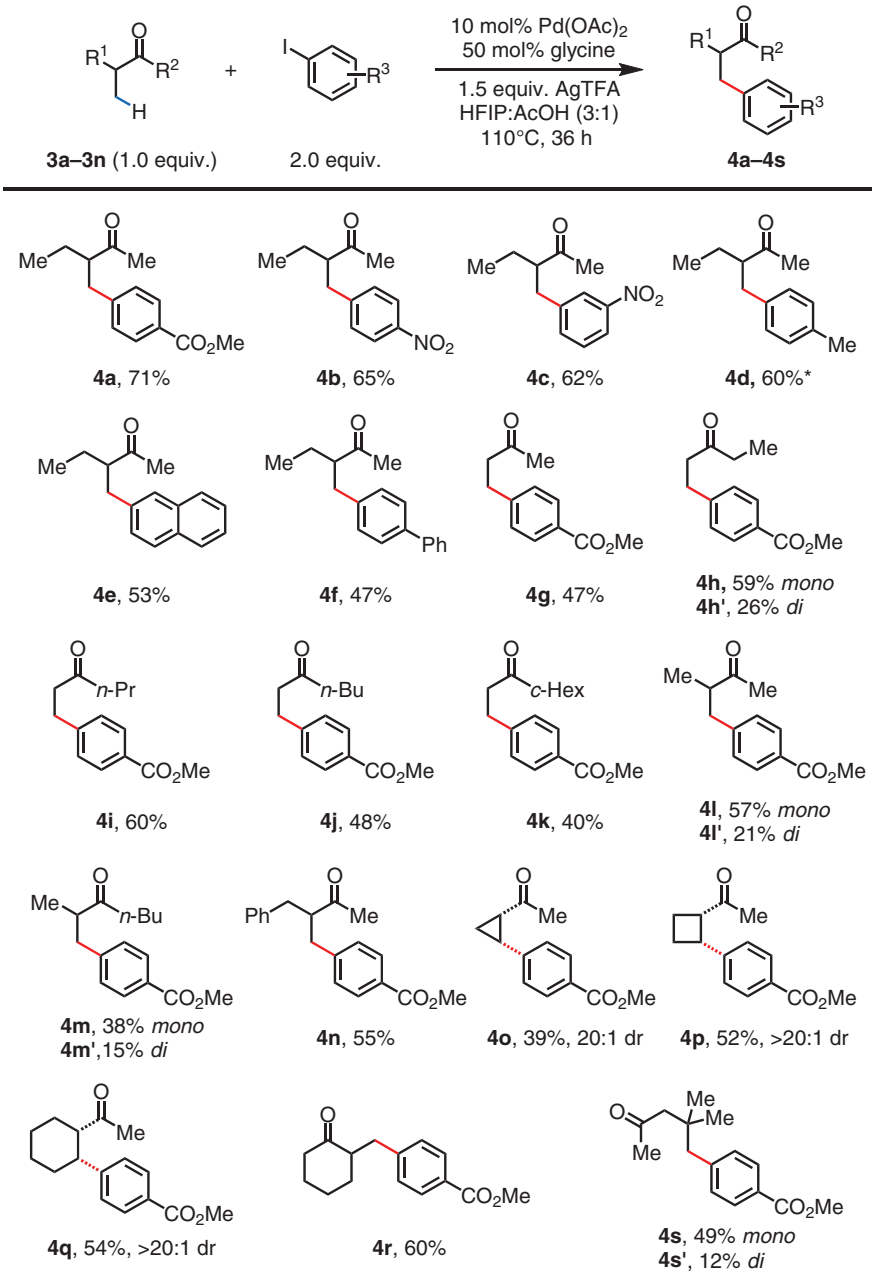

Fig. 3. Palladium-catalyzed C(sp^3)–H arylation of ketones. Pr, propyl; Bu, butyl; Hex, hexyl; dr, diastereomeric ratio.

For each entry number (in boldface), data are reported as isolated yield. See supplementary materials for experimental details. * Reaction performed at 130°C with 3.0 equiv. aryl iodide.

was used instead of glycine, the arylation of 2-ethyl-5-(trifluoromethyl)benzaldehyde (**5a**) provided the desired product **6a** with an enantiomeric ratio (er) of 85:15 (table S3, entry 4). Consequently, we speculated that a more sterically encumbered amino acid should lead to superior enantioselectivity. When we performed the reaction using L-*tert*-leucine (R″ = *tert*-butyl), we achieved excellent enantioselectivity (98:2 er), albeit in only 30% NMR yield (table S3, entry 5). Reducing the ratio of ligand-to-Pd from 4:1 to 2:1 resulted in a substantially enhanced yield (87%), without any erosion of enantioselectivity (table S3, entry 6). Apparently, sterically bulky L-*tert*-leucine is less prone to imine formation, allowing the free form of the amino acid to coordinate with Pd(II) and deactivate the catalyst. Finally, the addition of 3 equivalents of water led to nearly identical results (table S3, entry 8). However, the presence of water has proved to be beneficial to other aldehyde substrates.

Under optimized conditions, the enantioselective arylation of **5a** proceeded effectively with a wide range of aryl iodides bearing various functional groups at the para or meta position (**6a** to **6i** in Fig. 4). With respect to the scope of aldehydes, the reaction is compatible with ester (**6j**), trifluoromethyl (**6k**), and halogen substituents (**6l** to **6n**). Halogen-substituted benzaldehydes exhibited higher reactivity, and the palladium catalyst loading could be reduced to 5 mol %. Moreover, the methylene C(sp^3)–H bond on longer side chains could also be activated (**6o** and **6p**), thus greatly expanding the scope of aldehydes for this reaction.

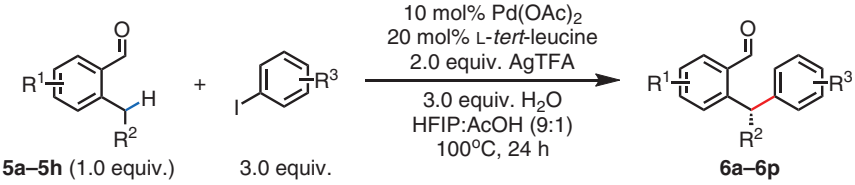

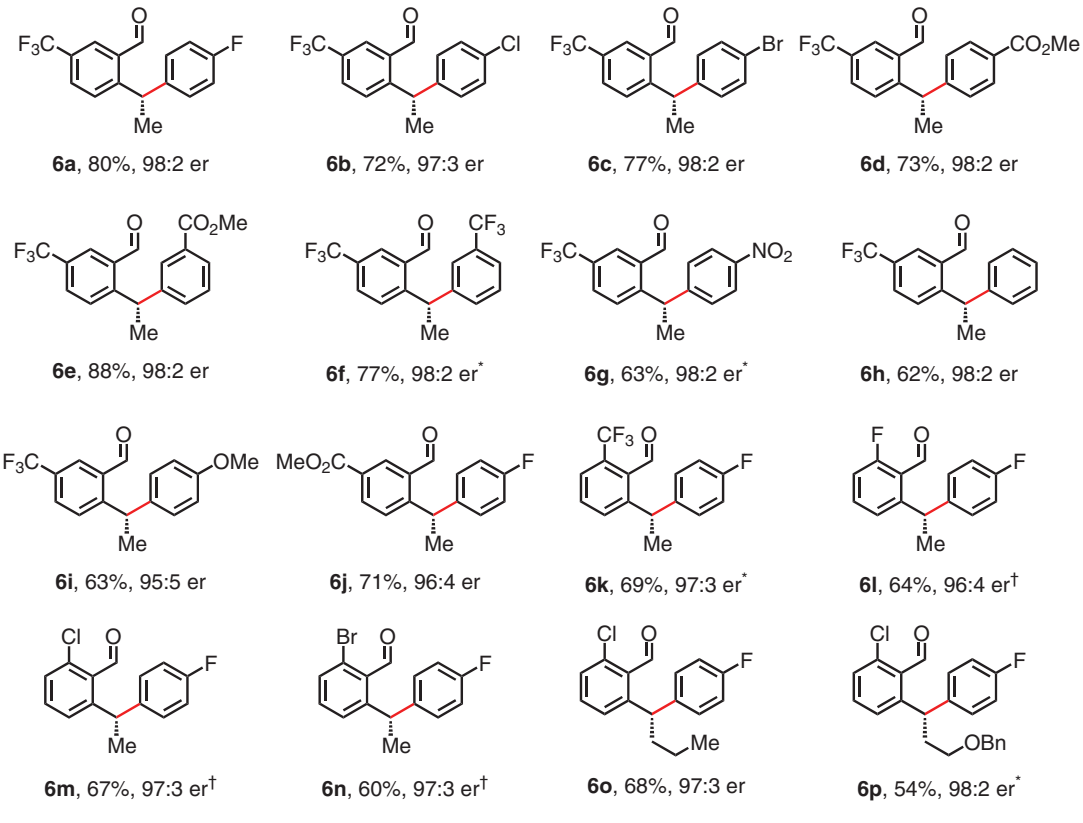

Fig. 4. Palladium-catalyzed enantioselective benzylic C(sp^3)–H arylation of aldehydes. HPLC, high-performance liquid chromatography.

For each entry number (in boldface), data are reported as isolated yield. Enantiomeric ratios (er) were determined by chiral HPLC analysis. See supplementary materials for experimental details. *Reaction performed at 110°C. †Reaction performed with 5 mol% $Pd(OAc)_2$ and 10 mol% L-*tert*-leucine.

REFERENCES AND NOTES

1. J. M. Brown, *Chem. Soc. Rev.* **22**, 25–41 (1993).
2. A. H. Hoveyda, D. A. Evans, G. C. Fu, *Chem. Rev.* **93**, 1307–1370 (1993).
3. C. G. Hartung, V. Snieckus, in *Modern Arene Chemistry*, D. Astruc, Ed. (Wiley, 2004), pp. 330–367.
4. R. A. Johnson, K. B. Sharpless, in *Catalytic Asymmetric Synthesis*, I. Ojima, Ed. (Wiley, ed. 2, 2005), pp. 231–280.
5. Z. Li, H. Yamamoto, *Acc. Chem. Res.* **46**, 506–518 (2013).
6. X. Chen, K. M. Engle, D.-H. Wang, J.-Q. Yu, *Angew. Chem. Int. Ed.* **48**, 5094–5115 (2009).
7. O. Daugulis, H.-Q. Do, D. Shabashov, *Acc. Chem. Res.* **42**, 1074–1086 (2009).
8. L. Ackermann, R. Vicente, A. R. Kapdi, *Angew. Chem. Int. Ed.* **48**, 9792–9826 (2009).
9. L. V. Desai, K. L. Hull, M. S. Sanford, *J. Am. Chem. Soc.* **126**, 9542–9543 (2004).
10. D. A. Colby, R. G. Bergman, J. A. Ellman, *Chem. Rev.* **110**, 624–655 (2010).
11. J. Wencel-Delord, T. Dröge, F. Liu, F. Glorius, *Chem. Soc. Rev.* **40**, 4740–4761 (2011).
12. C.-H. Jun, H. Lee, J.-B. Hong, *J. Org. Chem.* **62**, 1200–1201 (1997).
13. F. Mo, G. Dong, *Science* **345**, 68–72 (2014).
14. R. B. Bedford, S. J. Coles, M. B. Hursthouse, M. E. Limmert, *Angew. Chem. Int. Ed.* **42**, 112–114 (2003).
15. T. E. Lightburn, M. T. Dombrowski, K. L. Tan, *J. Am. Chem. Soc.* **130**, 9210–9211 (2008).
16. C. U. Grünanger, B. Breit, *Angew. Chem. Int. Ed.* **47**, 7346–7349 (2008).
17. D.-H. Wang, M. Wasa, R. Giri, J.-Q. Yu, *J. Am. Chem. Soc.* **130**, 7190–7191 (2008).
18. J. He *et al.*, *Science* **343**, 1216–1220 (2014).
19. B.-F. Shi, N. Maugel, Y.-H. Zhang, J.-Q. Yu, *Angew. Chem. Int. Ed.* **47**, 4882–4886 (2008).
20. D.-H. Wang, K. M. Engle, B.-F. Shi, J.-Q. Yu, *Science* **327**, 315–319 (2010).
21. W. Gong, G. Zhang, T. Liu, R. Giri, J.-Q. Yu, *J. Am. Chem. Soc.* **136**, 16940–16946 (2014).
22. F. C. McIntire, *J. Am. Chem. Soc.* **69**, 1377–1380 (1947).
23. R. C. Larock, in *Comprehensive Organic Transformations* (Wiley, ed. 2, 1999), pp. 1197–1620.
24. M. T. Pirnot, D. A. Rankic, D. B. C. Martin, D. W. C. MacMillan, *Science* **339**, 1593–1596 (2013).
25. Z. Huang, G. Dong, *J. Am. Chem. Soc.* **135**, 17747–17750 (2013).
26. T. Kang, Y. Kim, D. Lee, Z. Wang, S. Chang, *J. Am. Chem. Soc.* **136**, 4141–4144 (2014).
27. P. Gao *et al.*, *J. Am. Chem. Soc.* **137**, 12231–12240 (2015).
28. M. Nakanishi, D. Katayev, C. Besnard, E. P. Kündig, *Angew. Chem. Int. Ed.* **50**, 7438–7441 (2011).
29. S. Anas, A. Cordi, H. B. Kagan, *Chem. Commun.* **47**, 11483–11485 (2011).
30. T. Saget, S. J. Lemouzy, N. Cramer, *Angew. Chem. Int. Ed.* **51**, 2238–2242 (2012).

ACKNOWLEDGMENTS

We gratefully acknowledge The Scripps Research Institute and the NIH (National Institute of General Medical Sciences grant 2R01GM084019) for financial support. F.-L.Z. thanks Wuhan University of Technology and T.-J.L. thanks Jiangsu Normal University for financial support. J.-Q.Y. and F.-L.Z. conceived the experimental concept; F.-L.Z. performed the arylation of primary C–H bonds; K.H. developed the enantioselective C–H arylation; T.-J.L. developed conditions for the β-arylation of ketones; and H.P. performed enantioselective C–H arylation. Metrical parameters for the structure of compound **S2** (see supplementary materials) are available free of charge from the Cambridge Crystallographic Data Centre under reference number CCDC 1434263.

SUPPLEMENTARY MATERIALS

www.sciencemag.org/content/351/6270/252/suppl/DC1
Supplementary Text
Tables S1 to S9
NMR Spectra
HPLC Spectra
X-ray Crystallographic Data
Reference (*31*)

2 November 2015; accepted 4 December 2015
10.1126/science.aad7893

ASTRONOMY

ASASSN-15lh: A highly super-luminous supernova

Subo Dong,[1]* B. J. Shappee,[2] J. L. Prieto,[3,4] S. W. Jha,[5] K. Z. Stanek,[6,7] T. W.-S. Holoien,[6,7] C. S. Kochanek,[6,7] T. A. Thompson,[6,7] N. Morrell,[8] I. B. Thompson,[2] U. Basu,[6] J. F. Beacom,[6,7,9] D. Bersier,[10] J. Brimacombe,[11] J. S. Brown,[6] F. Bufano,[12] Ping Chen,[13] E. Conseil,[14] A. B. Danilet,[6] E. Falco,[15] D. Grupe,[16] S. Kiyota,[17] G. Masi,[18] B. Nicholls,[19] F. Olivares E.,[4,20] G. Pignata,[4,20] G. Pojmanski,[21] G. V. Simonian,[6] D. M. Szczygiel,[21] P. R. Woźniak[22]

We report the discovery of ASASSN-15lh (SN 2015L), which we interpret as the most luminous supernova yet found. At redshift z = 0.2326, ASASSN-15lh reached an absolute magnitude of $M_{u,AB}$ = −23.5 ± 0.1 and bolometric luminosity L_{bol} = (2.2 ± 0.2) × 10^{45} ergs s^{-1}, which is more than twice as luminous as any previously known supernova. It has several major features characteristic of the hydrogen-poor super-luminous supernovae (SLSNe-I), whose energy sources and progenitors are currently poorly understood. In contrast to most previously known SLSNe-I that reside in star-forming dwarf galaxies, ASASSN-15lh appears to be hosted by a luminous galaxy (M_K ≈ −25.5) with little star formation. In the 4 months since first detection, ASASSN-15lh radiated (1.1 ± 0.2) × 10^{52} ergs, challenging the magnetar model for its engine.

Only within the past two decades has the most luminous class of supernovae (super-luminous supernovae, SLSNe) been identified (*1*). Compared with the most commonly discovered SNe (Type Ia), SLSNe are more luminous by over two magnitudes at peak and rarer by at least 3 orders of magnitude (*2*). Like normal SNe, SLSNe are classified by their spectra as either SLSN-I (hydrogen-poor) or SLSN-II (hydrogen-rich). Yet, the physical characteristics of SLSNe may not be simple extensions from their low-luminosity counterparts (*1*). In particular, the power source for SLSNe-I is poorly understood (*3*). Adding to the puzzle, SLSNe tend to explode in low-luminosity, star-forming dwarf galaxies (*4*–*6*). The recent advent of wide-area, untargeted transient surveys has made the systematic discovery and investigation of the SLSNe population possible [(*7*, *8*) and references therein].

The All-Sky Automated Survey for SuperNovae [ASAS-SN; www.astronomy.ohio-state.edu/~assassin (*9*)] scans the visible sky every two to three nights to depths of V ≈ 16.5 to 17.3 mag using a global network of 14-cm telescopes (*9*) in an untargeted search for new transients, particularly bright supernovae.

On 14 June 2015 (universal time dates are used throughout this paper), ASAS-SN triggered on a new source located at RA = $22^h02^m15^s.45$ Dec = −61°39′34″.6 (J2000), coinciding with a galaxy of then unknown redshift, APMUKS(BJ) B215839.70–615403.9 (*10*). Upon confirmation with our follow-up telescopes, we designated this new source ASASSN-15lh and published its coordinates (*11*).

By combining multiple epochs of ASAS-SN images, we extended the detections to fainter fluxes, finding prediscovery images of ASASSN-15lh from 8 May 2015 (V = 17.39 ± 0.23 mag), and the light curve through 19 September 2015 is shown in Fig. 1. The ASAS-SN light curve peaked at V = 16.9 ± 0.1 on approximately t_{peak} ~ JD2457179 (2015 June 05) based on a parabolic fit to the lightcurve (Fig. 1, dashed line). Follow-up images were taken with the Las Cumbres Observatory Global Telescope Network (LCOGT) 1-m telescopes, and the BV light-curves with the galaxy contribution subtracted are also shown.

We obtained an optical spectrum (3700 to 9200 Å) of ASASSN-15lh on 21 June 2015 with the du Pont 100-inch telescope. The steep spectral slope with relatively high blue flux motivated *Swift* UltraViolet and Optical Telescope (UVOT)/X-Ray Telescope (XRT) (*12*) target-of-opportunity observations starting on 24 June 2015. The six-band *Swift* light curve spanning from the ultraviolet (UV) to the optical (1928 to 5468 Å) is shown in Fig. 1. The *Swift* spectral energy distribution (SED), peaking in the UV, indicates that the source has a high temperature. We derive a 3σ x-ray flux limit of <1.6 × 10^{-14} ergs s^{-1} cm^{-2} (0.3 to 10 keV) from a total XRT exposure of 81 ks taken between 24 June and 18 September 2015.

The du Pont spectrum is mostly featureless (Fig. 2A, first from the top), except for a deep, broad absorption trough near ~5100 Å (observer frame). SNID (*13*), a commonly used SN classification software that has a spectral library of most types of supernovae except SLSN, failed to find a good SN match. However, we noticed a resemblance between the trough and a feature attributed to O II absorption near 4100 Å (rest frame) in the spectrum of PTF10cwr/SN 2010gx, a SLSN-I at z = 0.230 (*3*, *14*, *15*). Assuming that the ASASSN-15lh absorption trough (full width at half maximum of ~10^4 km s^{-1}) was also due to the same feature indicated a similar redshift of z ~ 0.23. An optical spectrum (3250 to 6150 Å) obtained on the Southern African Large Telescope (SALT) revealed a clear Mg II absorption doublet (λλ2796, 2803) at z = 0.232, confirming the redshift expected from our tentative line identification. Subsequent Magellan/Clay (6 July) and SALT (7 July) spectra refined the redshift to z = 0.2326 (Fig. 2, C and D). The available rest frame spectra show continua with steep spectral slope, relatively high blue fluxes, and several broad absorption features also seen in PTF10cwr/SN 2010gx (Fig. 2A, features "a," "b," and "c") and without hydrogen or helium features, which is consistent with the main spectral features of SLSNe-I (*1*, *3*). The broad absorption feature near 4400 Å (Fig. 2, "d") seen in PTF10cwr/SN 2010gx is not present in ASASSN-15lh. ASASSN-15lh thus has some distinct spectral characteristics in comparison with PTF10cwr/SN 2010gx and some other SLSNe-I (*3*).

Using a luminosity distance of 1171 Mpc (standard *Planck* cosmology at z = 0.2326), Galactic extinction of $E(B-V)$ = 0.03 mag (*16*), assuming no host extinction (thus, the luminosity derived is likely a lower limit), and fitting the *Swift* and LCOGT flux measurements to a simple blackbody (BB) model, we obtain declining rest-frame temperatures of T_{BB} from 2.1 × 10^4 to 1.3 × 10^4 K and bolometric luminosities of L_{bol} = 2.2 × 10^{45} to 0.4 × 10^{45} ergs s^{-1} at rest-frame phases relative to the peak of t_{rest} ~ 15 and ~50 days, respectively (Fig. 3). ASASSN-15lh's bolometric magnitude declines at a best-fit linear rate of 0.048 mag day^{-1}, which is practically identical to SLSN-I iPTF13ajg (*17*) at 0.049 mag day^{-1} during similar phases (~10 to ~50 days). Subsequently, the luminosity and temperature reach a "plateau" phase with slow changes, and a similar trend is also seen for iPTF13ajg though with sparser coverage. Overall,

[1]Kavli Institute for Astronomy and Astrophysics, Peking University, Yi He Yuan Road 5, Hai Dian District, Beijing 100871, China. [2]Carnegie Observatories, 813 Santa Barbara Street, Pasadena, CA 91101, USA. [3]Núcleo de Astronomía de la Facultad de Ingeniería, Universidad Diego Portales, Av. Ejército 441, Santiago, Chile. [4]Millennium Institute of Astrophysics, Santiago, Chile. [5]Department of Physics and Astronomy, Rutgers, The State University of New Jersey, 136 Frelinghuysen Road, Piscataway, NJ 08854, USA. [6]Department of Astronomy, The Ohio State University, 140 W. 18th Avenue, Columbus, OH 43210, USA. [7]Center for Cosmology and AstroParticle Physics (CCAPP), The Ohio State University, 191 W. Woodruff Avenue, Columbus, OH 43210, USA. [8]Las Campanas Observatory, Carnegie Observatories, Casilla 601, La Serena, Chile. [9]Department of Physics, The Ohio State University, 191 W. Woodruff Avenue, Columbus, OH 43210, USA. [10]Astrophysics Research Institute, Liverpool John Moores University, 146 Brownlow Hill, Liverpool L3 5RF, UK. [11]Coral Towers Observatory, Cairns, Queensland 4870, Australia. [12]INAF-Osservatorio Astrofisico di Catania, Via S.Sofia 78, 95123, Catania, Italy. [13]Department of Astronomy, Peking University, Yi He Yuan Road 5, Hai Dian District, 100871, P. R. China. [14]Association Francaise des Observateurs d'Etoiles Variables (AFOEV), Observatoire de Strasbourg 11, rue de l'Université, F-67000 Strasbourg, France. [15]Harvard-Smithsonian Center for Astrophysics, 60 Garden Street, Cambridge, MA 02138, USA. [16]Department of Earth and Space Science, Morehead State University, 235 Martindale Drive, Morehead, KY 40351, USA. [17]Variable Star Observers League in Japan (VSOLJ), 7-1 Kitahatsutomi, Kamagaya, Chiba 273-0126, Japan. [18]The Virtual Telescope Project, Via Madonna de Loco 47, 03023 Ceccano, Italy. [19]Mt Vernon Observatory, 6 Mt Vernon pl, Nelson, New Zealand. [20]Departamento Ciencias Fisicas, Universidad Andres Bello, Av. Republica 252, Santiago, Chile. [21]Warsaw University Astronomical Observatory, Al. Ujazdowskie 4, 00-478 Warsaw, Poland. [22]Los Alamos National Laboratory, Mail Stop B244, Los Alamos, NM 87545, USA.
*Corresponding author. E-mail: dongsubo@pku.edu.cn

the temperature and luminosity time evolution resemble iPTF13ajg, but ASASSN-15lh has a systematically higher temperature at similar phases. The estimated BB radius of ~5×10^{15} cm near the peak is similar to those derived for other SLSNe-I (*3*, *17*). These similarities in the evolution of key properties support the argument that ASASSN-15lh is a member of the SLSN-I class, but with extreme properties.

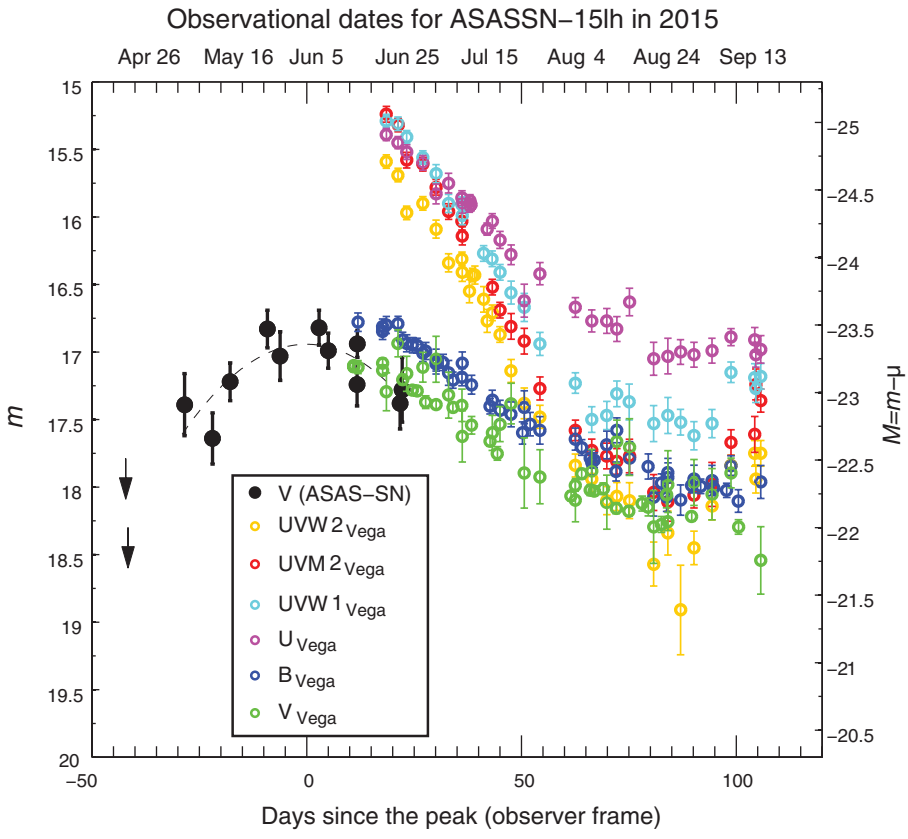

Fig. 1. Multi-band light curve of ASASSN-15lh. The *V*-band ASAS-SN light curve is shown as black solid dots, and upper limits are represented by black arrows. *Swift* and LCOGT 1-m data are shown as open circles.

The absolute magnitudes (AB) in the rest-frame *u*-band are shown in Fig. 4. Using either T_{BB} or the spectra, there is little K-correction (*18*) in converting from *B*-band to rest-frame u_{AB} with $K_{B \to u_{AB}} = -0.1$. The solid red points at $t_{rest} \gtrsim 10$ days include *B*-band data. Before ~10 days, we lack measurements in blue bands. To estimate $M_{u,AB}$ at these earlier epochs, we assumed the $B - V = -0.3$ mag color and K-corrections found for the later epochs with *Swift* photometry. We estimate an integrated bolometric luminosity radiated of ~$(1.1 \pm 0.2) \times 10^{52}$ ergs over 108 days in the rest frame. Although our estimates at $t_{rest} \lesssim 10$ days should be treated with caution, we can securely conclude that the peak $M_{u,AB}$ is at or brighter than −23.5 ± 0.1, with a bolometric luminosity at or greater than $(2.2 \pm 0.2) \times 10^{45}$ ergs s^{-1}. Both values are without precedent for any supernova recorded in the literature. In Fig. 4, we compare ASASSN-15lh with a sample of SLSNe-I (*3*, *17*). Although its spectra resemble the SLSNe-I subclass, ASASSN-15lh stands out from the luminosity distribution of known SLSNe-I, whose luminosities are narrowly distributed around $M \sim -21.7$ (*2*, *19*). In table S1, we list the peak luminosities of the five most luminous SNe discovered to date, including both SLSN-I and SLSN-II. The spectral correspondence and similarities in temperature, luminosity, and radius evolutions between ASASSN-15lh and some SLSNe-I lead to the conclusion that ASASSN-15lh is the most luminous supernova yet discovered. Even though we find that SLSN-I is the most plausible classification of ASASSN-15lh, it is important to consider other interpretations given its distinct properties. We discuss alternative physical interpretations of ASASSN-15lh in the supplementary text, and given all the currently available data, we conclude that it is most likely a supernova, albeit an extreme one.

Fig. 2. Rest-frame spectra of ASASSN-15lh (black) compared with SLSN-I PTF10cwr/SN 2010gx (red). (**A**) The spectra are offset for clarity, labeled with phases and telescopes, and ranked by descending T_{BB} (given on the right) from the top. The ASASSN-15lh spectra are blue and featureless, except for broad absorption features labeled "a," "b," and "c" (marked in blue), which match those of PTF10cwr/SN 2010gx at similar T_{BB}. Absorption features "a" at ~4100 Å and "d" at ~4400 Å (marked in red) in PTF10cwr/SN 2010gx are commonly attributed to O II (*3*, *15*). The ~4400 Å feature is not present in ASASSN-15lh. (**B**) Close-ups of the 4100 Å features, whose evolution in shape, depth, and velocity as a function of T_{BB} is similar for both supernovae. (**C** and **D**) The ASASSN-15lh host redshift ($z = 0.2326$) is determined from the Mg II doublets seen in the SALT and Clay MagE spectra, with EW 0.55 ± 0.05 and 0.49 ± 0.05 Å in (C) and (D), respectively.

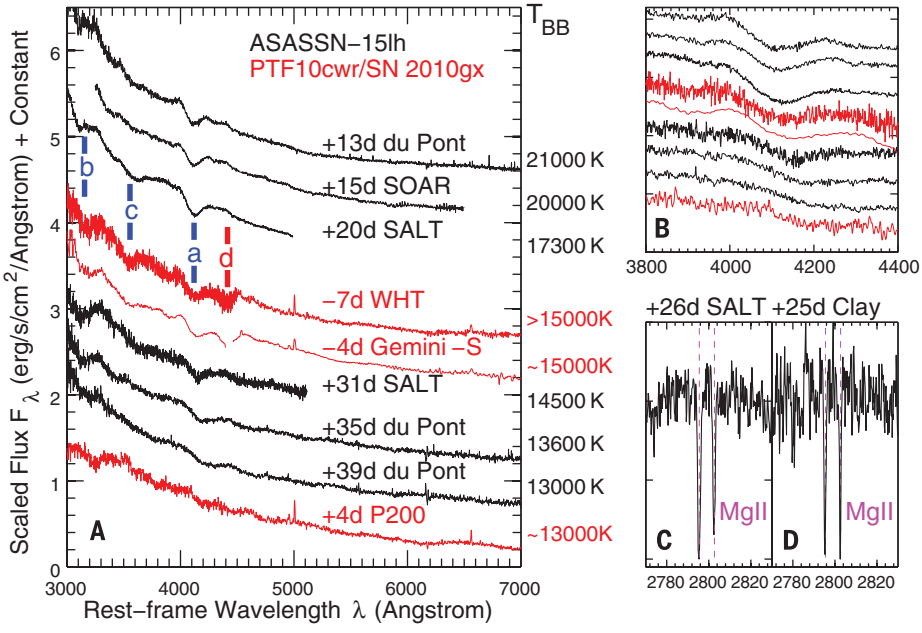

The rate of events with similar luminosities to ASASSN-15lh is uncertain. On the basis of a simple model of transient light curves in ASAS-SN observations tuned to reproduce the magnitude distribution of ASAS-SN Type Ia supernovae (supplementary text), the discovery of one ASASSN-15lh–like event implies a rate of $r \simeq 0.6\ \mathrm{Gpc^{-3}\ yr^{-1}}$ (90% confidence: $0.21 < r < 2.8$). This is at least 2 times and can be as much as 100 times smaller than the overall rate of SLSNe-I, $r \simeq 32\ \mathrm{Gpc^{-3}\ yr^{-1}}$ (90% confidence: $6 < r < 109$) from (*2*), and suggests a steeply falling luminosity function for such supernovae.

For a redshift of $z = 0.2326$, the host galaxy of ASASSN-15lh has $M_K \approx -25.5$, which is much more luminous than the Milky Way. We estimate an effective radius for the galaxy of 2.4 ± 0.3 kpc and a stellar mass of $M_* \approx 2 \times 10^{11}\ M_\odot$. This is in contrast to the host galaxies of other SLSNe, which tend to have much lower M_* (*4*–*6*). However, given the currently available data, we cannot rule out the possibility that the host is a dwarf satellite galaxy seen in projection. The lack of narrow hydrogen and oxygen emission lines from the galaxy superimposed in the supernova spectra implies little star formation (SFR) < 0.3 $M_\odot\ \mathrm{yr^{-1}}$ by applying the conversions in (*20*). Las Cumbres Observatory Global Telescope (LCOGT) astrometry places ASASSN-15lh within 0″.2 (750 pc) of the center of the nominal host. A detailed discussion of the host properties is provided in the supplementary text.

The power source for ASASSN-15lh is unknown. Traditional mechanisms invoked for normal SNe likely cannot explain SLSNe-I (*3*). The lack of hydrogen or helium suggests that shock interactions with hydrogen-rich circumstellar material, invoked to interpret some SLSNe, cannot explain SLSNe-I or ASASSN-15lh. SLSN-I post-peak decline rates appear too fast to be explained by the radioactive decay of ^{56}Ni (*3*)—the energy source for Type Ia supernovae. Both the decline rate of the late-time light curve and the integral method (*21*) will allow tests of whether ASASSN-15lh is powered by ^{56}Ni, and we estimate that $\gtrsim 30\ M_\odot$ of ^{56}Ni would be required to produce ASASSN-15lh's peak luminosity. Another possibility is that the spindown of a rapidly rotating, highly magnetic neutron star (a magnetar) powers the extraordinary emission (*22*–*24*). To match the peak L_{bol} and time scale of ASASSN-15lh, the light-curve models of (*23*) imply a magnetar spin period and magnetic field strength of $P \simeq 1$ ms and $B \simeq 10^{14}$ G, respectively, assuming that all of the spindown power is thermalized in the stellar envelope. If efficient thermalization continues, this model predicts a $L_{\mathrm{bol}} \propto t^{-2}$ power-law at late times. The total observed energy radiated so far ($1.1 \pm 0.2 \times 10^{52}$ ergs) strains a magnetar interpretation because, for $P \lesssim 1$ ms, gravitational wave radiation should limit the total rotational energy available to $E_{\mathrm{rot}}^{\mathrm{max}} \sim 3 \times 10^{52}$ ergs (*25*) and the total radiated energy to a third of $E_{\mathrm{rot}}^{\mathrm{max}}$, which is ~$10^{52}$ ergs (*23*).

The extreme luminosity of ASASSN-15lh opens up the possibility of observing such supernovae in the early universe. An event similar to ASASSN-15lh could be observed with the Hubble Space Telescope out to $z \sim 6$, and with the James Webb Space Telescope out to $z \gtrsim 10$ (*19*). A well-observed local counterpart will be critical in making sense of future observations of the transient high-redshift universe.

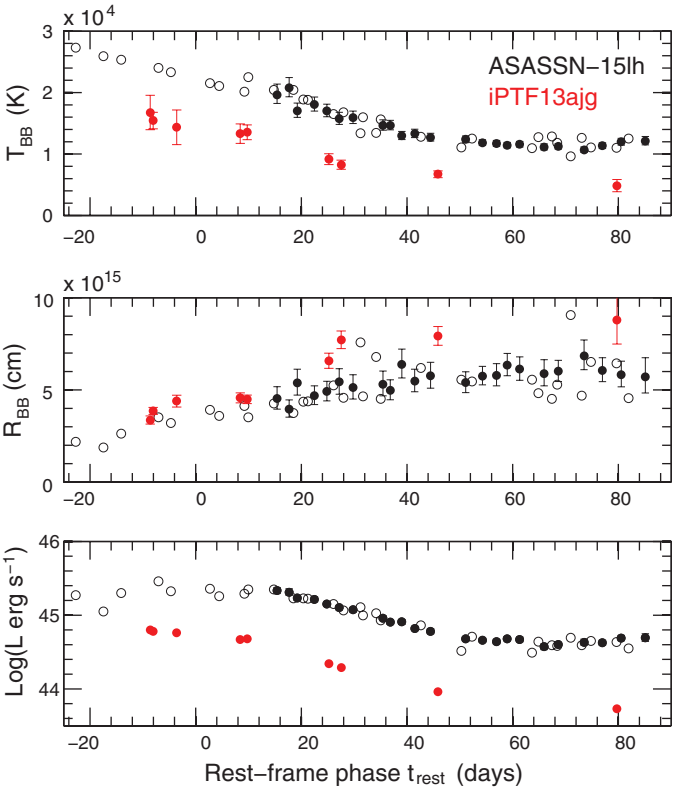

Fig. 3. Time evolution of blackbody temperatures, radii and bolometric luminosities for ASASSN-15lh (black) and SLSN-I iPTF13ajg (red). Solid black dots show estimates derived from the full UV and optical bands, whereas the open circles show those from optical only. For $t_{\mathrm{rest}} < 10$ days, only *V*-band is available, and the temperatures are estimated on the basis of linear extrapolation from MJD = 57191 – 57241.

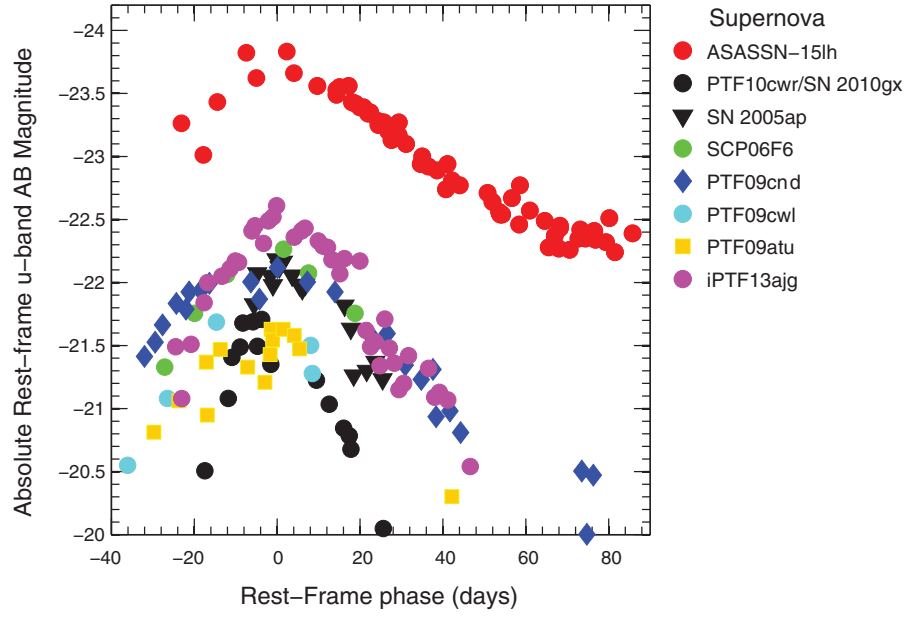

Fig. 4. Rest-frame absolute magnitude light curve of ASASSN-15lh near peak compared with other SLSNe-I. Estimates of $M_{u,\mathrm{AB}}$ for ASASSN-15lh at $t_{\mathrm{rest}} \gtrsim 10$ days are derived from *B*-band fluxes, which are subject to small K-corrections, whereas the less reliable $M_{u,\mathrm{AB}}$ estimates are based on *V*-band only for $t_{\mathrm{rest}} \lesssim 10$ days. The comparison sample (*3*, *17*) includes the most luminous SLSNe-I previously known. At $M_{u,\mathrm{AB}} = -23.5$, ASASSN-15lh stands out from the SLSNe-I luminosity distribution (*2*, *19*). Its peak bolometric absolute magnitude is more than ~1 mag more luminous than any other SLSN-I.

REFERENCES AND NOTES

1. A. Gal-Yam, *Science* **337**, 927–932 (2012).
2. R. M. Quimby, F. Yuan, C. Akerlof, J. C. Wheeler, *Mon. Not. R. Astron. Soc.* **431**, 912–922 (2013).
3. R. M. Quimby *et al.*, *Nature* **474**, 487–489 (2011).
4. J. D. Neill *et al.*, *Astrophys. J.* **727**, 15 (2011).
5. R. Stoll *et al.*, *Astrophys. J.* **730**, 34 (2011).
6. R. Lunnan *et al.*, *Astrophys. J.* **787**, 138 (2014).
7. R. M. Quimby, in *IAU Symposium*, A. Ray, R. A. McCray, Eds. (International Astronomical Union, 2014), vol. 296, pp. 68–76.
8. M. Nicholl *et al.*, *Mon. Not. R. Astron. Soc.* **452**, 3869–3893 (2015).
9. B. J. Shappee *et al.*, *Astrophys. J.* **788**, 48 (2014).
10. S. J. Maddox, G. Efstathiou, W. J. Sutherland, J. Loveday, *Mon. Not. R. Astron. Soc.* **243**, 692 (1990).
11. B. Nicholls *et al.*, *Astronomer's Telegram* **7642**, 1 (2015).
12. D. N. Burrows *et al.*, *Space Sci. Rev.* **120**, 165–195 (2005).
13. S. Blondin, J. L. Tonry, *Astrophys. J.* **666**, 1024–1047 (2007).
14. A. Pastorello *et al.*, *Astrophys. J.* **724**, L16–L21 (2010).
15. C. Inserra *et al.*, *Astrophys. J.* **770**, 128 (2013).
16. E. F. Schlafly, D. P. Finkbeiner, *Astrophys. J.* **737**, 103 (2011).
17. P. M. Vreeswijk *et al.*, *Astrophys. J.* **797**, 24 (2014).
18. D. W. Hogg, I. K. Baldry, M. R. Blanton, D. J. Eisenstein, *ArXiv Astrophysics e-prints:astro-ph/0210394* (2012).
19. C. Inserra, S. J. Smartt, *Astrophys. J.* **796**, 87 (2014).
20. S. Savaglio, K. Glazebrook, D. Le Borgne, *Astrophys. J.* **691**, 182–211 (2009).
21. B. Katz, D. Kushnir, S. Dong, http://arxiv.org/abs/1301.6766 (2013).
22. P. Bodenheimer, J. P. Ostriker, *Astrophys. J.* **191**, 465 (1974).
23. D. Kasen, L. Bildsten, *Astrophys. J.* **717**, 245–249 (2010).
24. S. E. Woosley, *Astrophys. J.* **719**, L204–L207 (2010).
25. B. D. Metzger, D. Giannios, T. A. Thompson, N. Bucciantini, E. Quataert, *Mon. Not. R. Astron. Soc.* **413**, 2031–2056 (2011).
26. O. Yaron, A. Gal-Yam, *Publ. Astron. Soc. Pac.* **124**, 668–681 (2012).

ACKNOWLEDGMENTS

We acknowledge B. Zhang, L. Ho, A. Gal-Yam, and B. Katz for comments; NSF AST-1515927, OSU CCAPP, Mt. Cuba Astronomical Foundation, TAP, SAO, CAS grant XDB09000000 (S.D.); NASA Hubble Fellowship (B.J.S.); FONDECYT grant 1151445, MAS project IC120009 (J.L.P.); NSF CAREER award AST-0847157 (S.W.J.); U.S. Department of Energy (DOE) DE-FG02-97ER25308 (T.W.-S.H.); NSF PHY-1404311 (J.F.B.); D. Victor for donating equipment (BN); FONDECYT postdoctoral fellowship 3140326 (F.O.E.), and Los Alamos National Laboratory Laboratory Directed Research and Development program (P.R.W). B.J.S. is a Hubble and Carnegie-Princeton Fellow. All data used in this paper are made public, including the photometric data (tables S1 to S6) and spectroscopic data at public repository WISeREP (*26*) (http://wiserep.weizmann.ac.il).

SUPPLEMENTARY MATERIALS

www.sciencemag.org/content/351/6270/257/suppl/DC1
Materials and Methods
Supplementary Text
Figures S1 to S5
Tables S1 to S6
References (*27*–*65*)

10 July 2015; accepted 24 November 2015
10.1126/science.aac9613

PALEOANTHROPOLOGY

Early human presence in the Arctic: Evidence from 45,000-year-old mammoth remains

Vladimir V. Pitulko,[1]*† Alexei N. Tikhonov,[2]* Elena Y. Pavlova,[3] Pavel A. Nikolskiy,[4] Konstantin E. Kuper,[5] Roman N. Polozov[6]

Archaeological evidence for human dispersal through northern Eurasia before 40,000 years ago is rare. In west Siberia, the northernmost find of that age is located at 57°N. Elsewhere, the earliest presence of humans in the Arctic is commonly thought to be circa 35,000 to 30,000 years before the present. A mammoth kill site in the central Siberian Arctic, dated to 45,000 years before the present, expands the populated area to almost 72°N. The advancement of mammoth hunting probably allowed people to survive and spread widely across northernmost Arctic Siberia.

Evidence for human habitation in the Arctic before the Last Glacial Maximum (LGM), which spans 26.5 to 19 thousand years ago (ka) (*1*), is very rare (Fig. 1A and fig. S1). It has only become available in the past 20 years, with the discoveries of the Mamontovaya Kurya site (*2*) in the European Arctic and the Yana Rhinoceros Horn Site (RHS) in Arctic Siberia (*3*). Before these discoveries, researchers held that humans could not have started populating the Arctic regions until the Pleistocene-Holocene boundary (*4*). The recent discoveries indicate the presence of people in the Arctic at least at the end of marine isotope stage 3 (MIS 3), around 28,000 ^{14}C years before the present (yr B.P.) or slightly earlier, whereas older sites are found south of 55°N.

Archaeological evidence for human dispersal throughout northern Eurasia dated to the first half of MIS 3 is known from different areas (*5*–*10*). In Siberia, this evidence is concentrated far south of the Arctic circle (*7*–*11*). In addition to some dozen sites with age estimates within ~45 to 30 ka, which are well supported by reliable data, there are several controversial localities in northeast Europe (*12*, *13*), the Urals (*14*), and Siberia (*9*, *10*). Thus, the relevant archaeological record for all of northern Eurasia amounts to 15 to 20 contexts with a northern latitudinal limit of 55°N (fig. S1). In west Siberia, a human fossil with an early modern human genome was recently found at 57°N and produced a direct radiocarbon date of 45,000 yr B.P.; however, these remains were not found in an archaeological context (*15*). Thus, the archaeological record for northern Eurasia has not suggested human presence in the Arctic that early, although there is evidence firmly dated to ~30 ka (*3*).

Ice sheet expansion during MIS 4 did not affect most of the Siberian Arctic (*16*). Interglacial (MIS 3) environmental conditions varied across the Eurasian Arctic (*17*–*21*) but were overall beneficial for the growth of late Pleistocene large herbivore populations, including mammoths, in various parts of the region (*22*–*25*). At the end of MIS 3, mammoths moved into deglaciated areas (*26*) and offered an unlimited food source, supporting the pre-LGM human settlement now corroborated for both the European and eastern Siberian Arctic (*2*, *3*, *25*, *26*).

The central Siberian Arctic was also populated by mammoths for a long time (*22*, *27*). Reconstructed fluctuations of their population numbers (*22*) largely follow the pattern seen among the mammoth populations in the New Siberian Islands and Northern Yana-Indighirka lowland. One of the highest peaks of the mammoth population numbers occurred around 44 to 42 ka (*25*).

In 2012, a team led by one of us (Tikhonov) excavated a partial carcass of a woolly mammoth (*Mammuthus primigenius*, Blumenbach, 1799) from frozen sediments exposed in a coastal bluff on the eastern shore of Yenisei Bay, 1.8 km north of the Sopochnaya Karga (SK) meteorological station, at 71°54′19.2″N and 82°4′23.5″E (Fig. 1B). The exposure stratigraphy there is composed of several clear structural elements (*28*).

Several radiocarbon dates help anchor this sequence in time (Fig. 1, C and D, and table S1). The peat layer (bed 3) is dated to 36,000 ± 2500 ^{14}C yr B.P. (LE-9822). A small willow branch fragment from bed 3 yielded an age of 47,600 +10,200/–4400 ^{14}C yr B.P. (LE-9821). Bed 4, which marks the beginning of the taberite sediments, produced a date of 18,200 +2600/–2200 ^{14}C yr B.P. (LE-9823). This sequence is above bed 1, which holds the mammoth carcass. Considering these dates, the age of the SK mammoth can be estimated at about 40 ka. A direct date on tibia bone, 44,570 +950/–700 ^{14}C yr B.P. (table S2), is consistent with the stratigraphy and the surrounding deposit dates (Fig. 1D). Thus, the SK mammoth carcass is a rare in situ specimen from

[1]Institute for the History of Material Culture, Russian Academy of Sciences, 18 Dvortsovaya Naberezhnaya, St. Petersburg 191186, Russia. [2]Zoological Institute, Russian Academy of Sciences, 1 Universitetskaya Naberezhnaya, St. Petersburg, 199034, Russia. [3]Arctic and Antarctic Research Institute, 38 Bering Street, St. Petersburg, 199397, Russia. [4]Geological Institute, Russian Academy of Sciences, 7 Pyzhevskiy Pereulok, Moscow, 119017, Russia. [5]Budker Institute of Nuclear Physics, Russian Academy of Sciences, Siberian Branch, 11 Academician Lavrentiev Avenue, Novosibirsk, 630090, Russia. [6]St. Petersburg Pediatric Medical University, 2 Litovskaya Street, St. Petersburg, 194100, Russia.
*These authors contributed equally to this work.
†Corresponding author. E-mail: pitulkov@gmail.com

the early phase of MIS 3 when mammoth populations in Taimyr were slowly growing (*22*, *25*). Additional dates (*28*) independently received on mammoth remains concur (table S3).

The SK mammoth is an exceptionally complete mammoth skeleton (*28*) with a small amount of preserved soft tissue, including the remains of the fat hump and the penis. It is more complete than other recent finds from Taimyr, known as the Kastyktakh (*29*) and Jarkov mammoths (*30*). The large amount of fat at the hump indicates that the mammoth was in a good physical condition. This was a young male around 15 years old, according to the tooth change model (*31*).

Its bones exhibit a number of unusual injuries (Figs. 2 and 3 and figs. S2 to S4). Damage is seen on the left scapula (Fig. 2B and fig. S2), the left jugal bone (Fig. 3), the fifth left rib (fig. S3, A to C), and the second right rib (fig. S3, D and E). Unequivocal postmortem damage is also recorded on the tip of the right tusk and the mandible, the left coronoid process of which is broken off (*28*).

A small rounded hole, filled with sediment particles, was discovered on the internal side of the left jugal bone after it was separated from the skull during the excavation (Fig. 3). The bone is uniformly patinated and has no evidence of recent damage. To clarify the character of this unusual injury, the bone was studied with x-ray computed tomography (XCT) (Fig. 3, D to F).

The shape of the injury (Fig. 3G) suggests that the tip of the weapon that damaged the jugal bone had a thinned symmetric outline (the cross-tip section at the point of entry measures 3.4 mm at the short axis and 5.1 mm at the long axis) and was relatively sharp (the height of an equilateral triangle with a base of 5.1 mm is 3.42 mm). In most cases, bone or ivory weapons have a conical tip that is symmetric and quite acute (~30° to 40°) at the end (*3*, *32*, *33*), but they are relatively fragile and often break as they penetrate bones (*33*). In this case, the tool resisted breaking and inflicted injury on the cranial bones. The blade retained its weapon characteristics and kept enough energy to go through the cheekbone surface, penetrating deeply into the bone. The blow was evidently very strong and was suffered by the animal from the left back and from top down (Fig. 3A), which is only possible if the animal was lying down on the ground.

This injury itself is probably the result of a missed blow, targeting the base of the trunk. This specific hunting method is still practiced in Africa by elephant hunters, who target the base of the trunk to cut major arteries and cause mortal bleeding (*34*). This blow becomes necessary after the animal has been sufficiently injured, and the SK mammoth displays numerous injuries in the thoracic area (to ribs and the left scapula).

The most remarkable injury is to the fifth left rib, caused by a slicing blow, inflicted from the front and somewhat from above downward (Fig. 2B and fig. S3C). The incision is filled in with well-rounded sand particles from the matrix deposits. Although it was a glancing blow, it was strong enough to go through skin and muscles and damage the bone. A similar but less powerful blow also damaged the second right front rib (Fig. 2A and fig. S3, D and E). Such blows were aimed at internal organs and/or blood vessels.

The SK mammoth was also hit in the left scapula at least three times. Two of these injuries, judging from the location of the dents at the distal (top, in an anatomic skeletal position) edge of the scapula, left of the spine, were imparted by a weapon, which went downward through the skin and muscles, moving from the top and side (Fig. 2B and fig. S2, A and D). These markings indicate injuries evidently left by relatively light throwing spears.

A much more powerful blow damaged the spine of the left scapula (Fig. 2B and fig. S2). It may have been imparted by a thrusting spear, practically straight from the front at the level of the coracoid process. The weapon went through the shoulder skin and muscle, almost completely perforating the spine of the scapula. The blow produced a lattice of cracks, and the bone curved in the direction of the impact. Taking into account the scapula's location in the skeleton and the estimated height of this mammoth, the point of impact would be approximately 1500 mm high; i.e., at the height of an adult human's shoulder. This area is the weakest on the scapula, but it usually remains intact even on bones found separately, including bones of younger mammoth individuals.

The SK mammoth remains also display postmortem damage, which indicates human activity. First, the ramus of the mandible is broken. These bones are quite strong: even when found isolated in much harsher taphonomic conditions, they often remain complete. However, in anthropogenic contexts, mammoth mandibles are mostly lacking one or both coronoid processes. Such mandible treatment may reflect tongue extraction. The Yana collection showed that mammoth tongue was often consumed by the hunters, perhaps as a ritual food or a delicacy (*33*).

The only preserved tusk of the SK mammoth (the right tusk) shows traces of human modification. These could be expected to be focused around the alveolar region, reflecting an attempt to separate the outside of the tusk by chopping. Instead, that portion remained intact (Fig. 2E), whereas the tip of the tusk shows evidence of impact. Several relatively thin subparallel spalls were removed (fig. S4); the tip of the tusk, normally quite blunt (*35*, *36*), served as a platform for these removals.

The natural breakage pattern found on mammoth tusks (*36*) and on those of recent elephants (*37*) is completely different from the pattern on the SK mammoth tusk. At the same time, such a technique is quite different from the ivory technology known in arctic Siberia in late MIS 3 (*38*). However, the same approach might have been used to produce ivory tools with asymmetric working parts that are known in the younger archaeological sites nearby (*39*).

These removals aimed to obtain long thin slivers of ivory with sharp edges, which were usable as butchering tools in places where quality lithic raw material is hardly available. In the modern estuarine area of the Yenisei, it is completely absent. Ivory flakes have a sharp cutting edge and can be used as cutting or scraping implements. Rarely, such objects are found in Siberian Arctic Stone Age sites (*39*), specifically in regions where lithic raw material is available in small nodules only.

Thus, the SK mammoth bone remains provide well-supported evidence for human involvement in its death. These are: (i) a lesion on the jugal

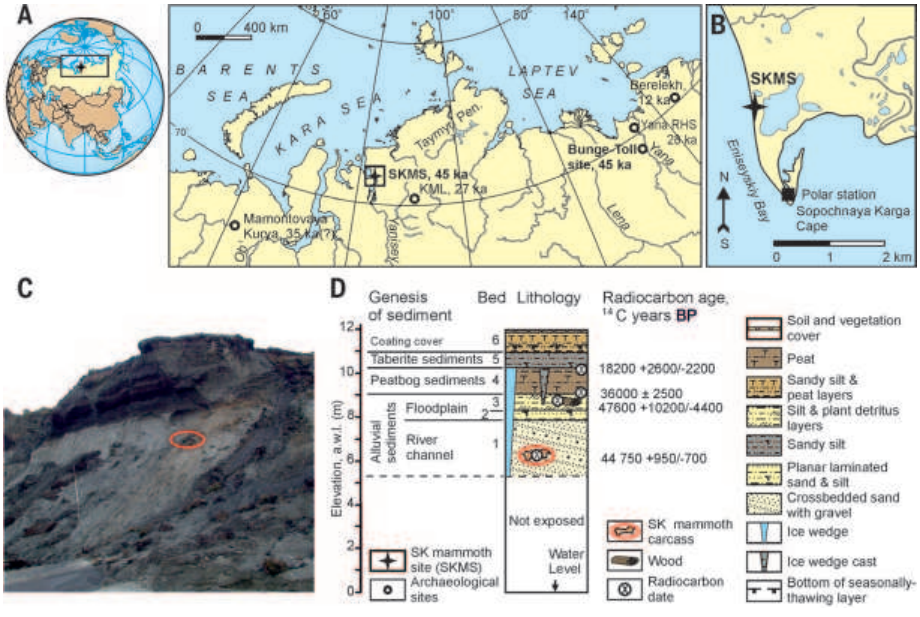

Fig. 1. Geographic, stratigraphic, and dating overview for the Siberian Arctic. (**A**) Dated archaeological contexts (*2*, *3*) and geological sites mentioned in the text: SKMS, SK mammoth site; KML, Kastyktakh mammoth site (*29*). (**B**) Location of the SK mammoth site. (**C**) General view of the exposure before the excavations. (**D**) Lithology and cryostratigraphy of the SK mammoth site.

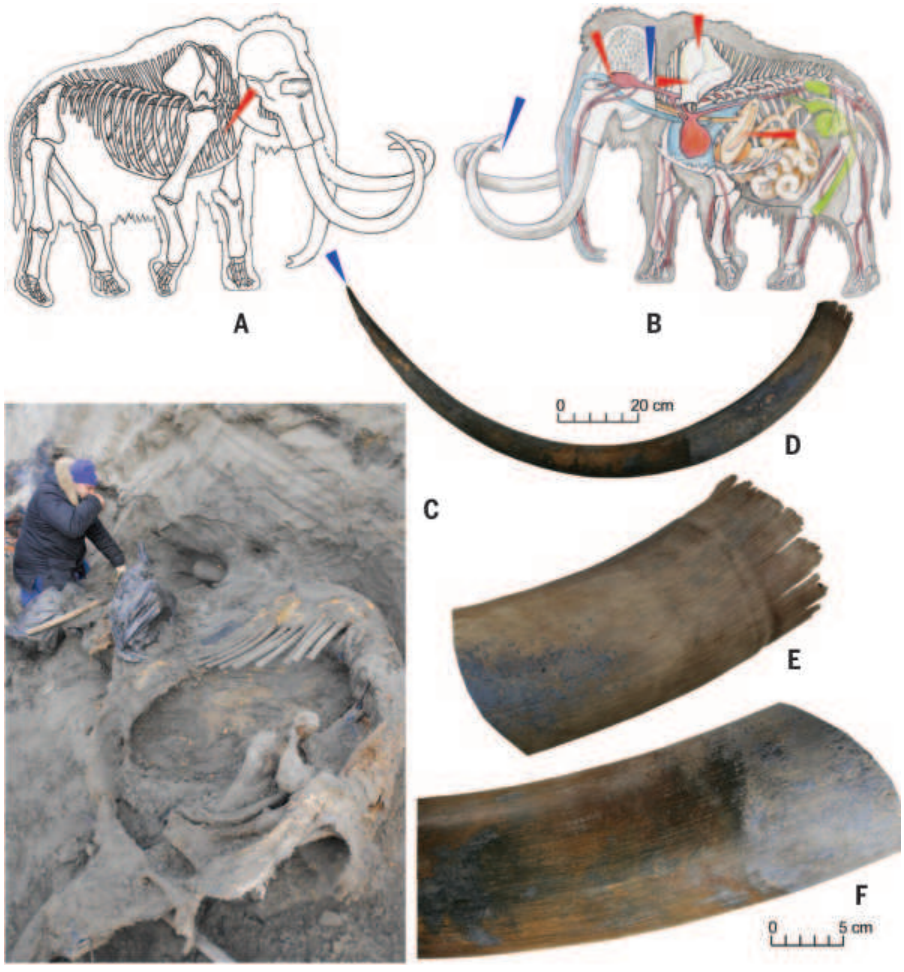

Fig. 2. Taphonomy of the SK mammoth and the inventory map for perimortem (red arrows) and postmortem damages (blue arrows) found on bones. (**A**) Mammoth skeleton, right view. (**B**) Mammoth skeleton and internal organs, left view. (**C**) Excavations of the carcass from channel deposits unit. (**D**) Right mammoth tusk with worked tip. (**E**) Undamaged alveolar part of the tusk, with extensive vivianite crust. (**F**) Unpatterned traces on the right tusk surface left by hard particles of the matrix sediments.

bone, (ii) a butchery mark on the fifth left rib (the most solid evidence), and (iii) the worked distal end of the right tusk. The same butchery pattern is well known for mammoth bones from the Yana RHS complex (*33*). In particular, it is repeatedly documented for mammoth ribs (Fig. 4). The bone lesion found on the rib of the SK mammoth fully replicates that pattern (Fig. 4G). All together, these findings leave no doubt that people were present in the central Siberian Arctic by 44,570 +950/–700 ^{14}C yr B.P. (GrA-57723), or 49,150 to 47,100 calendar yr B.P.

Independently, another locality in the eastern Siberian Arctic (Fig. 1A) produced evidence for human habitation that also dates to early MIS 3 (*28*). The Bunge-Toll site yielded remains of bison, rhinoceros, and mammoth. Among those, a left humerus of a Pleistocene wolf exhibited an unusual pathology, resulting from an injury, on its external lateral surface. Standard x-rays and XCT show that the pathology is a result of a penetrating injury inflicted by a sharp weapon (fig. S5). Such trauma could only have been caused by a human. Direct ^{14}C dating of the bone indicates that this episode occurred 44,650 +950/–700 (GrA-57022); i.e., contemporaneously with the SK mammoth kill. These two incidents suggest that even during the early phases of MIS 3, humans inhabited the Arctic quite widely, although the population was probably small and remained sparse for a long time.

The SK mammoth kill, along with the Bunge-Toll site, confirms the presence of humans in the Arctic much earlier than previously suggested. This is a rare case of unequivocal evidence for clear human involvement, even if there is no artifact association (*40*). Apparently, humans' ability to survive in the Arctic environment, and their spread within the region as early as 45 ka, represents an important cultural and adaptational shift. We speculate that adaptation changes that ensured human survival there may be related to innovations in mammoth hunting. Sustained development of the populations, secured by an abundant food source, could have led to their rapid spread

Fig. 3. Human-inflicted lesion on the left jugal bone of the SK mammoth head. (**A**) Mammoth skull with the marked direction of the penetrating wound (solid red arrow) documented by a lesion on the jugal bone [(B) to (F)] and desired direction of the impact (dashed red arrow) in the area of the nasal opening. (**B**) Jugal bone, external side. (**C**) Jugal bone, internal side with a hole. (**D**) XCT image of the impact area. (**E**) Longitudinal section of the impact area. (**F**) Cross section of the impact area. (**G**) Three-dimensional model of the tool tip.

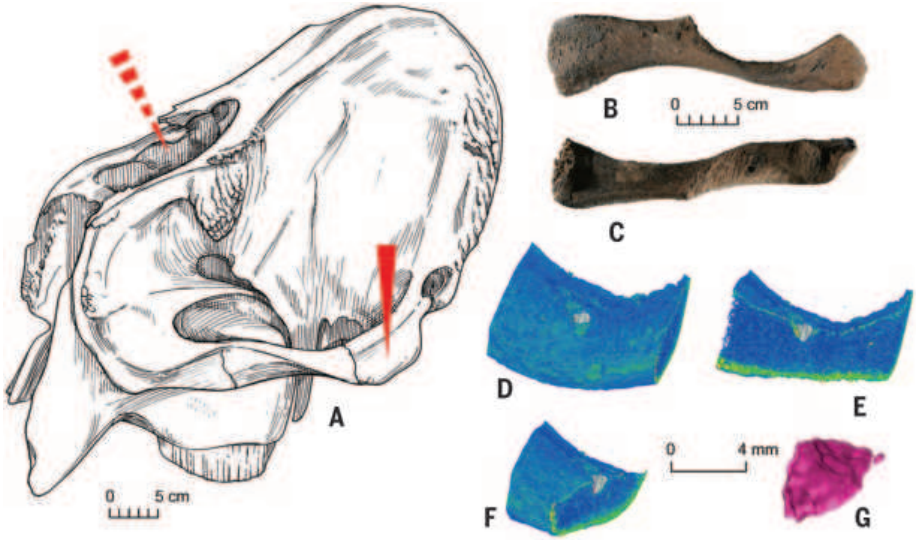

Fig. 4. Mammoth ribs with hunting lesions collected at Yana RHS [(A) to (F)], showing the mechanism for the formation of bone injury on the fifth rib of the SK mammoth (G). (**A**) Mammoth rib with embedded lithic tool fragment. (**B**) Mammoth rib with two injuries that retain lithics. (**C**) View of the upper cut at (B). (**D**) View of the lower cut at (B). (**E**) Bone injury with no lithic in it but clearly left by the same action as for (A) and (B). (**F**) Bone injury that resulted from sliding of the lithic implement that removed part of the bone. (**G**) Hunting lesion on the fifth left rib of the SK mammoth; compare to (A) to (F) and note the same scale for all images.

across the Siberian Arctic. The early arrival of humans in the area close to the Bering land bridge may have provided an opportunity for humans to enter the New World before the LGM.

REFERENCES AND NOTES

1. P. U. Clark *et al.*, *Science* **325**, 710–714 (2009).
2. P. Pavlov, J. I. Svendsen, S. Indrelid, *Nature* **413**, 64–67 (2001).
3. V. V. Pitulko *et al.*, *Science* **303**, 52–56 (2004).
4. N. K. Vereshchagin, *Polar Record* **17**, 3–12 (1974).
5. M. V. Anikovich *et al.*, *Science* **315**, 223–226 (2007).
6. A. P. Derevianko, M. V. Shunkov, *Archaeol. Ethnol. Anthropol. Eurasia* **19**, 12–40 (2004).
7. L. V. Lbova, *Paleolithic of the NW Trans-Baikal Zone* (Buryat NC SO RAN, Ulan-Udhe, Russia, 2000).
8. N. F. Lisitsyn, *The Upper Paleolithic of Chulim-Yenisei Region* (Archaeologica Petropolitana, St. Petersburg, Russia, 2000).
9. J. Chlachula, N. I. Drozdov, N. D. Ovodov, *Boreas* **32**, 506–520 (2003).
10. T. Goebel, M. Aksenov, *Antiquity* **69**, 349–357 (1995).
11. T. Sato *et al.*, *Quat. Int.* **179**, 101–107 (2008).
12. V. V. Pitulko, P. A. Nikolskiy, A. E. Basilyan, E. Y. Pavlova, in *The Quaternary in all of its variety. Basic issues, results, and major trends of further research. Proceedings of the VII All-Russian Quaternary Conference*, P. Korsakova, V. V. Kolka, L. D. Chistyakova, Eds. (Geological Institute, Kola Research Center RAS, Apatity and St. Petersburg, Russia, 2011), pp. 146–149.
13. J. I. Svendsen *et al.*, *Quat. Sci. Rev.* **29**, 3138–3156 (2010).
14. Y. B. Serikov, J. Chlachula, *Quat. Int.* **326–327**, 261–273 (2014).
15. Q. Fu *et al.*, *Nature* **514**, 445–449 (2014).
16. J. I. Svendsen *et al.*, *Quat. Sci. Rev.* **23**, 1229–1271 (2004).
17. A. A. Andreev *et al.*, *Boreas* **32**, 484–505 (2003).
18. H.-W. Hubberten *et al.*, *Quat. Sci. Rev.* **23**, 1333–1357 (2004).
19. A. V. Sher, S. A. Kuzmina, T. V. Kuznetsova, L. D. Sulerzhitsky, *Quat. Sci. Rev.* **24**, 533–569 (2005).
20. F. Kienast *et al.*, *Quat. Sci. Rev.* **30**, 2134–2159 (2011).
21. A. V. Lozhkin, P. M. Anderson, *Quat. Sci. Rev.* **30**, 2160–2181 (2011).
22. L. D. Sulerzhitsky, *Proc. Zool. Inst* **263**, 163–183 (1995).
23. L. D. Sulerzhitsky, F. A. Romanenko, *Ambio* **28**, 251–255 (1999).
24. Y. V. Kuzmin, L. A. Orlova, *Earth Sci. Rev.* **68**, 133–169 (2004).
25. P. A. Nikolskiy, L. D. Sulerzhitsky, V. V. Pitulko, *Quat. Sci. Rev.* **30**, 2309–2328 (2011).
26. A. K. Markova, A. Y. Puzachenko, T. van Kolfschoten, J. van der Plicht, D. V. Ponomarev, *Quat. Int.* **292**, 4–14 (2013).
27. R. D. E. MacPhee *et al.*, *J. Archaeol. Sci.* **29**, 1017–1042 (2002).
28. See the supplementary text on *Science* Online.
29. I. K. Kirillova, F. K. Shidlovskiy, V. V. Titov, *Quat. Int.* **276-277**, 269–277 (2012).
30. D. Mol *et al.*, *Quat. Int.* **142-143**, 186–202 (2006).
31. L. V. Roth, J. Shoshani, *J. Zool. (Lond.)* **214**, 567–588 (1988).
32. V. V. Pitulko, P. A. Nikolskiy, *World Archaeol.* **44**, 21–42 (2012).
33. P. Nikolskiy, V. Pitulko, *J. Archaeol. Sci.* **40**, 4189–4197 (2013).
34. S. F. Kulik, *Safari. Travels in Eastern, Central, and Southern Africa* (Mysl, Moscow, 1971).
35. N. K. Vereschagin, A. N. Tikhonov, *Proc. Zool. Inst.* **149**, 3–15 (1986).
36. N. K. Vereshchagin, A. N. Tikhonov, *Cranium* **16**, 2–48 (1999).
37. G. Haynes, *Mammoths, Mastodonts & Elephants. Biology, Behavior, and the Fossil Record* (Cambridge Univ. Press, 1991).
38. V. V. Pitulko, E. Y. Pavlova, P. A. Nikolskiy, *World Archaeol.* **47**, 333–389 (2015).
39. V. V. Pitulko, *The Zhokhov Island Site and Ancient Habitation in the Arctic* (Simon Frazer Univ., Burnaby, British Columbia, Canada, 2013).
40. S. M. Kenady, M. C. Wilson, R. F. Schalk, R. R. Mierendorf, *Quat. Int.* **233**, 130–141 (2011).

ACKNOWLEDGMENTS

We thank E. Solinder and A. Bystrov (SK weather station), the Taimyr Region administration, and Norilsk Nickel mining company. We are also grateful to P. Ivanov (photography); A. Mashezerskaya (drawings); V. Stegantseva (illustrations); N. Slobodina (translation); and N. Burova, A. Sementsov, and J. van der Plicht (radiocarbon dating). The SK mammoth remains are currently stored at the Zoological Institute, St. Petersburg, Russia. When the study ends, they will be moved to the Taimyr Regional Museum for permanent storage and display (Dudinka, Taimyr Autonomous District, Russia), and they can then be resampled if needed while a bulk sample of the organic deposit from the inside of the SK mammoth stays at the Zoological Institute in St. Petersburg. The Yana site materials and finds from the Bunge-Toll site are stored at the Institute for the History of Material Culture, St. Petersburg, Russia), as a part of the materials collected under the Zhokhov-Yana research project. All collected skeletal elements of the Kastyktakh mammoth are with the Ice Age Museum, Moscow, Russia. This project was supported by the Russian Foundation of Basic Research (grant Nr 13-06-12044 to V.V.P.); publication is supported by the Rock Foundation (New York, USA).

SUPPLEMENTARY MATERIALS

www.sciencemag.org/content/351/6270/260/suppl/DC1
Materials and Methods
Supplementary Text
Figs. S1 to S5
Tables S1 to S3
References (*41*–*57*)

19 July 2015; accepted 4 December 2015
10.1126/science.aad0554

PHYTOPLANKTON

The fate of photons absorbed by phytoplankton in the global ocean

Hanzhi Lin,[1]* Fedor I. Kuzminov,[1] Jisoo Park,[2] SangHoon Lee,[2] Paul G. Falkowski,[1,3]† Maxim Y. Gorbunov[1]†

Solar radiation absorbed by marine phytoplankton can follow three possible paths. By simultaneously measuring the quantum yields of photochemistry and chlorophyll fluorescence in situ, we calculate that, on average, ~60% of absorbed photons are converted to heat, only 35% are directed toward photochemical water splitting, and the rest are reemitted as fluorescence. The spatial pattern of fluorescence yields and lifetimes strongly suggests that photochemical energy conversion is physiologically limited by nutrients. Comparison of in situ fluorescence lifetimes with satellite retrievals of solar-induced fluorescence yields suggests that the mean values of the latter are generally representative of the photophysiological state of phytoplankton; however, the signal-to-noise ratio is unacceptably low in extremely oligotrophic regions, which constitute 30% of the open ocean.

For several decades, chlorophyll concentrations based on remotely sensed variations in ocean color have been used to derive global phytoplankton productivity (*1*, *2*). Primary productivity models implicitly include physiological processes, but their explicit representation has, thus far, been elusive (*3*, *4*). Variable chlorophyll fluorescence is the most sensitive, nondestructive signal detectable in the upper ocean that reflects instantaneous phytoplankton photophysiology (*5*–*7*). Over the past two decades, many hundreds of thousands of discrete in situ measurements of variable fluorescence have been made using ship-based active fluorometers. These instruments, primarily designed to quantify the quantum yield of photochemistry (F_v/F_m) (F_v, variable fluorescence; F_m, maximal fluorescence) in photosystem II (PSII), the reaction center responsible for splitting water, have been used to follow phytoplankton photophysiology in response to iron fertilization (*8*), across eddies (*9*, *10*), along meridional transects (*11*), and in response to many other phenomena (*12*, *13*). Although active variable fluorescence measurements have become almost routine, by themselves, they do not allow closure on the fate of light absorbed by phytoplankton. Here we report the fraction of sunlight absorbed by phytoplankton that is actually used to form chemical bonds in the global ocean. Further, we compare the spatial distributions of photochemical energy conversion to the pattern inferred from space-based retrievals of solar-induced fluorescence yields.

[1]Environmental Biophysics and Molecular Ecology Program, Department of Marine and Coastal Sciences, Rutgers, The State University of New Jersey, 71 Dudley Road, New Brunswick, NJ, USA. [2]Korea Polar Research Institute, 26 Songdomirae-ro, Yeonsu-Gu, Incheon, Republic of Korea. [3]Department of Earth and Planetary Sciences, Rutgers, The State University of New Jersey, Piscataway, NJ, USA.
*Present address: Institute of Marine and Environmental Technology, University of Maryland Center for Environmental Science, Baltimore, MD 21202, USA. **†Corresponding author. E-mail: falko@marine.rutgers.edu (P.G.F.); gorbunov@marine.rutgers.edu (M.Y.G.)**

The biophysical basis of fluorescence measurements derives from the three possible fates of solar energy absorbed by any photosynthetic organism (*14*). Absorbed photons can (i) generate photochemical reactions leading to the production of organic matter (with the rate k_p), (ii) be dissipated as heat (k_t), or (iii) be emitted back to the environment as fluorescence (k_f) (*15*). In a dark-adapted state or under low irradiance (when k_t is constant), the quantum yield of chlorophyll fluorescence, ϕ_f [$= k_f/(k_p + k_t + k_f)$], is inversely related to the quantum yield of photochemistry in PSII, $\phi_p = k_p/(k_p + k_t + k_f) = F_v/F_m$.

Substitution and rearrangement lead to

$$\phi_f = \phi_{fm}\,(1 - F_v/F_m) \qquad (1)$$

where ϕ_{fm} [$= k_f/(k_t + k_f)$] is the maximum fluorescence yield obtained when photochemistry is nil (e.g., at saturating background light).

This biophysical model predicts an inverse linear relationship between the quantum yield of photochemistry and that of chlorophyll fluorescence. However, by the early 1980s it was realized that exposure to high continuous irradiance can lead to a suite of thermal dissipative mechanisms, collectively called nonphotochemical quenching (NPQ) (*16*). These reactions markedly decrease the quantum yield of fluorescence at high background light. Hence, the relationship between chlorophyll fluorescence and photochemistry, described in Eq. 1, becomes highly nonlinear as NPQ phenomena play an increasingly larger role in energy dissipation.

Calculating the budget of absorbed solar radiation requires measurements of the quantum yields of at least two pathways; for example, photochemistry and fluorescence. Although the development and use of variable fluorescence techniques over the past two decades have provided unprecedented information about photochemical conversion in phytoplankton in situ, these instruments are unable to measure the absolute quantum yields of fluorescence. To overcome this basic limitation, we constructed an extremely sensitive sea-going instrument that measures chlorophyll fluorescence lifetimes in the picosecond time domain (*17*). The fluorescence lifetime can be quantitatively related to the absolute quantum yield of fluorescence (*18*)

$$\phi_f = \tau/\tau_n \qquad (2)$$

where τ_n is the intrinsic (or natural) lifetime constant for chlorophyll a molecules (*17*). Thus, the longer the lifetime, the higher the quantum yield of fluorescence.

Between 2008 and 2014, we obtained >150,000 discrete chlorophyll fluorescence lifetime measurements from the Pacific, Atlantic, Arctic, and Southern Oceans. These measurements constitute the map of quantum yields of chlorophyll fluorescence from phytoplankton in the upper

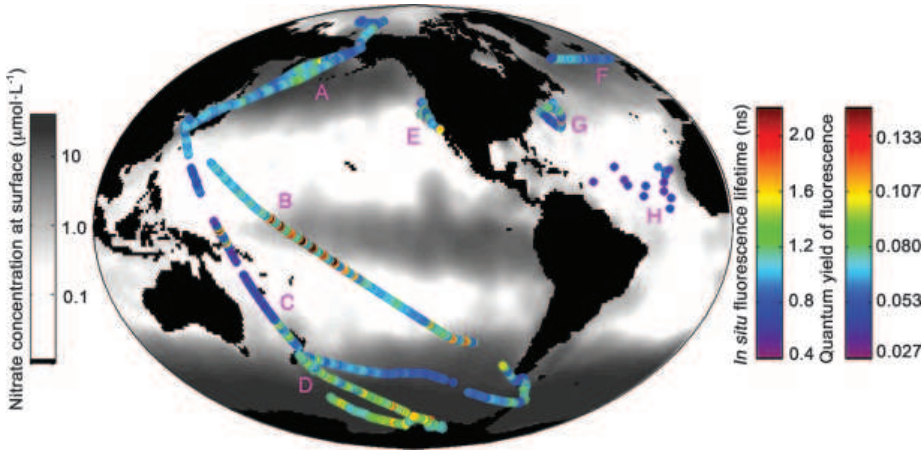

Fig. 1. Global distribution of ship-based measurements of chlorophyll fluorescence lifetimes and the derived quantum yields of fluorescence (Eq. 2) in the upper ocean, superimposed on the climatological map of surface nitrate concentrations in the world ocean (*32*). Periods of in situ sampling were (**A**) July–August 2011, (**B**) October–November 2011, (**C**) October–November 2010, (**D**) January 2012, (**E**) July 2014, (**F**) September 2010, (**G**) May 2014, and (**H**) August 2008.

ocean (Fig. 1). The nighttime in situ lifetimes ranged from 0.5 to 2.7 ns, with a mean of 1.13 ± 0.33 ns (Fig. 2). This naturally dark-adapted condition corresponds to a state in which all functional reaction centers are open and NPQ is absent. These values span the entire range of published lifetimes of in vivo chlorophyll fluorescence obtained from cultured phytoplankton (*17*) and reflect extraordinary variability in phytoplankton physiology in the global ocean. The general pattern of the fluorescence lifetimes in the central gyres of the global ocean is rather featureless, although phytoplankton growth is subject to both macro- and micronutrient limitation (*14*). The shortest fluorescence lifetimes (<1 ns) were observed along continental margins, in the Antarctic convergence, and in the subtropical Atlantic and Pacific oceans. These lifetime distributions support the hypothesis that phytoplankton in the central gyres are acclimated to broad scales and persistent nutrient limitation (*11*, *12*). In contrast, the longest fluorescence lifetimes were observed in high-nutrient–low-chlorophyll (HNLC) regions of the equatorial Pacific Ocean and the Southern Ocean, where primary production is limited by the paucity of iron (*19*), a micronutrient that is critical for the function of PSII (*20*, *21*). The exceptionally high values of fluorescence lifetimes in these areas of the global ocean are consistent with extremely

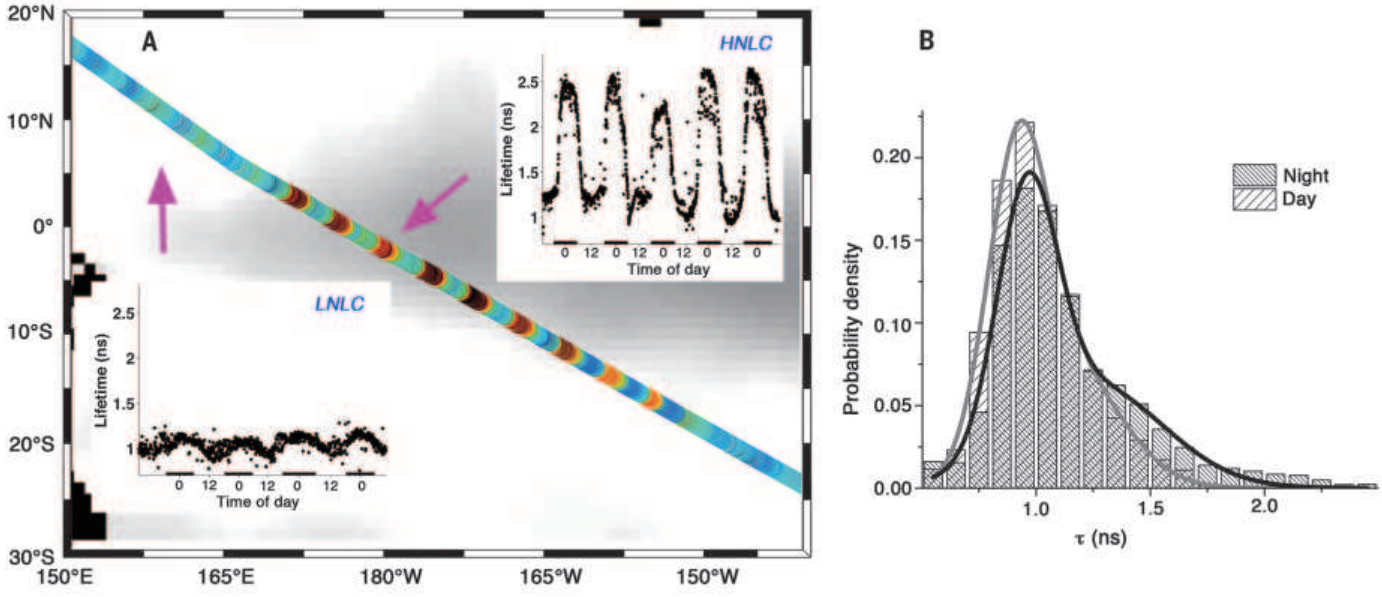

Fig. 2. (A) Representative diel cycles of chlorophyll fluorescence lifetimes in HNLC and LNLC regions of the Pacific Ocean obtained in October 2011. The color bar for lifetimes is the same as in Fig. 1. (**B**) Histograms of the fractional frequency of lifetime measurements in daytime and at night, respectively. The mean value of nighttime lifetimes is 1.13 ± 0.33 ns and that of daytime lifetimes is 1.02 ± 0.22 ns.

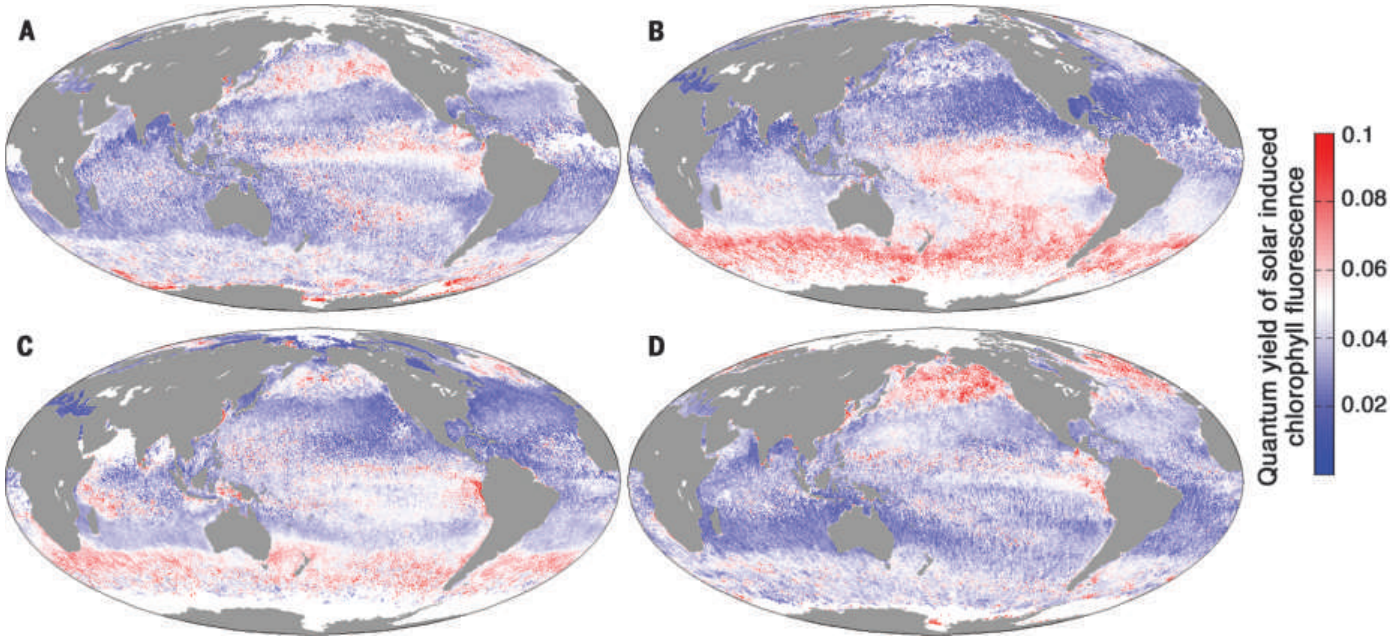

Fig. 3. Global seasonal maps of quantum yields of solar-induced chlorophyll fluorescence in the upper ocean. (**A**) Boreal winter (21 December 2011 to 20 March 2012); (**B**) boreal spring (21 March to 20 June 2012); (**C**) boreal summer (21 June to 20 September 2012); and (**D**) boreal autumn (21 September to 20 December 2012).

low F_v/F_m values and indicative of a large fraction of nonfunctional PSII reaction centers and energetically uncoupled antenna pigment-protein complexes (*21*–*23*).

There is a strong diel cycle in fluorescence lifetimes; in general, lifetimes were longer at night than during daytime, in spite of a marked reduction in the quantum yields of photochemistry under strong sunlight (Fig. 2). The more than fivefold variability in dark-adapted fluorescence lifetimes in situ far exceeds that predicted by Eq. 1. However, this dynamic range is greatly attenuated in high light, when NPQ processes are activated. For example, exceptionally long lifetimes (>2 ns) measured in a dark-adapted state in HNLC regions decrease by more than twofold in high light, whereas relatively short lifetimes (~1 ns) in low-nutrient–low-chlorophyll (LNLC) regions decrease by only 30% under the same conditions (Fig. 2A). Regardless of the molecular mechanisms responsible for NPQ, the net result for high light conditions is increased thermal dissipation of absorbed light in PSII, leading to both reductions in photochemical energy conversion efficiency and in the range of variability of the quantum yields of fluorescence.

With the launch of the Moderate Resolution Imaging Spectroradiometer (MODIS) and Medium Resolution Imaging Spectrometer (MERIS) satellites, which possess the capability of remotely detecting solar-induced chlorophyll fluorescence signals from the global ocean, it became theoretically possible to calculate the quantum yield of chlorophyll fluorescence from space (*24*–*26*). However, the theoretical basis for estimating the relationship between chlorophyll fluorescence and photochemistry was developed before there was an understanding of NPQ (*24*). We therefore examined how the measured in situ fluorescence lifetimes are related to satellite-derived estimates of the quantum yield of chlorophyll a fluorescence.

Statistical analyses (effective sample size >20,000) by both Pearson's linear correlation coefficient and two nonparametric Kendall's tau and Spearman's rho coefficients revealed a weak linear correlation ($P < 0.01$) between these satellite-derived solar-induced fluorescence yields and the ship-based measurements (table S1). Satellite-based estimates of the quantum yield are derived from observations of the surface ocean at times close to local noon (*27*). Hence, the remotely sensed estimates inevitably are obtained at very high irradiances and are strongly influenced by NPQ, a phenomenon that is extremely difficult to quantify in global biophysical models. NPQ is not only critically dependent on pigment composition within the light-harvesting antennae of the phytoplankton (which, in turn, is affected by phytoplankton community composition), but also on upper ocean turbulence as it affects the light field experienced by the community (*28*), as well as nutrient stress (*19*). Despite these complications, qualitative comparison of satellite-derived maps of quantum yields of chlorophyll fluorescence (Fig. 3) reveals basic trends that often, but not always, correspond to in situ lifetime measurements. For example, in the Southern Ocean (an HNLC region), satellite-derived quantum yields are high and correlate with long lifetimes. In this iron-limited region of the world oceans, there is a well-documented reduction in photosynthetic energy conversion efficiency as a result of impairment of PSII reaction centers and potential energetic uncoupling of the antenna pigment-protein complexes (*7*, *22*). In the LNLC regions of the central oceanic gyres of the North and South Pacific and the North Atlantic, measured fluorescence lifetimes are significantly shorter than in HNLC regions. Although the mean fluorescence yield based on the satellite retrievals for the oligotrophic open ocean is 0.043 (Fig. 4) and is generally concordant with the values measured in situ, the high estimates of quantum yields obtained from the space-based platform (Fig. 3) are not corroborated by in situ lifetime measurements. Further, the range of estimated quantum yields derived from satellite-based measurements (more than sixfold) is far larger than that of the in situ lifetimes measured at high irradiances (about threefold). Indeed, the range of the estimated quantum yields of fluorescence in the global ocean (~0.02 to 0.15) appears to exceed that of our current biophysical understanding of photochemistry in phytoplankton. What might be the source of this discrepancy?

In the central ocean gyres, where surface chlorophyll concentrations are very low (<0.1 mg m^{-3}), the fluorescence signals propagated to space are extremely weak. As a result, the current algorithms used to calculate quantum yields of fluorescence become increasingly uncertain [Fig. 4 and (*26*, *29*)]. The relationship between measured lifetimes and satellite-derived quantum yields diverges. In contrast to the satellite-derived yields, which have significant "noise," the in situ lifetime measurements remain extremely precise (within 5%) even at the lowest chlorophyll concentrations found in the upper ocean. Another factor behind this discrepancy is the effect of pigment packaging within a phytoplankton cell (*25*, *30*, *31*), which is most pronounced in larger cells and reduces the observed quantum yields, as compared to their true "molecular" values inferred from lifetime measurements. Similarly, the uncertainties of the current algorithms for remote sensing retrievals of phytoplankton absorption coefficients (*25*) further reduce the accuracy of satellite-based estimates of the quantum yields.

Although quantum yields of chlorophyll fluorescence obtained from current satellite sensors

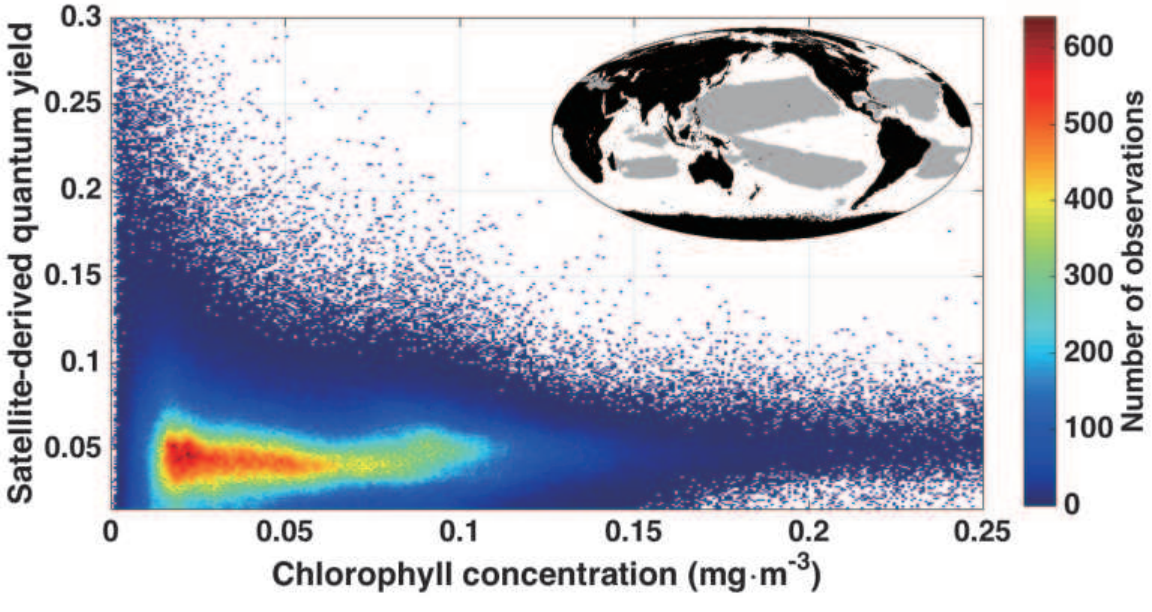

Fig. 4. Variations in MODIS retrievals of the quantum yields of chlorophyll fluorescence (sample size $n = 5.17 \times 10^6$) with chlorophyll abundance (*17*). The mean value of these satellite-derived quantum yields is 0.043. The average value of in situ lifetime measurements at noon (between 10 a.m and 2 p.m local time) is 0.99 ± 0.2 ns, which corresponds to the quantum yield of 0.066 ± 0.013. (**Inset, top right**) Global distribution (10-year average) of chlorophyll concentrations in the boreal summer. The gray area indicates oligotrophic regions with chlorophyll concentrations below 0.1 mg m_{-3}, this area covers ~30% of the global ocean.

have many inherent inaccuracies, this approach to understanding global photophysiology of phytoplankton should not be abandoned. We suggest that relating the space-based estimates to in situ measurements of chlorophyll fluorescence lifetimes will provide a pathway to understanding photobiological energy utilization and dissipation processes on a global scale. For example, the maximal average photochemical energy conversion efficiency (ϕ_P) at night in the global ocean, obtained simultaneously with our lifetime measurements, is 0.35 ± 0.11 (fig. S2). Given an average nighttime lifetime of 1.13 ns (Fig. 2), we deduce that thermal energy dissipation accounts for ~60% of the photosynthetically active quanta absorbed by phytoplankton globally. In contrast, under optimal growth conditions in the laboratory, an average phytoplankton cell uses ~65% of the absorbed quanta for photochemistry and dissipates <35% as heat. The fact that thermal dissipation of absorbed quanta by phytoplankton in the upper ocean is so high strongly implies that a large fraction of cells have impaired or nonfunctional PSII reaction centers and/or uncoupled photosynthetic antennae. We conclude that, although photochemical energy conversion to biomass in the oceans accounts for half of the global carbon fixed per annum, the overall energy conversion efficiency is relatively low and is limited by nutrient supply.

REFERENCES AND NOTES

1. D. Antoine, J. M. Andre, A. Morel, *Global Biogeochem. Cycles* **10**, 57–69 (1996).
2. C. B. Field, M. J. Behrenfeld, J. T. Randerson, P. Falkowski, *Science* **281**, 237–240 (1998).
3. M. J. Behrenfeld, E. Boss, D. A. Siegel, D. M. Shea, *Global Biogeochem. Cycles* **19**, GB1006 (2005).
4. M. J. Behrenfeld, P. G. Falkowski, *Limnol. Oceanogr.* **42**, 1–20 (1997).
5. P. G. Falkowski, Z. Kolber, *Aust. J. Plant Physiol.* **22**, 341–355 (1995).
6. Z. Kolber, P. G. Falkowski, *Limnol. Oceanogr.* **38**, 1646–1665 (1993).
7. G. H. Krause, E. Weis, *Annu. Rev. Plant Physiol.* **42**, 313–349 (1991).
8. P. W. Boyd *et al*., *Nature* **407**, 695–702 (2000).
9. T. S. Bibby, M. Y. Gorbunov, K. W. Wyman, P. G. Falkowski, *Deep Sea Res. Part II Top. Stud. Oceanogr.* **55**, 1310–1320 (2008).
10. P. G. Falkowski, D. Ziemann, Z. Kolber, P. K. Bienfang, *Nature* **352**, 55–58 (1991).
11. M. J. Behrenfeld *et al*., *Nature* **442**, 1025–1028 (2006).
12. D. J. Suggett, C. M. Moore, A. E. Hickman, R. J. Geider, *Mar. Ecol. Prog. Ser.* **376**, 1–19 (2009).
13. D. Tchernov *et al*., *Proc. Natl. Acad. Sci. U.S.A.* **101**, 13531–13535 (2004).
14. P. Falkowski, J. A. Raven, *Aquatic Photosynthesis* (Princeton Univ. Press, Princeton, NJ, ed. 2, 2007).
15. W. L. Butler, R. J. Strasser, *Proc. Natl. Acad. Sci. U.S.A.* **74**, 3382–3385 (1977).
16. M. Bradbury, N. R. Baker, *Proc. R. Soc. London Ser. B* **220**, 251–264 (1983).
17. Information on materials and methods is available on *Science* Online.
18. J. R. Lakowicz, *Principles of Fluorescence Spectroscopy* (Springer Science+Business Media, New York, ed. 3, 2006).
19. C. M. Moore *et al*., *Nat. Geosci.* **6**, 701–710 (2013).
20. J. A. Raven, M. C. W. Evans, R. E. Korb, *Photosynth. Res.* **60**, 111–150 (1999).
21. I. R. Vassiliev *et al*., *Plant Physiol.* **109**, 963–972 (1995).
22. P. G. Falkowski, R. M. Greene, R. J. Geider, *Oceanography* **5**, 84–91 (1992).
23. P. S. Schrader, A. J. Milligan, M. J. Behrenfeld, *PLOS ONE* **6**, e18753 (2011).
24. M. R. Abbott, R. M. Letelier, "Algorithm theoretical basis document: Chlorophyll fluorescence (MODros. Inf. Serv. Product Number 20)" (Ocean Biology Processing Group, NASA's Earth Observing System, 1999).
25. M. J. Behrenfeld *et al*., *Biogeosciences* **6**, 779–794 (2009).
26. Y. Huot, B. A. Franz, M. Fradette, *Remote Sens. Environ.* **132**, 238–253 (2013).
27. A. Savtchenko *et al*., *Adv. Space Res.* **34**, 710–714 (2004).
28. A. C. Alderkamp, H. J. W. de Baar, R. J. W. Visser, K. R. Arrigo, *Limnol. Oceanogr.* **55**, 1248–1264 (2010).
29. T. J. Browning, H. A. Bouman, C. M. Moore, *Global Biogeochem. Cycles* **28**, 510–524 (2014).
30. A. Bricaud, H. Claustre, J. Ras, K. Oubelkheir, *J. Geophys. Res. Oceans* **109**, C11010 (2004).
31. A. Morel, A. Bricaud, *Deep-Sea Res.* **28**, 1375–1393 (1981).

ACKNOWLEDGMENTS

We thank E. Boyle, P. Quinn, K. Thamatrakoln, and V. Fadeev for providing ship time and the captains and crews of research vessels *Oceanus*, *Knorr*, *Melville*, *Akademik Yoffe*, and *Araon*. This research was supported by grants NNX08AC24G from the NASA Ocean Biology and Biogeochemistry Program and SI-1334 from the Strategic Environmental Research and Development Program to M.Y.G. and P.G.F. H.L. and F.I.K. were supported by Institute of Marine and Coastal Sciences postdoctoral fellowships and the Bennett L. Smith Endowment to P.G.F. M.Y.G and F.I.K. were in part supported by grant 14-17-00451 from the Russian Science Foundation. J.P. and S.L. were supported by grant PP15020 from the Korea Polar Research Institute. All fluorescence data are deposited at PANGAEA (Publishing Network for Geoscientific and Environmental Data) under accession number PDI-11228.

SUPPLEMENTARY MATERIALS

www.sciencemag.org/content/351/6270/264/suppl/DC1
Materials and Methods
Figs. S1 to S4
Table S1
References (*32*–*52*)

30 March 2015; accepted 9 December 2015
10.1126/science.aab2213

NEURAL CIRCUITS

Inhibition protects acquired song segments during vocal learning in zebra finches

Daniela Vallentin,[1,2]* Georg Kosche,[1,2]* Dina Lipkind,[3] Michael A. Long[1,2]†

Vocal imitation involves incorporating instructive auditory information into relevant motor circuits through processes that are poorly understood. In zebra finches, we found that exposure to a tutor's song drives spiking activity within premotor neurons in the juvenile, whereas inhibition suppresses such responses upon learning in adulthood. We measured inhibitory currents evoked by the tutor song throughout development while simultaneously quantifying each bird's learning trajectory. Surprisingly, we found that the maturation of synaptic inhibition onto premotor neurons is correlated with learning but not age. We used synthetic tutoring to demonstrate that inhibition is selective for specific song elements that have already been learned and not those still in refinement. Our results suggest that structured inhibition plays a crucial role during song acquisition, enabling a piece-by-piece mastery of complex tasks.

Humans (*1*) and several other animal species (*2*–*4*) learn motor sequences by imitation. In the observer, a sensory percept must inform relevant motor circuits involved in the generation of the target behavior, but little is known about the neural mechanisms underlying this process. We address this issue in the male zebra finch, which acquires its courtship song by listening to (movie S1) (*5*) and imitating (*6*–*9*) a tutor. The forebrain nucleus HVC acts as an important sensorimotor interface because it receives direct connections from higher-order auditory centers (*10*–*12*) and generates commands essential for song production (*13*–*15*). In the juvenile zebra finch, tutor song exposure influences structural plasticity within HVC (*16*), a process that is thought to be crucial for song imitation (*17*). The tutor song has also been shown to drive network activity within HVC (*18*), but the responses of individual HVC premotor neurons during observational learning had not yet been explored.

We performed intracellular recordings in identified HVC neurons projecting to the robust nucleus of the arcopallium (RA) of 10 awake juvenile zebra finches during exposure to their tutor song. In 13 out of 29 of these HVC premotor neurons, tutor song playback caused spiking activity (Fig. 1, A to C). In those neurons, the timing of the evoked spikes was often highly precise across trials (see supplementary materials), demonstrating that exposure to the tutor song is sufficient to drive patterned spiking activity within HVC and may serve an instructive role for the developing HVC premotor circuit. We also observed reliably timed tutor-evoked spiking in RA (18 neurons in

[1]NYU Neuroscience Institute and Department of Otolaryngology, New York University Langone Medical Center, New York, NY 10016, USA. [2]Center for Neural Science, New York University, New York, NY 10003, USA. [3]Laboratory of Vocal Learning, Department of Psychology, Hunter College, New York, NY 10065, USA.
*These authors contributed equally to this work.
†Corresponding author. E-mail: mlong@med.nyu.edu

three birds) (fig. S1) that was presumably driven by HVC. In contrast, tutor song playback did not evoke a suprathreshold response in HVC premotor neurons of awake adult zebra finches (Fig. 1D, 0 of 24 cells in seven birds) and had only a minimal impact on subthreshold activity in those neurons (Fig. 1, D to F).

To directly investigate sensory-evoked synaptic events in HVC premotor neurons in awake zebra finches, we used in vivo whole-cell voltage clamp recordings (fig. S2). Using a fluorescent retrograde tracer injected into RA, we targeted HVC premotor neurons with two-photon microscopy guidance. In both juveniles (25 cells in 7 birds) and adults (15 cells in 5 birds), excitatory events could be evoked by the tutor song (fig. S3); this suggests that the observed lack of spiking in the adult bird is not explained by a decrease in the strength of sensory afferents from auditory projections to HVC. Our results seemed inconsistent with previous findings in which HVC projection neuron spiking could be reliably driven by song playback in urethane-anesthetized adult zebra finches (*19*). Because urethane has been shown to act as an antagonist for GABAergic transmission (*20*), we reasoned that synaptic inhibition might suppress tutor song–evoked excitation in HVC of awake adult zebra finches. To test that hypothesis, we locally infused a $GABA_A$ antagonist (gabazine) and recorded HVC premotor neurons during tutor song exposure in adults (Fig. 1G). Once local inhibition was attenuated, HVC premotor neurons exhibited tutor song–evoked patterned spiking responses (Fig. 1, G to I) similar to that seen in juvenile zebra finches (Fig. 1, A to C). This finding indicates that inhibition can effectively silence sensory inputs onto HVC premotor neurons in the adult zebra finch.

Local circuit interneurons are likely to be the sole source of inhibition in HVC (*21*), and they exhibit song selective auditory responses in the awake adult zebra finch (*22*, *23*). Thus, the lack of a tutor song response in HVC premotor neurons in adulthood may be due to a stronger recruitment of the inhibitory network. To address this idea, we performed juxtacellular recordings of HVC interneurons during tutor song presentation in both juvenile (34 cells in 10 birds) and adult (15 cells in 4 birds) zebra finches (Fig. 2, A to D). Across all ages tested, interneurons increased their spiking activity to tutor song playback relative to a silent baseline period (fig. S4), and we observed that the tutor song could evoke precise spiking activity in some cases (Fig. 2B). When considering all data across both juvenile and adult zebra finches, however, we noticed no consistent age-related difference in the regularity of interneuron firing across trials (Fig. 2C). Because the song learning process has been shown to be highly variable across individuals (*6*) (fig. S5), we reexamined our database on the similarity of recent song recordings from each bird to the tutor song. We found that interneuron firing precision in response to the tutor song tended to correlate with the extent of acoustic similarity to that song (Fig. 2D).

Because HVC interneurons densely interconnect with HVC premotor neurons (*24*, *25*), they are well poised to directly inhibit HVC premotor neurons during tutor song presentation. Using two-photon targeted voltage-clamp recordings in awake birds, we found that inhibitory currents onto HVC premotor neurons were often reliably evoked by tutor song playback (Fig. 2, E to H, and fig. S6). Consistent with our results concerning HVC interneuron firing, we found no evidence for an age-related change in the regularity or strength of tutor song–evoked inhibition onto HVC premotor neurons (fig. S7). Additionally, we found no age-related change in the amplitude or frequency of spontaneous inhibitory events (fig. S8) and a developmental decrease in the amount of current needed to hold premotor neurons at 0 mV, which could reflect a down-regulation of tonic inhibition. However, in both juvenile and adult zebra finches, we found that the inhibitory charge, event frequency and amplitude, and regularity of inhibition across trials were significantly correlated with song imitation accuracy (Fig. 2, E to L, and fig. S6). These results demonstrate that the maturation of sensory-evoked inhibition in HVC matches the bird's learning progress rather than its developmental stage.

What function might this inhibition serve? We hypothesized that precisely timed inhibition in HVC could selectively target portions of the song that have been adequately learned, thereby suppressing the effect of sensory inputs on premotor neurons during those times and preventing further plasticity in motor output. We tested two predictions stemming from this idea. One prediction is that all premotor neurons should receive the inhibitory signal synchronously, which would allow for robust suppression of sensory inputs on the entire premotor system. A second prediction is that the global inhibitory signal should vary in strength as a function of how well each segment of the song has been learned, with stronger inhibition associated with better-learned segments. To test the first prediction, we considered 11 cases

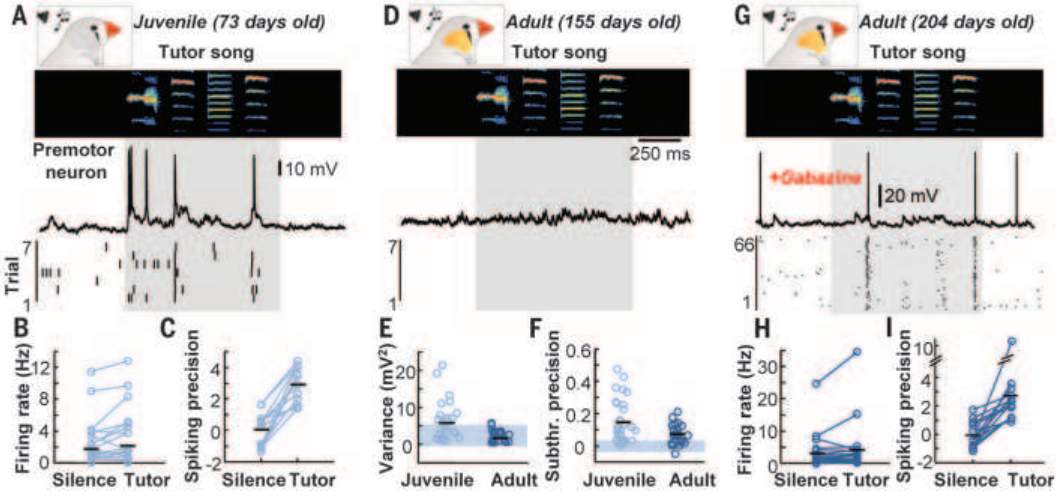

Fig. 1. Responses of HVC premotor neurons to the tutor song are developmentally suppressed. (**A**) Example intracellular recording from an HVC premotor neuron in an awake juvenile zebra finch during tutor song presentation (sonogram frequency: 0.5 to 7.5 kHz). Below is a spike raster plot showing seven repetitions from the same neuron; the shaded region indicates the time of tutor song exposure with an additional 50 ms after the end of the song. (**B**) Firing rate of HVC premotor neuron firing in juvenile zebra finches [silence, 1.7 ± 2.7 Hz; tutor, 2.1 ± 3.3 Hz; $P = 0.114$, repeated-measures analysis of variance (ANOVA)]. (**C**) Spiking precision (see materials and methods) of HVC premotor neuron firing in juvenile zebra finches (silence, 0.0 ± 1.1; tutor, 3.0 ± 1.2; $P = 0.007$, repeated-measures ANOVA). (**D**) Example HVC premotor neuron recording in an awake adult bird during tutor song presentation, with spike raster below. (**E**) Membrane potential variance of HVC premotor neurons was greater in juveniles (5.8 ± 5.3 mV^2) than in adults (2.3 ± 1.6 mV^2) ($P = 0.004$, Wilcoxon rank sum test); the shaded region denotes the 95% confidence interval. (**F**) Subthreshold precision in HVC premotor neurons was greater in juveniles (0.16 ± 0.14) than in adults (0.08 ± 0.06) ($P = 0.025$, Wilcoxon rank sum test). (**G**) Tutor song responses from an HVC premotor neuron in an awake adult bird after local gabazine infusion (0.01 mM). (**H**) Firing rate during silence (3.6 ± 5.8 Hz) and during tutor song presentation (4.6 ± 8.2 Hz) ($n = 14$ neurons; $P < 0.001$, repeated-measures ANOVA) after local gabazine infusion. (**I**) Spiking precision was greater during the tutor song presentation (2.7 ± 2.5) than during silence (−0.1 ± 0.9) ($P = 0.016$, repeated-measures ANOVA).

in which multiple HVC premotor neurons (mean: 3.5 ± 1.3 neurons per bird) were recorded in the same bird (Fig. 3A). We found that tutor song–evoked inhibition was often highly correlated across neurons (Fig. 3B), and this effect was monotonically related to the degree of learning (Fig. 3D). The excitatory current profiles, however, seemed to be unique for each neuron (Fig. 3C) and did not significantly change with song learning (Fig. 3E). Our results are consistent with a global entrainment of a motor circuit by an inhibitory network whose coherent song responsiveness may effectively suppress certain segments of the tutor song in a learning-dependent manner.

Zebra finches often learn individual song elements in series, focusing on specific passages at certain times (*7*). To test the second prediction of our model—that local inhibition in HVC is accurately targeting the syllables of the tutor song that the zebra finch had learned—we used a previously established method for controlling the learning process of individual song syllables (*7*, *26*). Zebra finches were first trained using a synthetic tutor that produced four concatenated copies of a single syllable "A" (Fig. 4A). Once the song "AAAA" was learned, the tutoring paradigm was altered to introduce an additional syllable

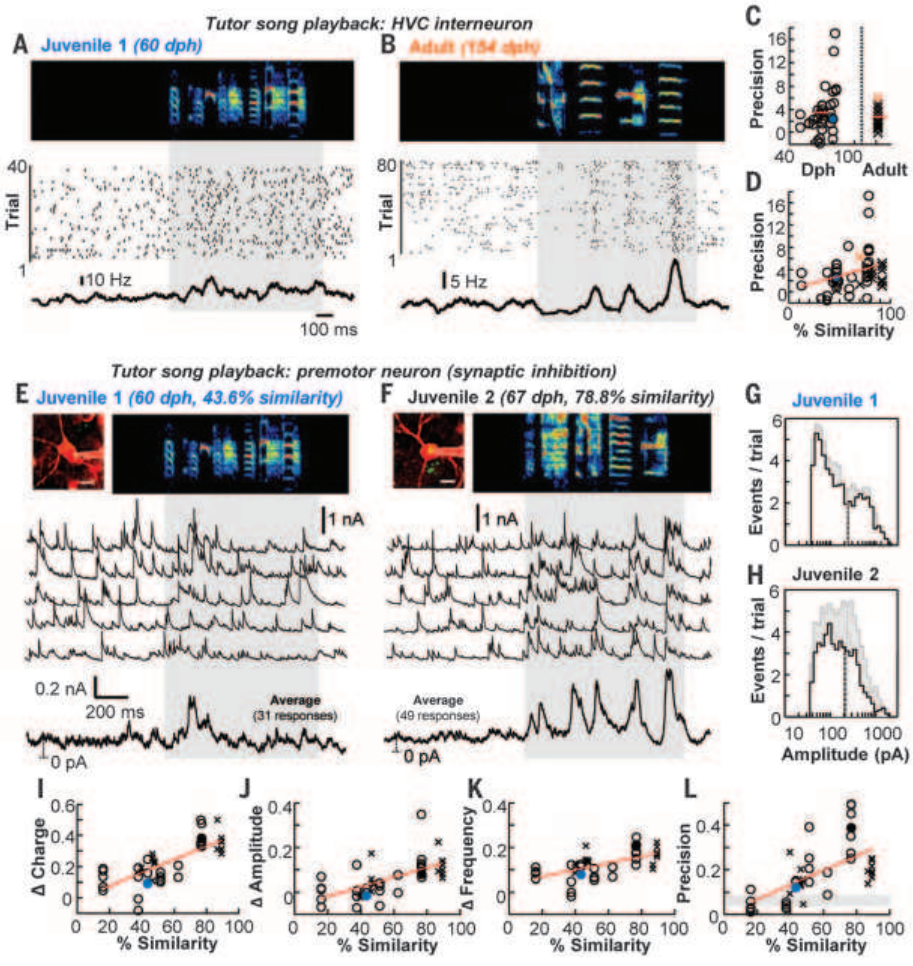

Fig. 2. Tutor song–evoked inhibition strengthens and sharpens with improved song performance. (**A** and **B**) Awake spiking activity of example HVC interneurons recorded in a juvenile (A) and an adult (B) bird during silence and tutor song presentation dph, days post-hatch. (**C**) Across the population, the precision of HVC interneuron firing did not differ between juveniles (3.8 ± 4.0 Hz) and adults (2.9 ± 1.7 Hz) (P = 0.51, Wilcoxon rank sum test). (**D**) Spiking precision of HVC interneurons depending on performance (P = 0.056, linear mixed-effect model). The solid circles and colored crosses represent data shown in the examples to the left. (**E** and **F**) Awake voltage-clamp recordings of inhibitory currents onto two HVC premotor neurons (images at top; scale bar, 10 μm) in response to a tutor song. For each cell, five single sweeps are presented as well as an average. The dotted line represents the distance from baseline (0 pA). (**G** and **H**) Amplitude histograms of detected inhibitory events during silence (black) and tutor song (gray) for juveniles 1 (G) and 2 (H). Mean of the amplitude distribution is indicated as a dashed vertical line. (**I** to **L**) Changes in tutor song–evoked inhibition onto HVC premotor neurons as a function of performance. Increasing similarity to the tutor song is associated with an increase (P < 0.01, linear mixed-effect model) in the inhibitory charge (I), amplitude (J), and frequency (K) of inhibitory events, and in the precision of inhibition across trials (L) (shaded region = 95% confidence interval). The solid circles represent data shown in the examples above.

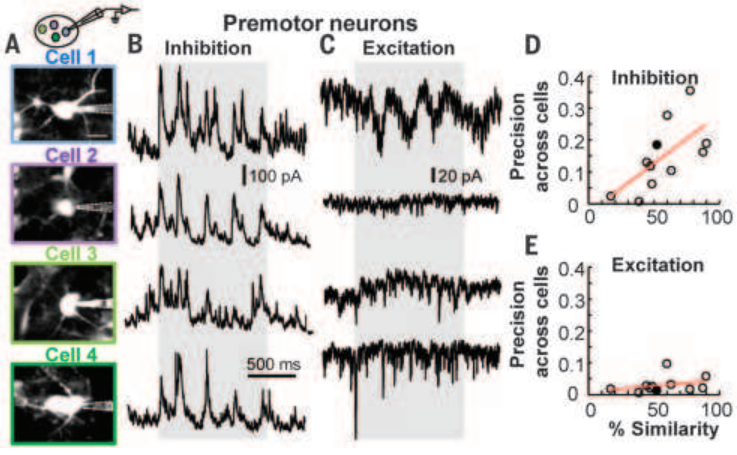

Fig. 3. Learning is associated with synchronous network inhibition. (**A**) Recording schematic and two-photon images of four recorded HVC premotor neurons in the same zebra finch. Scale bar, 10 μm. (**B** and **C**) Average inhibitory (B) and excitatory (C) current traces of premotor neurons shown in (A) during tutor song presentation. (**D**) Regularity of tutor song–evoked inhibitory currents across different neurons within one bird significantly increases with learning (P < 0.05, Pearson linear correlation). The solid circles represent data shown in the examples to the left. (**E**) Regularity of tutor song–evoked excitatory currents across different neurons within one bird does not significantly change depending on performance (P = 0.35, Pearson linear correlation).

"B." Juvenile finches can eventually copy the new song "ABAB" (Fig. 4A), which leads to two distinct learning phases: an early learning phase in which "A" is performed well and "B" is performed poorly (Fig. 4, B and C), followed by a later learning phase in which both "A" and "B" are performed well (Fig. 4, D and E). We could exploit this artificially induced learning trajectory to address whether inhibition can be specifically directed toward portions of the song that have already been learned. In the early learning phase, when juveniles could perform syllable "A" well and not "B," interneuron firing (Fig. 4F) as well as inhibitory currents onto HVC premotor neurons (Fig. 4G) preferentially targeted the learned syllable (Fig. 4, H and I). Zebra finches at the later learning stage, which produced a good copy of both "A" and "B," showed equivalent interneuron firing and synaptic inhibition across both syllable types (Fig. 4, J to M). In contrast, excitatory currents did not change their relative timing across learning conditions (fig. S9).

Our results show that the activity of a motor circuit can be directly driven by sensory afferents during song learning. Specifically, exposure to the tutor song can elicit precise spiking in HVC premotor neurons of the juvenile bird (fig. S10A). This result is reminiscent of the "mirroring" previously observed in mammalian motor systems (*27*) as well as in other songbird species (*28*) in which motor neurons respond to actions that are observed in others, but the temporal similarity between the tutor song–evoked firing patterns and singing-related activity in individual HVC neurons of the juvenile remains unknown.

A previous experiment (*17*) demonstrated the necessity of tutor song–dependent HVC dynamics during vocal learning. In that study, juvenile zebra finches were unable to imitate the tutor when HVC activity was optogenetically scrambled during the presentation of the tutor song. These results are consistent with the idea that precise sensory-driven activity may have a pivotal role in establishing song-related premotor sequences.

We demonstrated a loss of auditory responsiveness in HVC of the adult bird, but we were able to use GABA antagonists to unmask tutor song–evoked spiking, thereby highlighting the role of inhibition in the suppression of these responses. Auditory-evoked responses were suppressed in all adults, even those that poorly copied the tutor song, indicating that the phasic inhibitory currents that are central to this study are not the only factor mediating this phenomenon. We did not find an age-related increase in tonic inhibition, which could have explained these results. Future studies could investigate the role of other developmentally regulated factors, such as intrinsic neuronal properties or chloride reversal potential, that could contribute to the further suppression of sensory inputs during development.

We also found that inhibition during song learning can precisely target specific portions of the song that have already been mastered (fig. S10B). As a result, certain components of the HVC sequence representing unlearned aspects of the song may be left "exposed" to the influence of the incoming auditory stream. These neurons may then fire in a patterned way in response to the tutor song until an appropriate behavior is established. After the song has been learned completely, inhibition can shield HVC premotor neurons from the impact of the tutor song (fig. S10C). We do not yet understand the mechanisms that compare the current song performance to the tutor song and then transform this information into a change in inhibition throughout learning. This process is likely to be primarily mediated through an increase in the regularity of inhibitory neuron firing across trials, which is driven from inputs from higher-order auditory centers (*10*–*12*).

In sensory systems, inhibitory network maturation can result in the closure of critical periods (*29*). However, this procedure is strongly dependent on the developmental stage of the animal,

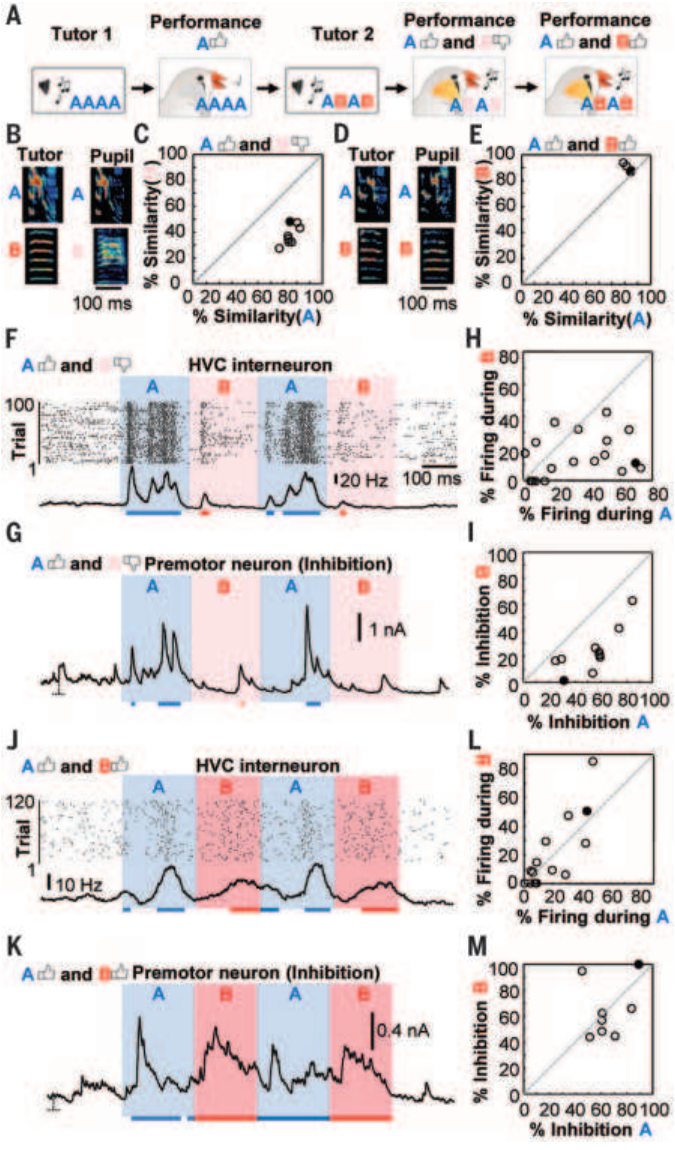

Fig. 4. Inhibition accurately targets learned portions of the tutor song. (**A**) Schematic of the training procedure. (**B**) Example syllables produced by a juvenile during an early learning phase in which syllable A is copied with 82.5% similarity and syllable B is copied with 48.8% similarity. (**C**) Syllable performance for eight individuals in their early learning stage singing a good copy of A (77.9 ± 4.7% similarity) and a poor copy of B (42.2 ± 7.6% similarity). (**D**) Example syllables produced by a juvenile during a late learning phase in which both syllable A and B are copied well (85.7% and 88.9% similarity, respectively). (**E**) Syllable performance for four individual adults in their final learning stage singing a good copy of A (84.6 ± 1.9% similarity) and B (89.7 ± 2.2% similarity). (**F** and **G**) HVC interneuron activity (F) and inhibitory currents onto an HVC premotor neuron (G) during ABAB presentation recorded in two juvenile zebra finches performing a good copy of A (similarity: 75.6% and 84.6%, respectively) and a poor copy of B (similarity: 36.0% and 44.7%). The red and blue horizontal lines represent periods in which either the interneuron firing rate or HVC premotor neuron inhibition exceeds a 95% confidence interval. (**H** and **I**) Percentage of time that interneuron firing rates (n = 18 cells) (H) or HVC premotor inhibition (n = 10 cells) (I) exceeded the 95% confidence interval threshold across a population of four and five birds, respectively, that copied syllable A well and B poorly. (**J** and **K**) HVC interneuron activity (J) and HVC premotor neuron inhibition (K) during ABAB presentation recorded in a juvenile zebra finch performing a good copy of syllables A (similarity: 85.7% and 79.8%) and B (similarity: 88.9% and 94.9%). (**L** and **M**) Percentage of time that interneuron firing rates (n = 14 cells) (L) or HVC premotor inhibitory current amplitudes (n = 8 cells) (M) exceeded the 95% confidence interval threshold in two birds, respectively, that copied syllables A and B well.

whereas the inhibitory network changes observed in HVC are correlated not with age but with song performance (fig. S10C). Additionally, because the extent of tutor imitation is variable across birds and even within the span of a single bird's song, the maturation of HVC inhibition proceeds in a self-directed, nonuniform manner. This stands in stark contrast to sensory systems, where inhibitory maturation primarily relies on external factors such as visual experience (*30*–*32*). Despite these differences, our findings offer the opportunity to potentially enable latent afferent streams to engage with motor circuits through the manipulation of local inhibition. Using this approach, we may help to extend (*29*) or reopen critical periods (*33*) in order to rebuild or refine skilled behaviors throughout life.

REFERENCES AND NOTES

1. Y. Blandin, L. Lhuisset, L. Proteau, *Q. J. Exp. Psychol. A* **52**, 957–979 (1999).
2. G. Fiorito, P. Scotto, *Science* **256**, 545–547 (1992).
3. A. Whiten, *J. Comp. Psychol.* **112**, 270–281 (1998).
4. B. Kenward, C. Rutz, A. A. S. Weir, A. Kacelnik, *Anim. Behav.* **72**, 1329–1343 (2006).
5. M. Konishi, *Z. Tierpsychol.* **22**, 770–783 (1965).
6. O. Tchernichovski, P. P. Mitra, T. Lints, F. Nottebohm, *Science* **291**, 2564–2569 (2001).
7. P. Ravbar, D. Lipkind, L. C. Parra, O. Tchernichovski, *J. Neurosci.* **32**, 3422–3432 (2012).
8. P. H. Price, *J. Comp. Physiol. Psychol.* **93**, 260–277 (1979).
9. K. Immelman, Song development in the zebra finch and other estrilidid finches. In *Bird Vocalizations*, R. A. Hinde, Ed. (Cambridge Univ. Press, 1969), pp. 61–74.
10. F. Nottebohm, D. B. Kelley, J. A. Paton, *J. Comp. Neurol.* **207**, 344–357 (1982).
11. E. E. Bauer *et al*., *J. Neurosci.* **28**, 1509–1522 (2008).
12. E. Akutagawa, M. Konishi, *J. Comp. Neurol.* **518**, 3086–3100 (2010).
13. E. T. Vu, M. E. Mazurek, Y. C. Kuo, *J. Neurosci.* **14**, 6924–6934 (1994).
14. M. A. Long, M. S. Fee, *Nature* **456**, 189–194 (2008).
15. D. Aronov, A. S. Andalman, M. S. Fee, *Science* **320**, 630–634 (2008).
16. T. F. Roberts, K. A. Tschida, M. E. Klein, R. Mooney, *Nature* **463**, 948–952 (2010).
17. T. F. Roberts, S. M. Gobes, M. Murugan, B. P. Ölveczky, R. Mooney, *Nat. Neurosci.* **15**, 1454–1459 (2012).
18. T. A. Nick, M. Konishi, *J. Neurobiol.* **62**, 231–242 (2005).
19. R. Mooney, *J. Neurosci.* **20**, 5420–5436 (2000).
20. D. Accorsi-Mendonça, R. M. Leão, J. F. Aguiar, W. A. Varanda, B. H. Machado, *Am. J. Physiol. Regul. Integr. Comp. Physiol.* **292**, R396–R402 (2007).
21. S. Scotto-Lomassese, C. Rochefort, A. Nshdejan, C. Scharff, *Eur. J. Neurosci.* **25**, 1663–1668 (2007).
22. P. L. Rauske, S. D. Shea, D. Margoliash, *J. Neurophysiol.* **89**, 1688–1701 (2003).
23. J. N. Raksin, C. M. Glaze, S. Smith, M. F. Schmidt, *J. Neurophysiol.* **107**, 2185–2201 (2012).
24. G. Kosche, D. Vallentin, M. A. Long, *J. Neurosci.* **35**, 1217–1227 (2015).
25. R. Mooney, J. F. Prather, *J. Neurosci.* **25**, 1952–1964 (2005).
26. D. Lipkind, O. Tchernichovski, *Proc. Natl. Acad. Sci. U.S.A.* **108** (suppl. 3), 15572–15579 (2011).
27. G. Rizzolatti, L. Craighero, *Annu. Rev. Neurosci.* **27**, 169–192 (2004).
28. J. F. Prather, S. Peters, S. Nowicki, R. Mooney, *Nature* **451**, 305–310 (2008).
29. T. K. Hensch, *Annu. Rev. Neurosci.* **27**, 549–579 (2004).
30. B. Morales, S. Y. Choi, A. Kirkwood, *J. Neurosci.* **22**, 8084–8090 (2002).
31. Y. T. Li, W. P. Ma, C. J. Pan, L. I. Zhang, H. W. Tao, *J. Neurosci.* **32**, 3981–3991 (2012).
32. M. Pecka, Y. Han, E. Sader, T. D. Mrsic-Flogel, *Neuron* **84**, 457–469 (2014).
33. D. G. Southwell, R. C. Froemke, A. Alvarez-Buylla, M. P. Stryker, S. P. Gandhi, *Science* **327**, 1145–1148 (2010).

ACKNOWLEDGMENTS

Supported by NIH grant R01NS075044, the New York Stem Cell Foundation, and Deutsche Forschungsgemeinschaft grant VA 742/1-2. We thank R. Froemke, J. Goldberg, G. Maimon, D. Okobi, B. Ölveczky, and R. Tsien for comments on earlier versions of this manuscript; K. Katlowitz, K. Kuchibhotla, and J. Merel for assistance with statistics and analysis; and O. Tchernichovski for valuable discussions and for providing the birds used in this study. Supplement contains additional data. The authors declare no competing financial interests. Author contributions: D.V., G.K., and M.A.L. designed the research; D.V., G.K., and D.L. performed the research; D.V., G.K., D.L., and M.A.L. analyzed the data; D.L. contributed reagents and analytic tools; and D.V., G.K., and M.A.L. wrote the paper.

SUPPLEMENTARY MATERIALS

www.sciencemag.org/content/351/6270/267/suppl/DC1
Materials and Methods
Figs. S1 to S10
Movie S1
References (*34*–*39*)

24 August 2015; accepted 30 November 2015
10.1126/science.aad3023

MUSCLE PHYSIOLOGY

A peptide encoded by a transcript annotated as long noncoding RNA enhances SERCA activity in muscle

Benjamin R. Nelson,[1,2]* Catherine A. Makarewich,[1,2]* Douglas M. Anderson,[1,2] Benjamin R. Winders,[1,2] Constantine D. Troupes,[3,4] Fenfen Wu,[5] Austin L. Reese,[6,7] John R. McAnally,[1,2] Xiongwen Chen,[3,4] Ege T. Kavalali,[6,7] Stephen C. Cannon,[5] Steven R. Houser,[3,4] Rhonda Bassel-Duby,[1,2] Eric N. Olson[1,2]†

Muscle contraction depends on release of Ca^{2+} from the sarcoplasmic reticulum (SR) and reuptake by the Ca^{2+}adenosine triphosphatase SERCA. We discovered a putative muscle-specific long noncoding RNA that encodes a peptide of 34 amino acids and that we named dwarf open reading frame (DWORF). DWORF localizes to the SR membrane, where it enhances SERCA activity by displacing the SERCA inhibitors, phospholamban, sarcolipin, and myoregulin. In mice, overexpression of DWORF in cardiomyocytes increases peak Ca^{2+} transient amplitude and SR Ca^{2+} load while reducing the time constant of cytosolic Ca^{2+} decay during each cycle of contraction-relaxation. Conversely, slow skeletal muscle lacking DWORF exhibits delayed Ca^{2+} clearance and relaxation and reduced SERCA activity. DWORF is the only endogenous peptide known to activate the SERCA pump by physical interaction and provides a means for enhancing muscle contractility.

Intracellular Ca^{2+} cycling is vitally important to the function of striated muscles and is altered in many muscle diseases. Upon electrical stimulation of the myocyte plasma membrane, Ca^{2+} is released from the sarcoplasmic reticulum (SR) and binds to the contractile apparatus triggering muscle contraction (*1*). Relaxation occurs as Ca^{2+} is pumped back into the SR by the sarco-endoplasmic reticulum Ca^{2+} adenosine triphosphatase (SERCA). SERCA activity is inhibited by the small transmembrane peptides phospholamban (PLN), sarcolipin (SLN), and myoregulin (MLN; also known as MRLN) in vertebrates and by sarcolamban A and B (sclA and sclB) in invertebrates, which diminish sarcoplasmic reticulum (SR) Ca^{2+} uptake and myocyte contractility (*2*–*7*).

Recently, we discovered the small open reading frame (ORF) of MLN within a transcript annotated as a long noncoding RNA (lncRNA) (*4*). We hypothesized that a subset of transcripts currently annotated as lncRNAs may encode small proteins that have evaded annotation efforts, a notion supported by recent proteomic analyses (*8*–*10*). To identify potential peptides, we searched presumably noncoding RNA transcripts for hypothetical ORFs using PhyloCSF; this method uses codon substitution frequencies (*11*). From these transcripts, we discovered a previously unrecognized ORF of 34 codons within a muscle-specific transcript, which we call dwarf open reading frame (*Dworf*) (fig. S1). The *Dworf* RNA transcript is annotated as NONCODE lncRNA gene NONMMUG026737 (*12*) in mice and lncRNA LOC100507537 in the University of California,

[1]Department of Molecular Biology, University of Texas Southwestern Medical Center, Dallas, TX 75390, USA. [2]Hamon Center for Regenerative Science and Medicine, University of Texas Southwestern Medical Center, Dallas, TX 75390, USA. [3]Department of Physiology, Temple University School of Medicine, Philadelphia, PA 19140, USA. [4]Department of Cardiovascular Research Center, Temple University School of Medicine, Philadelphia, PA 19140, USA. [5]Department of Neurology, University of Texas Southwestern Medical Center, Dallas, TX 75390, USA. [6]Department of Neuroscience, University of Texas Southwestern Medical Center, Dallas, TX 75390, USA. [7]Department of Physiology, University of Texas Southwestern Medical Center, Dallas, TX 75390, USA.
*These authors contributed equally to this work. **†Corresponding author. E-mail: eric.olson@utsouthwestern.edu**

Santa Cruz, human genome (fig. S2A). With only 34 codons, DWORF is currently the third smallest full-length protein known to be encoded by the mouse genome.

The murine *Dworf* transcript is encoded in three exons on chromosome 3 (fig. S2A). The ORF begins in exon 1, which encodes the first four amino acids of the protein, and the remaining protein is encoded in exon 2. Use of alternative splice acceptors between exons 1 and 2 produces two transcripts that differ by a three-nucleotide insertion. The ORF is conserved to lamprey, the most distant vertebrate genome available (fig. S2B), and scores positively with PhyloCSF (fig. S2C). The C terminus is hydrophobic and is predicted to encode a tail-anchored transmembrane peptide (*13*–*15*). The N terminus is less stringently conserved, but most sequences contain multiple charged residues (primarily lysine and aspartic acid) in this region. Unless otherwise noted, further studies focused on the murine homolog of DWORF.

Northern blot analysis showed that the mRNA transcript is robustly expressed in the heart (Fig. 1A).

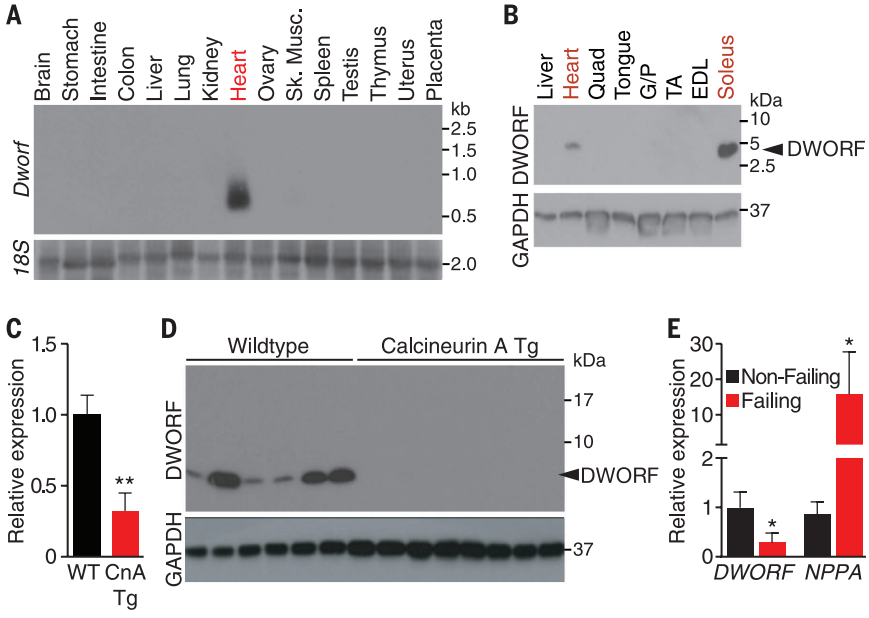

Fig. 1. Muscle-specific expression of the DWORF peptide. (**A**) Northern blot of adult mouse tissues showing *Dworf* RNA expression. (**B**) Western blot of adult mouse tissues with the DWORF-specific antibody reveals a single band at the predicted size of 3.8 kD. Quad, quadriceps; G/P, gastrocnemius/plantaris; TA, tibialis anterior; EDL, extensor digitorum longus. (**C**) Detection of *Dworf* RNA by qRT-PCR in 6-month-old WT and αMHC-CnA mice. Mean ± SEM; WT, $n = 4$; Tg, $n = 5$. (**D**) Western blot analysis of heart homogenates from WT and αMHC-calcineurin mice immunoblotted with DWORF-specific antibody. (**E**) qRT-PCR analysis of human ischemic heart failure tissue showing reduced *DWORF* mRNA in failing hearts, whereas atrial natriuretic peptide (*NPPA*) is significantly increased. Means ± SEM; nonfailing, $n = 8$; failing, $n = 8$.

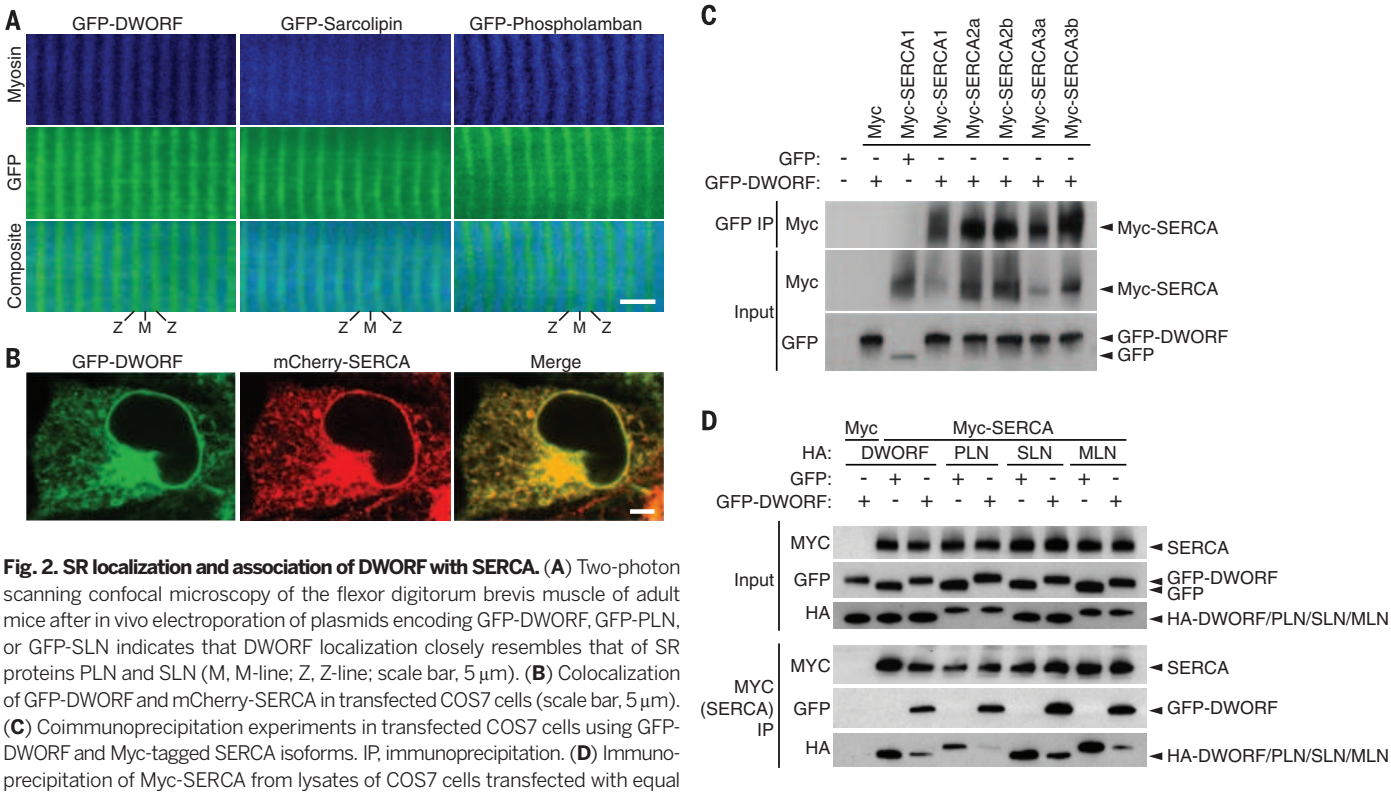

Fig. 2. SR localization and association of DWORF with SERCA. (**A**) Two-photon scanning confocal microscopy of the flexor digitorum brevis muscle of adult mice after in vivo electroporation of plasmids encoding GFP-DWORF, GFP-PLN, or GFP-SLN indicates that DWORF localization closely resembles that of SR proteins PLN and SLN (M, M-line; Z, Z-line; scale bar, 5 μm). (**B**) Colocalization of GFP-DWORF and mCherry-SERCA in transfected COS7 cells (scale bar, 5 μm). (**C**) Coimmunoprecipitation experiments in transfected COS7 cells using GFP-DWORF and Myc-tagged SERCA isoforms. IP, immunoprecipitation. (**D**) Immunoprecipitation of Myc-SERCA from lysates of COS7 cells transfected with equal amounts of HA-DWORF, -PLN, -SLN, or -MLN and Myc-SERCA with fivefold overexpression of either GFP or GFP-DWORF. Coexpression of GFP-DWORF reduced the pull-down of HA-tagged peptides in association with SERCA, which indicated that DWORF binding to SERCA excludes binding of PLN, SLN, or MLN.

By quantitative reverse transcription polymerase chain reaction (qRT-PCR), *Dworf* RNA was also detected in heart and soleus, a postural muscle group of the hindlimb containing the greatest enrichment of slow-twitch muscle fibers in mice (fig. S3A), as well as diaphragm, which contains some slow-twitch fibers but is primarily a fast-twitch muscle in mice (*16*, *17*). Notably, *Dworf* was not detected in the quadriceps, a fast-twitch muscle group, or in cardiac atrial muscle. *Dworf* is not expressed in the prenatal heart but gradually increases in abundance postnatally (fig. S3B).

Cloning of the *Dworf* 5′ untranslated region in frame with an ORF lacking a start codon efficiently initiates translation of the ORF (fig. S4). To further confirm that the transcript encodes a protein, we raised a polyclonal rabbit antibody against the N-terminal 12 amino acids of the predicted protein. Western blotting revealed a single band at the expected molecular mass of 3.8 kD in soleus and heart but not in other tissues (Fig. 1B).

Given its abundance in heart tissue, we examined whether *Dworf* mRNA or protein expression changes in response to pathological cardiac signaling. Indeed, in mice bearing a cardiac-specific α-myosin heavy chain (αMHC) promoter driven calcineurin transgene, which serve as a model of hypertrophic heart disease that progresses to dilated cardiomyopathy by 6 months of age (*18*), *Dworf* mRNA was down-regulated in dilated transgenic hearts of 6-month-old mice (Fig. 1C). Notably, DWORF protein was more dramatically down-regulated than the mRNA in these hearts (Fig. 1D). *DWORF* mRNA was also down-regulated in ischemic failing human hearts, which potentially links changes in *DWORF* expression with human heart failure (Fig. 1E).

We investigated the subcellular distribution of DWORF in skeletal muscle fibers by electroporation of a green fluorescent protein (GFP)–DWORF expression vector into the flexor digitorum brevis muscle of the mouse foot (*19*). Multiphoton excitation microscopy to simultaneously visualize GFP and myosin (using second harmonic generation) showed that GFP-DWORF localizes in an alternating pattern with myosin (Fig. 2A), a distribution consistent with the location of the SR. GFP-SLN and GFP-PLN were individually expressed in the flexor digitorum brevis muscle for comparison. The apparent co-localization of GFP-DWORF, GFP-SLN, and GFP-PLN was striking, including transverse and lengthwise striations typical of SR. The subcellular distribution of GFP-DWORF in transfected COS7 cells also overlaps with that of mCherry-SERCA1 in the endoplasmic reticulum (ER) and perinuclear regions (Fig. 2B).

Because GFP-DWORF colocalizes to the SR with SERCA, we tested whether the two proteins physically interact. COS7 cells were cotransfected with GFP or GFP-DWORF and Myc-tagged SERCA1, 2a, 2b, 3a, or 3b. Immunoprecipitation with a GFP antibody coprecipitated GFP-DWORF with all isoforms of SERCA but did not pull down SERCA in GFP transfected samples lacking DWORF (Fig. 2C). We next examined whether coexpression of DWORF with SERCA would affect complex formation between SERCA and PLN, SLN, or MLN. Indeed, we observed a reduction in the binding of hemagglutinin (HA) epitope–tagged peptides HA-PLN, -SLN, and -MLN with SERCA when coexpressed with GFP-DWORF (Fig. 2D and fig. S5), which suggested that binding of DWORF

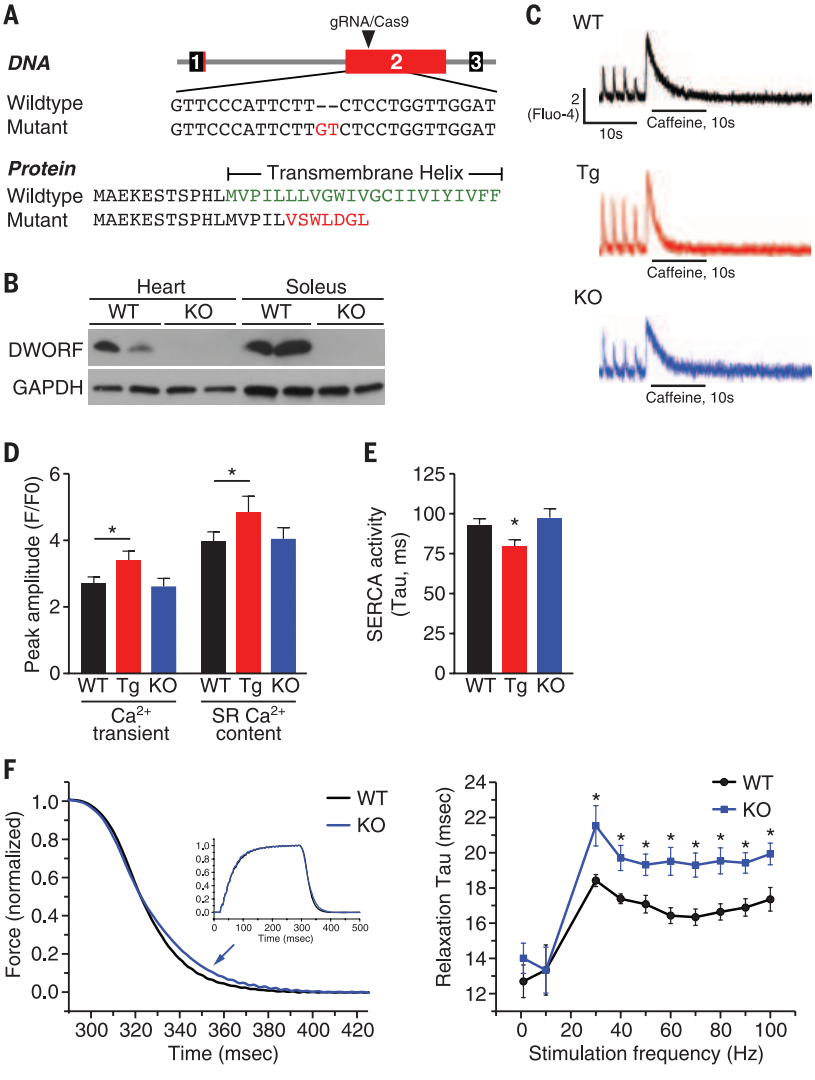

Fig. 3. Consequences of DWORF gain and loss of function. (**A**) A CRISPR gRNA was generated to target the coding sequence of exon 2. An allele containing a 2-bp insertion was chosen for further experiments. The mutation is expected to produce a truncated protein lacking the transmembrane domain. (**B**) Western blot showing the absence of DWORF protein in the cardiac ventricle and soleus muscle of *Dworf* KO mice. (**C**) Representative Ca^{2+} transients and SR load measurements recorded in fluo-4–loaded cardiomyocytes from WT, αMHC-DWORF (Tg), and *Dworf* KO mice. (**D**) Mean amplitude of pacing-induced Ca^{2+} transients in fluo-4–loaded cardiomyocytes from WT, Tg, and KO mice and caffeine-induced Ca^{2+} transients triggered by rapid application of 10 mM caffeine to quantify SR load. Ca^{2+} signal is shown as fluorescence ratio (F/F_0) with the fluorescence intensity (F) normalized to the minimal intensity measured between 0.5 Hz contractions at diastolic phase (F_0). $P < 0.05$, $n = 6$. (**E**) Average decay-time constants (Tau) of pacing-induced Ca^{2+} transients in WT, Tg, and *Dworf* KO cardiomyocytes measured by fitting a single exponential to the Ca^{2+} transient decay trace. This parameter is indicative of SERCA activity. $P < 0.05$, $n = 8$. (**F**) Isometric force was measured from soleus muscles mounted ex vivo and stimulated by 0.2-ms current pulses applied at a range of frequencies. (Left) Force decay was slower in *Dworf* KO muscles (arrow) after fully fused tetanic contractions as shown for 90 Hz (inset). (Right) Slower relaxation for *Dworf* KO muscles occurred for stimulus frequencies sufficient to produce twitch fusion (>20 Hz); however, unfused twitches at low frequency showed no difference in relaxation rates. $P < 0.05$, $n = 6$.

and PLN, SLN, or MLN to SERCA is mutually exclusive. We mutated residues on the M6 transmembrane helix of SERCA1, which are known to interact with PLN, and performed pull-down experiments (*20*). We observed a reduction in SERCA interaction with GFP-DWORF comparable to that of GFP-PLN, which suggested that both peptides bind to similar regions of the SERCA pump (fig. S6) (*20*). Coexpression of Myc-SERCA2a with various ratios of GFP-DWORF and GFP-PLN followed by immunoprecipitation with Myc-specific antibody (anti-Myc) and immunoblotting with GFP-specific antibody indicated that DWORF and PLN have similar binding affinities for SERCA (fig. S7).

To assess the functions of DWORF in vivo, we generated mouse models of gain and loss of function. DWORF overexpression in the heart was achieved by expressing untagged DWORF under the control of the cardiomyocyte-specific αMHC promoter in transgenic mice. Two transgenic (Tg) founders that overexpressed the protein were selected for further studies. Other proteins involved in Ca^{2+} handling were largely unaffected in these transgenic mice (figs. S8 and S9).

We used the CRISPR/Cas9 system to disrupt the coding frame of *Dworf* in mice. A single-guide RNA (gRNA) was designed to target the coding sequence of exon 2 before the transmembrane region (Fig. 3A). Original generation F_0 pups were screened for indels, and a founder with a 2–base pair (2-bp) insertion that disrupts the ORF after codon 16 was chosen for further analysis. Heterozygous *Dworf* knockout (KO) mice yielded homozygous mutant offspring at expected Mendelian ratios. Western blots of ventricular and soleus muscle probed with DWORF-specific antibody showed that the DWORF protein was eliminated in muscle tissues of homozygous mutant mice (Fig. 3B). To our surprise, the *Dworf* transcript was up-regulated about fourfold in the *Dworf* KO tissue (fig. S10A), which suggested a potential feedback mechanism to enhance *Dworf* expression. Several notable RNA transcripts were not changed in *Dworf* KO mice, including those encoding the Ca^{2+}-handling proteins SERCA2 and PLN and the cardiac stress markers *Myh7* and atrial natriuretic peptide (*Nppa*). Western blot analysis of heart (fig. S10B) and soleus muscle (fig. S10C) homogenates revealed no detectable changes in protein expression level, phosphorylation state (fig. S11), or oligomerization of major Ca^{2+}-handling proteins.

We examined whether Ca^{2+} flux was altered in adult cardiomyocytes from wild-type (WT), αMHC-DWORF Tg, and *Dworf* KO mice using the fluorescent Ca^{2+} indicator dye, fluo-4. Isolated cardiomyocytes were loaded with fluo-4, mounted on a temperature-controlled perfusion chamber, and electrically stimulated at 0.5 Hz to initiate intracellular Ca^{2+} transients, which were monitored by epifluorescence. Peak systolic Ca^{2+} transient amplitude and SR Ca^{2+} load were significantly increased in Tg myocytes (Fig. 3, C and D). The pacing-induced Ca^{2+} transient decay rate was significantly enhanced in the Tg myocytes of both αMHC-DWORF Tg lines (Fig. 3E and fig. S12), which suggested that SERCA is more active in these cells (i.e., has a lower tau value). The decay rate of caffeine-induced Ca^{2+} transients was unchanged in Tg myocytes, which indicates that the activity of the Na^+/Ca^{2+} exchanger (NCX) is not altered (fig. S13A). Tg myocytes had higher baseline measurements of contractility—as measured by fractional shortening, peak Ca^{2+} transient amplitude, and Ca^{2+} transient decay rate—and responded less to β-adrenergic stimulation by isoproterenol, likely because they function at close to maximally active levels under baseline conditions (figs. S12 and S13, and table S1). In the absence of increased protein abundance of SERCA or changes in other known Ca^{2+} handling proteins, these findings indicate that SERCA activity is increased in muscle cells overexpressing DWORF.

The effect of *Dworf* ablation on skeletal muscle contractile function was assessed by measuring twitch force at multiple stimulation frequencies in isolated soleus muscles from WT and KO mice (*21*). We did not observe significant differences in peak muscle force between genotypes and saw no differences in relaxation rates at low, non-tetanic stimulation frequencies; however, at tetanus-inducing frequencies, relaxation rates were significantly slowed in *Dworf* KO muscles after tetanus (Fig. 3F). The effect on posttetanic relaxation times may suggest that *Dworf* expression is particularly beneficial for recovery from periods of prolonged contraction and Ca^{2+} release.

Oxalate-supported Ca^{2+}-dependent Ca^{2+}-uptake measurements in muscle homogenates provide a direct quantification of SERCA enzymatic activity (*21*, *22*). We used this technique to measure SERCA activity in hearts of WT, Tg, and KO mice. Hearts overexpressing DWORF showed an apparent increase in SERCA activity at lower concentrations of Ca^{2+} substrate in both of our transgenic lines quantified as a higher affinity of SERCA for Ca^{2+} (reduction in K_{Ca}), and *Dworf* KO hearts exhibited a less obvious, but still significant, decrease in the affinity of SERCA for Ca^{2+}, as indicated by an increase in K_{Ca} (Fig. 4A, fig. S14A, and table S2). We did not observe

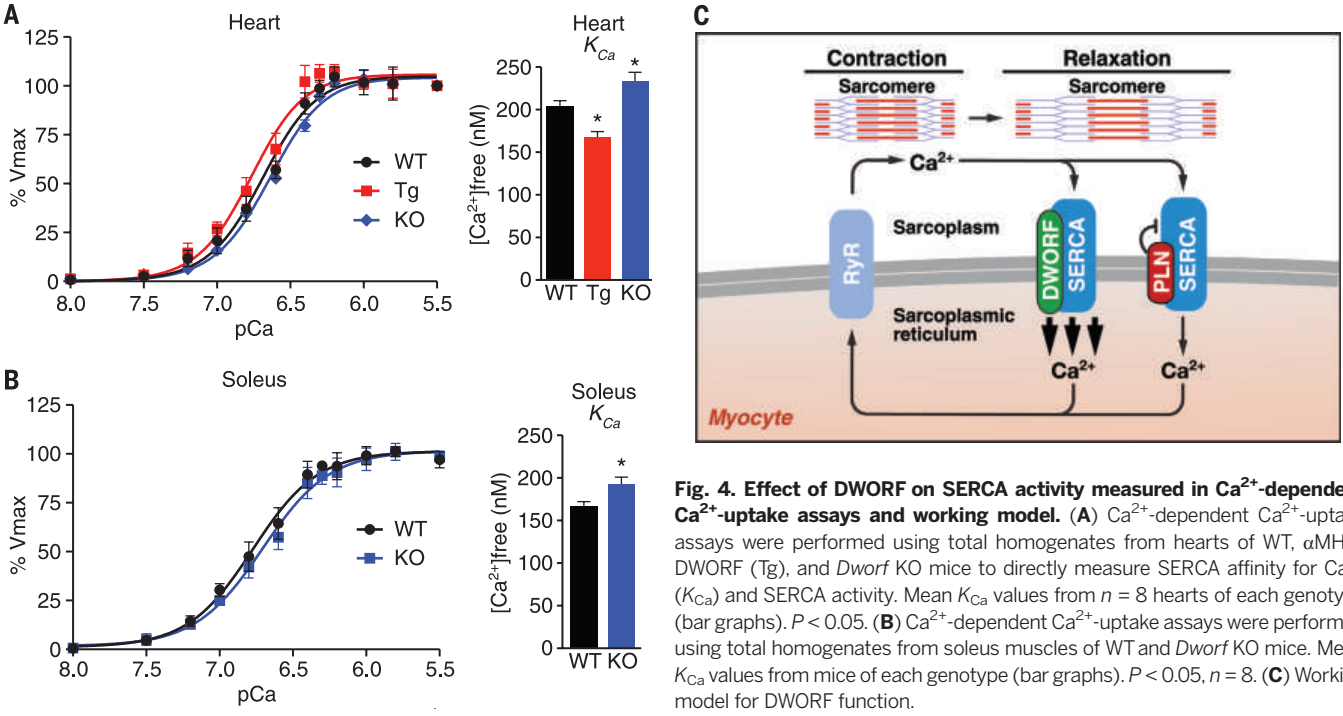

Fig. 4. Effect of DWORF on SERCA activity measured in Ca^{2+}-dependent Ca^{2+}-uptake assays and working model. (**A**) Ca^{2+}-dependent Ca^{2+}-uptake assays were performed using total homogenates from hearts of WT, αMHC-DWORF (Tg), and *Dworf* KO mice to directly measure SERCA affinity for Ca^{2+} (K_{Ca}) and SERCA activity. Mean K_{Ca} values from $n = 8$ hearts of each genotype (bar graphs). $P < 0.05$. (**B**) Ca^{2+}-dependent Ca^{2+}-uptake assays were performed using total homogenates from soleus muscles of WT and *Dworf* KO mice. Mean K_{Ca} values from mice of each genotype (bar graphs). $P < 0.05$, $n = 8$. (**C**) Working model for DWORF function.

changes in the maximal rate of Ca^{2+} pump activity (V_{max}) in any of our genotypes (table S2). Because DWORF is most abundant in the slow-twitch soleus muscle group, we also measured SERCA activity in soleus homogenates from WT and KO mice and used quadriceps muscles as a control, because DWORF is not expressed in this muscle group. Analysis of homogenates from the soleus muscle of *Dworf* KO mice revealed a decreased apparent affinity of SERCA for Ca^{2+} as compared with homogenates from WT muscles (Fig. 4B and table S3). These differences were not observed in quadriceps muscle (figs. S14B and table S4).

To determine whether DWORF directly activates SERCA or does so through displacement of its endogenous inhibitors, we cotransfected COS7 cells with SERCA2a and DWORF in the presence or absence of PLN, SLN, and MLN (*4*). We found that coexpression of DWORF alone with SERCA2a did not change the apparent affinity of SERCA for Ca^{2+}, but it relieved the inhibition by PLN in a dose-dependent manner (fig. S15). Threefold overexpression of DWORF was sufficient to return SERCA activity to baseline levels when coexpressed with PLN, SLN, or MLN (fig. S16). These results indicate that DWORF counteracts the effect of inhibitory peptides rather than directly stimulating SERCA pump activity, which is consistent with the lack of primary sequence similarity between DWORF and SERCA inhibitors (fig. S17).

Based on gain- and loss-of-function studies, our results demonstrate that DWORF enhances SR Ca^{2+} uptake and myocyte contractility through its displacement of the inhibitory peptides PLN, SLN, and MLN from SERCA (Fig. 4C). Because DWORF increases the activity of the SERCA pump, it represents an attractive means of enhancing cardiac contractility in settings of heart disease. Finally, our results underscore the likelihood that many transcripts currently annotated as noncoding RNAs encode peptides with important biological functions. These small peptides may evolve rapidly as singular functional domains that fine-tune the activities of larger preexisting molecular complexes, rather than having intrinsic biologic effects themselves. In this regard, small peptides may be uniquely suited to act as key factors in evolutionary adaptation and speciation.

REFERENCES AND NOTES

1. D. M. Bers, *Nature* **415**, 198–205 (2002).
2. D. H. MacLennan, M. Asahi, A. R. Tupling, *Ann. N. Y. Acad. Sci.* **986**, 472–480 (2003).
3. E. G. Kranias, R. J. Hajjar, *Circ. Res.* **110**, 1646–1660 (2012).
4. D. M. Anderson *et al.*, *Cell* **160**, 595–606 (2015).
5. N. C. Bal *et al.*, *Nat. Med.* **18**, 1575–1579 (2012).
6. E. G. Magny *et al.*, *Science* **341**, 1116–1120 (2013).
7. G. W. Dorn 2nd, J. D. Molkentin, *Circulation* **109**, 150–158 (2004).
8. S. A. Slavoff *et al.*, *Nat. Chem. Biol.* **9**, 59–64 (2013).
9. M. C. Frith *et al.*, *PLOS Genet.* **2**, e52 (2006).
10. B. R. Nelson, D. M. Anderson, E. N. Olson, *Circ. Res.* **114**, 18–20 (2014).
11. M. F. Lin, I. Jungreis, M. Kellis, *Bioinformatics* **27**, i275–i282 (2011).
12. C. Xie *et al.*, *Nucleic Acids Res.* **42** (D1), D98–D103 (2014).
13. E. L. Sonnhammer, G. von Heijne, A. Krogh, *Proc. Int. Conf. Intell. Syst. Mol. Biol.* **6**, 175–182 (1998).
14. A. Krogh, B. Larsson, G. von Heijne, E. L. Sonnhammer, *J. Mol. Biol.* **305**, 567–580 (2001).
15. M. Goujon *et al.*, *Nucleic Acids Res.* **38** (Web Server), W695–W699 (2010).
16. A. N. Guido, G. E. Campos, H. S. Neto, M. J. Marques, E. Minatel, *Anat. Rec. (Hoboken)* **293**, 1722–1728 (2010).
17. S. Schiaffino, C. Reggiani, *Physiol. Rev.* **91**, 1447–1531 (2011).
18. J. D. Molkentin *et al.*, *Cell* **93**, 215–228 (1998).
19. B. R. Nelson *et al.*, *Proc. Natl. Acad. Sci. U.S.A.* **110**, 11881–11886 (2013).
20. M. Asahi, Y. Kimura, K. Kurzydlowski, M. Tada, D. H. MacLennan, *J. Biol. Chem.* **274**, 32855–32862 (1999).
21. A. R. Tupling *et al.*, *Am. J. Physiol. Cell Physiol.* **301**, C841–C849 (2011).
22. B. A. Davis, A. Schwartz, F. J. Samaha, E. G. Kranias, *J. Biol. Chem.* **258**, 13587–13591 (1983).

ACKNOWLEDGMENTS

We thank C. Long for advice and expertise, N. Beetz for cDNA, J. Cabrera for graphics, S. Johnson for technical support, and the University of Texas Southwestern Medical Center Live Cell Imaging Core Facility under the direction of K. Luby-Phelps. This work was supported by grants from the NIH (HL-077439, HL-111665, HL-093039, DK-099653, U01-HL-100401, and AR-063182), Fondation Leducq Networks of Excellence, Cancer Prevention and Research Institute of Texas, and the Robert A. Welch Foundation (grant I-0025 to E.N.O.). B.R.N. was support by a National Institute of Arthritis and Musculoskeletal Diseases, NIH, Ruth L. Kirschstein National Research Service Award (NRSA) (F30AR067094).

SUPPLEMENTARY MATERIALS

www.sciencemag.org/content/351/6270/271/suppl/DC1
Materials and Methods
Figs. S1 to S17
Tables S1 to S4
References (*23*–*36*)

11 September 2015; accepted 23 November 2015
10.1126/science.aad4076

METABOLISM

AMP-activated protein kinase mediates mitochondrial fission in response to energy stress

Erin Quan Toyama,[1]* Sébastien Herzig,[1]* Julien Courchet,[2] Tommy L. Lewis Jr.,[2] Oliver C. Losón,[3] Kristina Hellberg,[1] Nathan P. Young,[1] Hsiuchen Chen,[3] Franck Polleux,[2] David C. Chan,[3] Reuben J. Shaw[1]†

Mitochondria undergo fragmentation in response to electron transport chain (ETC) poisons and mitochondrial DNA–linked disease mutations, yet how these stimuli mechanistically connect to the mitochondrial fission and fusion machinery is poorly understood. We found that the energy-sensing adenosine monophosphate (AMP)–activated protein kinase (AMPK) is genetically required for cells to undergo rapid mitochondrial fragmentation after treatment with ETC inhibitors. Moreover, direct pharmacological activation of AMPK was sufficient to rapidly promote mitochondrial fragmentation even in the absence of mitochondrial stress. A screen for substrates of AMPK identified mitochondrial fission factor (MFF), a mitochondrial outer-membrane receptor for DRP1, the cytoplasmic guanosine triphosphatase that catalyzes mitochondrial fission. Nonphosphorylatable and phosphomimetic alleles of the AMPK sites in MFF revealed that it is a key effector of AMPK-mediated mitochondrial fission.

Metabolic stresses that inflict damage to mitochondria trigger mitochondrial fragmentation, leading to degradation of defective mitochondria (mitophagy) or apoptosis in cases of severe damage (*1*). This response enables the consolidation of the still-intact functional elements of mitochondria, while allowing for physical segregation of dysfunctional mitochondrial components into depolarized daughter organelles that are targeted for mitophagy (*2*, *3*). Similarly, proper mitochondrial fission facilitates timely apoptosis (*4*–*7*). Mitochondrial fragmentation is also associated with mitochondrial dysfunction, such as in diseases associated with mitochondrial DNA (mtDNA) mutations (*8*). Conversely, mitochondrial fusion is thought to promote oxidative phosphorylation (*9*), to spare mitochondria from mitophagy (*10*, *11*), and to allow biodistribution of fatty acids for fuel utilization under nutrient-limited conditions to maintain metabolite pools and efficient adenosine triphosphate (ATP) production (*12*).

A central metabolic sensor activated by a wide variety of mitochondrial insults is the adenosine

[1]Molecular and Cell Biology Laboratory and Howard Hughes Medical Institute, Salk Institute for Biological Studies, La Jolla, CA 92037, USA. [2]Department of Neuroscience, Zuckerman Mind Brain Behavior Institute and Kavli Institute for Brain Science, Columbia University, New York, NY 10032, USA. [3]Division of Biology and Biological Engineering, California Institute of Technology, Pasadena, CA 91125, USA.
*These authors contributed equally to this work.
†Corresponding author. E-mail: shaw@salk.edu

monophosphate (AMP)–activated protein kinase (AMPK) (*13*). Under conditions when intracellular ATP concentrations decrease, increased intracellular AMP directly binds to the γ regulatory subunit of AMPK, facilitating AMPK activation by the upstream protein kinase LKB1. Upon activation, AMPK restores intracellular energy levels through direct phosphorylation of multiple downstream substrates that inhibit ATP-consuming biosynthetic pathways and stimulate catabolic ATP-regenerating processes. Because mitochondria supply the majority of cellular ATP, the maintenance of mitochondrial function is critical to maintaining overall energetic homeostasis (*14*), but the question of whether AMPK plays direct roles in different aspects of mitochondrial biology has not been well examined. AMPK has previously been tied to mitochondrial integrity through its direct phosphorylation and activation of the highly conserved autophagy kinase ULK1 (Atg1 in yeast) (*15*, *16*), which promotes mitophagy. In comparison, although mitochondrial fission and fusion rates are known to respond to changes in cellular metabolism, the molecular details of how changes in cellular bioenergetics and nutrients couple to the fission and fusion machinery remain poorly understood (*17*). For example, cells treated with mitochondrial inhibitors or bearing mtDNA-linked mutations undergo mitochondrial fragmentation, but much of the biochemical underpinning for these effects remains obscure. Inhibition of mitochondrial fusion due to aberrant processing of Optic atrophy 1 (OPA1, an inner mitochondrial membrane fusion GTPase) is a proposed mechanism (*17*–*21*), but it is thought to require a loss of mitochondrial membrane potential, which does not occur with many fragmentation-inducing stimuli.

We examined whether AMPK plays a part in the dynamic response of mitochondria to lowered ATP concentrations. To this end, we treated human U2OS osteosarcoma cells with the electron transport chain (ETC) complex I inhibitor rotenone or complex III inhibitor antimycin A for 1 hour and assessed their mitochondrial morphology. Confocal microscopy of endogenous TOM20 staining revealed extensive fragmentation of mitochondria caused by both inhibitors (Fig. 1A, top row). Time-lapse microscopy with MitoTracker dye to visualize live fusion and fission events revealed extensive mitochondrial fragmentation within 30 min after the addition of rotenone (Fig. 1B and movie S1). Treatment with either rotenone or antimycin A led to the rapid activation of AMPK and phosphorylation of its well-established downstream substrates acetyl coenzyme A carboxylase (ACC), Raptor, and ULK1 within 15 min (Fig. 1C).

We next used CRISPR/Cas9 to genetically disrupt the two catalytic subunits of AMPK (AMPKα1 and AMPKα2) in U2OS cells (AMPK double knockout, DKO) (fig. S1A). We demonstrated that both AMPK catalytic subunits must be genetically removed in U2OS cells to fully abolish AMPK signaling in this cell type (Fig. 1C and fig. S1B), similar to what is observed in other cell types (*22*). In AMPK DKO U2OS cells, the effect of rotenone or antimycin A on mitochondrial fragmentation was significantly attenuated (Fig. 1, A and D), as visualized by TOM20 staining at fixed time points (Fig. 1A) and by time-lapse microscopy (Fig. 1B and movie S2), despite comparable effects on oxygen consumption rates (fig. S1C). Lentivirus was used to stably reconstitute a wild-type AMPKα1 or AMPKα2 cDNA into the AMPK DKO U2OS cells to confirm that the loss of mitochondrial fragmentation was not an artifact of the chosen AMPK DKO clone. In cells treated with rotenone and antimycin A, either reconstituted AMPKα1 or AMPKα2 was sufficient to restore mitochondrial fragmentation and phosphorylation of downstream substrates, suggesting that either of the α subunits is capable of mediating these responses in U2OS cells (Fig. 1, A and D, and fig. S1D).

Some stimuli that acutely trigger mitochondrial fragmentation lead to proteolytic cleavage and inactivation of the OPA1 GTPase that mediates inner mitochondrial membrane fusion (*17*–*21*). We therefore compared the induction of AMPK activation with the induction of OPA1 proteolytic cleavage. Although the ETC uncoupler CCCP (carbonyl cyanide *m*-chlorophenyl hydrazone) promoted OPA1 processing, this effect was absent in cells treated with rotenone or antimycin A (fig. S1E), supporting reports that a loss of mitochondrial membrane potential is required for OPA1 cleavage (*17*–*20*). Immunoblotting of wild-type and AMPK DKO cells after CCCP treatment revealed that OPA1 cleavage was independent of AMPK status, reinforcing that these are two independent biochemical events. AMPK is activated by a loss of ATP due to ETC inhibition, whereas OPA1 cleavage is induced only after the more extensive mitochondrial damage that accompanies a loss of mitochondrial membrane potential.

We next examined whether direct pharmacological activation of AMPK in the absence of mitochondrial inhibitor treatment would be sufficient to induce mitochondrial fission. The small molecule A769662 and related compounds (MT63-78 and 991) were isolated from high throughput screens for AMPK activators (*23*–*25*). All of the A769662-related compounds are thought to bind in a cleft between the AMPK α and β subunits, in contrast to AMP-mimetic compounds such as AICAR (5-aminoimidazole-4-carboxamide ribonucleotide), which bind to nucleotide binding pockets in AMPKγ subunits to trigger activation of AMPK kinase complexes (*26*). Treatment of U2OS cells with A769662 for 1 hour resulted in mitochondrial fragmentation equivalent to that which occurred after rotenone or antimycin A treatment (compare Fig. 2, A to C, with Fig. 1, A, B, and D). This effect was almost fully ablated in the AMPK DKO U2OS cells (Fig. 2, A and B, and fig. S2A). Similarly, the cell-permeable AMP-mimetic AICAR increased the percentage of cells with short mitochondria, an effect ablated in the AMPK DKO U2OS cells (Fig. 2, A and B). The effects of these two mechanistically distinct direct AMPK activators on mitochondrial fragmentation were restored in the AMPK DKO U2OS cells that were stably reconstituted with either wild-type AMPKα1 or AMPKα2 cDNAs (Fig. 2, A and B), which also restored full downstream AMPK signaling (fig. S2B).

We also assessed AMPK induction of mitochondrial fragmentation in SV40-immortalized murine embryonic fibroblasts (MEFs) bearing floxed alleles of AMPKα1 (*Prkaa1*) and AMPKα2 (*Prkaa2*) that we derived de novo from embryonic day–13 mouse embryos to ensure equivalent starting mitochondrial populations. These cells were transduced with adenoviruses bearing either the Cre recombinase or the FlpO recombinase to obtain parallel treated cultures in which both AMPKα1 and AMPKα2 were deleted or that were exposed to a nontargeting control recombinase, respectively. Immunoblotting confirmed efficient deletion of AMPKα1 and AMPKα2 and a loss of downstream signaling only in the Cre-treated cells (fig. S2C). Mitochondrial networks in MEFs are shorter and less tubulated under basal conditions compared with those in U2OS cells, but treatment with rotenone further induced fragmentation of mitochondria in wild-type MEFs, which was largely ablated in the AMPK DKO MEFs (Fig. 2, D and E). Direct activation of AMPK with MT63-78 (a more potent A769662 derivative) (*25*) induced acute mitochondrial fragmentation in MEFs to an extent comparable to that with rotenone treatment, which was also attenuated in the AMPK DKO MEFs (Fig. 2, D and E). The observation that mechanistically distinct AMPK activators can consistently induce fragmentation to the same extent as ETC inhibitors, across cell types with morphometrically distinct mitochondrial networks, suggests that AMPK may directly regulate some component (s) of the mitochondrial fission and fusion machinery to mediate these events.

Previously, our laboratory has used proteomic and bioinformatics approaches to identify AMPK substrates (*15*, *27*–*29*). In one screen for AMPK substrates, we identified a protein named C2orf33, which subsequently was renamed mitochondrial fission factor (MFF). MFF is a mitochondrial outer-membrane protein that was discovered in an RNA interference screen aimed at identifying factors required for mitochondrial fission (*30*). Mitochondrial fission involves the recruitment of the GTPase dynamin-related protein 1 (DRP1) from the cytosol to the mitochondrial surface to catalyze the fission reaction. Genetic analysis has demonstrated that MFF is the dominant receptor for DRP1 in most mammalian cell types examined to date (*31*–*33*). MFF contains two predicted candidate AMPK phosphorylation sites, Ser^{155} and Ser^{172} in human MFF, which lie between the DRP1-interacting region at the amino terminus and the mitochondrial targeting transmembrane domain at the carboxyl terminus (Fig. 3A and fig. S3A). MFF was directly phosphorylated by recombinant AMPK, and, although mutation of Ser^{172} attenuated most of the in vitro phosphorylation, it was only fully ablated when Ser^{155} was also mutated (Fig. 3B). We used phosphomotif antibodies directed against the AMPK optimal substrate motif (*27*) or the optimal 14-3-3 binding

motif to determine whether they recognize MFF phosphorylated at Ser[155] or Ser[172] in vivo. FLAG-tagged variants of MFF cDNAs were stably introduced into wild-type MEFs, and treatment of the cells with AICAR increased MFF phosphorylation (Fig. 3C). A nonphosphorylatable Ser172Ala mutation abolished interaction with the antibody to the 14-3-3 binding motif, whereas a nonphosphorylatable Ser155Ala mutation abolished the interaction with the antibody to the AMPK substrate motif, and mutation of either site alone did not affect the AICAR-induced phosphorylation of the other site (Fig. 3C). Phosphorylation of either site was largely ablated in the AMPK DKO MEFs (Fig. 3D).

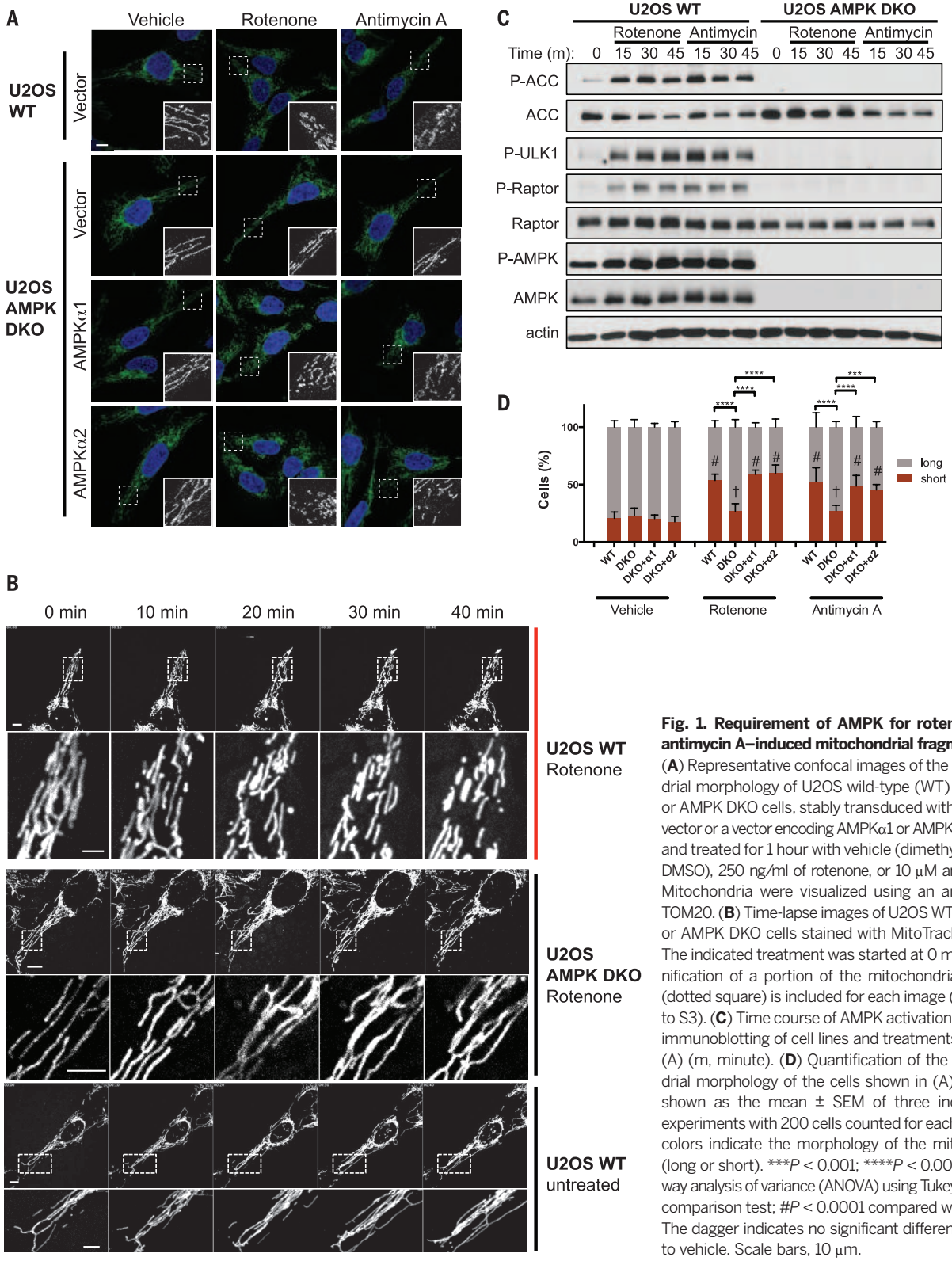

Fig. 1. Requirement of AMPK for rotenone- and antimycin A–induced mitochondrial fragmentation. (**A**) Representative confocal images of the mitochondrial morphology of U2OS wild-type (WT) (parental) or AMPK DKO cells, stably transduced with an empty vector or a vector encoding AMPKα1 or AMPKα2 cDNAs, and treated for 1 hour with vehicle (dimethyl sulfoxide, DMSO), 250 ng/ml of rotenone, or 10 μM antimycin A. Mitochondria were visualized using an antibody to TOM20. (**B**) Time-lapse images of U2OS WT (parental) or AMPK DKO cells stained with MitoTracker Green. The indicated treatment was started at 0 min. A magnification of a portion of the mitochondrial network (dotted square) is included for each image (movies S1 to S3). (**C**) Time course of AMPK activation by protein immunoblotting of cell lines and treatments shown in (A) (m, minute). (**D**) Quantification of the mitochondrial morphology of the cells shown in (A). Data are shown as the mean ± SEM of three independent experiments with 200 cells counted for each replicate; colors indicate the morphology of the mitochondria (long or short). ***$P < 0.001$; ****$P < 0.0001$ by two-way analysis of variance (ANOVA) using Tukey's multiple comparison test; #$P < 0.0001$ compared with vehicle. The dagger indicates no significant difference relative to vehicle. Scale bars, 10 μm.

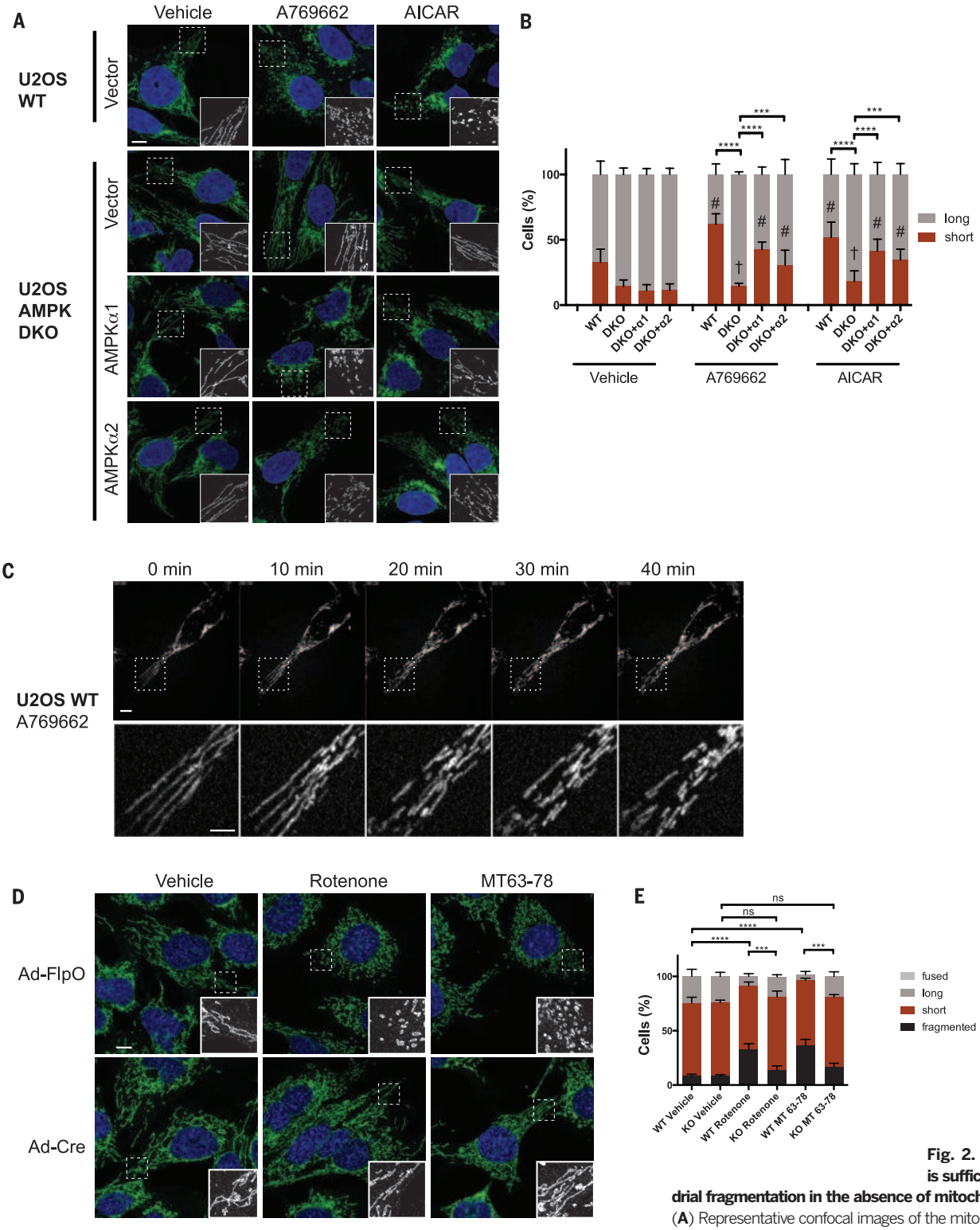

Fig. 2. AMPK activation is sufficient for mitochondrial fragmentation in the absence of mitochondrial inhibitors. (**A**) Representative confocal images of the mitochondrial morphology of WT (parental) or AMPK DKO U2OS cells, stably transduced with an empty vector or a vector encoding human AMPKα1 or AMPKα2 cDNAs, and treated for 1 hour with vehicle (DMSO), 300 μM A769662, or 2 mM AICAR. Mitochondria were visualized using an antibody to TOM20. (**B**) Quantification of the mitochondrial morphology of cells shown in (A). (**C**) Time-lapse images of WT (parental) U2OS cells stained with MitoTracker Green and treated with 300 μM A769662 at 0 min. A magnification of a portion of the mitochondrial network (dotted square) is included for each image (bottom panel; movie S4). (**D**) Representative confocal images of the mitochondrial morphology of AMPKα1$^{fl/fl}$α2$^{fl/fl}$ (fl, floxed) MEFs transduced with FlpO (control)– or Cre-encoding adenoviruses (Ad) and treated for 1 hour with vehicle (DMSO), 100 ng/ml of rotenone, or 50 μM MT63-78. Mitochondria were visualized using an antibody to TOM20. (**E**) Quantification of the mitochondrial morphology of cells shown in (D). Data in (B) and (E) are shown as the mean ± SEM of three independent experiments with 200 cells counted for each replicate and statistically analyzed as in Fig. 1 (ns, not significant). Scale bars, 10 μm.

To examine endogenous MFF phosphorylation, we developed a phosphospecific antibody to phospho-Ser^{172} (P-Ser^{172}), which we validated for phosphospecificity and induction in cells either expressing an activated allele of AMPK or treated with metabolic stress (fig. S3, B and C). Multiple alternatively splice isoforms of MFF have been documented, and one of the differentially spliced exon boundaries in MFF occurs just after Ser^{172} (fig. S3D) (*34*). However, direct examination of transiently expressed cDNAs of MFF splice isoforms revealed that the antibody to P-Ser^{172} recognized the cognate site in an AMPK-dependent manner in three of four isoforms tested (fig. S3D). To next ascertain whether the antibody to P-Ser^{172} recognized endogenous MFF, we used MEFs genetically lacking MFF (fig. S4A). AICAR treatment induced reactivity of endogenous MFF with the antibody to MFF P-Ser^{172} in wild-type but not in the *Mff*-null MEFs (fig. S4B). Next, we immunoblotted parallel lysates from AMPK wild-type and genetically matched DKO MEFs treated with rotenone or MT63-78, in which AMPK was critical for mitochondrial shortening (Fig. 2, D and E). This revealed that endogenous MFF P-Ser^{172} was increased in wild-type but not AMPK DKO MEFs after receiving these stimuli (fig. S4C). In time-course experiments, MFF P-Ser^{172} was fully induced within 15 min of treatment of wild-type MEFs with rotenone, paralleling the timing of

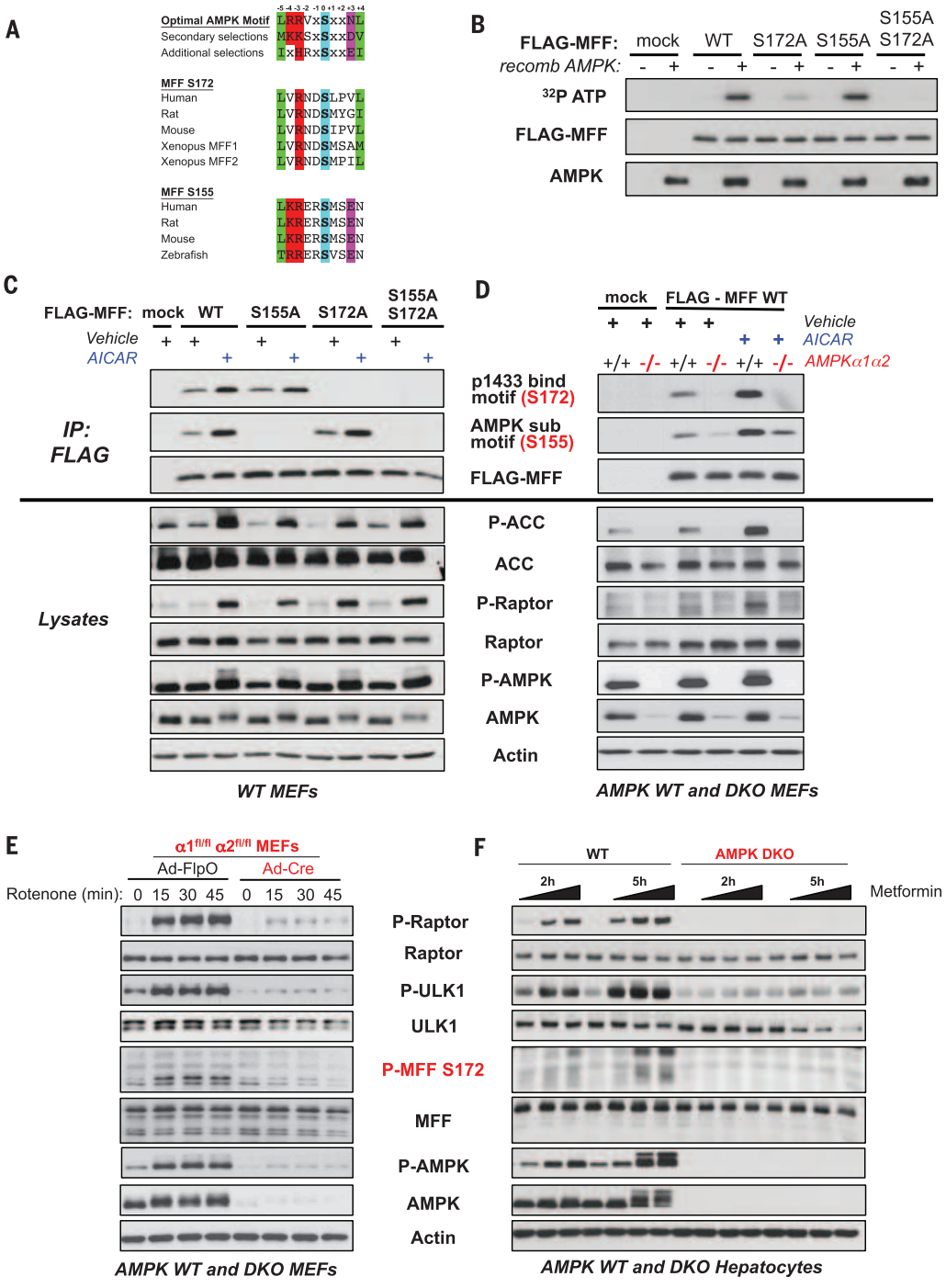

Fig. 3. MFF is a conserved substrate of AMPK. (**A**) ClustalW alignment of two conserved sites on MFF that match the AMPK optimal substrate motif. Ser^{172} (S172) matches the well-defined AMPK motif found in most substrates (*27*, *39*), and Ser^{155} (S155) contains additional selections including +4N that also have been previously described (*39*). (**B**) Incorporation of γ-^{32}P-ATP into MFF in vitro. Human embryonic kidney–293 T cells transfected with empty vector (mock), WT MFF, or the indicated MFF mutants were lysed, and the FLAG immunoprecipitates were combined with recombinant (recomb) active AMPK where indicated and γ-^{32}P-ATP in an in vitro kinase reaction. Proteins were resolved on a SDS–polyacrylamide gel electrophoresis gel, and parallel nonradioactive kinase assays were immunoblotted as indicated. (**C**) Phosphorylation of MFF mutants. WT MEFs stably expressing a control vector (mock), WT MFF, or the indicated MFF mutants were treated with vehicle or 2 mM AICAR for 1 hour. FLAG immunoprecipitates and lysates were immunoblotted with the indicated antibodies and phosphomotif antibodies that recognize phosphorylated Ser^{172} or Ser^{155}. (**D**) Phosphorylation in WT ($^{+/+}$) or AMPK DKO ($^{-/-}$) MEFs stably expressing a control vector (mock) or WT MFF. Cells were treated with vehicle or 2 mM AICAR for 1 hour and processed as in (C). (**E**) Protein immunoblot showing the time course of AMPK activation in WT and AMPK DKO MEFs, as generated in Fig. 2D, after treatment with 250 ng/ml of rotenone for the indicated times. Phosphorylation of endogenous MFF was detected by the antibody to MFF P-Ser^{172}. (**F**) Protein immunoblot of primary hepatocytes prepared from WT or AMPK DKO livers and treated with increasing concentrations of metformin (0, 0.5, 1.0, and 2.0 mM), showing phosphorylation of endogenous MFF as detected by the antibody to MFF P-Ser^{172}.

mitochondrial fragmentation and phosphorylation of other AMPK substrates (Fig. 3E). Mitochondrial morphology is altered in hepatocytes upon genetic deletion of AMPK (*15*); we therefore also examined MFF in this cell type. AICAR treatment of primary hepatocytes induced phosphorylation of endogenous MFF Ser^{172} and other AMPK substrates (fig. S4D). Another mitochondrial inhibitor that activates AMPK is metformin, the most-widely prescribed type 2 diabetes drug in the United States and worldwide (*2*). Metformin treatment of hepatocytes resulted in

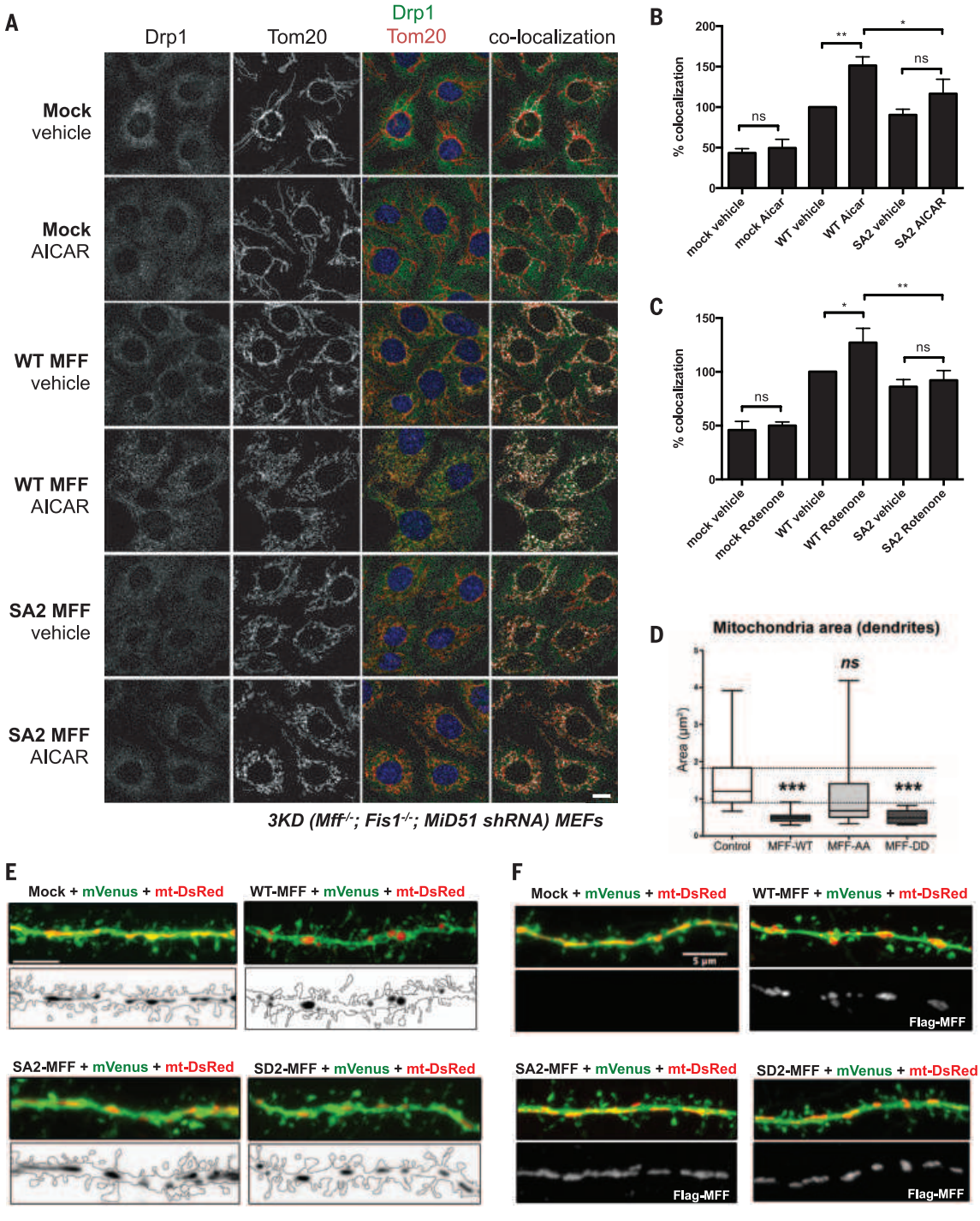

Fig. 4. MFF Ser^{155} and Ser^{172} are required for recruitment of DRP1 to mitochondria after AMPK activation. (**A**) Representative images of 3KD MEFs stably transduced with a control vector (mock), WT MFF, or the SA2 MFF mutant, treated for 1 hour with vehicle (DMSO) or 2 mM AICAR and fixed and visualized with antibodies to endogenous TOM20 and DRP1. The merge of both channels as well as the result of the colocalization highlighter plugin (ImageJ) are shown. Scale bar, 10 µm. (**B**) Quantification of mitochondrial DRP1 in samples shown in (A) (details are included in the supplementary materials). Data are shown as the mean ± SEM of four independent experiments, each with at least five images representing >40 cells per condition. *P < 0.05; **P < 0.01 by one-way ANOVA. (**C**) Quantification of mitochondrial DRP1 after treatment with 250 ng/ml of rotenone for 1 hour, as in panels (A) and (B). (**D**) Quantification of the in vivo dendritic mitochondrial area upon overexpression of mVenus, mt-DsRED, and the indicated construct (AA, SA2; DD, SD2). Data are shown as 0 to 100% whisker box plots with the 25th, 50th, and 75th percentiles as the lower, middle, and upper boundaries of the box, respectively. Data were analyzed using a nonparametric Kruskal-Wallis ANOVA with Dunn's multiple comparisons ($n_{Control}$ = 19 neurons, $n_{MFF\text{-}WT}$ = 19 neurons, $n_{MFF\text{-}AA}$ = 27 neurons, and $n_{MFF\text{-}DD}$ = 26 neurons from four distinct animals per genotype). ***P < 0.001. (**E**) Maximum projection images of layer 2/3 postnatal day–30 apical dendrite branches, demonstrating mitochondrial morphology upon expression of the labeled constructs via in utero electroporation at embryonic day 15.5. The upper panel in each section is the merge of mVenus and mt-DsRED; the lower panel shows the outline of the cell and mt-DsRED. (**F**) Maximum projection images of 21-day in vitro apical dendrite collaterals from cortical neurons electroporated with the indicated constructs via ex utero electroporation at embryonic day 15.5. The upper panel in each section is the merge of mVenus and mt-DsRED; the lower panel shows MFF expression via staining by the antibody to FLAG. Scale bars, 5 µm.

phosphorylation of endogenous MFF Ser^{172} in a dose- and time-dependent manner, paralleling AMPK phosphorylation of Raptor and ULK1—effects which were abolished in AMPK DKO hepatocytes (Fig. 3F).

To test the effects of AMPK phosphorylation on MFF function, we first used MEFs that we have previously reported as lacking most functional DRP1 receptors [*Mff*$^{-/-}$, *Fis1*$^{-/-}$, and *Mid51* short hairpin–mediated RNA interference (shRNA), referred to as 3KD MEFs] (fig. S5A) (*31*). Mitochondrial shortening that was induced by AICAR in wild-type cells was abolished in the 3KD cells (fig. S5B). Reconstitution of the 3KD cells with wild-type MFF cDNA demonstrated that MFF expression alone was sufficient to restore mitochondrial fragmentation in response to AICAR (fig. S5C). Subsequent analysis of MEFs that were genetically disrupted only for MFF (*Mff*$^{-/-}$) revealed they were also completely defective for AICAR-induced fragmentation (fig. S5D).

As the major receptor for DRP1, MFF is required for steady-state localization of DRP1 to the mitochondria (*31*, *33*). Reconstitution of the 3KD MEFs with a wild-type MFF cDNA revealed a much greater colocalization of endogenous DRP1 to the mitochondria when MFF expression was restored, as compared with the control vector (Fig. 4, A and B). Treatment of cells with AICAR further increased colocalization of endogenous DRP1 with TOM20 in 3KD MEFs reconstituted with wild-type MFF, but this treatment failed to do so in the luciferase control 3KD MEFs (Fig. 4, A and B). This increase in DRP1 and TOM20 colocalization was attenuated in the cells stably expressing nonphosphorylatable Ser155Ala-Ser172Ala (SA2) mutant MFF, though amounts of MFF and DRP1 were comparable across these stable cell lines (fig. S5E). Similar effects on DRP1 and TOM20 colocalization were observed in response to rotenone treatment in cells bearing wild-type versus SA2 MFF (Fig. 4C and fig. S5F). These data indicate that basal DRP1 localization to mitochondria is largely normal in the SA2 cells but that AICAR and rotenone induce acute recruitment of DRP1 to the mitochondria, and this effect is abolished when AMPK cannot phosphorylate Ser^{155} and Ser^{172} in MFF. To model the effects of AMPK phosphorylation, we created phosphomimetic Ser155Asp-Ser172Asp (SD2) and Ser155Glu-Ser172Glu (SE2) mutants. Despite being expressed at equal levels to wild-type MFF protein (fig. S6A), both the SD2 and SE2 MFF mutants displayed gain-of-function activity when introduced into 3KD or *Mff*$^{-/-}$ MEFs, resulting in shortened mitochondria even in the absence of stimuli, comparable to those induced by AICAR in cells expressing wild-type MFF (fig. S6, B to E). Moreover, neither AICAR nor MT63-78 treatment further shortened the mitochondria in SD2- and SE2-expressing cells (fig. S6, C to E). Fragmented mitochondria are correlated with increased production of reactive oxygen species (*35*). Consistent with this, among all the 3KD cell lines, SD2- and SE2-MFF expressing cells exhibited the greatest accumulation of reactive oxygen species after rotenone treatment (fig. S6F).

To examine the function of the AMPK-dependent phosphorylation of MFF in vivo, in a cell type in which the AMPK pathway plays critical roles and in which mitochondrial homeostasis is paramount (*36*, *37*), we expressed wild-type, SA2, or SD2 MFF cDNAs in layer 2/3 cortical pyramidal neurons using in utero cortical electroporation (*36*). Co-electroporation of cDNAs encoding myristoylated (m)Venus and mt-DsRed enabled quantitative imaging of mitochondrial morphology in dendritic segments of single neurons 3 weeks after birth (fig. S7, A and B). In control neurons, mitochondria morphology in the dendrites of pyramidal neurons is elongated (Fig. 4D). In contrast, enforced equivalent expression of wild-type or SD2 but not SA2 MFF resulted in fragmented mitochondria in the dendrites (Fig. 4, D and E). All three forms of MFF (wild-type, SA2, and SD2) were targeted to mitochondria and expressed at similar levels (Fig. 4F and fig. S7C). These results indicate that MFF is sufficient to induce fragmentation of neuronal mitochondria in vivo and that this effect requires phosphorylation of Ser$^{155/172}$.

AMPK is rapidly activated by mitochondrial stress and acutely triggers mitochondrial fission, at least in part via phosphorylation of MFF. This rapid AMPK-dependent induction of mitochondrial fission may serve as one way for the cell to prepare to initiate mitophagy of those mitochondrial fragments that have extensive damage (*38*). Though AMPK is a highly conserved sensor of mitochondrial damage across eukaryotes, MFF is one of the first AMPK substrates to have been discovered to directly control mitochondrial biology. AMPK is also known to induce mitochondrial biogenesis in various tissues (*13*), and AMPK directly phosphorylates and activates the first component of the autophagy cascade, the kinase ULK1 (*15*). Thus, AMPK emerges as a master regulator of mitochondrial homeostasis, coupling fission to mitophagy and, after prolonged energy stress, signaling the nucleus to initiate biogenesis of new mitochondria to replace the damaged ones.

REFERENCES AND NOTES

1. P. Mishra, D. C. Chan, *Nat. Rev. Mol. Cell Biol.* **15**, 634–646 (2014).
2. G. Benard *et al.*, *J. Cell Sci.* **120**, 838–848 (2007).
3. G. Twig *et al.*, *EMBO J.* **27**, 433–446 (2008).
4. S. Montessuit *et al.*, *Cell* **142**, 889–901 (2010).
5. M. Karbowski *et al.*, *J. Cell Biol.* **159**, 931–938 (2002).
6. R. J. Youle, M. Karbowski, *Nat. Rev. Mol. Cell Biol.* **6**, 657–663 (2005).
7. D. R. Green, L. Galluzzi, G. Kroemer, *Science* **345**, 1250256 (2014).
8. J. Q. Kwong, M. S. Henning, A. A. Starkov, G. Manfredi, *J. Cell Biol.* **179**, 1163–1177 (2007).
9. M. Liesa, O. S. Shirihai, *Cell Metab.* **17**, 491–506 (2013).
10. L. C. Gomes, G. Di Benedetto, L. Scorrano, *Nat. Cell Biol.* **13**, 589–598 (2011).
11. A. S. Rambold, B. Kostelecky, N. Elia, J. Lippincott-Schwartz, *Proc. Natl. Acad. Sci. U.S.A.* **108**, 10190–10195 (2011).
12. A. S. Rambold, S. Cohen, J. Lippincott-Schwartz, *Dev. Cell* **32**, 678–692 (2015).
13. B. B. Kahn, T. Alquier, D. Carling, D. G. Hardie, *Cell Metab.* **1**, 15–25 (2005).
14. M. M. Mihaylova, R. J. Shaw, *Nat. Cell Biol.* **13**, 1016–1023 (2011).
15. D. F. Egan *et al.*, *Science* **331**, 456–461 (2011).
16. J. Kim, M. Kundu, B. Viollet, K. L. Guan, *Nat. Cell Biol.* **13**, 132–141 (2011).
17. P. Mishra, V. Carelli, G. Manfredi, D. C. Chan, *Cell Metab.* **19**, 630–641 (2014).
18. S. Ehses *et al.*, *J. Cell Biol.* **187**, 1023–1036 (2009).
19. N. Ishihara, Y. Fujita, T. Oka, K. Mihara, *EMBO J.* **25**, 2966–2977 (2006).
20. B. Head, L. Griparic, M. Amiri, S. Gandre-Babbe, A. M. van der Bliek, *J. Cell Biol.* **187**, 959–966 (2009).
21. S. Duvezin-Caubet *et al.*, *J. Biol. Chem.* **281**, 37972–37979 (2006).
22. K. R. Laderoute *et al.*, *Mol. Cell. Biol.* **26**, 5336–5347 (2006).
23. B. Cool *et al.*, *Cell Metab.* **3**, 403–416 (2006).
24. B. Xiao *et al.*, *Nat. Commun.* **4**, 3017 (2013).
25. G. Zadra *et al.*, *EMBO Mol. Med.* **6**, 519–538 (2014).
26. M. F. Calabrese *et al.*, *Structure* **22**, 1161–1172 (2014).
27. D. M. Gwinn *et al.*, *Mol. Cell* **30**, 214–226 (2008).
28. M. M. Mihaylova *et al.*, *Cell* **145**, 607–621 (2011).
29. Y. Li *et al.*, *Cell Metab.* **13**, 376–388 (2011).
30. S. Gandre-Babbe, A. M. van der Bliek, *Mol. Biol. Cell* **19**, 2402–2412 (2008).
31. O. C. Losón, Z. Song, H. Chen, D. C. Chan, *Mol. Biol. Cell* **24**, 659–667 (2013).
32. Q. Shen *et al.*, *Mol. Biol. Cell* **25**, 145–159 (2014).
33. H. Otera *et al.*, *J. Cell Biol.* **191**, 1141–1158 (2010).
34. S. Ducommun *et al.*, *Cell. Signal.* **27**, 978–988 (2015).
35. X. Qi, N. Qvit, Y. C. Su, D. Mochly-Rosen, *J. Cell Sci.* **126**, 789–802 (2013).
36. J. Courchet *et al.*, *Cell* **153**, 1510–1525 (2013).
37. G. Mairet-Coello *et al.*, *Neuron* **78**, 94–108 (2013).
38. R. J. Youle, A. M. van der Bliek, *Science* **337**, 1062–1065 (2012).
39. J. W. Scott, D. G. Norman, S. A. Hawley, L. Kontogiannis, D. G. Hardie, *J. Mol. Biol.* **317**, 309–323 (2002).

ACKNOWLEDGMENTS

This research was supported by NIH grants R01DK080425, R01CA172229, and P01 CA120964 to R.J.S; R01GM062967 and R01GM110039 to D.C.C; R01NS089456 to F.P.; and K99NS091526 to T.L.L. Work in the laboratory of R.J.S. was also supported in part by the Leona M. and Harry B. Helmsley Charitable Trust (grant 2012-PG-MED002). E.Q.T. and N.P.Y. were supported by American Cancer Society fellowships (122123-PF-12-029-01-TBE and 123016-PF-PF-12-191-01-TBE, respectively). S.H. was supported by a European Molecular Biology Organization (EMBO) Long Term Fellowship (ALTF 1101-2013). K.H. was funded by a George E. Hewitt Foundation for Medical Research fellowship. O.C.L. was supported by an American Physiological Society William Townsend Porter predoctoral fellowship. R.J.S. is the William R. Brody Chair at the Salk Institute and a Howard Hughes Medical Institute Early Career Scientist. We thank A. Singh and G. Kasof at Cell Signaling Technology for developing the antibody to MFF P-Ser^{172} in conjunction with E.Q.T. and R.J.S. We thank the Waitt Biophotonics Core and Flow Cytometry Core at the Salk Institute for use of their instruments, which are supported by the Salk Institute (grant CCSG P30 CA014195). We thank C. Merkwirth and M. Adams for helpful discussions and M. Chun for critical reading of the manuscript.

SUPPLEMENTARY MATERIALS

www.sciencemag.org/content/351/6270/275/suppl/DC1
Materials and Methods
Supplementary Text
Figs. S1 to S7
Reference (*40*)
Movies S1 to S5

28 April 2015; accepted 9 December 2015
10.1126/science.aab4138

RNA BIOCHEMISTRY

Transcriptome-wide distribution and function of RNA hydroxymethylcytosine

Benjamin Delatte,[1]*† Fei Wang,[2]* Long Vo Ngoc,[3]*‡ Evelyne Collignon,[1] Elise Bonvin,[1] Rachel Deplus,[1] Emilie Calonne,[1] Bouchra Hassabi,[1] Pascale Putmans,[1] Stephan Awe,[4] Collin Wetzel,[5]§ Judith Kreher,[4]‖ Romuald Soin,[3] Catherine Creppe,[1] Patrick A. Limbach,[5] Cyril Gueydan,[3] Véronique Kruys,[3] Alexander Brehm,[4] Svetlana Minakhina,[2]¶ Matthieu Defrance,[1] Ruth Steward,[2] François Fuks[1]#

Hydroxymethylcytosine, well described in DNA, occurs also in RNA. Here, we show that hydroxymethylcytosine preferentially marks polyadenylated RNAs and is deposited by Tet in *Drosophila*. We map the transcriptome-wide hydroxymethylation landscape, revealing hydroxymethylcytosine in the transcripts of many genes, notably in coding sequences, and identify consensus sites for hydroxymethylation. We found that RNA hydroxymethylation can favor mRNA translation. Tet and hydroxymethylated RNA are found to be most abundant in the *Drosophila* brain, and Tet-deficient fruitflies suffer impaired brain development, accompanied by decreased RNA hydroxymethylation. This study highlights the distribution, localization, and function of cytosine hydroxymethylation and identifies central roles for this modification in *Drosophila*.

In DNA, vertebrate Tet methyldioxygenases (Tet1, Tet2, and Tet3) catalyze hydroxylation of 5-methylcytosine to 5-hydroxymethylcytosine (*1*–*3*). Tet also catalyzes the formation of hydroxymethylcytosine in RNA (referred to here as hmrC) (*4*, *5*). To date, however, the distribution, localization, and functional relevance of hmrC remain unknown.

In the present study, we have sought to provide a better understanding of hmrC. For ease of interpreting results, we analyzed hmrC in *Drosophila melanogaster* because (i) cytosine methylation in *Drosophila* DNA is either absent or very low, being restricted to specific cellular contexts (*6*, *7*), and (ii) we have found no evidence of DNA hydroxymethylation in this organism (fig. S1). To detect 5hmC RNA modification, we used an antibody raised against 5-hydroxymethylcytosine (*8*, *9*). To confirm that it will bind to hmrC, we performed dot blot experiments using in vitro transcribed templates containing either unmethylated, methylated, or hydroxymethylated cytosines (table S1). The antibody to 5hmC specifically detected 5hmC-containing RNA. In addition, detection of 5hmC was abolished after ribonuclease (RNase) A treatment (fig. S2A).

We detected hmrC in dot blot experiments on total RNA extracted from *Drosophila* S2 cells (Fig. 1A and fig. S2, B and C). Isolation of polyadenylated RNA from S2 cells followed by immunoblotting showed strong enrichment in hmrC signal as compared with that of total cellular RNA (Fig. 1B and fig. S2, D and E). No signal was detected in fractions enriched in small RNAs or ribosomal RNAs (Fig. 1C and fig. S3, A and B). *Drosophila* possesses only one conserved Tet ortholog, *CG43444* (dTet) (*10*, *11*). Depletion of dTet in S2 cells, by using RNA interference for dTet (dTet KD), revealed a 54% decrease in *dTet* transcripts, as compared with control cells (Fig. 1D). Dot blotting with antibody to 5hmC showed a similar decrease in hmrC—44%—upon dTet knockdown (Fig. 1D and fig. S3, C and D).

To map the hmrC modification landscape in a transcriptome-wide manner, we adapted a recently used method [methylated RNA immunoprecipitation followed by sequencing (MeRIP-seq)] (*12*, *13*), which we call hMeRIP-seq. This method involves immunoprecipitation of hmrC-containing RNA with the antibody to 5hmC followed by next-generation sequencing. hMeRIP-seq in S2 cells yielded 3058 significantly enriched regions ("hmrC peaks," $P < 10^{-10}$) within 1597 coding gene transcripts (fig. S4, A to C, and table S2). Examples of enrichment profiles are shown in Fig. 2A. Several key controls were performed so as to ensure the validity and stringency of our experimental approach: (i) Further bioinformatic analyses demonstrated that our hMeRIP-seq experiments did not merely coprecipitate abundant RNA fragments

[1]Laboratory of Cancer Epigenetics, Faculty of Medicine, ULB Cancer Research Center (U-CRC), Université Libre de Bruxelles (ULB), Brussels, Belgium. [2]Waksman Institute, Department of Molecular Biology and Biochemistry, Cancer Institute of New Jersey, Rutgers University, Piscataway, NJ, USA. [3]Laboratory of Molecular Biology of the Gene, Faculty of Sciences, Université Libre de Bruxelles, Gosselies, Belgium. [4]Institut für Molekularbiologie und Tumorforschung, Philipps-Universität Marburg, Marburg, Germany. [5]Department of Chemistry, University of Cincinnati, Cincinnati, OH, USA.
*These authors contributed equally to this work. †Present address: Division of Signaling and Gene Expression, La Jolla Institute for Allergy and Immunology, La Jolla, CA 92037, USA. ‡Present address: Section of Molecular Biology, University of California, San Diego, La Jolla, CA 92093, USA. §Present address: Department of Cancer Biology, University of Cincinnati, Cincinnati, OH, USA. ‖Present address: Roche Diagnostics, 68305 Mannheim, Germany. ¶Present address: Robert Wood Johnson Medical School, Department of Medicine, Rutgers University, Piscataway, NJ, USA.
#Corresponding author. E-mail: ffuks@ulb.ac.be

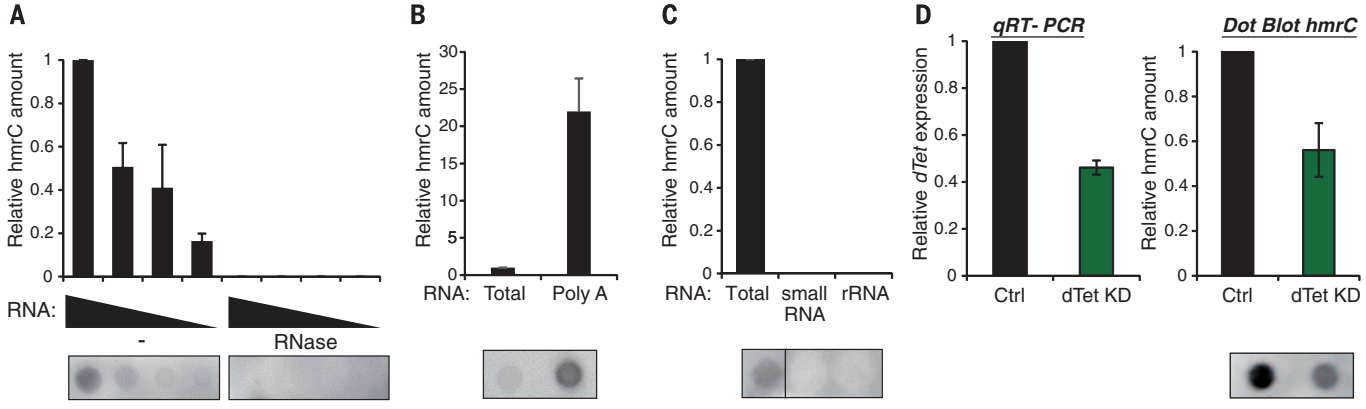

Fig. 1. RNA hydroxymethylation by dTet in *Drosophila* S2 cells. (**A**) Dot blotting on total RNA from *Drosophila* S2 cells with antibody to 5hmC, treated or not with RNase A (serially halved amounts of RNA, starting at 1 μg). Data are mean ± SD (n = 4 experiments run) with a representative blot shown. (**B**) Immunoblotting with anti-5hmC antibody was performed on polyadenylated and total RNA from S2 cells. Data are mean ± SD (n = 3 experiments run). (**C**) hmrC content of total RNA as well as fractions enriched in small RNA or rRNA was assessed by dot blotting. Data are mean ± SD (n = 3 experiments run). A vertical line indicates juxtaposition of lanes within the same blot, exposed for the same time. (**D**) dTet knockdown leads to reduced hmrC levels. (Left) Quantitative RT-PCR analysis. (Right) Dot blotting. Data are mean ± SD (n = 4 experiments run).

nonspecifically (Fig. 2B and fig. S5); (ii) up to 79.4% of hmrC sites showed significant reduction levels in hMeRIP-seq upon dTet depletion as compared with that of control S2 cells, with 85.5% of the sites showing a more than fourfold reduction in hmrC levels (Fig. 2C and fig. S6); and (iii) replicate hMeRIP-seq experiments by using an additional antibody to 5hmC showed strong agreement between experiments performed with the two 5hmC antibodies (fig. S7 and table S3).

The distribution of hmrC peaks revealed by hMeRIP-seq analyses was significantly nonrandom

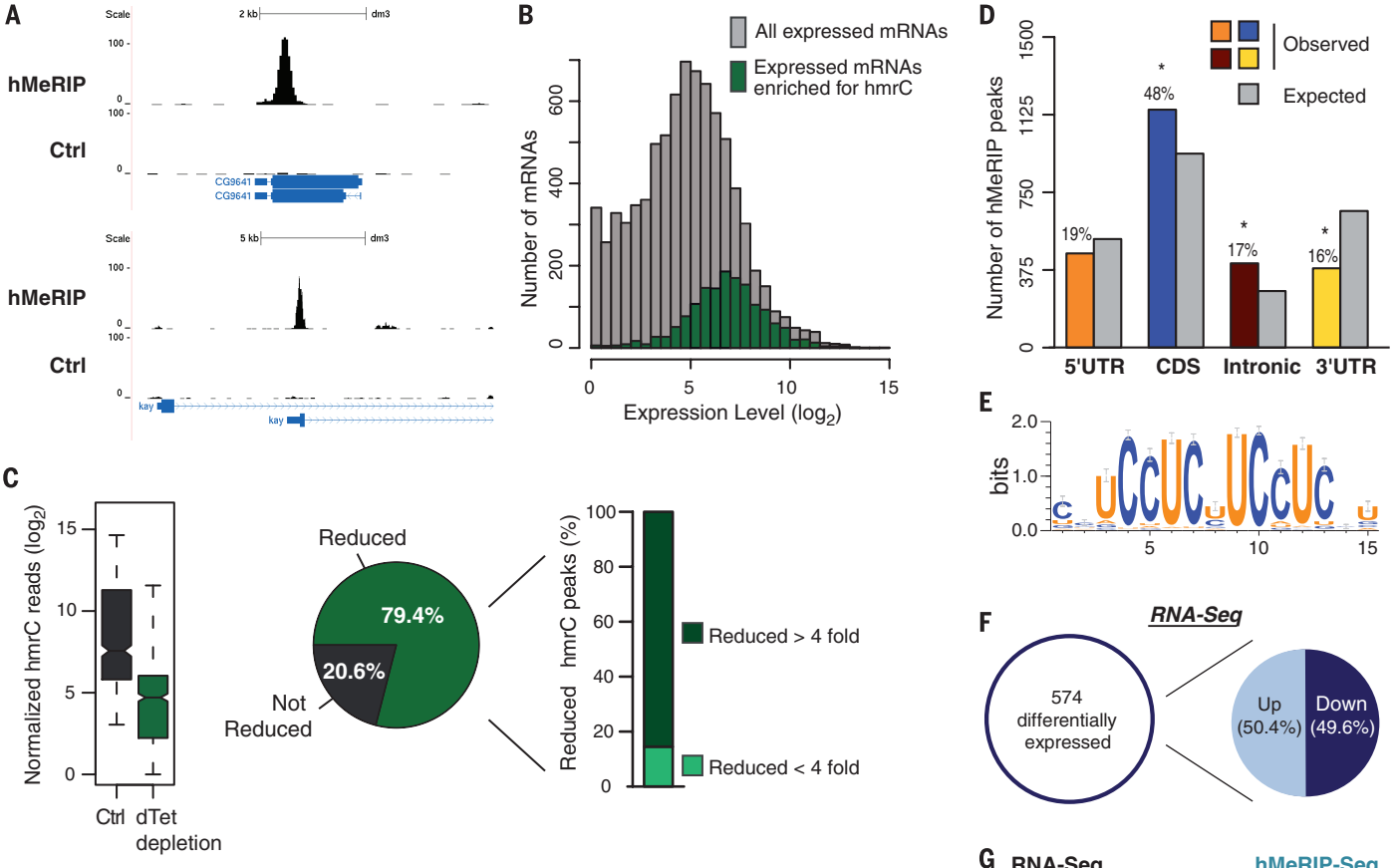

Fig. 2. Transcriptome-wide distribution of hmrC in *Drosophila* cells. (**A**) Representative UCSC Genome Browser plot from hMeRIP-seq data. (**B**) Distribution of all expressed (gray) or hmrC-enriched (green) transcripts, showing the number of mRNAs as a function of their expression levels. In hMeRIP-seq, enrichment in both abundant and less abundant fragments was observed. (**C**) hMeRIP-seq in cells depleted of dTet shows reduced hmrC levels at the majority of target regions. (Left) Box plot of the normalized number of hmrC reads in dTet-depleted cells versus control cells. (Center) Pie chart showing the percentage of reduced hmrC peaks, with (right) a more than fourfold reduction at most targets. (**D**) Distribution of hmrC peaks according to the type of structural element within the transcript. *$P < 10^{-5}$). (**E**) Sequence motif identified within hmrC peaks. (**F**) RNA-seq performed on dTet-knockdown and control S2 cells. (**G**) Partial overlap between hMeRIP-seq and RNA-seq data sets.

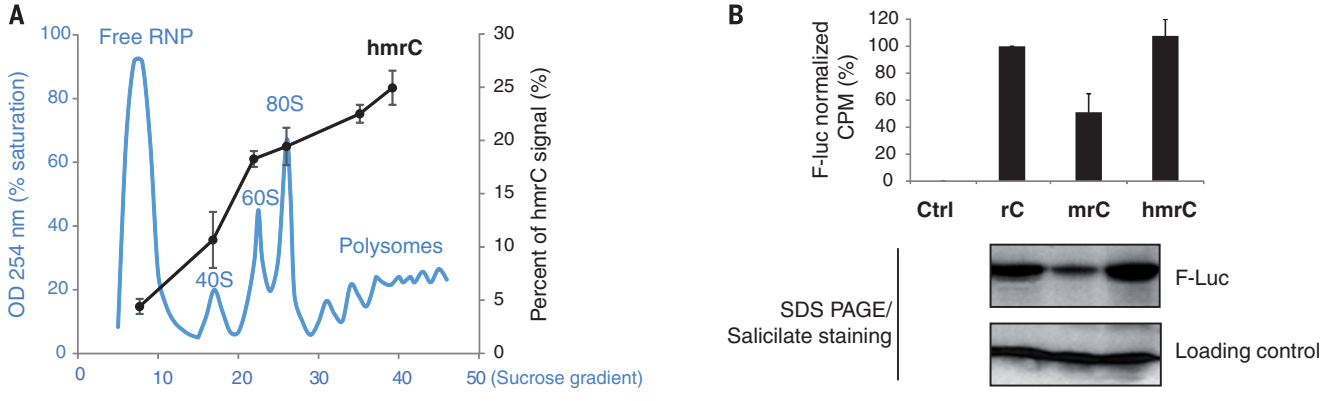

Fig. 3. RNA hydroxymethylation can favor mRNA translation. (**A**) Sucrose gradient fractionation followed by dot-blot quantification shows that active translation is associated with a high hmrC content. Data are mean ± SD (n = 3 experiments run). (**B**) In vitro translation of C-, mC-, and hmC-containing RNAs, as measured by incorporation of ^{35}S-radiolabeled methionine, shows that methylation decreases translation and hydroxymethylation restores it. Shown are the normalized scintillation counts (top) and the results of SDS–polyacrylamide gel electrophoresis (SDS-PAGE) followed by fluorography (bottom). Data are mean ± SD (n = 3 experiments run).

($P < 10^{-5}$), with many of these peaks found in coding sequences (48%) (Fig. 2D). Further analyses identified an overrepresented motif with occurrences in a large proportion of peaks (64%) and which tends to be highly UC-rich, containing UCCUC repeats (Fig. 2E and fig. S8A). Gene Ontology analysis of the hmrC targets showed enrichment for genes involved in basic cellular processes and notably in the regulation of embryogenesis and development (fig. S8B and table S6). In addition, exons were more enriched in hmrC than introns (fig. S9D). Thus, the above data present the hmrC-enriched transcriptome, revealing the presence of this modification in specific mRNA regions and in specific sequence contexts.

Next, we knocked down *dTet* expression in S2 cells and performed RNA-sequencing (RNA-seq) experiments in order to assess how many mRNAs might be regulated by dTet. We found the expression of 574 mRNAs to change after dTet depletion (50.4% were more abundant, whereas 49.6% were less abundant) (Fig. 2F; fig. S9, A to C; and table S4). Examples of mRNAs whose levels either increased or decreased upon dTet knockdown are shown in fig. S9, A and B. A positive correlation was observed between transcript abundance and the presence of hmrC peaks (Fig. 2B and fig. S5). We then compared these dTet-regulated mRNAs with the targets identified by hMeRIP-seq and found a slight but significant percentage (26%, $P < 10^{-43}$) of the dTet-regulated mRNAs to contain at least one hmrC peak (Fig. 2G, figs. S9C and S11, and table S5). It is worth mentioning that dTet contains an N-terminal CXXC Zn-finger domain, which likely explains the reported ability of mammalian Tets to regulate gene expression independently of their catalytic activity (*14*, *15*). It thus remains possible that dTet might affect gene expression via its CXXC domain, independently of its ability to hydroxylate methylated RNA (fig. S10, A and B). This domain, however, is likely not required for the role of dTet in *Drosophila* brain development (see below) because flies where dTet CXXC is deleted are still viable and show no specific phenotype (*11*).

To examine how cytosine hydroxymethylation might affect mRNA function, we examined the distribution of hmrC as a function of the mRNA translational status in *Drosophila* S2 cells. For this, we performed standard sucrose-gradient fractionation followed by dot blotting. A correlation between hmrC abundance and active mRNA translation was observed; fractions with low translation activity (free mRNAs and monosomes) were found to be poor in hmrC, whereas mRNAs heavily loaded with ribosomes (polysome fractions) showed a high hmrC content (Fig. 3A). We also assessed how mrC distributes across polysome fractions and found it to be high in monosomes and low in polysomes (fig. S12). Next, we examined whether mRNA hydroxymethylation might affect mRNA translation. In vitro translation of

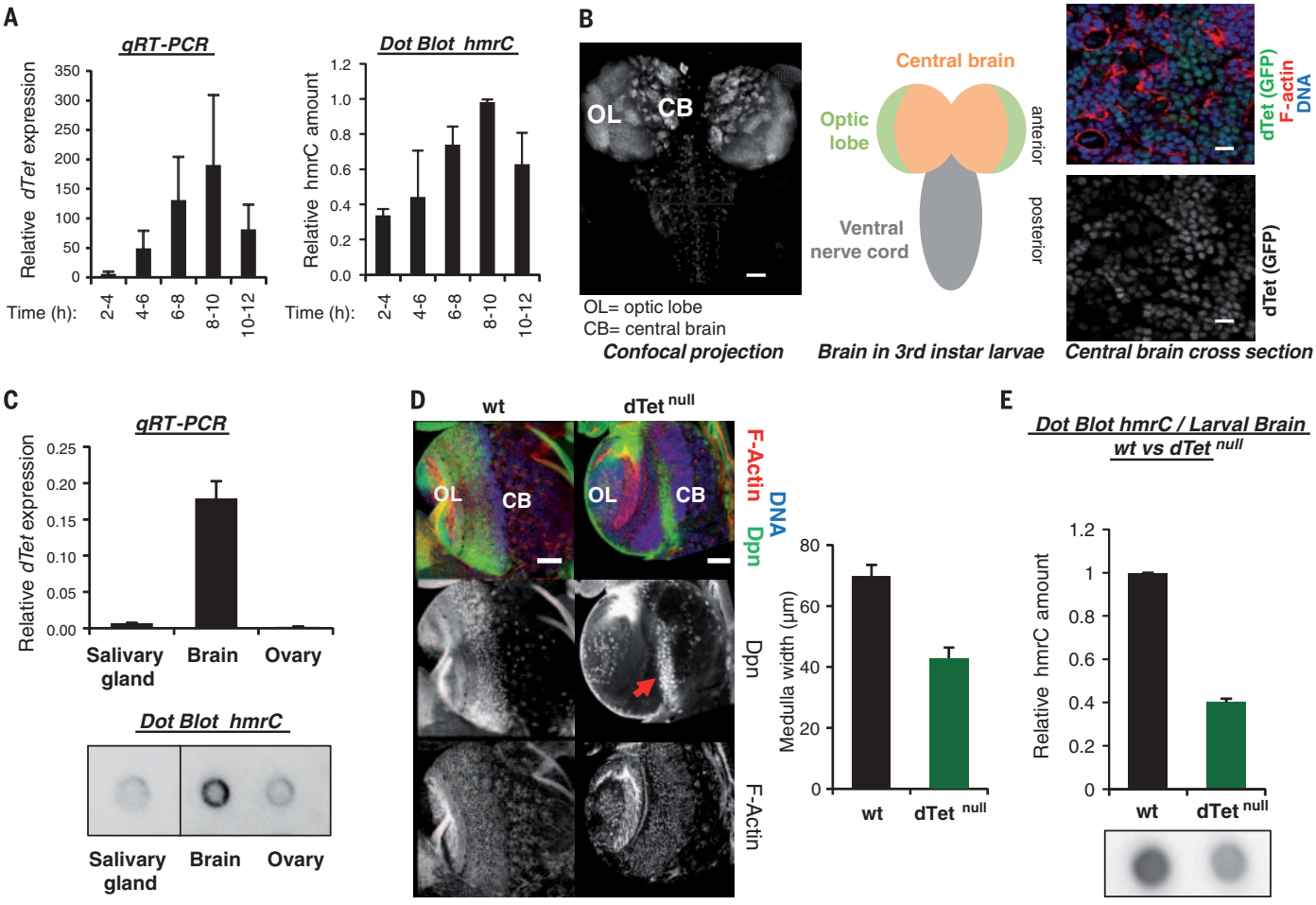

Fig. 4. dTet-deficient fruitflies show impaired brain development, accompanied by decreased RNA hydroxymethylation. (**A**) *dTet* expression and hmrC levels during *Drosophila* embryogenesis. Data are mean ± SD (n = 4 experiments run). (**B**) (Left) Pattern of endogenous GFP-tagged dTet in the larval brain. Scale bar, 50 µm. (Center) Scheme of the larval brain. (Right) Confocal brain section showing the expression of endogenous dTet (green) and F-actin (red). DNA, blue. Scale bar, 10 µm. (**C**) (Top) *dTet* expression in the salivary gland, brain, and ovary. Data are mean ± SD (n = 3 experiments run). (Bottom) Immunoblotting with 5hmC antibody in RNA from salivary gland, brain, and ovary. Vertical line indicates juxtaposition of lanes within the same blot, exposed for the same time. (**D**) (Left) $dTet^{null}$ brains are smaller than wild-type brains. Dpn (neuroblasts), green; F-actin, red; DNA, blue. Scale bar, 50 µm. (Right) Average width of the medulla region containing the neuroblasts (left, red arrow). Error bars represent 95% confidence intervals ($p < 2.4\ 10^{-9}$) for 20 brain lobes. (**E**) Brains of dTet-deficient larvae show a decrease in hmrC. Data are mean ± SD (n = 3 experiments run).

unmodified, methylated, and hydroxymethylated Firefly Luciferase–encoding RNA templates in rabbit reticulocyte lysate showed a decrease in translation of methylated RNAs. In contrast, hmrC-modified templates gave rise to near-control protein levels (Fig. 3B), suggesting that hydroxymethylation can restore the translation efficiency of previously methylated substrates.

We next sought to assess hmrC in vivo in fruitflies. To determine the timing of *dTet* expression and of the appearance of hmrC during early embryogenesis of *D. melanogaster*, we performed quantitative reverse transcription polymerase chain reaction (RT-PCR) to measure *dTet* transcript levels, and immunoblotting to estimate levels of hmrC. We found that *dTet* levels correlate positively with hmrC levels during fruitfly embryogenesis (Fig. 4A and fig. S13A). We also analyzed a publicly available database of RNA-seq results from different stages of *D. melanogaster* development and found that in third-instar larvae, *dTet* expression is highest in the central nervous system (fig. S13B). These findings suggest that dTet-mediated hydroxymethylation of RNA could play a role in the fruitfly brain. To confirm and extend these observations, we generated transgenic *Drosophila* flies expressing a *GFP-dTet* fusion construct under the control of the endogenous dTet promoter (called *dTet-Mi*). The green fluorescent protein (GFP)–tagged dTet protein was detected throughout the larval brain, the highest levels being detected in the optic lobe and central brain (Fig. 4B).

It was of interest to assess whether the fly brain contains high levels of hmrC. To this end, in addition to the brain, we used ovary [because this was the organ chosen to show the role of dTet in DNA m6A demethylation (*11*)]. We also used another organ, the salivary gland, from which we could extract enough RNA to measure hmrC levels. Quantitative RT-PCR and dot blotting showed higher dTet expression and hmrC content in the brain than in the ovary or in the salivary gland of the fruitfly (Fig. 4C). Hence, by revealing that the hmrC signal is highest in the brain, these data support the argument for the importance of hmrC in this organ.

We wished to evaluate RNA hydroxymethylation levels in a complete loss-of-function mutant of dTet (fig. S13, C and D). In agreement with recent observations (*11*), dTet-deficient animals survived through the larval stages but died at the pupal stage (no adult animals survived; $n > 5000$ dTet-null animals analyzed) (fig. S13E). Morphological defects were observed at larval stages: The brains of mutant larvae were smaller than those of normal larvae and showed abnormal organization of neuroblasts in their central part (Fig. 4D). To quantify the observed changes, we measured the width of the medulla region (based on 20 examined brains). We found it to be significantly reduced in $dTet^{null}$ animals ($P < 2.4 \times 10^{-9}$), likely reflecting a lower number of neuroblasts (Fig. 4D). To measure the effects of dTet loss on the RNA hydroxymethylation level, we performed immunoblotting analyses with antibody to 5hmC on brains from $dTet^{null}$ and wild-type larvae. These experiments showed a decreased hmrC content in the brains of dTet-deficient larvae (Fig. 4E and fig. S14).

Our understanding of the posttranscriptional modifications that decorate RNA, a regulatory layer positioned between DNA and proteins, is in its infancy. We have conducted a study addressing the distribution, localization, and function of cytosine hydroxymethylation in RNA, using *Drosophila melanogaster* as a model. Our work has yielded the following key findings: (i) It provides a picture of the hydroxymethylated transcriptome, (ii) reveals an unrecognized function for hmrC, and (iii) suggests a central role for this RNA modification and dTet in the *Drosophila* brain. All in all, we expect this study to change the way we think about the roles played by cytosine hydroxymethylation and the Tet proteins. Our findings open new research prospects in an emerging realm of biological regulation: epitranscriptomics.

REFERENCES AND NOTES

1. S. Kriaucionis, N. Heintz, *Science* **324**, 929–930 (2009).
2. M. Tahiliani *et al.*, *Science* **324**, 930–935 (2009).
3. R. M. Kohli, Y. Zhang, *Nature* **502**, 472–479 (2013).
4. I. Rácz, I. Király, D. Lásztily, *Planta* **142**, 263–267 (1978).
5. L. Fu *et al.*, *J. Am. Chem. Soc.* **136**, 11582–11585 (2014).
6. G. Raddatz *et al.*, *Proc. Natl. Acad. Sci. U.S.A.* **110**, 8627–8631 (2013).
7. S. Takayama *et al.*, *Genome Res.* **24**, 821–830 (2014).
8. E. M. Kallin *et al.*, *Mol. Cell.* **48**, 266–276 (2012).
9. H. Wu *et al.*, *Genes Dev.* **25**, 679–684 (2011).
10. T. L. Dunwell, L. J. McGuffin, J. M. Dunwell, G. P. Pfeifer, *Cell Cycle* **12**, 3357–3365 (2013).
11. G. Zhang *et al.*, *Cell* **161**, 893–906 (2015).
12. K. D. Meyer *et al.*, *Cell* **149**, 1635–1646 (2012).
13. D. Dominissini *et al.*, *Nature* **485**, 201–206 (2012).
14. R. Deplus *et al.*, *EMBO J.* **32**, 645–655 (2013).
15. K. Williams *et al.*, *Nature* **473**, 343–348 (2011).

ACKNOWLEDGMENTS

We thank L. Droogmans for advice, as well as A. Rao and J. Kadonaga for continued support. We also thank Y. N. Jan for providing the antibody to Dpn. R.D., B.H., C.C., and E.B. were supported by the Belgian Fonds de la Recherche Scientifique (FNRS). B.D. was supported by the FNRS (« Aspirant ») and a Belgian American Educational Foundation (BAEF) fellowship. L.V.N. was supported by the Belgian Fund for Research Training in Industry and Agriculture and a BAEF fellowship. E.Co. was supported by a "l'Oréal" fellowship, and M.D. was supported by the WBHealth grant (CanDx) from the Walloon Region. F.F. is a ULB Professor. F.F.'s lab was funded by grants from the FNRS and Télévie, the Interuniversity Attraction Poles (P7/03) program, the Action de Recherche Concertée (ARC) (AUWB-2010-2015 ULB-No 7), the WB Health program, the Belgian Fondation contre le Cancer, and the Fonds Gaston Ithier. F.W. was supported by a Charles and Johanna Busch graduate fellowship and the work at Rutgers by a NIH grant (RO1 GM089992) to R.S. V.K. was supported by the ARC (AV.12/17) as well as Brachet and Van Buuren Funds. P.A.L. received financial support from the National Science Foundation (NSF CHE 1212625 and 1507357). The authors declare no conflicts of interest. All sequencing data have been deposited to the Gene Expression Omnibus as series GSE66090.

SUPPLEMENTARY MATERIALS

www.sciencemag.org/content/351/6270/282/suppl/DC1
Materials and Methods
Figs. S1 to S14
Tables S1 to S6
References (*16*–*35*)

8 May 2015; accepted 8 December 2015
10.1126/science.aac5253

GENE REGULATION

Transcription factors LRF and BCL11A independently repress expression of fetal hemoglobin

Takeshi Masuda,[1] Xin Wang,[2] Manami Maeda,[1] Matthew C. Canver,[3] Falak Sher,[3] Alister P. W. Funnell,[4] Chris Fisher,[5] Maria Suciu,[5] Gabriella E. Martyn,[4] Laura J. Norton,[4] Catherine Zhu,[1] Ryo Kurita,[6] Yukio Nakamura,[6,7] Jian Xu,[3,8] Douglas R. Higgs,[5] Merlin Crossley,[4] Daniel E. Bauer,[3] Stuart H. Orkin,[3,9] Peter V. Kharchenko,[2]* Takahiro Maeda[1]*

Genes encoding human β-type globin undergo a developmental switch from embryonic to fetal to adult-type expression. Mutations in the adult form cause inherited hemoglobinopathies or globin disorders, including sickle cell disease and thalassemia. Some experimental results have suggested that these diseases could be treated by induction of fetal-type hemoglobin (HbF). However, the mechanisms that repress HbF in adults remain unclear. We found that the LRF/ZBTB7A transcription factor occupies fetal γ-globin genes and maintains the nucleosome density necessary for γ-globin gene silencing in adults, and that LRF confers its repressive activity through a NuRD repressor complex independent of the fetal globin repressor BCL11A. Our study may provide additional opportunities for therapeutic targeting in the treatment of hemoglobinopathies.

During human development, the site of erythropoiesis changes from the embryonic yolk sac to the fetal liver and then, in newborns, to the bone marrow, where it persists through adulthood. Coincidentally, there is a "globin switch" from embryonic to fetal globin genes in utero, and then a second switch from fetal to adult globin expression soon after birth. This process has been studied for more than 60 years (*1*). The latter transition from fetal to adult

hemoglobin is marked by a switch from a fetal tetramer consisting of two α and two γ subunits (HbF: $\alpha_2\gamma_2$) to an adult tetramer containing two α-like and two β-like globin subunits (HbA: $\alpha_2\beta_2$).

Mutations in the adult globin gene cause hemoglobinopathies such as thalassemia and sickle cell disease (SCD). These diseases are among the most common monogenic inherited human disorders and represent emerging public health challenges (*2*). For example, the number of children born with SCD is expected to exceed 14 million worldwide in the next 40 years (*3*).

Molecular genetic and clinical evidence indicates that elevated levels of fetal-type hemoglobin (HbF) in adults ameliorate SCD and β-thalassemia pathogenesis (*1*, *4*). Thus, a promising approach is to pharmacologically inactivate a silencer(s) of fetal globin expression in order to reactivate HbF production in adult erythroid cells. Nuclear factors that regulate globin switching have been identified, but how they function cooperatively or independently in fetal globin repression is not fully understood.

Leukemia/lymphoma-related factor (LRF), encoded by the *ZBTB7A* gene, is a ZBTB transcription factor that binds DNA through C-terminal C2H2-type zinc fingers and presumably recruits a transcriptional repressor complex through its N-terminal BTB domain (*5*). To assess the effects of LRF loss on the erythroid transcriptome, we inactivated the *Zbtb7a* gene in erythroid cells of adult mice (*6*). We then performed RNA sequencing (RNA-seq) analysis using splenic erythroblasts from control and LRF conditional knockout (*Zbtb7a*$^{F/F}$ *Mx1-Cre*$^{+}$) mice (LRF KO mice) (Fig. 1A). Efficient *Zbtb7a* deletion was confirmed by Western blot and RNA-Seq reads (fig. S1, A and B) (*7*). Wild-type mice express two embryonic β-like globin genes: *Hbb-bh1* and *Hbb-y* (*8*, *9*). Although both genes are expressed at early embryonic stages, *Hbb-bh1* is the ortholog of human γ-globin (*10*, *11*). LRF-deficient adult erythroblasts showed significant induction of *Hbb-bh1*, but not *Hbb-y*, with a moderate reduction in adult globin levels (fig. S2A). These results were validated by quantitative polymerase chain reaction (qPCR) (fig. S2B). Isoelectric focusing of peripheral blood hemolysates revealed unique bands corresponding to embryonic globin proteins in peripheral blood from LRF KO mice (Fig. 1B).

We used a humanized mouse model to investigate whether LRF loss would reactivate human fetal globin expression in vivo. To do so, we established LRF KO mice harboring the human β-globin gene cluster as a yeast artificial chromosome transgene (βYAC) (*12*) (fig. S2C). Human γ-globin transcripts, but not those of embryonic β-globin (HBE1), were significantly induced in LRF-deficient erythroblasts and constituted 6 to 12% of total human β-like globins in peripheral blood (Fig. 1C and fig. S2D). The magnitude of γ-globin induction in LRF/βYAC mice approximated that seen in BCL11A/βYAC mice (*13*).

We next determined whether LRF loss could induce HbF in human erythroid cells. To this end, we used human CD34^{+} hematopoietic stem and progenitor cell (HSPC)–derived primary erythroblasts and determined γ-globin expression levels upon short hairpin RNA (shRNA)–mediated LRF knockdown (LRF KD) (fig. S3A). LRF expression was markedly induced upon erythroid differentiation over a 2-week period (Fig. 2A). LRF KD significantly increased the percentage of γ-globin mRNA (Fig. 2B and fig. S3, B and C) and protein expression (fig. S3D) relative to adult globin. HbF levels in LRF KD cells were greater than those seen in parental or scrambled-shRNA transduced cells (Fig. 2C and fig. S3E). Because LRF KO mice exhibit a mild macrocytic anemia due to inefficient erythroid terminal differentiation (*14*), we assessed the effects of LRF deficiency on human erythroid differentiation. We observed a delay in differentiation upon LRF KD relative to controls (fig. S4A and supplementary text).

HSPC-derived erythroid cells tend to display relatively high basal levels of HbF (Fig. 2C). Moreover, it is difficult to exclude the possibility that the effects of LRF KD may be the result of a subpopulation of cells expressing aberrantly high HbF

[1]Division of Hematology, Department of Medicine, Brigham and Women's Hospital, Harvard Medical School, Boston, MA 02115, USA. [2]Department of Biomedical Informatics, Harvard Medical School, Boston, MA 02115, USA. [3]Division of Hematology/Oncology, Boston Children's Hospital, Department of Pediatric Oncology, Dana-Farber Cancer Institute, Harvard Stem Cell Institute, Department of Pediatrics, Harvard Medical School, Boston, MA 02115, USA. [4]School of Biotechnology and Biomolecular Sciences, University of New South Wales, Sydney, NSW 2052, Australia. [5]Medical Research Council, Molecular Haematology Unit, Weatherall Institute of Molecular Medicine, Oxford University, Oxford, UK. [6]Cell Engineering Division, RIKEN BioResource Center, Tsukuba, Ibaraki, Japan. [7]Comprehensive Human Sciences, University of Tsukuba, Tsukuba, Ibaraki, Japan. [8]Children's Research Institute, Department of Pediatrics, University of Texas Southwestern Medical Center, Dallas, TX 75390, USA. [9]Howard Hughes Medical Institute, Boston, MA 02115, USA.
***Corresponding author. E-mail: peter.kharchenko@post.harvard.edu (P.V.K.); tmaeda@partners.org (T.M.)**

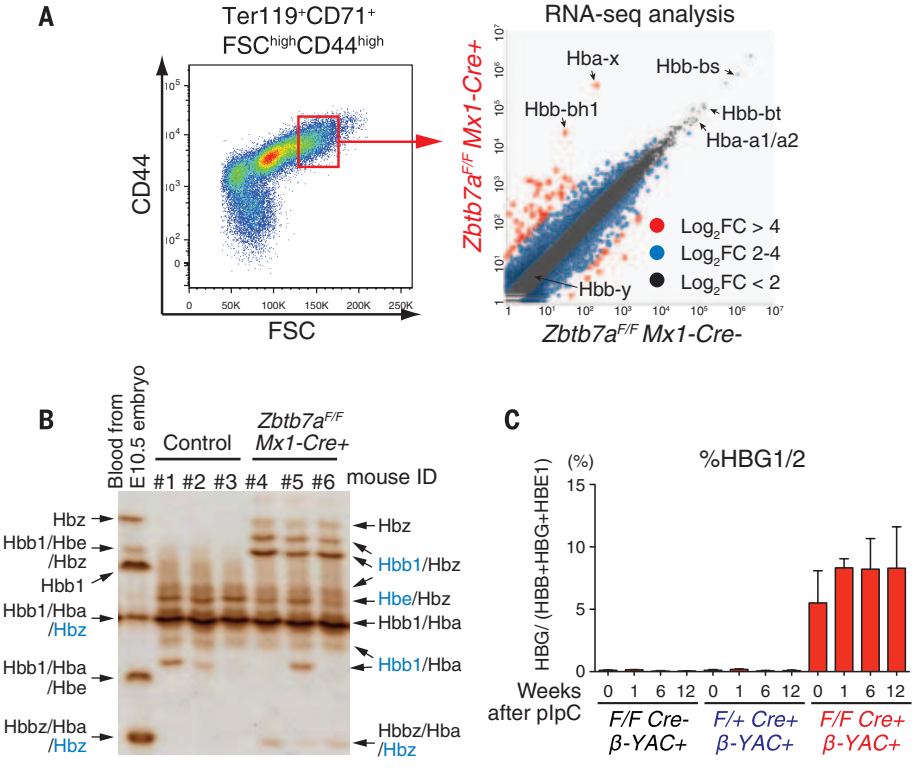

Fig. 1. Induced *Zbtb7a* deletion reactivates embryonic/fetal globin expression in adult mice. (**A**) RNA-seq analysis of splenic erythroblasts from control and LRF KO mice. Mice were injected with polyinosinic-polycytidylic acid, and splenic erythroblasts were harvested 2 months later. Each dot represents an individual gene; differentially expressed genes are depicted according to FPM (fragments per million mapped reads) values. (**B**) Isoelectric focusing of peripheral blood hemolysates and subsequent peptide mass fingerprinting with matrix-assisted laser desorption/ionization–time-of-flight mass spectrometry (MALDI-TOF MS). Embryonic globins (Hbz and Hbbz) are evident in samples from LRF KO mice. Globins shown in blue were detected at a much lower level. (**C**) Levels of human γ-globin (HBG) transcripts were monitored by qPCR before and after LRF depletion. Error bars denote SD. We observed a low level of γ-globin expression before induction of LRF KO, likely due to leaky Cre activity (*24*).

levels. To circumvent these problems, we used a human immortalized erythroid line (HUDEP-2), which undergoes terminal differentiation upon doxycycline removal (fig. S5A) (*15*). This line possesses an advantage over lines currently used for globin switching studies because it expresses predominantly adult hemoglobin (HbA), with very low background HbF expression (*15*). Using CRISPR/cas9 gene modification, we knocked out *ZBTB7A* in HUDEP-2 cells (fig. S5B). We did not observe a significant difference in erythroid differentiation between control and *ZBTB7A* KO HUDEP-2 cells, as evidenced by morphologic and fluorescence-activated cell sorting (FACS) analyses (fig. S5, C and D). To evaluate genome-wide

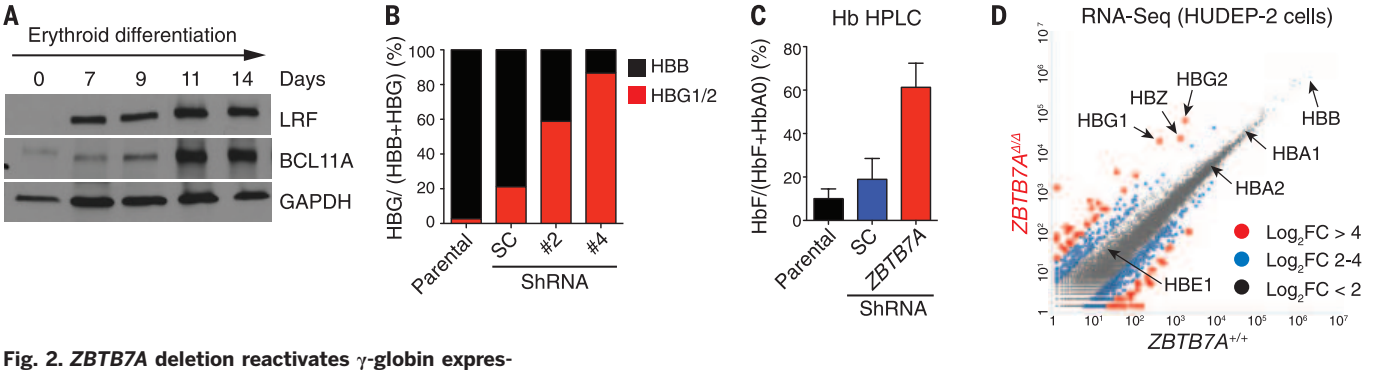

Fig. 2. *ZBTB7A* deletion reactivates γ-globin expression in human erythroblasts. (**A**) Time course analysis of LRF and BCL11A protein levels by Western blot. GAPDH was used as a loading control. (**B**) Bar graphs show proportions of γ-globin to total β-globin transcripts measured by qPCR on day 15. (**C**) Bar graphs show proportions of HbF relative to adult globin (HbA0) on day 15. Means of two independent samples per condition are shown. Error bars denote SD. (**D**) RNA-seq analysis of control and LRF KO HUDEP-2 cells. Differentially expressed genes are indicated according to FPM values. (**E**) Representative HPLC profiles of control and *ZBTB7A*$^{\Delta/\Delta}$ HUDEP-2 clones. Control: HUDEP-2_Cas9.

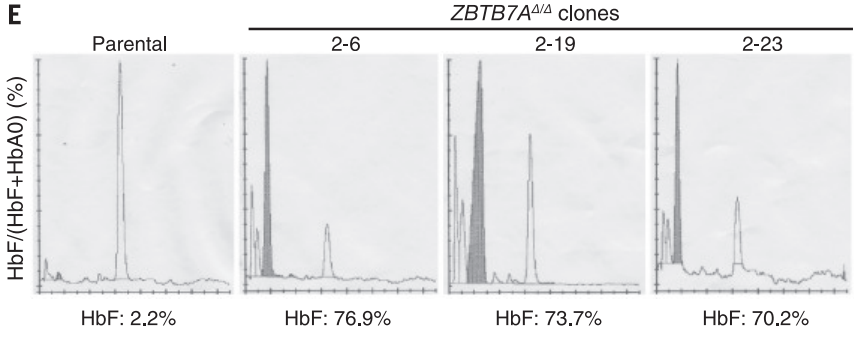

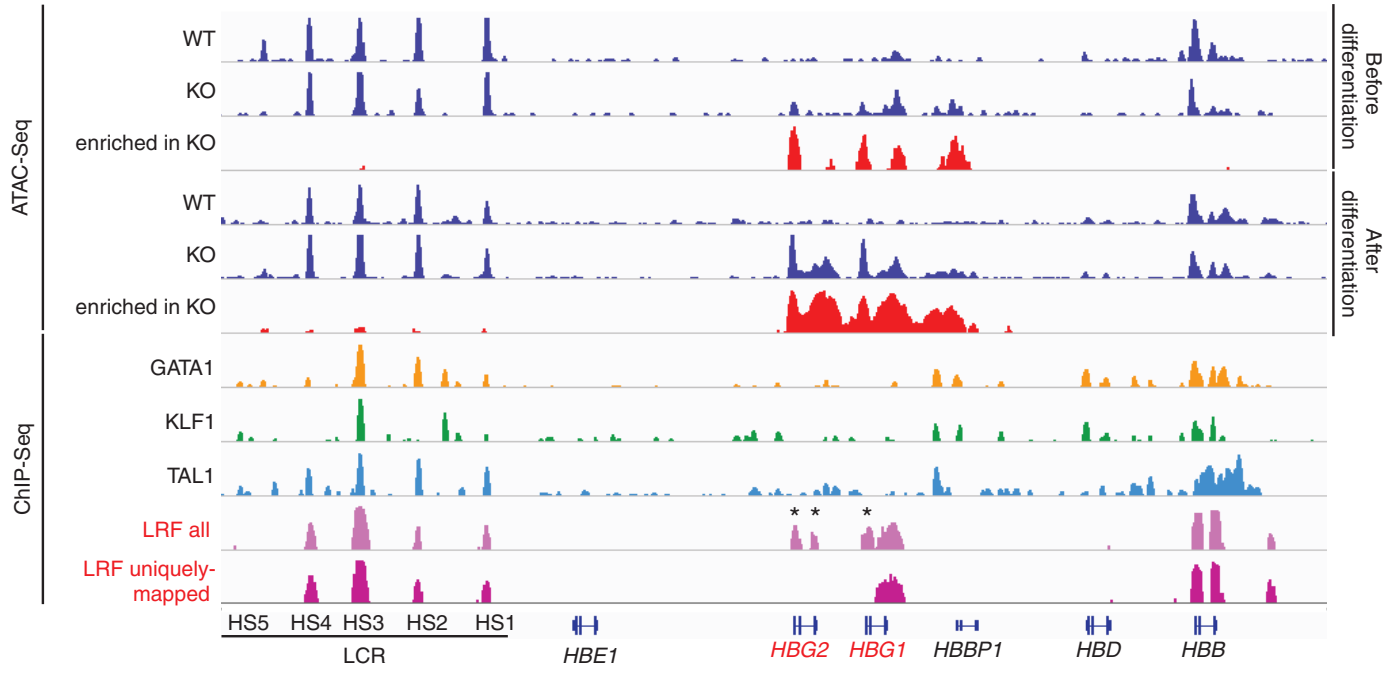

Fig. 3. LRF occupies the γ-globin gene and maintains local chromatin compaction. LRF ChIP-seq and ATAC-seq signals at the β-globin cluster (HUDEP-2 cells) are shown, along with ChIP-seq enrichment for GATA1, KLF1, and TAL1 (*25*). Regions showing statistically significant ATAC-seq differences between LRF KO and wild-type HUDEP-2 cells are depicted in red. Because of high sequence similarity of *HBG1* and *HBG2*, we analyzed LRF occupancy sites at the γ-globin locus using two different mapping methods: one mapping all mappable fragments ("LRF all") and the other mapping only uniquely mappable fragments ("LRF uniquely mapped"). In the "LRF all" track, fragments mappable to either *HBG1* or *HBG2* were randomly distributed between both genes (marked by asterisks).

gene expression changes promoted by *ZBTB7A* deletion, we performed RNA-seq analysis. Wild-type HUDEP-2 cells exhibited gene expression patterns similar to those of HSPC-derived basophilic erythroblasts (fig. S6). As expected, γ-globin transcripts, but not those of embryonic ε-globin, were markedly induced in *ZBTB7A* KO HUDEP-2 cells (Fig. 2D and fig. S7A). Levels of adult β-globin transcripts in *ZBTB7A* KO cells were approximately half those seen in control cells (fig. S7A); γ-globin transcripts constituted more than 60% of total β-like globins (fig. S7B). Induction of γ-globin was also validated at the protein level (fig. S7, C and D). We then established three independent *ZBTB7A* KO HUDEP-2 clones (fig. S7E) and determined HbF levels in each by high-performance liquid chromatography (HPLC). All three clones exhibited HbF levels greater than 60%, whereas that of parental cells was less than 3% (Fig. 2E). Notably, the HbF reactivation occurred without changes in levels of transcripts encoding known HbF repressors, including BCL11A (fig. S7F). BCL11A protein levels were also unchanged in *ZBTB7A* KO cells (fig. S5B).

To determine LRF occupancy sites genome-wide, we performed chromatin immunoprecipitation and sequencing (ChIP-seq) with an antibody to LRF, using HSPC-derived proerythroblasts and HUDEP-2 cells. These experiments exhibited strong correlations and concordance among the replicates (fig. S8A). We identified 5684 and 10,385 LRF binding sites in HSPC-derived proerythroblasts and HUDEP-2 cells, respectively (fig. S8B). The most enriched motif identified in either cell type was consistent with that previously identified in vitro using CAST (cyclic amplification and selection of targets) analysis (*16*), confirming antibody specificity (figs. S9 and S10). Genes differentially expressed in control and *ZBTB7A* KO cells were significantly enriched for LRF binding sites (Fisher's exact test, $P < 1.6 \times 10^{-5}$ and $P < 8.3 \times 10^{-13}$ for undifferentiated and differentiated conditions, respectively). It is also notable that LRF occupancy sites differ from those of the known γ-globin repressors SOX6 and BCL11A (*17*) (fig. S8C).

In support of a direct role of LRF at the β-globin cluster, we observed several significant LRF-ChIP binding signals at adult (*HBB*) and fetal (*HBG1* and *HBG2*) globin genes and at upstream hypersensitivity (HS) sites within the locus control region (LCR) (Fig. 3 and supplementary text). To assess the local chromatin accessibility at the β-globin cluster in the presence or absence of LRF, we performed ATAC-seq [assay for transposase-accessible chromatin with high-throughput sequencing (*18*)]. In control HUDEP-2 cells, the *HBB* gene and LCR HS sites, but not the γ-globin genes, exhibited ATAC-seq nucleosome-free signals (Fig. 3). In contrast, strong chromatin accessibility was evident at the γ-globin genes in *ZBTB7A*$^{\Delta/\Delta}$ cells before differentiation, and the signal was amplified upon differentiation. Strikingly, differential enrichment of ATAC signals in *ZBTB7A*$^{\Delta/\Delta}$ cells was evident only at the γ-globin genes (Fig. 3) but not at the *HBB* gene or HS sites, indicating that chromatin in the latter is accessible regardless of *ZBTB7A* genotype. Thus, although LRF binds to the *HBB* gene and HS sites as well as to the γ-globin genes, LRF depletion specifically opens chromatin at the γ-globin genes.

To identify a repressor complex interacting with LRF in an unbiased fashion, we performed a yeast two-hybrid screen with the human LRF-BTB domain as bait. A total of 360 positive clones were processed out of 52.1 million potential binding events. LRF-interacting proteins with high confidence included four ZBTB proteins, three NuRD/CHD family proteins, and two chromatin remodelers (fig. S11, A and B). Given their abundance in erythroid cells (fig. S12A) and their potential repressor function, we focused on three factors (GATAD2B, CHD3, and CHD8) for further validation. Interactions of LRF with each were validated by immunoprecipitation (fig. S12B). Because NuRD complex components are implicated in globin switching (*17*, *19*, *20*), we examined the LRF-GATAD2B interaction in more detail. Immunoprecipitation of human proerythroblast lysates with an antibody to LRF pulled down GATAD2B and other NuRD complex components (Fig. 4A). The interactions were also validated in mouse erythroid cells (fig. S10C). Although BCL11A reportedly interacts with NuRD components (*21*, *22*), we did not detect BCL11A in the NuRD complexes containing LRF in either human or mouse erythroid cells (Fig. 4A and fig. S12C). For reciprocal validation, we performed immunoprecipitation in human erythroid cell lysates with antibodies to GATAD2B or MTA2; as expected, both antibodies pulled down LRF (Fig. 4B). BCL11A was readily detected in MTA2-containing protein complexes, as reported (*22*). Consistent with our findings, LRF was not identified as a BCL11A-interacting protein in proteomic affinity screens in erythroid cells (*21*, *22*).

Finally, to determine whether LRF and BCL11A suppress γ-globin expression via distinct mechanisms, we established *ZBTB7A/BCL11A* double-knockout (DKO) HUDEP-2 cells (fig. S12D) and compared HbF in these cells to that in *ZBTB7A* or *BCL11A* single-KO HUDEP-2 cells. DKO cells exhibited a significantly greater fetal/adult β-globin ratio than did either *ZBTB7A* or *BCL11A* single-KO cells (fig. S12, E and F). The HbF levels of DKO cells were at 91 to 94% of total Hb (Fig. 4, C and D).

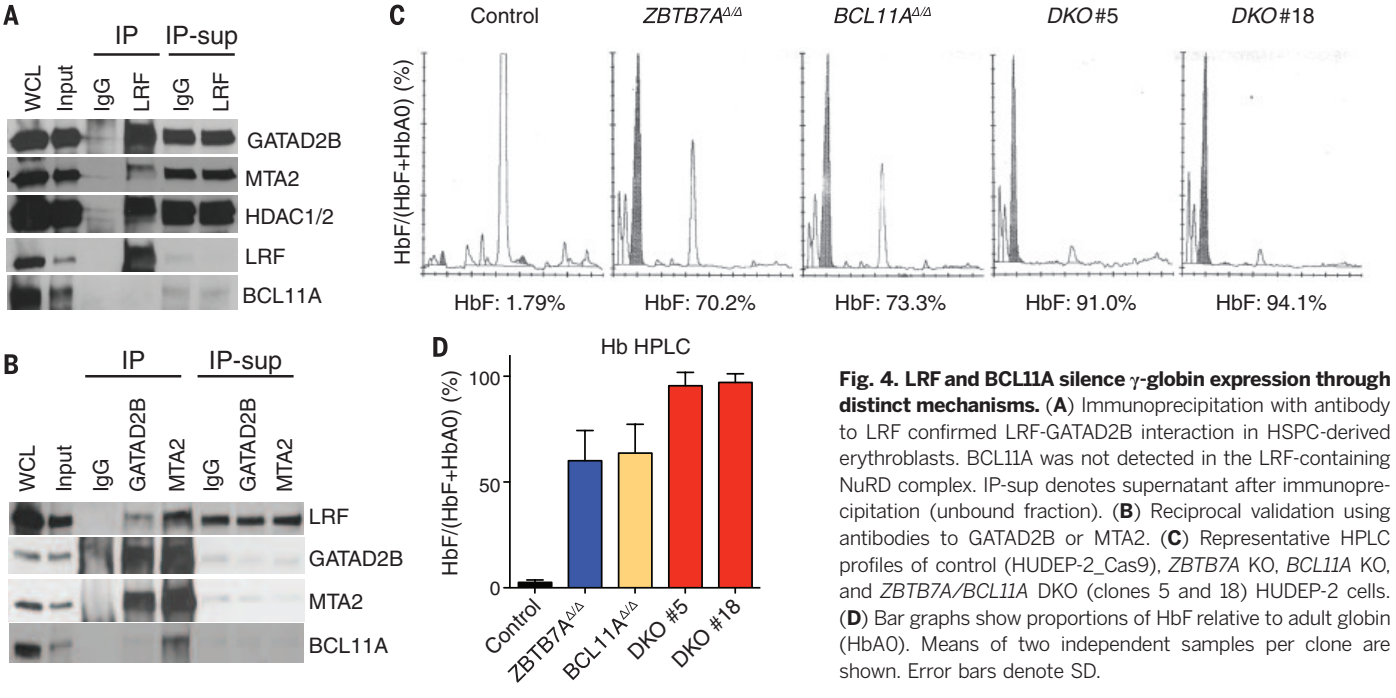

Fig. 4. LRF and BCL11A silence γ-globin expression through distinct mechanisms. (**A**) Immunoprecipitation with antibody to LRF confirmed LRF-GATAD2B interaction in HSPC-derived erythroblasts. BCL11A was not detected in the LRF-containing NuRD complex. IP-sup denotes supernatant after immunoprecipitation (unbound fraction). (**B**) Reciprocal validation using antibodies to GATAD2B or MTA2. (**C**) Representative HPLC profiles of control (HUDEP-2_Cas9), *ZBTB7A* KO, *BCL11A* KO, and *ZBTB7A/BCL11A* DKO (clones 5 and 18) HUDEP-2 cells. (**D**) Bar graphs show proportions of HbF relative to adult globin (HbA0). Means of two independent samples per clone are shown. Error bars denote SD.

These data suggest that LRF and BCL11A represent a primary fetal globin repressive activity in adult erythroid cells (fig. S13).

Our results show that LRF is a potent repressor of embryonic/fetal β-like globin expression in adult erythroid cells. We postulate that LRF depletion opens local chromatin at the γ-globin genes, thereby enabling erythroid transcriptional activators to induce γ-globin expression. Furthermore, we propose that LRF silences γ-globin expression independently of BCL11A, as implied by our observations that (i) LRF inactivation in mice specifically reactivates *Hbb-bh1*, but not *Hbb-y*, expression, whereas BCL11A depletion induces both of these embryonic globins (*13*); (ii) LRF directly binds to the *HBG1* gene, whereas BCL11A reportedly targets intergenic region(s), the LCR, and sequences between *HBG1* and *HBD* (*17*, *23*); (iii) the LRF-NuRD complex in adult erythroid cells lacks BCL11A; and (iv) *ZBTB7A/BCL11A* DKO HUDEP-2 cells exhibit significantly greater γ-globin expression than do either *ZBTB7A* or *BCL11A* single-KO cells.

Our work suggests that the two NuRD-associated pathways, in which LRF and BCL11A are respectively involved, are responsible for turning off fetal globin expression in order to switch over to adult globin. These findings may enable the development of therapies to turn on fetal globin expression in individuals with human hemoglobinopathies displaying defective adult globin gene expression.

REFERENCES AND NOTES

1. G. Stamatoyannopoulos, *Exp. Hematol.* **33**, 259–271 (2005).
2. S. Pleasants, *Nature* **515**, S2 (2014).
3. F. B. Piel, S. I. Hay, S. Gupta, D. J. Weatherall, T. N. Williams, *PLOS Med.* **10**, e1001484 (2013).
4. D. E. Bauer, S. C. Kamran, S. H. Orkin, *Blood* **120**, 2945–2953 (2012).
5. S. U. Lee, T. Maeda, *Immunol. Rev.* **247**, 107–119 (2012).
6. S. U. Lee *et al.*, *Blood* **121**, 918–929 (2013).
7. See supplementary materials on *Science* Online.
8. P. D. Kingsley, J. Malik, K. A. Fantauzzo, J. Palis, *Blood* **104**, 19–25 (2004).
9. M. H. Baron, J. Isern, S. T. Fraser, *Blood* **119**, 4828–4837 (2012).
10. K. Chada, J. Magram, F. Costantini, *Nature* **319**, 685–689 (1986).
11. P. D. Kingsley *et al.*, *Blood* **107**, 1665–1672 (2006).
12. K. R. Peterson *et al.*, *Proc. Natl. Acad. Sci. U.S.A.* **90**, 7593–7597 (1993).
13. J. Xu *et al.*, *Science* **334**, 993–996 (2011).
14. T. Maeda *et al.*, *Dev. Cell* **17**, 527–540 (2009).
15. R. Kurita *et al.*, *PLOS ONE* **8**, e59890 (2013).
16. T. Maeda *et al.*, *Nature* **433**, 278–285 (2005).
17. J. Xu *et al.*, *Genes Dev.* **24**, 783–798 (2010).
18. J. D. Buenrostro, P. G. Giresi, L. C. Zaba, H. Y. Chang, W. J. Greenleaf, *Nat. Methods* **10**, 1213–1218 (2013).
19. J. W. Rupon, S. Z. Wang, K. Gaensler, J. Lloyd, G. D. Ginder, *Proc. Natl. Acad. Sci. U.S.A.* **103**, 6617–6622 (2006).
20. M. Amaya *et al.*, *Blood* **121**, 3493–3501 (2013).
21. V. G. Sankaran *et al.*, *Science* **322**, 1839–1842 (2008).
22. J. Xu *et al.*, *Proc. Natl. Acad. Sci. U.S.A.* **110**, 6518–6523 (2013).
23. V. G. Sankaran *et al.*, *Nature* **460**, 1093–1097 (2009).
24. I. T. Chan *et al.*, *J. Clin. Invest.* **113**, 528–538 (2004).
25. M. Y. Su *et al.*, *J. Biol. Chem.* **288**, 8433–8444 (2013).

ACKNOWLEDGMENTS

We thank P. Jarolim, D. Dorfman, and other members of BWH Hematology laboratory for help on HPLC analysis; J. Hughes, J. Eglinton, J. Sharp, C. Babbs, K. di Gleria, D. Chen, and P. Schupp for technical support and assistance; E. Lamar for critical reading of the manuscript; and S-U. Lee, H. Yi, Y. Ishikawa and other members of the Maeda lab for help and advice. Supported by National Institute of Diabetes and Digestive and Kidney Diseases (NIDDK) Predoctoral National Research Service Award for M.D./Ph.D. Fellowship F30DK103359-01A1 (M.C.C.), NIDDK Career Development Award K08DK093705 and Doris Duke Charitable Foundation Innovations in Clinical Research Award 2013137 (D.E.B.), NIH grants P01HL032262 and P30DK049216 (Center of Excellence in Molecular Hematology) (S.H.O.), NIH grant 5K25AG037596 and Ellison Medical Foundation grant AG-NS-0965-12 (P.V.K.), and NIH grants R01 AI084905 and R56 DK105001 and an American Society of Hematology Bridge Program grant (T. Maeda). All reagents described in this manuscript (mouse models, plasmids) are available to the scientific community upon request. Sequencing data are available at the NCBI Gene Expression Omnibus (GEO accession number GSE74977). T. Masuda, M. Maeda, and T. Maeda are contributors to a patent application filed on behalf of Brigham and Women's Hospital related to therapeutic targeting of LRF/NuRD interaction.

SUPPLEMENTARY MATERIALS

www.sciencemag.org/content/351/6270/285/suppl/DC1
Materials and Methods
Supplementary Text
Figs. S1 to S14
References (*26*–*64*)

28 August 2015; accepted 7 December 2015
10.1126/science.aad3312

NEW ENGLAND BioLabs® Inc.

In the know, wherever you go.

Introducing the NEBpubs™ app from New England Biolabs.

Looking for an easy and more environmentally-friendly way to catch up on your favorite NEB publications? Try the NEBpubs app! Available for both iPad® and Android™, the app contains interactive editions of our NEB Expressions newsletter, as well as all of our popular technical guides and product brochures. As if that weren't enough, you'll also get access to exclusive videos, animations, audio clips and other interactive content. *The NEBpubs app keeps you in the know, wherever you go!*

> *"The NEBpubs app is stellar. It's as beautiful and complete as you would expect from NEB – the same quality you get in their catalogs and publications...I'm a big fan of the NEB Expressions, so having them downloadable and available offline is helpful."*
>
> – Jason, Assistant Teaching Professor, University of Missouri

Get started today: www.neb.com/NEBpubs

Download on the App Store

GET IT ON Google play

NEW ENGLAND BIOLABS® and NEB® are registered trademarks of New England Biolabs, Inc. NEBPUBS™ is a trademark of New England Biolabs, Inc.
APPLE® and iPAD® are registered trademarks of Apple, Inc. GOOGLE PLAY™ and ANDROID™ are trademarks of Google, Inc.

myIDP: A career plan customized for you, by you.

For your career in science, there's only one Science

my IDP
ScienceCareers

Recommended by leading professional societies and the NIH

Features in myIDP include:

- Exercises to help you examine your skills, interests, and values.
- A list of 20 scientific career paths with a prediction of which ones best fit your skills and interests.
- A tool for setting strategic goals for the coming year, with optional reminders to keep you on track.
- Articles and resources to guide you through the process.
- Options to save materials online and print them for further review and discussion.
- Ability to select which portion of your IDP you wish to share with advisors, mentors, or others.
- A certificate of completion for users that finish myIDP.

Visit the website and start planning today!
myIDP.sciencecareers.org

ScienceCareers In partnership with:

advancing the life sciences 1912-2012 FASEB Federation of American Societies for Experimental Biology

UCSF University of California San Francisco

Medical College of Wisconsin

Burroughs Wellcome Fund

AAAS 2016 ANNUAL MEETING | WASHINGTON, DC FEBRUARY 11–15

Global Science Engagement

The 2016 meeting focuses on how the scientific enterprise can meet global challenges in need of innovation and international collaboration.

aaas.org/meetings

See Inside for Details:

President's Address / Registration Rates
Plenary Lectures / Topical Lectures
Seminars / Symposia Tracks

AAAS 2016 ANNUAL MEETING

Join Us in Washington, DC

Learn about science and technology addressing current and future global challenges.

- Seminars on food security; personalized medicine; preserving artifacts; and communicating science
- 130+ symposia in 14 disciplinary tracks covering the latest research advances
- Network with colleagues and attend career development workshops

Connect with us

@AAASmeetings #AAASmtg

facebook.com/AAAS.Science

www.aaas.org/meetings

Reporters: The EurekAlert! website hosts the AAAS Annual Meeting Newsroom. For details please visit eurekalert.org/aaasnewsroom

Dear Colleagues:

On behalf of the AAAS Board of Directors, it is my honor to invite you to join us in Washington, DC for the 2016 AAAS Annual Meeting, February 11–15. The AAAS Annual Meeting is the most widely recognized global science gathering with cutting-edge scientific sessions, valuable networking opportunities, and broad international media coverage.

The 2016 meeting theme—*Global Science Engagement*—focuses on how the scientific enterprise can meet global challenges in need of innovation and international collaboration.

We hope you will join us in Washington, DC.

Geraldine Richmond, Ph.D.
AAAS President and Program Chair
Presidential Chair and Professor of Chemistry
University of Oregon

PRESIDENT'S ADDRESS

Geraldine Richmond
AAAS President and Program Chair
Presidential Chair in Science and Professor of Chemistry
University of Oregon

Thursday, February 11
6:00 p.m. – 7:00 p.m.

Dr. Geri Richmond's research using laser spectroscopy and computational methods focuses on understanding the chemistry and physics that occur at complex interfaces, with relevance to important problems in energy production, environmental remediation, and atmospheric chemistry. She is a member of the National Academy of Sciences and American Academy of Arts and Sciences and is a fellow of the American Chemical Society (ACS), American Physical Society (APS), American Association for the Advancement of Science (AAAS), and the Association for Women in Science. Richmond has served in leadership roles on many international, national, and state governing and advisory boards. She is a member of the National Science Board and is the U.S. Science Envoy to the Lower Mekong River Countries of Vietnam, Laos, Cambodia, Burma, and Thailand. She is founding and current director of COACh, an organization that has helped career advancement for thousands of scientists and engineers in the U.S., Asia, Africa, and Latin America. Awards for her scientific accomplishments include the ACS Olin-Garvan Medal, the Spiers Medal of the Royal Society of Chemistry, the ACS Joel H. Hildebrand Award in Theoretical and Experimental Studies of Liquids, and the APS Davisson-Germer Prize. Awards for outreach and science capacity-building efforts include the Presidential Award for Excellence in Science and Engineering Mentoring, the ACS Award for Encouraging Women in the Chemical Sciences, the Council on Chemical Research Diversity Award, and the ACS Charles L. Parsons Award.

PLENARY LECTURES

All plenary lectures will be held in the Washington Marriott Wardman Park.

Christopher Dye
Director of Strategy, Office of the Director General, World Health Organization

A Problem Shared: Teaming Up to Fight Epidemic Diseases

Friday, February 12
5:00 p.m. – 6:00 p.m.

Jennifer Doudna
Professor of Chemistry and Molecular and Cell Biology, University of California, Berkeley

The CRISPR-Cas9 Genome Editing Revolution

Saturday, February 13
5:00 p.m. – 6:00 p.m.

Jad Abumrad
Host and Producer, Radiolab

Lecture title to be announced

Sunday, February 14
5:00 p.m. – 6:00 p.m.

TOPICAL LECTURES

Friday, February 12

Thaisa Storchi Bergmann
Professor of Physics and Astronomy, Federal University of Rio Grande do Sul, Brazil
Supermassive Black Holes and the Evolution of the Universe

May-Britt Moser
Professor of Neuroscience, Norwegian University of Science and Technology
Brain, Space, and Memory

Gary Machlis
Science Advisor to the Director, U.S. National Park Service
The Near-Horizon Future of Science in National Parks

Saturday, February 13

Robin Murphy
Professor of Computer Science and Engineering, Texas A&M University
Disaster Management: Robots, Informatics, and People

Jennifer Richeson
John D. and Catherine T. MacArthur Professor of Psychology, Northwestern University
Coalition or Derogation? Psychological Perspectives on Race Relations in the 21st Century

David Spiegelhalter
Professor for the Public Understanding of Risk, Cambridge University
Can Your Lifestyle Make You Older or Younger? Metaphors for Communicating Chronic Risks

Sunday, February 14

GEORGE SARTON MEMORIAL LECTURE IN THE HISTORY AND PHILOSOPHY OF SCIENCE
David Kaiser
Germeshausen Professor of the History of Science, Massachusetts Institute of Technology
Einstein's Legacy: Studying Gravity in War and Peace

JOHN P. MCGOVERN AWARD LECTURE IN THE BEHAVIORAL SCIENCES
Elizabeth Spelke
Professor of Psychology, Harvard University
Origins of Knowledge

Samuel Wasser
Endowed Chair and Director, Center for Conservation Biology, University of Washington
Forensic Science, Organized Crime, and the Illegal Ivory Trade: The Elephant in the Room

SEMINARS

Thursday, February 11

Communicating Science

Scientific and technological issues may trigger societal conflict when they intersect with personal or political views. Today's scientists and engineers are increasingly obligated to engage with public audiences about emerging issues in science and technology. This seminar builds connections between scientists, science communication and public engagement professionals who can support their efforts, and social scientists whose research can inform best practices. Participants will gain actionable knowledge and join a growing community focused on public engagement with science. The panels focus on policy engagement, communicating emerging science-society topics such as synthetic biology, and using visuals for science communication.

Organized by: Jeanne Braha, AAAS Center for Public Engagement with Science and Technology, Washington, DC

Scientists Engaging in Policy

MODERATOR: Erin Heath, AAAS Office of Government Relations, Washington, DC

SPEAKERS: Carrie Wolinetz, National Institutes of Health, Bethesda, MD
Arthur Lupia, University of Michigan, Ann Arbor
Jim Gates, University of Maryland, College Park

Communicating Synthetic Biology

MODERATOR: Andrew Maynard, Arizona State University, Tempe

SPEAKERS: Gretchen Gano, University of California, Berkeley
Kristala Prather, Massachusetts Institute of Technology, Cambridge
Natalie Kuldell, BioBuilder Educational Foundation, Cambridge, MA
Dietram Scheufele, University of Wisconsin, Madison

Using Visuals for Science Communication

MODERATOR: Lena Groeger, ProPublica, New York City

SPEAKERS: Matt Hansen, University of Maryland, College Park
Alberto Cuadra, AAAS/*Science*, Washington, DC
Gina Eosco, Eastern Research Group, Arlington, VA

Friday, February 12

Food Security

This seminar will explore food security in light of climate change and other disruptive events, changes in food production systems, and advances in technology and data-sharing. The first session focuses on managing the impacts of food shocks, coincidental extreme events that affect the stability of food production or markets, and climate projections for how weather hazards may contribute to food shocks. The next session examines approaches to sustainable intensification of agriculture, including agricultural censuses, farming practices, and the role of small farms. The final session addresses sustainable intensification specifically through use of open datasets and geospatial data to improve farming productivity and reduce environmental impacts and poverty.

Food Shocks: The Impact of Simultaneous Extreme Events on Global Food Systems

Organized by: Matt Goode and Sian Williams, U.K. Biotechnology and Biological Sciences Research Council, Swindon

SPEAKERS: Kirsty Lewis, Met Office Hadley Center for Climate Science and Services, Exeter, United Kingdom
Joshua W. Elliott, University of Chicago Computation Institute, IL
Tim Benton, Global Food Security Program, Swindon, United Kingdom

Multiple Paths to Ensuring Global Food Security

Organized by: Linda Young, U.S. Department of Agriculture (USDA), Washington, DC

SPEAKERS: Pietro Gennari, Food and Agriculture Organization of the United Nations, Rome, Italy
Catherine Woteki, USDA, Washington, DC
Seth Cook, International Institute for Environment and Development, London, United Kingdom

DISCUSSANT: Kenneth G. Cassman, University of Nebraska, Lincoln

Using Data to Enhance Food Productivity in Subsistence Farming

Organized by: Cindy Cox and Jawoo Koo, International Food Policy Research Institute (IFPRI), Washington, DC

SPEAKERS: Stanley Wood, Bill and Melinda Gates Foundation, Seattle, WA
Paul West, University of Minnesota, St. Paul
Ousmane Badiane, IFPRI, Washington, DC

Saturday, February 13

Precision and Personalized Medicine

Precision medicine and personalized medicine offer an opportunity to transform health care by customizing treatment to an individual's genetics. The United States and United Kingdom have recently made investments into initiatives that seek to accelerate progress in this research. This seminar discusses these efforts, and others that use large datasets from insurance companies to understand response patterns, engage patient organizations in research, and use genomic medicine for patients with rare inherited diseases, cancer, or infection. The seminar also addresses emerging questions about privacy and the public good, including computational methods and algorithms for analyzing big data.

Precision Medicine, Global Reach: Health Solutions from the Big Data Revolution

Organized by: Kristen T. Honey, AAAS Science and Technology Policy Fellow, U.S. Department of Energy, Washington, DC

SPEAKERS: Dhanurjay "DJ" Patil, White House Office of Science and Technology Policy, Washington, DC
John N. Aucott, Johns Hopkins University School of Medicine, Baltimore, MD
Lorraine Johnson, LymeDisease.org, Los Angeles, CA

Precision Medicine and Bioethics

Organized by: Lindsay R. Chura, British Embassy, Washington, DC

SPEAKERS: Hugh Whittall, Nutfield Council on Bioethics, London, United Kingdom
Richard Barker, Innovate UK, Swindon
Willem Ouwehand, University of Cambridge, United Kingdom

DISCUSSANT: Kathy Hudson, National Institutes of Health, Bethesda, MD

Personalized Medicine: Big Data and Machine Learning

Organized by: Gabriela Chira, European Commission

SPEAKERS: Karsten Borgwardt, ETH Zurich, Switzerland
Gunnar Rätsch, Memorial Sloan-Kettering Cancer Center, New York City
Florence Demenais, French Institute of Health and Medical Research (INSERM), Paris

Sunday, February 14

Protecting Cultural Heritage Sites and Artifacts

From the destruction of ancient sites in areas of conflict to discrediting fake artifacts, this seminar covers a range of preservation needs, techniques, and practices. The seminar highlights recent work in Syria, Mali, and Iraq using satellite images. Sessions demonstrate how forensic science and the humanities can work together to reveal the true history of objects and discusses technologies – such as 3-D printing, digital scanning, and a novel sensing system that captures spatial data – for preserving archaeological information, or for creating new products.

Cultural Heritage Destruction: Evidence and Emergency Responses

Organized by: Susan Wolfinbarger, AAAS Scientific Responsibility, Human Rights, and Law Program, Washington, DC; Katharyn Hanson, University of Pennsylvania Museum's Cultural Heritage Center, Philadelphia

SPEAKERS: Susan Wolfinbarger, AAAS, Washington, DC
Corine Wegener, Smithsonian Institution, Washington, DC
Morag Kersel, Depaul University, Chicago, IL

DISCUSSANT: Brian Daniels, University of Pennsylvania Museum's Cultural Heritage Center, Philadelphia

Faked or Changed? Using Science To Reconstruct Object Biography

Organized by: Marc Walton, Northwestern University, Evanston, IL; Katherine Faber, California Institute of Technology, Pasadena

SPEAKERS: Luigi Modini, U.S. Federal Bureau of Investigation, Chicago, IL
Marc Walton, Northwestern University, Evanston, IL
Joel Baden, Yale University, New Haven, CT; Candida Moss, University of Notre Dame, IN

DISCUSSANT: Francesca Casadio, Art Institute of Chicago, IL

Preserving World Heritage and Transforming Global Manufacturing with 3-D Scanning

Organized by: Björn Johansson, Chalmers University of Technology, Gothenburg, Sweden; Ram D. Sriram, National Institute of Standards and Technology, Gaithersburg, MD; Ramesh Jain, University of California, Irvine

SPEAKERS: Jan-Eric Sundgren, Volvo Group, Gothenburg, Sweden
Katsushi Ikeuchi, University of Tokyo, Japan
Lori Collins, University of South Florida, Tampa

DISCUSSANT: Adam Metallo, Smithsonian Institution, Landover, MD

SYMPOSIA TRACKS

Organizers are listed under symposia titles.

ANTHROPOLOGY, CULTURE, AND LANGUAGE

Global Variation in Health and Aging: Cultural Contexts and Quality of Life
Lynnette Leidy Sievert, University of Massachusetts, Amherst

I Can't Hear Myself Think! Noise and the Developing Brain from Infancy to Adulthood
Nan Bernstein Ratner, University of Maryland, College Park

Bilingualism Matters
Karen Emmorey, San Diego State University, CA

Evolutionary Biology Impacts on Medicine and Public Health
Cynthia Beall, Case Western Reserve University, Cleveland, OH; Randolph Nesse, Arizona State University, Tempe

Rethinking Child Language Disorders: Insights from Sign Language Research
Richard P. Meier, University of Texas, Austin

The Science of Human Evolution in Africa
Leslea Hlusko, University of California, Berkeley

Understanding Speakers of 7,000 Languages
Robert Munro, Idibon, San Francisco, CA

BEHAVIORAL AND SOCIAL SCIENCES

Aligning Publishing Incentives with Research Transparency and Integrity
Bobbie Spellman, University of Virginia, Charlottesville; Arthur Lupia, University of Michigan, Ann Arbor

Going Public: How Science Communicators Can Break Through the Noise
Arthur Lupia, University of Michigan, Ann Arbor; Kathleen Hall Jamieson, University of Pennsylvania, Philadelphia

How the Body Shapes the Mind
Susan Goldin-Meadow and Daniel Casasanto, University of Chicago, IL

Interpersonal Violence and Conflict Escalation: Situational Dynamics
William Alex Pridemore, State University of New York, Albany

Is the Risk of Alzheimer's and Dementia Declining? Evidence From Around the World
Kenneth Langa, University of Michigan, Ann Arbor

Trying on Identities: Science Engagement of Adolescents
Julia McQuillan, University of Nebraska, Lincoln

U.S. and Global Public Opinion on Science and Technology Issues
John C. Besley, Michigan State University, East Lansing

Virtues of U.S. Scientists Guiding Scientific Practice
Robert T. Pennock, Michigan State University, East Lansing; Jon D. Miller, University of Michigan, Ann Arbor

BIOLOGY AND NEUROSCIENCE

At a Loss for Words, or Losing Your Mind? New Views on Language Problems in Aging
Margaret Rogers, American Speech-Language-Hearing Association, Rockville, MD; Nan Bernstein Ratner, University of Maryland, College Park

Artificial Intelligence: Imagining the Future
Maria Spiropulu, California Institute of Technology, Pasadena

Discovery and Development of the CRISPR-Cas Genome Editing Technology
Hong Li, Florida State University, Tallahassee

Global Response to Human Gene Editing
Anne-Marie Mazza and Kevin Finneran, National Academies of Sciences, Engineering, and Medicine, Washington, DC

From Toxins to Culture: How Environment Shapes the Infant Brain
Marie-Francoise Chesselet, University of California, Los Angeles

Neuroplasticity: Insights in Neuronal Connectivity Illuminate Brain Function
Thomas Franke, New York University, New York City; Eric Nestler, Mount Sinai School of Medicine, New York City

Neuroscience Clues to the Chemistry of Addictions and Mood Disorders
Mary Baker, European Brain Council, Brussels, Belgium; Aidan Gilligan, SciCom–Making Sense of Science, Brussels, Belgium

Oral Cancer: Epidemiology, Mechanisms, and Early Detection
Mina Mina, University of Connecticut Health Center, Farmington

COMMUNICATION AND PUBLIC PROGRAMS

Opinion Writing: Strategies for Persuasive Public Communication
Laura Helmuth, Slate *magazine, Washington, DC; Bethany Brookshire,* Science News, *Washington, DC*

A Global Village of Public Engagement in Science
Satoru Ohtake, Japan Science and Technology Agency, Tokyo; Seunghwan Kim, Korea Foundation for the Advancement of Science and Creativity, Seoul, South Korea; Tateo Arimoto, National Graduate School for Policy Studies, Tokyo, Japan

Bridging the Science-Society Gap in Africa
Thandi Mgwebi, National Research Foundation, Pretoria, South Africa

GeoJournalism: Telling the Story of Science with Data, Maps, and Sensors
James Fahn, Internews' Earth Journalism Network, Albany, CA

Maker Culture and Creativity: The Global Maker Movement
Seunghwan Kim, Korea Foundation for the Advancement of Science and Creativity, Seoul, South Korea

Science in Unexpected Places: Innovative Ways to Engage the Public
Jennifer Cutraro, WGBH Educational Foundation, Boston, MA

Using Humor to Address Serious Topics
Kasha Patel, NASA Goddard Space Flight Center, Washington, DC

What Scientists Think About Public Engagement: New Data, Insights, and Directions
Anthony Dudo, University of Texas, Austin

EDUCATION

Meeting Global Climate Goals with Energy Education
Matthew Garcia, AAAS Science and Technology Policy Fellow, U.S. Department of Energy, Washington, DC; David Blockstein, Council of Energy Research and Education Leaders, Washington, DC

Advancing Science Through Afterschool STEM: Making the Case with Evidence
Anita Krishnamurthi, Afterschool Alliance, Washington, DC

After the Dover Intelligent Design Trial: Law, Politics, and Education
Ida Chow, Society for Developmental Biology, Bethesda, MD; Jay B. Labov, National Academy of Sciences, Washington, DC; Eugenie C. Scott, National Center for Science Education, Berkeley, CA

Building a Transdisciplinary Science Workforce to Meet Contemporary Health Challenges
Syril Pettit, Health and Enviornmental Sciences Initiative, Washington, DC

Enabling Effective Climate Literacy with Collective Impact
Tamara Shapiro Ledley, TERC, Cambridge, MA; Frank Niepold, National Oceanic and Atmospheric Administration, Silver Spring, MD; Lin Chambers, National Aeronautics and Space Administration (NASA), Hampton, VA

Incorporating Responsible Science into Academic Curricula
Lida Anestidou, National Academies of Sciences, Engineering, and Medicine, Washington, DC

Mathematics and Music
David Wright, Washington University, St. Louis, MO

Team Science and Convergence: Implications for Education
Katherine Bowman, Margaret Hilton, and Elizabeth O'Hare, National Research Council, Washington, DC

ENGINEERING, INDUSTRY, AND TECHNOLOGY

X-ray Imaging Innovations for Biomedicine
Ge Wang, Rensselaer Polytechnic Institute, Troy, NY; Mannudeep Kalra, Massachusetts General Hospital, Boston

Accelerating Energy-Climate Innovation
Daniel Sarewitz, Arizona State University, Tempe; John Alic, Consultant, Avon, NC

Cleaner Energy Solutions: What Can 21st Century Large-Scale Physics Deliver?
Silvana C. Westbury and Isabelle Boscaro-Clarke, Diamond Light Source, Didcot, United Kingdom

Does Hydraulic Fracturing Allow Gas to Reach Drinking Water?
David Marker, WESTAT, Rockville, MD

Global Science-Driven Entrepreneurship: Determined Pursuit of Innovative Success
Anice Anderson, Private Engineering Consulting, Carmel, IN; Katharine Blodgett Gebbie, National Institute of Standards and Technology, Gaithersburg, MD; Charles W. Clark, Joint Quantum Institute, Gaithersburg, MD

AAAS 2016 ANNUAL MEETING
GLOBAL SCIENCE ENGAGEMENT

Advance Registration Rates until January 19

	AAAS Member Rates for members in good standing	New Member Includes a year of AAAS membership	Non-Member Rates for all other attendees
Professional	$295	$380	$399
Postdoc	$235	$320	$335
K-12 Teacher	$235	$320	$335
Emeritus	$235	$320	$335
Student	$60	$70	$90

One-day rates are also available: **www.aaas.org/AM16reg**

Promoting Global Science, Technology, and Innovation Entrepreneurship: Best Practices
Sarah Staton and Sara Klucking, U.S. Department of State, Washington, DC

Rethinking Sustainable Housing in Sub-Saharan Africa
Esther Obonyo and Abraham Goldman, University of Florida, Gainesville

Smart Materials for Sustainable Infrastructure: Self-Healing Concrete and Asphalt
Stefanie Reiffert and Patrick Regan, Technical University of Munich, Germany

The Global Energy Landscape: 2050 and Beyond
Subhashree Mishra, David Rench McCauley, and Abigail Watrous, U.S. Department of Energy, Washington, DC

ENVIRONMENT, ECOLOGY, AND CLIMATE CHANGE

Sea Level Rise: Human and Scientific Challenges
Benjamin Hamlington, Old Dominion University, Norfolk, VA; Eric Lindstrom, NASA Earth Sciences Division, Washington DC; Michelle Covi, Mitigation and Adaptation Research Institute and Virginia Sea Grant, Norfolk, VA

The National Park System: A National Scientific Asset
Gary Machlis, U.S. Department of the Interior, National Park Service, Washington, DC; Megan F. McKenna, National Park Service, Fort Collins, CO

Advancing Knowledge of Global Amphibian Decline with International Collaboration
Karen Lips, University of Maryland, College Park; Patricia Burrowes, University of Puerto Rico, San Juan; Kelly Zamudio, Cornell Univeristy, Ithaca, NY

Air Pollution, Climate Change, and Policy in Asia
Zhanqing Li and Maureen Cribb, University of Maryland, College Park

Biodiversity, Scientists, and Religious Communities: Conservation Through Collaboration
Se Y. Kim and Jennifer Wiseman, AAAS Dialogue on Science, Ethics, and Religion, Washington, DC

Creating Resilient Cities in the Face of Global Sea Level Rise
Rita Teutonico and Tiffany Troxler, Florida International University, Miami

Dynamic Relationship Between Mountain Glaciers and Climate Change
Jeffrey Kargel, University of Arizona, Tucson

Empowering Environmental Research, Education, and Outreach in Congo Basin Forests
Mary Katherine Gonder, Drexel University, Philadelphia, PA; Thomas Smith, University of California, Los Angeles

Finding the Balance: Collaboration on Social-Ecological Tipping Points
Carrie Kappel, University of California, Santa Barbara

Global Soil Biodiversity: A Common Ground for Sustainability
Tandra Fraser, Colorado State University, Fort Collins

Global Urban Ecology Research: Addressing Novelty, Equity, and Uncertainty
Jessica Graybill, Colgate University, Hamilton, NY; Vivek Shandas, Portland State University, OR

Living with Earthquakes: Causes, Early Warning, and Damage Mitigation
David Kornhauser, Kyoto University, Japan

Sea Level Rise in a Warming World: Past is Prologue
Maureen Raymo, Columbia University Lamont-Doherty Earth Observatory, Palisades, NY

Tsunamis: An International Hazard
Costas Synolakis, University of Southern California, Los Angeles; Harry Yeh, Oregon State University, Corvallis; Philip Liu, Cornell University, Ithaca, NY

Unmanned Autonomous Systems for Climate and Environmental Research
Sally McFarlane, U.S. Department of Energy, Washington, DC

FOOD AND WATER RESOURCES

Climate Change and Agriculture: Revisiting the Evidence and Potential Solutions
Caron Gala, Council on Food, Agricultural, and Resource Economics, Washington, DC

Food Systems: Building Resilience and Partnering across Sectors
Rahel Byland, ETH Zurich, Switzerland; Ursula Oesterle, Mixing Bowl, Palo Alto, CA

Food, Water, Energy, and the American Indian Farmer
Maureen McCarthy, University of Nevada, Reno

Global Science to Protect Our Global Farm
Matt Goode, U.K. Biotechnology and Biological Sciences Research Council, Swindon; Jennifer Martin, National Institute of Food and Agriculture, Washington, DC

Pathogens Without Borders
John Bakum, Cornell University, Ithaca, NY

Unlocking Plant Genetic Diversity for Food and Nutritional Security
Patrick Byrne, Colorado State University, Fort Collins; Ann Marie Thro, National Institute of Food and Agriculture, Washington, DC; Wayne Smith, Texas A&M University, College Station

GLOBAL PERSPECTIVES AND ISSUES

Arctic Research as a Model for Responsible International Collaboration
David Moorman, Canada Foundation for Innovation, Ottawa

Engaging LGBT Scientists in the U.S. and Abroad
Arthur G. Fitzmaurice and Gregory Mack, National Science Foundation, Arlington, VA

Iran: Science Cooperation in a Post-Sanctions Era
Richard Stone, AAAS/Science, Washington, DC

Library of Alexandria and Global Research Engagement
Ronald LaPorte, University of Pittsburgh, PA; Faina Linkov, Magee Womens Research Institute, Pittsburgh, PA

Limiting our Planet's Nitrogen Footprint
James Galloway, University of Virginia, Charlottesville

Open Science: Global Perspectives and Prospects
Rene von Schomberg, European Commission, Brussels, Belgium

SESAME: A Scientific Source of Light in the Middle East
James Gillies, European Organization for Nuclear Research (CERN), Geneva, Switzerland; Antonella Varaschin, Infinera Corporation, Rome, Italy

Smart Cities: Utopia for Data Collection?
Eswaran Subrahmanian, Carnegie Mellon University, Pittsburgh, PA; Maryann Feldman, National Science Foundation, Arlington, VA; Ram D. Sriram, National Institute of Standards and Technology, Gaithersburg, MD

Statecraft and Scalpel: Regional and Global Health Diplomacy
Daan Du Toit, South Africa Department of Science and Technology, Pretoria; Satoru Ohtake, Japan Science and Technology Agency, Tokyo

Statisticians Building Global Science Capacity and Infrastructure
Rochelle Tractenberg, Georgetown University, Washington, DC; Eric Vance, Virginia Polytechnic Institute and State University, Blacksburg

Toward a Sustainable Future in the Middle East: Building Scientific Collaborations
Elizabeth Ann Nalley, Cameron University, Lawton, OK; Zafra Margolin Lerman, Malta Conferences Foundation, Evanston, IL

INFORMATION TECHNOLOGY AND COMPUTING

New Science Roadmaps for Global Research
Ben Shneiderman, University of Maryland, College Park

Citizen Science and Information Technology: Engaging People for a Better Planet
Daniel Rubenstein, Princeton University, NJ; Carla P. Gomes, Cornell University, Ithaca, NY; Barbara Illman, U.S. Forest Service, Madison, WI

Emergence of Intelligent Machines: Challenges and Opportunities
Bart Selman, Cornell University, Ithaca, NY; Francesca Rossi, University of Padova, Italy

Massively-Collaborative Global Research in Mathematics and Science
Edward Aboufadel, Grand Valley State University, Allendale, MI

Public-Private Partnerships to Accelerate Innovation in Intelligence Analysis
Alyson Wilson, North Carolina State University, Raleigh

The Confluence of Computing and Society: Emerging Themes in Socio-Technical Systems
Gregory D. Hager, Johns Hopkins University, Baltimore, MD; Ann Drobnis, Computing Community Consortium, Washington, DC

INTERNATIONAL AND SUSTAINABLE DEVELOPMENT

Accelerating Africa's Scientific Transformation
Diana Sanchez, CRDF Global, Arlington, VA

Enhancing African STEM Research and Capacity with International Collaboration
Molly Haragan and Emilio Bunge, Development Finance International Inc., Bethesda, MD

Mathematics Making a Difference in Africa
Evans Harrell, Georgia Institute of Technology, Atlanta

Sustainable Development Goals: Paths Forward
Margaret Collins, International Institute for Applied Systems Analysis, Laxenburg, Austria

Using Biodiversity Science for Conservation and Development
Molly Fannon and John Kress, Smithsonian Institution, Washington, DC

Win-Win or Lose-Lose: Poverty, Human Health, and Environmental Quality
Christopher B. Barrett, Cornell University, Ithaca, NY

MEDICAL SCIENCES AND PUBLIC HEALTH

Advancing Assistive Devices Through Global Olympic-Style Competition
Rahel Byland, ETH Zurich, Switzerland

Fighting Cancer and Chronic Infections with T Cell Therapy: Promise and Progress
Patrick Regan and Ulrich Marsch, Technical University of Munich,Germany

Improving Cancer Patient Care: Trade-Offs Between Efficacy and Toxicity
Gabriela Chira, European Commission, Brussels, Belgium

Lessons from the Ebola Outbreak: Designing Vaccine Trials for Emerging Diseases
M. Elizabeth Halloran, University of Washington, Seattle

Measles Vaccination: Global Challenges
M. Elizabeth Halloran, University of Washington, Seattle

New and Emerging Tobacco Products: Biomarkers of Exposure and Injury
Daniel Conklin, University of Louisville, KY; Judith Zelikoff, New York University, Tuxedo

Public Health Epigenomics: Integrating Environment and Human Health
Shaun McCullough, U.S. Environmental Protection Agency, Research Triangle Park, NC; Dana Dolinoy, University of Michigan, Ann Arbor

The Burden of Disease From Air Pollution
Aaron Cohen, Health Effects Institute, Boston, MA; Michael Brauer, University of British Columbia, Vancouver, Canada

The Impact of Convergence on Innovation Across Sectoral and Global Boundaries
Katherine Bowman, National Research Council, Washington, DC; Amanda Arnold, Square Set Stratgeies LLC, Washington, DC; Anice Anderson, Private Engineering Consulting, Carmel, IN

PHYSICS AND ASTRONOMY

Astroparticle Physics: Unraveling Mysteries of the Universe
Tajinder Panesor, Institute of Physics, London, United Kingdom

Ghost Hunters: The Search for New Types of Neutrinos
Katie Yurkewicz, Fermi National Accelerator Laboratory, Batavia, IL; Vincenzo Napolano, National Institute for Nuclear Physics, Rome, Italy

James Webb Space Telescope: Building a Global Observatory
Jason Kalirai, Margaret Meixner, and Joel Green, Space Telescope Science Institute, Baltimore, MD

Mapping the Northern and Southern Skies: Diversity and Research Capacity for Global Astronomy
Keivan Stassun, Vanderbilt University, Nashville, TN

Megascience Global Projects Seeded in Europe, Asia, and the United States
Maria Spiropulu, California Institute of Technology, Pasadena; David Gross, Unviersity of California, Santa Barbara

Planet Formation Seen with Radio Eyes
Mark T. Adams, National Radio Astronomy Observatory, Charlottesville, VA

Radio Astronomy on Three Continents: First Stars and the Epoch of Reionization
Bruce G. Elmegreen, IBM, Yorktown Heights, NY

Space Weather: A Low Frequency, High Impact Space Age Hazard
Michael Wiltberger, National Center for Atmospheric Research, Boulder, CO

Where Did Most of the Universe Go? Searching for Dark Matter
Terry O'Connor, U.K. Science and Technology Facilities Council, Swindon; Manuel Gnida, SLAC National Accelerator Laboratory, Menlo Park, CA

PUBLIC POLICY

A War on Science? Vaccines, Climate Change, GMOs, and the Role of Science
Mark A. Largent, Michigan State University, East Lansing; Christian Young, Alverno College, Milwaukee, WI

Childhood Stunting: Policy Solutions To Address a Global Burden with Long-Term Impacts
Sharon Bergquist, Bill and Melinda Gates Foundation, Seattle, WA

Federal Science and the Public Good: U.S. Agency Science-Based Decision-Making
Francesca T. Grifo, U.S. Environmental Protection Agency, Washington, DC

Forensic Sciences: Toward a Stronger Scientific Framework
Alicia Carriquiry, Iowa State University, Ames

Fostering Integrity in Science: An Action Agenda
Thomas Arrison, National Academy of Sciences, Washington, DC

Future Directions for International Science Advice
Peter Gluckman, New Zealand Ministry of Foreign Affairs and Trade, Wellington

Grand Visions for the Future of U.S. Science in a New Global Era
Pushpalatha Bhat, Fermi National Accelerator Laboratory, Batavia, IL

Integrating Science into Policymaking: What Works and Why
Stephen Davies and Geraldine Barry, European Commission Joint Research Center, Brussels, Belgium

Overcoming Barriers to Technology Innovation in Established Economic Sectors
Charles Weiss, Georgetown University, Bethesda, MD; William B. Bonvillian, Massachusetts Institute of Technology, Washington, DC

Peer Review for Public Trust
Brad Wible and Marcia McNutt, AAAS/Science, Washington, DC

Science Policy in the 2016 U.S. Presidential Election: Candidates' Visions for Science
Joanne P. Carney, AAAS Office of Government Relations, Washington, DC; Tobin Smith, American Association of Universities, Washington, DC; Jennifer Poulakidas, Association of Public and Land-grant Universities, Washington, DC

The Global Impact of Violence Against Children: Economic, Health, and Policy Perspectives
Susan Horton, University of Waterloo, Canada; Susan Bissell, United Nations Children's Fund (UNICEF), New York City

AAAS 2016 ANNUAL MEETING
GLOBAL SCIENCE ENGAGEMENT

AAAS, publisher of *Science*, thanks the sponsors and supporters of the 2016 Annual Meeting

European Commission

SUBARU

RESEARCH COUNCILS UK

HELMHOLTZ ASSOCIATION

THE KAVLI FOUNDATION

NANYANG TECHNOLOGICAL UNIVERSITY

for its generous support of the Science Journalism Awards

As of December 21, 2015

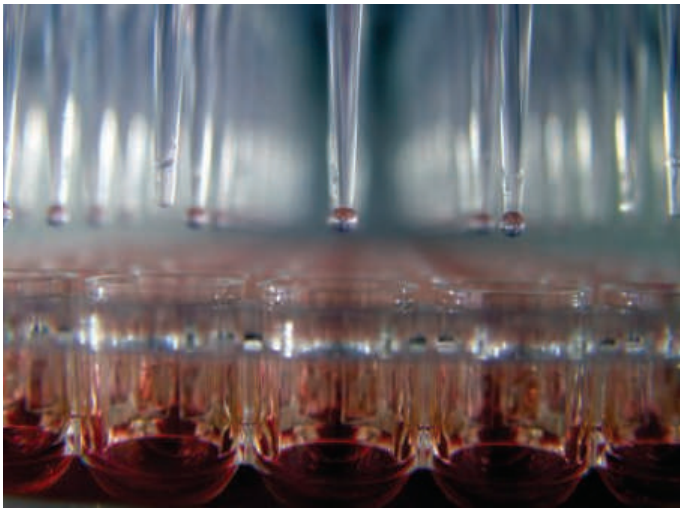

Automated sample preparation

Devices to prepare cells, nucleic acids, proteins, and other samples for analysis are becoming increasingly sophisticated, running faster and more accurately than ever before. In addition, their ease of use is making it possible to quickly train almost anyone to run automated sample preparation.
By Mike May

Automation increases the throughput and consistency of preparing samples for protein analysis, genetic sequencing, and other methods of data collection. The key challenges of automating sample preparation, explains Michael McGinley, core products manager for **Phenomenex** in Torrence, California, is "turning vision into reality." He adds, "It's all about how to get a sample from point 'A' to point 'B,' but that can be a Herculean task at times."

Traditionally, most automated sample preparation involves liquid handling, which uses robotics to dispense and collect specific amounts of liquids to, for example, add reagents or wash samples. These tasks remain fundamental to automated sample preparation, and such liquid-handling platforms work with various containers ranging from tubes to multiwell plates, to automatically prepare samples for various downstream processes, such as liquid and gas chromatography (LC and GC) and next-generation sequencing (NGS).

"The challenge for data collection is to prepare samples in a consistent manner, and automation can be used to reduce human error," says Eric Grumbach, a product manager at **Waters Corporation** in Milford, Massachusetts. "The health science marketplace has made the most of automation—using a conveyor line, barcode reading, and whole rooms of machinery to completely automate workflows. In many cases, the user simply inserts the sample and, sometime later, gets a result."

Two tactics

Overall, companies produce tools for automation in two ways. The sample preparation can either stand alone, meaning that it is used only to get a sample ready for analysis on another platform; or automated sample preparation can be integrated with an analytical platform, so that a sample is loaded, prepared, and analyzed within one device. Choosing an approach really depends on the user's requirements and the reason they want to add automation into their workflow. For instance, Grumbach says, "If you handle preparation separately then you're not tying up test instrumentation while samples are being prepared." However, when the preparation and analysis are integrated, user intervention is essentially eliminated after the samples and methods have been loaded onto the machine, and that frees lab members to do other things.

Many labs use a standalone approach with LC or GC to separate samples into components that can be analyzed on another platform, such as mass spectrometry (MS). LC, for example, pushes a sample and a liquid solvent through an adsorbent-filled column. The components of the sample move through the column at different rates based on how they interact with the adsorbent, and that separates them. In GC, the sample is instead vaporized for separation. Getting the best results from chromatography starts with sample preparation. For example, solid phase extraction (SPE) can be used to increase the concentration of targeted components before either LC or GC.

McGinley says of Phenomenex, "We live and breathe chemistries of separation," and this includes GC, LC, and SPE. He adds, "We're good at the chemistries and making sample preparation devices, but what do we do if the scale goes from 20 samples a day to 200 or 2,000?" In this case, the answer is to team up with an expert in liquid handling.

In 2015, Phenomenex and Switzerland-based **Tecan** combined their skills to automate SPE. The resulting platform consists of Phenomenex's SPE-chemistry products—Phenomenex Strata and Strata-X SPE sorbents—and Tecan's Freedom EVO, which provides robotic liquid handling. McGinley says, "This collaboration came out of being at a scientific conference with people from Tecan and finding a customer who wanted to use their robots and our assays." This system can run tubes or 96-well plates. McGinley adds, "You can start with a manual process and move to automation as needed."

One example of integrating sample analysis and detection involves titration, which measures a solution's concentration. Medical laboratories, for instance, use titration to measure chemicals in blood or urine samples. **Metrohm USA** in Riverview, Florida, automates this process. By focusing on one key task, Metrohm has made its automated

Upcoming Features

Genomics—February 12 ■ Tissue Analysis—March 4 ■ General Lab Equipment—April 29

PHOTO: © CALEB FOSTER/SHUTTERSTOCK.COM

titration platforms easier to use. "This technology is good for labs with multiple analysts who rotate through," says Lori Carey, Metrohm's titration product manager. "You just weigh the sample, put it on a tray, and press 'start.'" These platforms can also perform automated dilution of the sample, add a solvent if needed, and remove precise volumes. A range of scientists beyond those in medical laboratories can use these titration platforms. As an example, Carey mentions researchers working in environmental labs, who also require high-throughput capabilities.

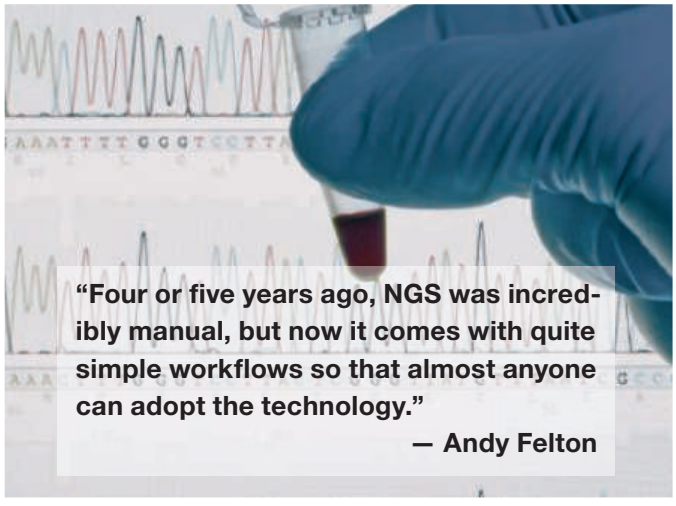

"Four or five years ago, NGS was incredibly manual, but now it comes with quite simple workflows so that almost anyone can adopt the technology."

— Andy Felton

Prepping proteins

To study specific proteins or peptides, scientists often label them. The labels can then be used to isolate specific proteins or peptides for further study. **Agilent Technologies** in Santa Clara, California simplifies protein isolation with its AssayMAP platform. David J. Edwards, senior director of mass spectrometry marketing in Agilent's life sciences and applied markets group, describes this platform as "a fully automated solution for high-throughput protein and peptide sample preparation and purification."

The AssayMAP Bravo Platform consists of the Agilent Bravo liquid handler and comes equipped with AssayMAP microchromatography technology, which features disposable cartridges that can accommodate a variety of separation chemistries. These chemistries include AssayMAP Affinity Purification, which can be used to attach an antibody to a target protein, for example.

Edwards says, "AssayMAP is especially effective when used upfront of LC/MS analyses, delivering consistent samples that allow users working in biopharma and proteomics to achieve superior mass spec results." The AssayMAP Bravo Platform uses the Bravo AssayMAP liquid-handling head, which contains precision-flow syringes. "The syringes enable liquid flow to be precisely controlled to accommodate quantitative protein/peptide binding and elution in a single pass and deliver reproducible and consistent coefficients of variation," Edwards says. In addition, AssayMAP comes with software that includes predefined workflows, but which can also be customized if the user wishes. The software eliminates "any need for the user to learn a scripting/instrument-control programming language," adds Edwards.

Agilent recently released an immobilized metal affinity chromatography (IMAC) cartridge for AssayMap that uses nitrilotriacetic acid (NTA) chelated with Fe(III) for phosphopeptide enrichment for LC/MS applications. "Phosphopeptide enrichment from complex mixtures is one of the most challenging sample preparation tasks to perform reproducibly for LC/MS," Edwards says. "The AssayMAP Fe(III) NTA cartridge addresses this challenge in a scalable, reproducible, and automated manner." This cartridge can be used as part of an LC/MS workflow to discover and characterize biomarkers and biotherapeutics or to analyze the selectivity and toxicity of candidate drugs.

Preparing DNA

For scientists looking to explore an organism's genes or isolate DNA for specific applications such as forensics, DNA sequencing is key. The high-throughput capabilities of NGS, however, only provide useful data if the right library is used. To build a library, scientists use enzymes to generate random DNA fragments of a specific size from their sample. Making the library, though, is more complicated than it sounds.

As Andy Felton, vice president of product management for Ion Torrent at **Thermo Fisher Scientific**, headquartered in Waltham, Massachusetts, explains: "Library preparation is a set of fairly complex molecular bioprocesses," and has traditionally required a lot of manual work. Consequently, it takes hours—at least two and up to seven, depending on the specific process being used. Felton adds, "There's always room for error with a manual process."

Thermo Fisher Scientific adapted its Ion Chef system to perform library construction. Instead of taking hours of hands-on time at the bench, Felton says, the Chef can build a library in just 15 minutes.

"Four or five years ago, NGS was incredibly manual," says Felton, "but now it comes with quite simple workflows so that almost anyone can adopt the technology." It's so easy to use that Felton says he could teach almost anyone how to set it up in less than an hour.

Besides being easier to use, the Ion Chef boosts the outcome of NGS. "Removing user interaction typically reduces the error rate and improves the overall repeatability of the results," Felton says. That really matters in clinical applications, which need less complex and extremely robust methods. The increasing simplification of NGS is also spreading the use of this technology, and Felton says it can be used for "measuring gene expression, target detection, metabolomics, epigenetics, and beyond." continued>

PHOTO: © DAMERAU/SHUTTERSTOCK.COM

Featured Participants

Agilent Technologies
www.agilent.com

Metrohm USA
www.metrohmusa.com

Phenomenex
www.phenomenex.com

QIAGEN
www.qiagen.com

Tecan
www.tecan.com

Thermo Fisher Scientific
www.thermofisher.com

Washington University School of Medicine in St. Louis
medicine.wustl.edu

Waters Corporation
www.waters.com

Identifying nucleic acids in the clinic

The throughput of NGS makes it useful for clinical settings in which researchers must analyze a large number of samples. By simplifying the sample-preparation steps in NGS, a wide variety of clinical applications become more practical. For instance, the growing interest in the health ramifications of the human microbiome—the microorganisms that live in and on us—generates the need to isolate and analyze these microbial samples.

As Markus Sprenger-Haussels—senior director, head of sample technologies product development for life sciences at Germany-based **QIAGEN**—explains, researchers use nucleic-acid extractions to study the composition of microorganisms in the human gut, for example. Unfortunately, about 95% of the NGS reads from such a sample are usually of human origin, not microbial. "So we developed a method to selectively isolate microbial DNA," Sprenger-Haussels says, "and after using it, 95% of the reads are from microbial DNA, which increases the amount of valuable information per sequencing run almost 20-fold." This enrichment method is included in QIAGEN's QIAamp DNA Microbiome Kit and the QIAamp FAST DNA Stool Mini Kit, which isolate microbial DNA for further analysis. Using these kits, "you can look at the correlation between certain disease states and the microbial community composition on the skin or in the colon," Sprenger-Haussels says.

In addition to NGS, today's medical experts also use assays based on the polymerase chain reaction (PCR). For instance, PCR can be used when treating cancer. To track the impact of a cancer treatment, an oncologist might use a liquid biopsy to analyze a patient's blood for signs of cancer. QIAGEN provides PCR-based tests that can be used manually or automated with the QIAsymphony sample preparation system to isolate circulating tumor cells, free circulating nucleic acids, and exosomes (vesicles released from cancer cells that can trigger tumor growth). "These all carry information about a [patient's] cancer," Sprenger-Haussels says, "and the QIAsymphony provides unmatched sensitivity due to its capacity to process large sample volumes." With respect to circulating tumor cells, for example, QIAGEN's AdnaSelect and AdnaDetect technology finds them 95% of the time if there are only five cancer cells in 5 milliliters of blood; and it detects them more than 70% of the time even when there are only two circulating tumor cells in 5 milliliters of blood.

QIAGEN's sample-preparation technology for PCR-based assays can also be used for prenatal diagnostics. "Just draw blood from the mother," Sprenger-Haussels says, "and it includes fetal DNA that can be analyzed for [Down syndrome] or other genetic disorders." Sprenger-Haussels adds, "There's no risk to the fetus, and it provides much higher accuracy than other noninvasive tests, like imaging."

Creating custom systems

Even with the various commercial options available for automating sample preparation, scientists sometimes need a custom system. Daniel Ory, professor of medicine, cell biology and physiology at **Washington University School of Medicine in St. Louis,** Missouri, and his colleagues create custom analytical systems for academic and industry scientists. He says, "The projects that we take can vary from a handful of samples to sample sets of thousands—3,000 to 4,000." Given that breadth of projects, Ory points out that each needs a different approach. The level of automation that Ory applies depends on the project's size. For instance, if a clinical project includes 1,000 samples, he might develop a method that uses 96-well plates. "There are lots of liquid-handling stations that can work with a multiwell format," he says. Nonetheless, many of the solutions turn out semiautomated. Ory says, "If we can get to a point with minimal manual work, that's the best, and that's what we aim for."

A lab or company's decision to automate sample preparation, however, includes an economic component. "Automation could cost hundreds of thousands of dollars," Grumbach says. "Automation also requires routine maintenance. Organizations often hire specialists specifically to care for these automation platforms." If a process does not include enough samples to justify that level of spending, it might make more sense to stick with a manual approach.

Regardless of the sample-preparation approach, Ory makes a key point: "Your project will only be as good as the quality of the data that comes out of it." To get the highest-quality data, a scientist must employ the best sample preparation. Moreover, the analytical system must be validated. As Ory explains: "If you have a sample set of 1,000 from a clinical study, you would like to know that sample number 1 and sample number 1,000 can be compared."

As tools for automating sample preparation become easier to set up and use, more scientists can incorporate the technology in their labs or in the clinic.

Mike May is a publishing consultant for science and technology.

DOI: 10.1126/science.opms.p1600101

Protein Extraction System

The Spot Hunter is a robotic system that is integrated with a fluorescence detection unit for the automatic extraction of selected protein spots after 2D electrophoresis. This new generation of proteomic workstation offers greater flexibility than other systems, improved accuracy, and reliability all within a minimal footprint. The Spot Hunter operates in three essential stages: First, an image is captured of the stained 2D gels using an application-specific, high-resolution charge-coupled device (CCD) camera. Next, the easy4 science software detects all protein spots and creates a target list, which it transfers to the picking unit. Finally, the selected spots are automatically extracted under contamination-free conditions and then transported into a standard microtiter plate. The high-throughput version can do this with up to four plates. The whole process conforms to good laboratory practice with the ability to enable exact backtracking to any spot. Three sizes are available including a high-throughput model for gels up to 340 mm × 290 mm.

HeroLab
For info: +49-(0)-6222-5802-0
www.herolab.com

Automated Microcomputed Tomography

The SkyScan 1275 is a highly automated, self-optimizing desktop X-ray microtomograph. The system takes advantage of new X-ray source technology and efficient flat-panel detectors to reduce scan time to just a few minutes without compromising image quality. The SkyScan 1275 software features 2D/3D image analysis, as well as a realistic 3D visualization that employs recent developments in reconstruction algorithms, accelerated by powerful new graphics cards, to give an additional gain in performance and speed. The outcome is the rapid and realistic visualization of results by volume rendering. Push-button operation with a preselected sequence of actions, including scanning, reconstruction, and volume rendering means that even routine users can successfully obtain high-quality results with the SkyScan 1275. The SkyScan 1275 has an object size range up to 96 mm in diameter and 120 mm in length. Optional stages for micropositioning and material testing allow scanning of a sample under a variety of conditions.

Bruker Corporation
For info: +32-3-877-5705
www.bruker.com/skyscan1275

NGS Platform

Two next-generation sequencing (NGS) systems deliver a comprehensive solution that simplifies targeted sequencing. Built upon the proven capabilities of Ion Torrent technology, the new Ion S5 and Ion S5 XL benchtop systems provide scientists with rapid, cost-effective, and flexible platforms that can be scaled for all research areas. These systems combine the ability to sequence gene panels and small genomes, as well as exomes, transcriptomes, and even custom assays on a single platform. The platforms are designed with "plug-and-play" cartridge-based reagents to make setting up and operating the sequencers easy and efficient. With reduced hands-on time and streamlined workflow, the Ion S5 and Ion S5 XL systems make targeted sequencing more accessible. The new systems require just 15 minutes of manual setup time per sequencing run and less than 45 minutes of hands-on work from DNA to data when using the Ion Chef System for automated Ion AmpliSeq library construction, template preparation, and chip loading.

Thermo Fisher Scientific
For info: 800-955-6288
www.thermofisher.com/ions5

Bioprocess Analysis Kits

A series of new kits comprising Gyrolab CHO-HCP Kits 2–5 and two Gyrolab Human IgG Titer Kits have been designed for analysis in bioprocess workflows. Combined with the automation and high throughput of Gyrolab systems, these kits facilitate increased productivity in process development and release testing. The four new Gyrolab CHO-HCP Kits 2–5 quantify host cell proteins (HCPs) from Chinese hamster ovary (CHO) cells used in bioprocessing of biotherapeutics. The kits have broad dynamic range and show low intra- and interassay variation. The new Gyrolab huIgG Kits for determination of human immunoglobin G (IgG) come in two configurations, high titer and low titer, and have been developed to accurately and robustly quantify intact human IgG during cell line development. With broad dynamic ranges of three to four logs for each kit, determination is enabled from 1 ng/ml up to 1 mg/ml IgG concentrations. Reliable methods to determine IgG titer are essential to ensure efficient process development.

Gyros
For info: +46-(0)-18-56-63-00
www.gyros.com

Automated DNA Preparation

The ThruPLEX Plasma-seq kit, which prepares DNA libraries for the analysis of cell-free DNA circulating in plasma, is now automated on Beckman Coulter's Biomek FX^P Laboratory Automation Workstation. ThruPLEX Plasma-seq's single-tube workflow is easily transferred to the Biomek FX^P Workstation to enable high-throughput automated preparation of Illumina next-generation sequencing (NGS) libraries of cell-free DNA for liquid biopsies. The Biomek FX^P Workstation, a proven tool for automated NGS sample prep, enables higher throughput and efficiency for processing these precious samples at even the lowest input amounts. The ready-to-run method creates up to 96 dual-barcoded libraries in about 3.5 hours—libraries that are compatible with Illumina NGS platforms. Automating ThruPLEX Plasma-seq reduces costly handling errors and potential sample loss while increasing reproducibility and, therefore, user confidence in sample quality. ThruPLEX Plasma-seq produces highly reproducible NGS libraries from less than 1 ng up to 30 ng of cell-free DNA in plasma.

Rubicon Genomics
For info: 734-677-4845
www.rubicongenomics.com

Electronically submit your new product description or product literature information! Go to www.sciencemag.org/products/newproducts.dtl for more information.

Newly offered instrumentation, apparatus, and laboratory materials of interest to researchers in all disciplines in academic, industrial, and governmental organizations are featured in this space. Emphasis is given to purpose, chief characteristics, and availability of products and materials. Endorsement by Science or AAAS of any products or materials mentioned is not implied. Additional information may be obtained from the manufacturer or supplier.

CALL FOR PAPERS! MANUSCRIPTS DUE MAY 1, 2016.

Make Waves with Your Bioelectronics Research

Publish in our Special Series, Advances in Bioelectronics.
We'll Waive all APCs. Use code: ADVSSBIO

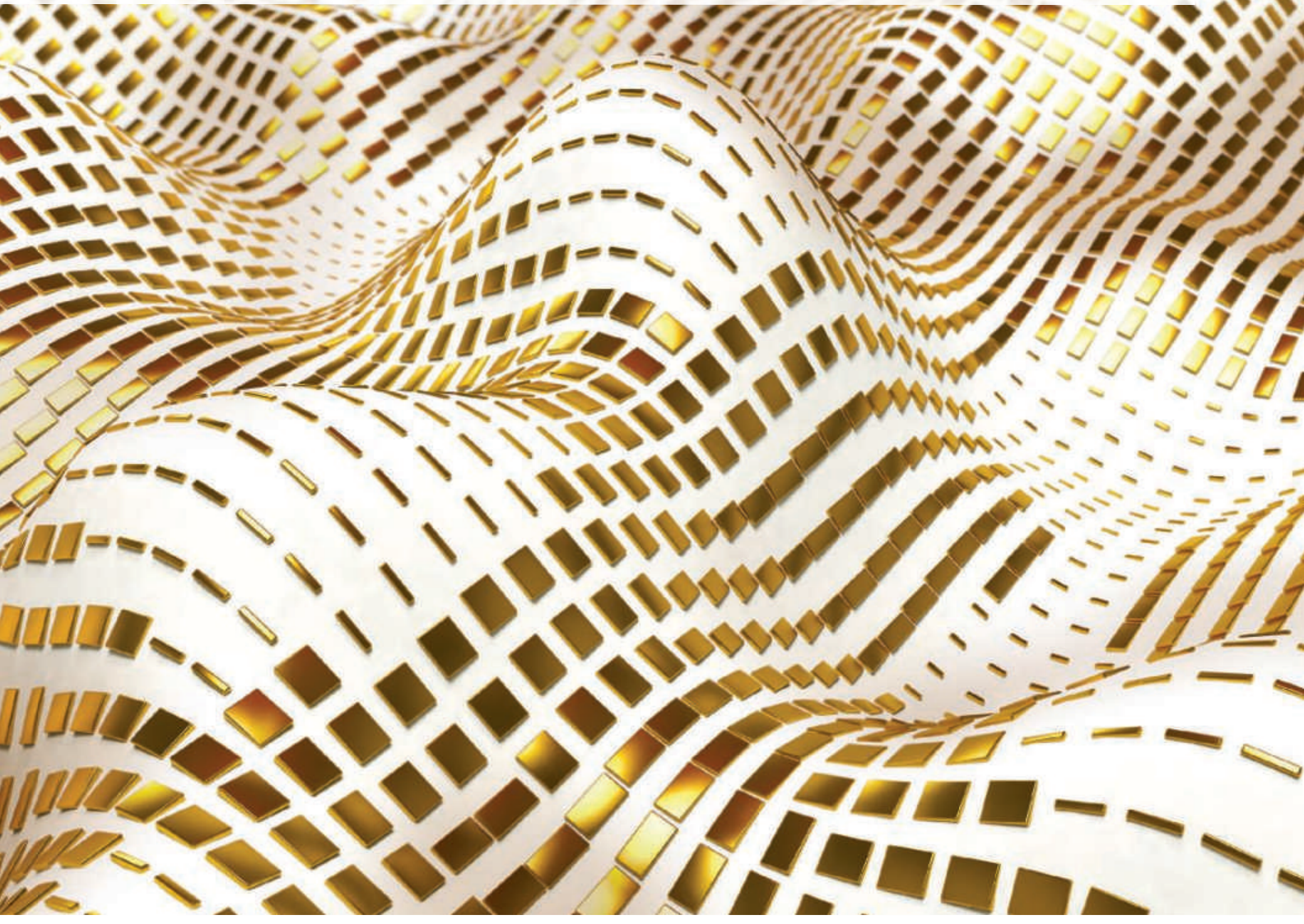

Illustration of an ultrathin cloak of nanoantennas (gold blocks) conformally coating an arbitrarily shaped surface, rendering it invisible with red light. Illustration: Valerie Altounian/Science, Vol. 349, No. 6254.

Science Advances, the new, open-access journal from AAAS, is making waves with original research that advances the frontiers of interdisciplinary science. We're now preparing an exciting Special Series, Advances in Bioelectronics, showcasing important work that has potential global impact.

You are invited to submit your research on bioelectronics to the series, and if our guest editors select your manuscript for publication, we'll waive all APCs. *Science Advances* offers expert editing, rapid publication, and all the marketing clout you'd expect from the publisher of *Science*.

Submit your research at ScienceAdvances.org

ScienceAdvances | AAAS
SIGNIFICANT RESEARCH. GLOBAL IMPACT

eppendorf

Visit us at the SLAS 2016
Booth 523

What`s Next?

NGS Sample Preparation and Library Construction

As a workflow oriented provider of lab equipment, Eppendorf offers instruments, consumables, and accessories that perfectly fit the NGS sample preparation and library construction workflow. Especially cumbersome steps are simplified or even fully automated.

- > Reproducible nucleic acid purification and library preparation with the Liquid Handling workstation ep*Motion*® 5075
- > Reliable DNA/RNA quantification with the Eppendorf BioSpectrometer® fluorescence
- > Mastercycler® pro with excellent block homogeneity and evaporation protection

www.eppendorf.com/NGS

Eppendorf®, the Eppendorf logo, Eppendorf BioSpectrometer®, ep*Motion*® and Mastercycler® are registered trademarks of Eppendorf AG, Germany.
U.S. Design Patents are listed on www.eppendorf.com/ip. All rights reserved, including graphics and images. Copyright © 2015 by Eppendorf AG.

Science Careers Advertising

For full advertising details, go to ScienceCareers.org and click For Employers, or call one of our representatives.

Tracy Holmes
Worldwide Associate Director
Science Careers
Phone: +44 (0) 1223 326525

THE AMERICAS

E-mail: advertise@sciencecareers.org

Fax: +1 (202) 289 6742

Tina Burks
Phone: +1 (202) 326 6577

Nancy Toema
Phone: +1 (202) 326 6578

Online Job Posting Questions
Phone: +1 (202) 312 6375

EUROPE / INDIA / AUSTRALIA / NEW ZEALAND / REST OF WORLD

E-mail: ads@science-int.co.uk

Fax: +44 (0) 1223 326532

Sarah Lelarge
Phone: +44 (0) 1223 326527

Kelly Grace
Phone: +44 (0) 1223 326528

Online Job Posting Questions
Phone: +44 (0) 1223 326528

JAPAN

Katsuyoshi Fukamizu (Tokyo)
E-mail: kfukamizu@aaas.org
Phone: +81 3 3219 5777

Hiroyuki Mashiki (Kyoto)
E-mail: hmashiki@aaas.org
Phone: +81 75 823 1109

CHINA / KOREA / SINGAPORE / TAIWAN / THAILAND

Ruolei Wu
Phone: +86 186 0082 9345
E-mail: rwu@aaas.org

All ads submitted for publication must comply with applicable U.S. and non-U.S. laws. *Science* reserves the right to refuse any advertisement at its sole discretion for any reason, including without limitation for offensive language or inappropriate content, and all advertising is subject to publisher approval. *Science* encourages our readers to alert us to any ads that they feel may be discriminatory or offensive.

ScienceCareers
FROM THE JOURNAL SCIENCE AAAS

ScienceCareers.org

POSITIONS OPEN

UNIVERSITY OF SOUTH CAROLINA
School of Medicine

TENURE-TRACK ASSISTANT PROFESSOR
University of South Carolina

The Department of Pathology, Microbiology, and Immunology at the University of South Carolina's School of Medicine invites applications for a tenure-track ASSISTANT PROFESSOR position in any area of Biomedical Sciences with expertise in Immunology, Inflammation or Microbiome research. This position is supported by USC Faculty Excellence Initiative. The successful candidate is expected to develop a strong extramurally funded research program complementing current faculty research interests (http://pmi.med.sc.edu/), and participate in teaching. The department is currently ranked in the top 15 among Pathology departments in the nation in NIH funding, and hosts several NIH-funded Research Centers including the Center for Complementary and Alternative Medicine, the Center of Biomedical Research Excellence on Dietary Supplements and Inflammation, and the IDeA Network of Biomedical Research Excellence. The department and Centers provide excellent mentoring opportunity to junior faculty. Candidates must have a PhD or equivalent, and at least 3 years of postdoctoral research experience. Competitive salary and startup funds are available. Please submit curriculum vitae and a statement of research and teaching interests with names of 3 references to Dr. Mitzi Nagarkatti, Chair, Department of Pathology, Microbiology, and Immunology, University of South Carolina School of Medicine, Columbia, SC 29208 or E-mail: **immunology@uscmed.sc.edu**. The search will start immediately and will continue until the position is filled. *USC Columbia is an Equal Opportunity Affirmative Action Employer and encourages applications from women and minorities and is responsive to the needs of dual career couples.*

KANSAS STATE UNIVERSITY College of Veterinary Medicine

HEAD AND PROFESSOR, DEPARTMENT OF ANATOMY AND PHYSIOLOGY

The College of Veterinary Medicine at Kansas State University invites applications and letters of nomination for the Head of the Department of Anatomy and Physiology. The successful candidate will have a Ph.D. or other earned doctoral degree in biomedical sciences or related, an outstanding history of scholarly achievement and continuing success in extramurally funded research, exceptional leadership, strong commitment to professional and graduate student education and the professional development of faculty, staff and students. Applicants should submit a single PDF that includes a letter of application addressing leadership philosophy and vision; curriculum vitae; and contact information for three individuals from whom letters of reference may be requested. Application and nomination materials should be sent to website: **geyestone@vet.k-state.edu.** For further information, please refer to website: **www.vet.k-state.edu/about/employment /opportunities.html**. Review of applications will begin immediately and continue until the position is filled. Applications should be submitted prior to **February 12, 2016**

Kansas State University is an Equal Opportunity Employer of individuals with disabilities and protected veterans and actively seeks diversity among its employees. Background check required.

Post Your Jobs
1 million candidates*
151,000 job applications*
Reach Scientists. Fill Positions.
ScienceCareers
employers.sciencecareers.org
*Jan–Dec 2014

Advance your career with expert advice from *Science* Careers.

Download Free Career Advice Booklets!
ScienceCareers.org/booklets

Featured Topics:
- Networking
- Industry or Academia
- Job Searching
- Non-Bench Careers
- And More

ScienceCareers
FROM THE JOURNAL SCIENCE AAAS

UNIL | Université de Lausanne

Faculty of Biology and Medicine

THE FACULTY OF BIOLOGY AND MEDICINE OF THE UNIVERSITY OF LAUSANNE, SWITZERLAND AND THE LAUSANNE UNIVERSITY HOSPITAL (CHUV) INVITE APPLICATIONS FOR THE POSITION OF

ASSOCIATE PROFESSOR OR TENURE-TRACK ASSISTANT PROFESSOR TOWARDS A POSITION OF ASSOCIATE PROFESSOR IN TRANSLATIONAL RESEARCH IN PSYCHIATRY AT THE DEPARTMENT OF PSYCHIATRY

Starting date: to be agreed

Your activities:

- Develop and lead translational research programs in the field of mood disorders, covering neuroscientific as well as psychiatric and psychotherapeutic aspects
- In collaboration with the clinical services of the Department of Psychiatry, implement recruitment programs in order to develop cohorts of patients to conduct translational research aimed in particular at identifying biomarkers and endophenotypes of mood disorders
- Within the framework of the National Center for Competence in Research (NCCR) *Synapsy* (www.nccr-synapsy.ch), participate in the development of an international research unit aimed at initiating collaborative cohort studies in order to improve the identification of early biomarkers
- Collaborate with national and international research groups
- Teach at pre- and postgraduate levels as well as to candidates for the specialization in psychiatry and psychotherapy
- Supervise master and doctoral theses

Your profile:

- MD, MD-PhD or PhD or qualifications deemed to be equivalent
- Demonstrated ability to:
  - Joint conduct of clinical activity and research
  - Conduct an internationally recognized research activity (substantial list of publications in peer-reviewed journals) in neuroscience, particularly neuroimaging and/or cellular and molecular neuroscience, focusing on the investigation of pathophysiological mechanisms in psychiatric disorders, as well as on the identification of biomarkers
  - Initiate and steer translational research programs that bring together clinicians and researchers in psychiatric neuroscience
  - Attract funding
- Excellent teaching and organizational skills
- Good working knowledge in French or the capacity to acquire it quickly

Your application:

The applications, in English, will include the motivation letter, the curriculum vitae, the list of publications with a copy of the five most relevant ones, a brief description of the research program and of teaching experience and a copy of diplomas. They should be sent by March 15th, 2016 as a single pdf file to www.unil.ch/iafbm/application.

The job description as well as a description of the Division are available on the Web at the address www.unil.ch/emplois « Postes académiques ». For further information, please contact Prof. Friedrich Stiefel (Frederic.Stiefel@chuv.ch), Head of Service.

Seeking to promote an equitable representation of women and men among their staff, the University and the Lausanne University Hospital encourage applications from women.

ScienceCareers online @sciencecareers.org

ScienceCareers online @sciencecareers.org

For recruitment in science, there's only one Science

Fantastic Recruiting Opportunity!

POSTDOC CAREERS | March 25, 2016

Be sure to promote your openings to the thousands of scientists who will be reading *Science* to find out about the latest postdoc opportunities.

Reserve ads by March 8 to guarantee space.

Produced by the *Science*/AAAS Custom Publishing Office.

SCIENCECAREERS.ORG

ScienceCareers
FROM THE JOURNAL SCIENCE AAAS

To book your ad: **advertise@sciencecareers.org**

The Americas
+202-326-6582

Japan
+81-3-3219-5777

Europe/RoW
+44(0)1223-326500

China/Korea/Singapore/Taiwan
+86-186-0082 9345

Fundación BBVA

9th edition

BBVA Foundation Frontiers of Knowledge Awards

The **BBVA Foundation Frontiers of Knowledge Awards** recognize and encourage fundamental advances in basic and applied research, as materialized in models and theories for understanding the natural and social worlds, technological innovations of broad impact and salient contributions to the creation, performance and conducting of the classical music of our time. Honors also go to outstanding contributions that advance understanding or deliver material progress with regard to two key challenges of the global society of the 21st century, climate change and development cooperation.

The **BBVA Foundation Frontiers of Knowledge Awards** are undertaken in collaboration with the **Spanish National Research Council (CSIC)**.

Fundación BBVA

Plaza de San Nicolás, 4
48005 Bilbao, Spain

Paseo de Recoletos, 10
28001 Madrid, Spain

www.fbbva.es

With the collaboration of

CSIC
Consejo Superior de Investigaciones Científicas

Categories

- Basic Sciences (Physics, Chemistry, Mathematics)
- Biomedicine
- Ecology and Conservation Biology
- Climate Change
- Information and Communication Technologies
- Economics, Finance and Management
- Development Cooperation
- Contemporary Music

Nominations

Nominations are invited from scientific and artistic societies, R&D centers, university and hospital departments, conservatories of music, orchestras, public agencies, and organizations working in the climate change and development areas, as well as other organizations and persons specified in the award conditions.

Deadline for submission

Nominations are open from January 1 through to June 30, 2016 at 23:00 GMT.

For more details and full entry conditions: www.fbbva.es/awards · awards-info@fbbva.es

Download the *Science* Careers jobs app from Science

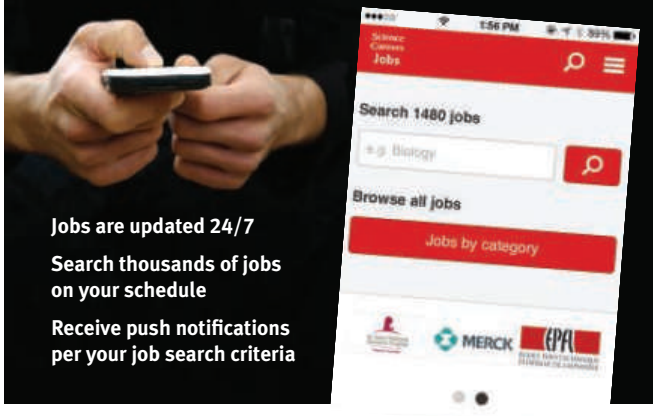

Jobs are updated 24/7

Search thousands of jobs on your schedule

Receive push notifications per your job search criteria

Get a job on the go.

Search worldwide for thousands of scientific jobs in academia, industry, and government. The application process is seamless, linking you directly to job postings from your customized push notifications.

Scan this code to download app or visit **apps.sciencemag.org** for information.

ScienceCareers | AAAS
FROM THE JOURNAL SCIENCE

ScienceCareers.org

Smithsonian Tropical Research Institute

RESEARCH POSITION IN ARCHAEOLOGY

The Smithsonian Tropical Research Institute (STRI; www.stri.si.edu), headquartered in the Republic of Panama, invites applicants interested in conducting archaeological research in the Neotropics to fill a permanent research position. The successful candidate is expected to develop a strong independent research program, supervise students, collaborate with other staff, and provide professional service.

STRI maintains modern research facilities, a library with extensive holdings in the natural and anthropological sciences, and support centers in Panama City, together with diverse stations for field work throughout the tropics. Staff scientists maintain cooperative research programs within a world-wide network of academic institutions. Opportunities for mentoring young scientists are available through a vigorous fellowship program, and formal teaching is possible through educational programs with affiliated universities.

We seek an archaeologist interested in doing research on prehistoric adaptations of native peoples to tropical ecosystems including in the fields of environmental archaeology, archaeobiology, landscape archaeology, and the development of social, cultural and economic systems. Other areas will be considered. Early to mid-career candidates are preferred but applicants at any level will be considered.

Minimum Qualifications: A Ph.D. and post-doctoral research experience, outstanding publication record, demonstrated success in obtaining grants, and a commitment to communicating science to the public.

To Apply: Interested candidates should submit a single PDF containing a summary of research accomplishments and interests, curriculum vitae, five significant reprints, and the names and contact information of three referees. **Send applications electronically as a single PDF to striarcheojob@si.edu**. Address inquiries to Dr. Fernando Santos-Granero, Chair, Search Committee on Archeology at: **SantosF@si.edu**. Review of applications will begin on **April 15, 2016**, and interviews will commence shortly thereafter.

STRI is an Equal Opportunity Employer and is committed to diversity in its workforce. Appointments are made regardless of nationality.

ScienceCareers online @sciencecareers.org

University of Zurich[UZH]

Faculty of Science

The Faculty of Science of the University of Zurich invites applications for a

Professorship in Molecular and Cellular Plant Physiology

in order to join the Department of Plant and Microbial Biology.

The Department of Plant and Microbial Biology conducts cutting-edge basic research in the areas of plant and microbial biology with a focus on molecular, genetic, genomic, and cell biological approaches. We seek innovative applicants with an outstanding track record in research and teaching who will strengthen and preferably bridge our existing interests in plant and microbial biology. The successful candidate will establish a complementary and independent research program in the field of Molecular and Cellular Plant Physiology, including but not limited to plant-microbe interactions, cellular and systemic transport processes, secondary metabolism and ecophysiology, or the biochemistry of physiological and developmental processes.

The successful candidate is expected to build up a strong research group in molecular and cellular plant physiology. Contributing to the existing undergraduate and graduate teaching efforts in plant biology (in English or German) will constitute an integral part of the position. The successful candidate should have demonstrated leadership skills to contribute to the further development of the department and is expected to acquire external funding. The position will be preferentially filled at the level of Full Professor. The position may be occupied as a part-time or shared professorship. The University of Zurich is an equal opportunity employer.

The University of Zurich provides generous research support, including funds for personnel and running expenses, and competitive start-up packages. Zurich's scientific environment includes a rich spectrum of research activities in plant biology and the life sciences in general, and provides extensive opportunities for collaborations within the University and with the ETH Zurich. Switzerland provides excellent opportunities for external funding of research. The University and the city of Zurich also offer a stimulating cultural and family-friendly environment.

Application packages should be uploaded to http://www.mnf.uzh.ch/MCPP in a single file containing a one-page summary; motivation letter; a full curriculum vitae; a vision statement of research and teaching interests outlining major unsolved problems and how they could be tackled; and the names and addresses of three potential referees. Application guidelines can be found on the above page. The deadline for applications is 29 February 2016. For further information, please contact Prof. Dr. Ueli Grossniklaus at grossnik@botinst.uzh.ch.

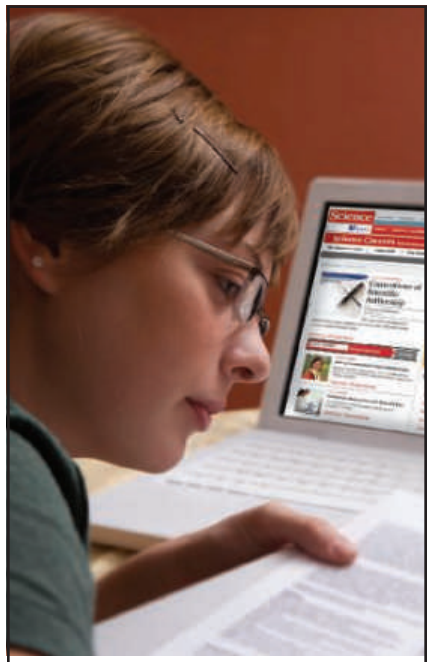

AAAS is here –
helping scientists achieve career success.

Every month, over 400,000 students and scientists visit ScienceCareers.org in search of the information, advice, and opportunities they need to take the next step in their careers.

A complete career resource, free to the public, *Science* Careers offers a suite of tools and services developed specifically for scientists. With hundreds of career development articles, webinars and downloadable booklets filled with practical advice, a community forum providing answers to career questions, and thousands of job listings in academia, government, and industry, *Science* Careers has helped countless individuals prepare themselves for successful careers.

As a AAAS member, your dues help AAAS make this service freely available to the scientific community. If you're not a member, join us. Together we can make a difference.

To learn more, visit
aaas.org/plusyou/sciencecareers

AAAS + U = Δ

Join the Conversation!

Twitter is a great way to connect with AAAS members and staff about the issues that matter to you most. Be a part of the discussion while staying up-to-date on the latest news and information about your personal member benefits.

Follow us @AAASmember and join the conversation with #AAAS

AAAS MemberCentral

MemberCentral.aaas.org

University of Zurich[UZH]

Faculty of Science

The Faculty of Science of the University of Zurich invites applications for an

Assistant Professorship in Plant Evolutionary Biology

in the framework of the University Research Priority Program «Evolution in Action: from Genomes to Ecosystems».

Evolutionary biology is a core area of biology, and understanding the mechanisms underlying evolutionary processes is of crucial importance for both basic and applied aspects of biology and medicine. Beyond the biological and medical fields, evolutionary concepts are an important theme in the social sciences and in economics. The University Research Priority Program (URPP) «Evolution in Action» is set within this wide area of research. It brings together multiple research groups of the Faculty of Science, the Faculty of Medicine, and the Faculty of Arts and plays an important integrative role for diverse disciplines at the University of Zurich (UZH). In the Plant Sciences, UZH conducts pioneering basic research and is strongly involved in the integrative, interdisciplinary structure of the URPP Evolution in Action.

We seek an innovative scientist with an outstanding track record in research and teaching, as well as the leadership skills and enthusiasm to build on the integrative structure of the URPP Evolution in Action and to further strengthen the integration of diverse disciplines. The successful candidate will establish a strong research group with a focus on Plant Evolutionary Biology, using novel approaches based on sequencing data and genome-wide analyses to address evolutionary questions. Possible research areas are: i) genetic and genomic studies at the population level, ii) molecular basis of adaptation and speciation, iii) evolution of developmental processes, iv) evolution of genomes and regulatory networks. In teaching, the successful candidate will contribute at the advanced level to graduate and undergraduate education (in English or German) in Biology.

The position will be filled as a non-tenure track Assistant Professorship but previous holders of such positions have subsequently obtained a permanent professorship at UZH. The UZH is an equal opportunity employer.

The UZH provides generous research support, including funds for personnel and running expenses. Zurich offers a stimulating scientific environment and extensive opportunities for collaborations within UZH and with ETH Zurich. Switzerland provides excellent research funding opportunities.

Application packages should be uploaded to http://www.mnf.uzh.ch/APPEB in a single file containing a one-page summary; motivation letter; a full curriculum vitae; a vision statement of research and teaching interests outlining major unsolved problems and how they could be tackled; and the names and addresses of three potential referees. Application guidelines can be found on the above page. The deadline for applications is 29 February 2016. For further information, please contact Prof. Dr. Ueli Grossniklaus at grossnik@botinst.uzh.ch.

ScienceCareers online @sciencecareers.org

By **Josh Shiode**

My adviser's best advice

Among my fellow graduate students, we called it the second-year slump, an affliction characterized by paralyzing doubts about one's abilities and future prospects. For me, though, it persisted. Even well into my third year, I found myself spending a lot of time worrying about whether I was headed in the right direction and questioning why I had even come to graduate school. "Am I cut out for this?" I asked myself. "And more important, do I even want to be here?"

I also struggled with whether I should tell my research adviser. I did talk with a few classmates who shared similar doubts about pursuing a career in academia, or even being able to finish our Ph.D.s in some reasonable number of years with the necessary accomplishments to be "successful." We speculated about "alternative career" options—but mostly in the way someone who has never set foot on a football field might talk about running the perfect play. We all vaguely knew of people who had ventured beyond academia, and figured their paths were theoretically open to us too, but none of us had any idea how we would actually go about it.

"He gave me room to find my own way as a Ph.D. scientist."

I thought that maybe my adviser could help, but the idea of sharing my doubts with him made me incredibly anxious. On the one hand, I felt I was not living up to expectations—mine or his—and talking to him about my doubts could at least partially explain my performance. On the other, I worried that telling him how I was feeling might jeopardize my graduate career. I could imagine him asking, "If you aren't here to make it in academia, why are you here at all?" I certainly wasn't ready for that level of finality. Advice from my older, wiser peers came down on both sides, which only served to reinforce my internal dithering.

In the end, not talking to him was probably never really an option for me; I wear my feelings on my sleeve, if not plastered on my forehead. So, in late spring of my third year, I asked my adviser if we could chat about "career stuff." Feeling both nervous and relieved, I told him about my doubts and asked for some time over the summer to pursue a few potentially interesting avenues, including ventures into teaching and science writing. Both would take time away from my research.

I could tell that my confession wasn't a complete surprise to my adviser, but he welcomed my honesty and encouraged me to take the time I needed to explore other interests, as long as my research progress didn't grind completely to a halt. He basically told me, "I support you 100%. You need to figure out what you want to do and what will make you happy." But he also said, "I'm an academic. My parents are academics. I have literally no help to offer you."

He had no idea how untrue that last statement was. Just supporting me in my exploration helped me tremendously. I don't know that I gained much insight that day about where I would eventually want to take my career, but I did feel a whole lot better.

It also turned out that, through colleagues, my adviser did know people I could talk to about new career directions. As I spent the next few years progressing through my Ph.D. research, he helped me connect with other Ph.D. scientists now working in policy, science communication, and tech companies in Silicon Valley. Through my own explorations and conversations with those people, I found that working at the interface of science and society—in education, communication, or policy—is what really excites me. After graduation I entered the world of science policy, where I continue to work today, almost 3 years later.

My adviser could have insisted that the only way to succeed in science was to keep my nose to the grindstone at all times, get a prize postdoc, and go on to a professorship. He could have told me he didn't want to work with someone who wasn't in grad school for the "right" reasons. But he didn't. He gave me room to find my own way as a Ph.D. scientist, and for that I'll be forever grateful. ■

Josh Shiode is a senior government relations officer at AAAS. For more on life and careers, visit sciencecareers.org. Send your story to SciCareerEditor@aaas.org.

ILLUSTRATION: ROBERT NEUBECKER

Published by AAAS